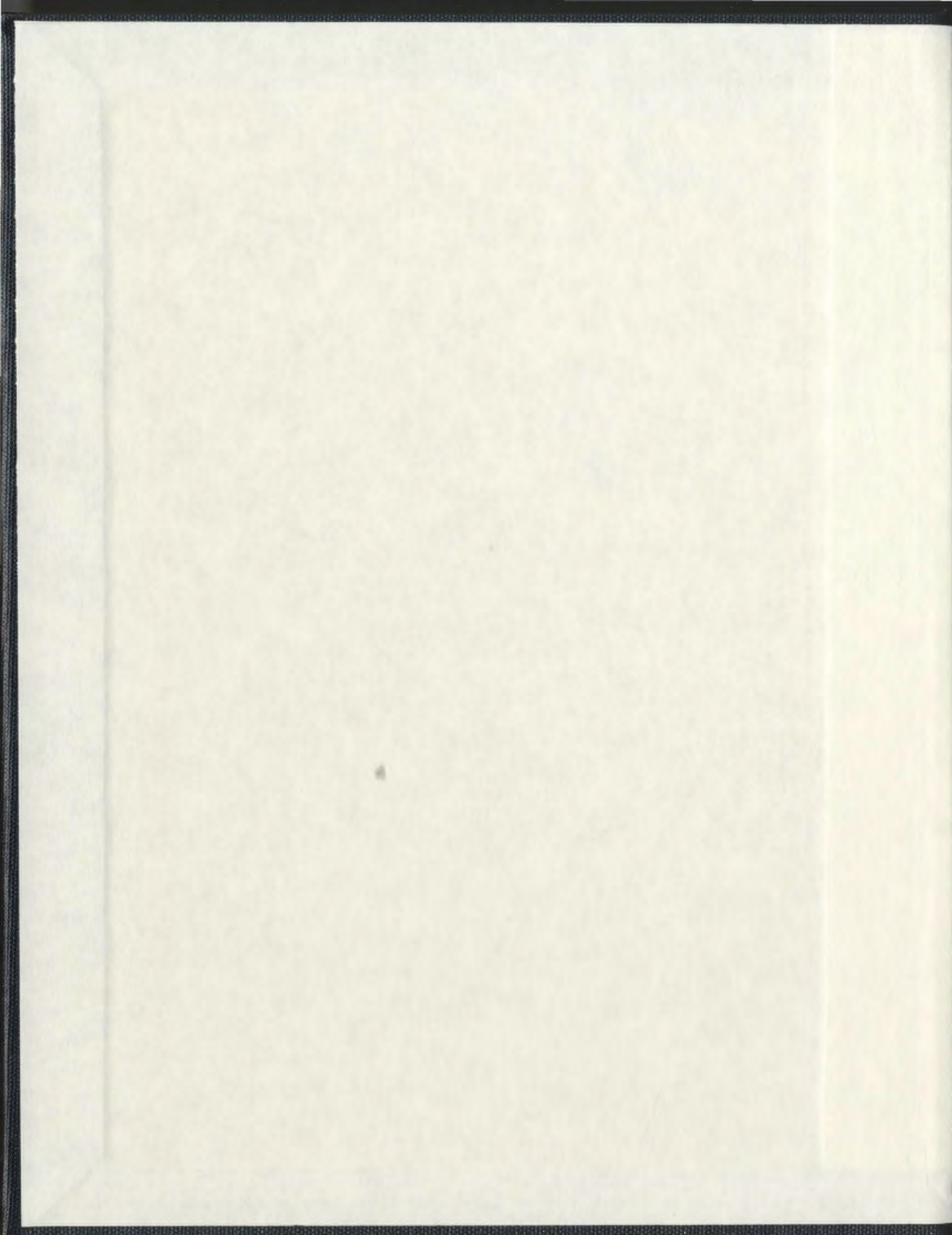


SYNTHETIC INVESTIGATIONS ON NEW CALIXSALENS  
AND MODIFIED THICALIXARENES

ALMEQDAD HABASHNEH



Synthetic Investigations on New Calixarenes  
and Modified Polycalixarenes

By

Atsuhisa Hatakeyama

B. Sc., M. Sc. (1994), Meiji University

Norfolk, Virginia

A thesis submitted to the School of Graduate  
Studies in partial fulfillment of the requirements for  
the degree of Doctor of Philosophy

Department of Chemistry  
Memorial University of Newfoundland

St. John's, Newfoundland

Canada

2004



Synthetic Investigations on New Calixsalens  
and Modified Thiocalixarenes

By

Almeqdad Habashneh

B. Sc., M. Sc. (1999), Mutah University

Karak, Jordan

A thesis submitted to the School of Graduate  
Studies in partial fulfillment of the requirements for  
the degree of Doctor of Philosophy

Department of Chemistry  
Memorial University of Newfoundland  
St. John's, Newfoundland  
Canada

2008

## Abstract

"Calix"-compounds have "cup"- or "basket"-like shapes which make them attractive synthetic targets for host-guest studies and for many other potential applications. The research described in this thesis deals with two sets of objectives. (a) The synthesis and characterization of new generation of calixsalens; and (b) The study of the reactions of thiacalix[4]arene 1,3-bistriflate and the chemistry of thiacalix[2]phenoxathiins

Calixsalens are dimeric compounds in which the two salen units are connected by methylene, ethylene or sulfonyl linking groups, and are usually prepared under Schiff-base macrocyclizations of bis-salicylaldehydes with diamines. Chiral Mn(III)-calixsalen complexes have been designed to serve as enantioselective epoxidation catalysts which act *via* a host-guest catalytic mechanism in which reactants can be included within the chiral cavities of the new complexes. New calixsalen ligands with large (chiral) cavities were synthesized by incorporating new linking groups between the two salen units. Modified low mol% Pd Suzuki conditions efficiently produced the desired targeted bis-salicylaldehydes which were used as the precursors for the desired calixsalen compounds.

The second part of this thesis describes the attempted modification of thiacalix[4]arene to form the narrow rim-functionalized arylethynyl derivative, using the Sonogashira reaction. However, the reactions employed produced instead an unexpected new phenoxathiin product under Cu(I)-catalyzed conditions. A host-guest complexation study was conducted with the new phenoxathiin and its *de-tert*-butylated analogue and both were shown to be moderate receptors for  $\text{Ag}^+$  and  $\text{Hg}^{2+}$  ions but not at all with the neutral  $\text{C}_{60}$  and  $\text{C}_{70}$  fullerenes.

## Acknowledgments

I would like express my deep gratitude to Dr. Paris E. Georghiou and Dr. Chet Jablonski for their supervision, guidance and patience. I would like also to thank them for providing support and a great learning environment.

Thanks also to Julie Collins and Dr. Celine Schneider for the X-ray structures and NMR spectra, and thanks to Linda Winsor for mass spectra.

Special thanks to my parents, and family for their continuous support. Thanks are also extended to the entire organic group and the staff in the Chemistry Department for their help, friendship and encouragement.

The financial support from the Department of Chemistry, the School of Graduate Studies, Memorial University of Newfoundland and NSERC were greatly appreciated.

## Table of Contents

<b>Abstract</b>	<b>ii</b>
<b>Acknowledgments</b>	<b>iii</b>
<b>Table of Contents</b>	<b>iv</b>
<b>List of Figures</b>	<b>vii</b>
<b>List of Schemes</b>	<b>xii</b>
<b>List of Tables</b>	<b>xvi</b>
<b>Glossary of Abbreviations</b>	<b>xvii</b>
<b>Dedication</b>	<b>xx</b>
<b>Part 1</b>	<b>1</b>
<b>Chapter 1.1 Introduction</b>	<b>2</b>
1.1.1 Schiff-base macrocycles	2
1.1.2 Mn(III)-salen asymmetric epoxidation catalysis	13
1.1.2.1 The Jacobsen-Katsuki methodology	14
1.1.2.2 Steric effects of the salen ligand on the enantioselectivity of epoxidation with Jacobsen-Katsuki catalysts	15
1.1.2.3 Advances in salen-based Mn catalysis	25
1.1.3 Host-guest catalysis and epoxidation reactions	29
1.1.4 Development of calixsalen complexes	43
1.1.5 References	47
<b>Chapter 1.2 Synthetic approaches towards the preparation of bisaldehydes</b>	<b>54</b>
1.2.1 Introduction	54
1.2.2 Strategies and retrosynthetic analysis	59
1.2.2.1 Retrosynthetic Route A	60

1.2.2.2 Retrosynthetic Route B	60
1.2.2.3 Retrosynthetic Route C	62
1.2.3 Synthesis of Bisaldehydes	62
1.2.3.1 Synthetic Route A	62
1.2.3.2 Synthetic Route B	65
1.2.3.3 Synthetic Route C	67
1.2.3.3.1 Suzuki-Miyaura coupling	69
1.2.3.3.2 De-methylation of phenol groups	77
1.2.3.3.3 <i>Ortho</i> -regioselective formylation of the bisphenols 53-56.	79
1.2.4 Summary	83
1.2.5 Experimental Section	84
1.2.6 References	100
<b>Appendix A: Selected NMR spectra for synthesized compounds described in Chapter 1.2</b>	102
<b>Chapter 1.3 Synthesis and Characterization of Calixsalens</b>	115
1.3.1 Macrocyclization methodologies	115
1.3.2 Results and discussion	126
1.3.2.1 Schiff base condensation of bisaldehyde <b>35</b>	126
1.3.2.2 Schiff base condensation of <i>meta</i> -bisaldehyde <b>40</b>	131
1.3.2.2.1 Schiff base macrocyclization of <b>40</b> in methanol THF	131
1.3.2.2.2 Schiff base macrocyclization of <b>40</b> in methanol	134
1.3.2.2.3 Schiff base macrocyclization of <b>40</b> in THF	137
1.3.2.2.4 Schiff base macrocyclization of <b>40</b> in dichloromethane	140

1.3.2.3 Schiff base condensation of bisaldehyde 47	155
1.3.2.4 Schiff base condensation of bisaldehyde 49	164
1.3.2.5 Complexation of 36, 41 and 48 with Mn <sup>3+</sup> , Ni <sup>2+</sup> and Cu <sup>2+</sup>	167
1.3.3 Summary	172
1.3.4 Experimental Section	174
1.3.5 References	179
<b>Part 2</b>	182
<b>Chapter 2.1 Modification of thiacalix[4]arene to form thiacalix[2]phenoxathiins—structural and complexation studies</b>	183
2.1.1 Introduction	183
2.1.2 Results and discussion	194
2.1.3 Complexation studies	208
2.1.4 Summary	217
2.1.5 Experimental Section	219
2.1.6 References	229
<b>Appendix B: Selected NMR spectra for synthesized compounds in Chapter 2.1 in numerical order</b>	235
<b>Appendix C: Complexation data for compounds 30 and 50 in Chapter 2.1</b>	242

## List of Figures

<b>Figure 1.1-1</b>	Achiral Robson-type macrocycles.	3
<b>Figure 1.1-2</b>	Chiral Robson-type macrocycles.	4
<b>Figure 1.1-3</b>	Polyaza macrocycles <b>22</b> and <b>23</b> .	7
<b>Figure 1.1-4</b>	Naphthalene-based tetraimine and tetraamine macrocycles <b>30-33</b> .	9
<b>Figure 1.1-5</b>	Peptide- and calixarene-like Schiff base macrocycle <b>34</b> and <b>36</b> .	10
<b>Figure 1.1-6</b>	Biscalix[4]arene Schiff base macrocycles <b>37a-c</b> .	11
<b>Figure 1.1-7</b>	Pyrrrole-containing macrocycles <b>39-43</b> .	12
<b>Figure 1.1-8</b>	Kochi's achiral Mn(III)-salen.	13
<b>Figure 1.1-9</b>	First-generation Jacobsen and Katsuki catalysts.	14
<b>Figure 1.1-10</b>	Various examples of Jacobsen- and Katsuki-type Mn(III)-salen catalysts.	15
<b>Figure 1.1-11</b>	Different approaches for an alkene to attack the oxo-Mn salen species.	16
<b>Figure 1.1-12</b>	Possible "side-on" approaches to an oxo-Mn-salen intermediate.	17
<b>Figure 1.1-13</b>	Proposed conformers for oxo-Mn-salen.	18
<b>Figure 1.1-14</b>	The axial conformer of the oxo-Mn species of the catalyst <b>72</b> bearing a carboxylic acid group.	20
<b>Figure 1.1-15</b>	Katsuki catalysts <b>73</b> and <b>74</b> .	22
<b>Figure 1.1-16</b>	"Planar" and "folded" oxo-Mn-salen species "X" and "Y" respectively, and their interactions with a <i>trans</i> alkene.	23
<b>Figure 1.1-17</b>	Jacobsen's catalysts <b>75</b> and <b>76</b> .	24
<b>Figure 1.1-18</b>	Different types of Mn(III)-salen catalysts.	26
<b>Figure 1.1-19</b>	$\beta$ -Ketoiminate salen <b>83</b> bearing a chiral ester auxiliary.	28

<b>Figure 1.1-20</b>	Perfluoro Mn(III)-salen complexes.	29
<b>Figure 1.1-21</b>	Cytochrome P-450 oxidation model.	30
<b>Figure 1.1-22</b>	Zeolite catalytic model.	32
<b>Figure 1.1-23</b>	Porphyrin enzyme mimic system for epoxidation.	36
<b>Figure 1.1-24</b>	“Strapped”-porphyrin <b>102</b> .	36
<b>Figure 1.1-25</b>	Enantioselective epoxidation catalysts bearing binaphthyl chiral auxiliaries <b>103-105</b> .	37
<b>Figure 1.1-26</b>	Clip porphyrin <b>106</b> .	38
<b>Figure 1.1-27</b>	$\alpha$ - and $\beta$ -Cyclodextrins <b>107</b> and <b>108</b> .	39
<b>Figure 1.1-28</b>	Sandwiched-porphyrin <b>109</b> .	40
<b>Figure 1.1-29</b>	Cyclodextrins <b>114</b> and <b>116</b> bearing a ketone functionality act as enantioselective catalysts for epoxidation <i>via</i> dioxirane intermediates.	42
<b>Figure 1.1-30</b>	Examples of calix[2]salens <b>117</b> .	43
<b>Figure 1.1-31</b>	X-ray crystal structure of <i>syn</i> -calix [2]salen Mn(III) complex <b>117d</b> .	44
<b>Figure 1.1-32</b>	Proposed mechanism of <i>syn</i> -calix[2]salen-epoxidation methodology.	45
<b>Figure 1.1-33</b>	Target calixsalens constructed from salen dimer <b>118</b> .	46
<b>Figure 1.2-1</b>	McAuliffe's Mn(III)-salen dimer.	55
<b>Figure 1.2-2</b>	Conformational isomers of bisaldehyde compounds <b>9-13</b> (R = H, or alkyl).	56
<b>Figure 1.3-1</b>	[2+2]-Condensation products of metal-templated Schiff base macrocyclization reactions.	116
<b>Figure 1.3-2</b>	MALDI-TOF mass spectrum producing mixture from Schiff base reaction of <b>35</b> .	128
<b>Figure 1.3-3a</b>	<sup>1</sup> H NMR (CDCl <sub>3</sub> ) spectrum of dimer <b>36</b> .	129

<b>Figure 1.3-3b</b>	$^{13}\text{C}$ NMR ( $\text{CDCl}_3$ ) spectrum of dimer <b>36</b> .	129
<b>Figure 1.3-4</b>	MALDI-TOF mass spectrum of the cyclized imine isolated by silica gel TLC.	135
<b>Figure 1.3-5a</b>	$^1\text{H}$ NMR ( $\text{C}_6\text{D}_6$ ) spectrum of <b>42</b> isolated by silica gel TLC.	136
<b>Figure 1.3-5b</b>	$^{13}\text{C}$ NMR ( $\text{CDCl}_3$ ) spectrum of <b>42</b> isolated by silica gel TLC.	136
<b>Figure 1.3-6</b>	<i>Syn</i> and <i>anti</i> conformations of bisaldehyde <b>40</b> .	137
<b>Figure 1.3-7a</b>	$^1\text{H}$ NMR Schiff base signals for the crude product from the reaction of <b>40</b> in THF solvent, $\text{Na}_2\text{CO}_3$ -free-reaction.	138
<b>Figure 1.3-7b</b>	$^1\text{H}$ NMR Schiff base signals for the crude product from the reaction of <b>40</b> in THF solvent, in the presence of $\text{Na}_2\text{CO}_3$ .	138
<b>Figure 1.3-8</b>	The MALDI-TOF mass spectrum product of Schiff base reaction of <b>40</b> THF solvent.	139
<b>Figure 1.3-9</b>	MALDI-TOF mass spectrum of the dimer <b>41</b> .	143
<b>Figure 1.3-10</b>	The $^1\text{H}$ NMR spectrum of dimer <b>41</b> in $\text{C}_6\text{D}_6$ .	144
<b>Figure 1.3-11</b>	The $^{13}\text{C}$ NMR spectrum of <b>41</b> in $\text{CDCl}_3$ .	145
<b>Figure 1.3-12a</b>	Structure and free energy of MMM-generated <i>saddle (boat)</i> conformer of <b>41</b> .	148
<b>Figure 1.3-12b</b>	Structure and free energy of <i>partial-pinched cone</i> conformer of <b>41</b> .	149
<b>Figure 1.3-12c</b>	Structure and free energy of MMM-generated <i>cone</i> conformer of <b>41</b> .	150
<b>Figure 1.3-12d</b>	Structure and free energy of MMM-generated <i>1,3-alternate</i> conformer of <b>41</b> .	151
<b>Figure 1.3-12e</b>	Structure and free energy of MMM-generated <i>1,2-alternate</i> conformer of <b>41</b> .	152
<b>Figure 1.3-13</b>	$^1\text{H}$ NMR spectra showing the Schiff base reaction of <b>40</b> in dichloromethane solvent at ambient temperature after: (a) 5 d; (b) 4 d; (c) 2 d; (d) 1 h.	154

<b>Figure 1.3-14</b>	The $^1\text{H}$ NMR spectrum of dimer <b>48</b> in $\text{CD}_2\text{Cl}_2$ .	157
<b>Figure 1.3-15</b>	The $^{13}\text{C}$ NMR spectrum of <b>48</b> in $\text{CD}_2\text{Cl}_2$ .	158
<b>Figure 1.3-16a</b>	Structure and free energy of MMM-generated <i>cone</i> conformer of <b>48</b> .	160
<b>Figure 1.3-16b</b>	Structure and free energy of MMM-generated 1,2- <i>alternate</i> conformer of <b>48</b> .	161
<b>Figure 1.3-16c</b>	Structure and free energy of MMM-generated 1,3- <i>alternate</i> conformer of <b>48</b> .	162
<b>Figure 1.3-16d</b>	Structure and free energy of MMM-generated <i>partial-pinched-cone</i> conformer of <b>48</b> .	163
<b>Figure 1.3-17</b>	The MALDI-TOF MS of Mn(II) complex <b>51</b> .	165
<b>Figure 1.3-18a</b>	Computer-generated model <sup>30</sup> of complex <b>51</b> showing the relative orientation of the M(III)-OH bonds, each of which are above the planes of the respective cyclohexyl groups;	166
<b>Figure 1.3-18b</b>	The chemical structure of <b>51</b> .	166
<b>Figure 1.3-19</b>	MALDI-TOF mass spectrum of the mono-metal-salen-macrocycles from the manganese complexation reaction with the mixture of salen-macrocycles <b>36-38</b> .	168
<b>Figure 2-1</b>	Calixarenes <b>1</b> and thiacalixarenes <b>2</b> .	184
<b>Figure 2-2</b>	The calix-like shape of thiacalixarenes <b>6</b> .	186
<b>Figure 2-3</b>	X-ray structure of monotriflate <b>42</b> .	201
<b>Figure 2-4</b>	X-ray structure stereoview of <b>30</b> : $\text{C}_6\text{H}_6$ .	205
<b>Figure 2-5</b>	X-ray structure stereoview of monotriflate <b>36</b> .	205
<b>Figure 2-6</b>	X-ray structure stereoview of 1,2-bistriflate <b>37</b> showing the orientation of the two molecules in the unit cell. The hydrogen atoms and the solvent molecule ( $\text{CHCl}_3$ ) have been removed for clarity.	206
<b>Figure 2-7</b>	X-ray structure stereoview of de- <i>tert</i> -butylated bis(phenoxathiin) <b>50</b> .	208

<b>Figure 2-8</b>	Thioporannulenes <b>51-56</b> and <i>tert</i> -butylcalix[4]naphthalene ( <b>57</b> ).	209
<b>Figure 2-9a</b>	MMM computer-generated hypothetical structures of supra- molecular complexes of C <sub>60</sub> with phenoxathiin <b>30</b> .	210
<b>Figure 2-9b</b>	MMM computer-generated hypothetical structures of supramolecular complexes of C <sub>60</sub> with tetra- <i>tert</i> -butylcalix[4]- naphthalene ( <b>57</b> ).	210
<b>Figure 2-10</b>	<sup>1</sup> H NMR titration curve of AgCO <sub>2</sub> CF <sub>3</sub> with <b>30</b> .	211
<b>Figure 2-11</b>	<sup>1</sup> H NMR titration curves for AgCO <sub>2</sub> CF <sub>3</sub> complexation with <b>50</b> .	212
<b>Figure 2-12a</b>	The <sup>1</sup> H NMR spectrum of the solution of Ag <sup>+</sup> and <b>30</b> in 1:9 CD <sub>3</sub> CN:CDCl <sub>3</sub> .	213
<b>Figure 2-12b</b>	The <sup>1</sup> H NMR spectrum of the solution of <b>30</b> in 1:9 CD <sub>3</sub> CN:CDCl <sub>3</sub> .	213
<b>Figure 2-13a</b>	The <sup>1</sup> H NMR spectrum of the solution of Ag <sup>+</sup> and <b>50</b> in 1:9 CD <sub>3</sub> CN:CDCl <sub>3</sub> .	213
<b>Figure 2-13b</b>	The <sup>1</sup> H NMR spectrum of the solution of <b>50</b> in 1:9 CD <sub>3</sub> CN:CDCl <sub>3</sub> .	213
<b>Figure 2-14a</b>	The <sup>1</sup> H NMR spectrum of the solution of Hg <sup>2+</sup> and <b>30</b> in 1.5:9 D <sub>3</sub> COD:CDCl <sub>3</sub> .	215
<b>Figure 2-14b</b>	The <sup>1</sup> H NMR spectrum of the solution of <b>30</b> in 1.5:9 D <sub>3</sub> COD:CDCl <sub>3</sub> .	215
<b>Figure 2-15a</b>	The <sup>1</sup> H NMR spectrum of the solution of Hg <sup>2+</sup> and <b>50</b> in 1.5:9 D <sub>3</sub> COD:CDCl <sub>3</sub> .	215
<b>Figure 2-15b</b>	The <sup>1</sup> H NMR spectrum of the solution of <b>50</b> in 1.5:9 D <sub>3</sub> COD:CDCl <sub>3</sub> .	215
<b>Figure 2-16</b>	500 MHz <sup>1</sup> H NMR titration curve of Hg(ClO <sub>4</sub> ) <sub>2</sub> with <b>30</b> .	216
<b>Figure 2-17</b>	500 MHz <sup>1</sup> H NMR titration curve of Hg(ClO <sub>4</sub> ) <sub>2</sub> with <b>50</b> .	216

## List of Schemes

<b>Scheme 1.1-1</b>	Generalized Schiff base macrocyclization reaction.	3
<b>Scheme 1.1-2</b>	Formation and complexation reactions of <b>15</b> .	5
<b>Scheme 1.1-3</b>	Asymmetric aldol condensation catalyzed by Zn(II) complex of <b>18</b> .	6
<b>Scheme 1.1-4</b>	Asymmetric Henry reaction catalyzed by Cu(II) complex of <b>24</b> .	8
<b>Scheme 1.1-5</b>	Schiff base reaction of formation of ferrocene-based macrocycle <b>29</b> .	8
<b>Scheme 1.1-6</b>	General metal-catalyzed epoxidation.	16
<b>Scheme 1.1-7</b>	Epoxidation of 2,2-dimethylchromene by achiral Mn(III)-salen <b>69</b> in the presence of a chiral additive.	19
<b>Scheme 1.1-8</b>	Reversing the conformation of epoxide <b>70a</b> by using catalyst <b>72</b> to form the enantiomer <b>71b</b> .	20
<b>Scheme 1.1-9</b>	Chiral Mn(III)-salen catalyst encapsulated within zeolite Y ( <b>90</b> ) for enantioselective epoxidation.	33
<b>Scheme 1.1-10</b>	Achiral Mn(III)-salen catalyst encapsulated within zeolite <b>94</b> for regioselective epoxidation.	34
<b>Scheme 1.1-11</b>	Chiral substituted iron(III)-porphyrin catalyst <b>99</b> for enantioselective epoxidation.	35
<b>Scheme 1.1-12</b>	Metal-porphyrin complex <b>111</b> bearing a $\alpha$ -CD for chiral photocatalytic oxygenation of chiral $\alpha$ -pinene <b>112</b> .	41
<b>Scheme 1.2-1</b>	Synthetic strategy for rigid ring-expanded calixsalens <b>1</b> .	54

<b>Scheme 1.2-2</b>	The first example of Suzuki-Miyaura coupling.	57
<b>Scheme 1.2-3</b>	Efficient ambient temperature conditions for Suzuki-Miyaura coupling.	58
<b>Scheme 1.2-4</b>	Cesium fluoride-catalyzed Suzuki-Miyaura coupling.	59
<b>Scheme 1.2-5</b>	Retrosynthesis of bisaldehyde <b>22</b> .	61
<b>Scheme 1.2-6</b>	Synthetic route <b>A</b> (R = isopropyl).	63
<b>Scheme 1.2-7</b>	Attempted protection of aldehyde group in <b>36</b> .	64
<b>Scheme 1.2-8</b>	Synthetic route <b>B</b> .	66
<b>Scheme 1.2-9</b>	Synthetic route <b>C</b> to boronic acid <b>43</b> (R = <i>tert</i> -butyl).	67
<b>Scheme 1.2-10</b>	Suzuki-Miyaura coupling reactions of <b>43</b> (R = <i>tert</i> -butyl).	69
<b>Scheme 1.2-11</b>	Suzuki-Miyaura coupling mechanism.	71
<b>Scheme 1.2-12</b>	Preparation of 1,8-bis(3- <i>tert</i> -butyl-4-methoxyphenyl)anthracene ( <b>52</b> ).	75
<b>Scheme 1.2-13</b>	Demethylation reactions of compounds <b>46–48</b> and <b>52</b> .	77
<b>Scheme 1.2-14</b>	Formylation reactions of phenols <b>57–60</b> (R = CHO).	80
<b>Scheme 1.3-1</b>	General mechanism for the Schiff base condensation reaction.	115
<b>Scheme 1.3-2</b>	Templated Schiff base macrocyclization reactions.	117
<b>Scheme 1.3-3</b>	Dimer <b>12</b> , trimer <b>13</b> and tetramer <b>14</b> formed under non-templated Schiff base macrocyclization.	118
<b>Scheme 1.3-4</b>	Template-free macrocyclization reactions to produce conjugated Schiff base macrocycles <b>17a–m</b> .	119

<b>Scheme 1.3-5</b>	Template-free macrocyclization reactions to produce Schiff base macrocycles <b>19a-c</b> .	121
<b>Scheme1.3-6</b>	Schiff base macrocyclization reaction of racemic mixture of 3,3'-diformyl-2,2'-binaphthol ( <b>20</b> ) with ( <i>R,R</i> )-1,2-diamino-1,2-diphenylethane ( <b>21</b> ).	122
<b>Scheme1.3-7</b>	Schiff base macrocyclization under microwave irradiation conditions.	123
<b>Scheme1.3-8</b>	McAuliffe's Mn(III)-salen dimer <b>31</b> .	123
<b>Scheme 1.3-9</b>	Ba(ClO <sub>4</sub> ) <sub>2</sub> -templated Schiff base macrocyclization reactions.	125
<b>Scheme1.3-10</b>	The Schiff base macrocyclization reaction of bisaldehyde <b>35</b> .	127
<b>Scheme 1.3-11</b>	Schiff base macrocyclization reaction of bisaldehyde <b>40</b> .	132
<b>Scheme1.3-12</b>	Proposed polymerization and cyclization process in the Schiff base reaction of <b>40</b> .	141
<b>Scheme1.3-13</b>	Macrocyclization reaction of bisaldehyde <b>47</b> .	156
<b>Scheme1.3-14</b>	Mn(II) template-assisted construction of the macrocyclic complex <b>51</b> .	164
<b>Scheme1.3-15</b>	Complexation reactions of <b>36</b> , <b>41</b> and <b>48</b> with Mn <sup>3+</sup> , Ni <sup>2+</sup> and Cu <sup>2+</sup> .	167
<b>Scheme 2-1</b>	Synthesis of calix[ <i>n</i> ]arenes <b>1</b> .	184
<b>Scheme 2-2</b>	The Sone synthesis of thiacalixarene <b>6</b> .	185
<b>Scheme 2-3</b>	Different synthetic approaches for thiacalixarene <b>6</b> .	186
<b>Scheme 2-4</b>	Modification of thiacalix[4]arene <b>6</b> .	188
<b>Scheme 2-5</b>	Synthetic approach towards aminothiacalix[4]arene <b>16</b> .	189

<b>Scheme 2-6</b>	Preparation of mono-, and diaminothiacalix[4]arenes <b>19</b> and <b>22</b> .	190
<b>Scheme 2-7</b>	Preparation of mono-, di- and tetraiodothiocalixarene <b>23-25</b> .	191
<b>Scheme 2-8</b>	Preparation of thiothiacalixarene <b>28</b> and thiacalix[2]thianthrenes <b>29</b> .	192
<b>Scheme 2-9</b>	Preparation of thiacalix[2]phenoxathiin ( <b>30</b> ).	193
<b>Scheme 2-10</b>	Upper-rim substitution of thiacalixarene <b>31</b> by acetylene.	194
<b>Scheme 2-11</b>	Narrow-rim substitution of calixarene <b>33</b> by acetylenes.	195
<b>Scheme 2-12</b>	Products from the reactions of <b>35</b> under Sonogashira conditions.	196
<b>Scheme 2-13</b>	Methylation reactions of 1,3-bistriflate <b>35</b> .	198
<b>Scheme 2-14</b>	A proposed mechanism of the migration reaction of triflate in <b>35</b> to form <b>37</b> .	199
<b>Scheme 2-15</b>	A proposed mechanism for reaction of <b>35</b> to form <b>30</b> .	202
<b>Scheme 2-16</b>	Reactions of <b>35</b> in the presence of phenols.	204
<b>Scheme 2-17</b>	De- <i>tert</i> -butylation reaction of tetra- <i>tert</i> -butylphenoxathiin <b>30</b> .	207

## List of Tables

<b>Table 1.1-1</b>	Asymmetric epoxidation of <i>cis</i> - $\beta$ -methylstyrene with different Mn(III)-salen catalysts.	21
<b>Table 1.2-1</b>	Effect of mol% of catalyst on yields of Suzuki-Miyaura coupling.	70
<b>Table 1.2-2</b>	Exact molecular mass analysis of Suzuki-Miyaura products.	74
<b>Table 1.2-3</b>	Yields and $^1\text{H}$ -, $^{13}\text{C}$ NMR summary analysis of <b>53-56</b> .	78
<b>Table 1.2-4</b>	Exact molecular masses for compounds <b>53-56</b> .	79
<b>Table 1.2-5</b>	Formylation reaction yields in THF and acetonitrile.	79
<b>Table 1.2-6</b>	$^1\text{H}$ -, $^{13}\text{C}$ NMR summary analysis of <b>57-60</b> .	81
<b>Table 1.2-7</b>	$^1\text{H}$ - and $^{13}\text{C}$ NMR summary analysis of <b>53-60</b> .	82
<b>Table 1.2-8</b>	Exact molecular masses for compounds <b>57-60</b> .	82
<b>Table 1.3-1</b>	Effect of concentration on the yields of <b>41</b> .	153
<b>Table 1.3-2</b>	Complexation of <b>41</b> and <b>48</b> with $\text{Mn}^{3+}$ , $\text{Ni}^{2+}$ and $\text{Cu}^{2+}$ .	170
<b>Table 1.3-3</b>	Calculated (MMFF94) <sup>30</sup> lowest-energy conformations of ligands <b>36</b> , <b>41</b> and <b>48</b> and complexes <b>54a1-3</b> and <b>54b1-3</b> (Scheme 1.3-15).	171
<b>Table 2-1</b>	Different Sonogashira conditions used with 1,3-bis(triflate) <b>35</b> .	197
<b>Table 2-2</b>	Cu-Pd conditions for the rearrangement reactions of <b>35</b> in toluene.	200

## Glossary of Abbreviations

APCI	atmospheric pressure chemical ionization
BPO	benzoyl peroxide
<i>t</i> -Bu or <i>t</i> -Bu	<i>tertiary</i> -butyl
<i>n</i> -BuLi	butyl lithium
<sup>13</sup> C NMR	carbon nuclear magnetic resonance
DACH	<i>trans</i> -1,2-diaminocyclohexane
d	day
DBU	1,5-diazabicyclo[5.4.0]undec-5-ene
DMA	<i>N,N</i> -dimethylacetamide
DME	1,2-dimethoxyethane
DMF	<i>N,N</i> -dimethylformamide
<i>ee</i>	enantiomeric excess
eq.	equivalent
Et	ethyl
h	hour
<sup>1</sup> H NMR	proton nuclear magnetic resonance spectroscopy
<i>J</i>	coupling constant (Hz)
<i>K<sub>assoc</sub></i>	association constant
LAH	Lithium aluminum hydride
LDA	Lithium diisopropyl amide

LDA	Lithium diisopropyl amide
Lit.	literature
MALDI-TOF	matrix-assisted laser desportion ionization-time of flight
<i>m</i> -CPBA	<i>meta</i> -chloroperbenzoic acid
Me	methyl
min	minute(s)
MMM	molecular mechanics modeling
MS	mass spectrometry
NBS	<i>N</i> -bromosuccinimide
NLO	mon-linear optics
<i>n</i> -Pr	<i>n</i> -propyl
<i>p</i>	<i>para</i>
Ph	phenyl
PLC	preparative thin layer chromatography
ppm	part per milion
Pr	propyl
<i>i</i> -Pr or <sup>t</sup> Pr	isopropyl
rt	room temperature
SHG	second harmonic generation
TBAF	Tetra- <i>n</i> -butylammonium flouride
THF	tetrahydrofuran
TLC	thin-layer chromatography

TMS

trimethylsilyl

TMACl

tetramethylammonium chloride

vs

*versus*

U.V.

Ultraviolet

**Dedication**

**To my Father Yousf Habashneh**

**To my Mom Aisha Houraini**

**And to my family**

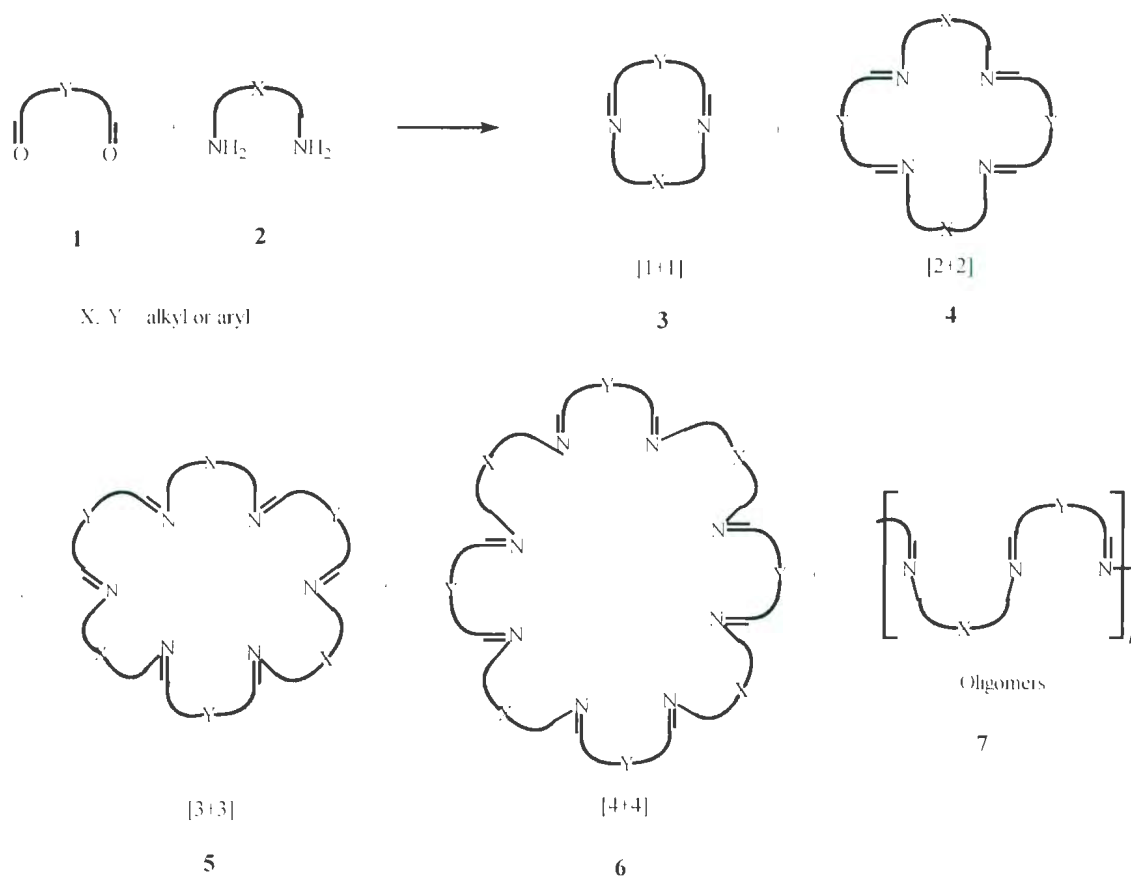
# Part 1

## Chapter 1.1 Introduction

### 1.1.1 Schiff base macrocycles.

Interest in developing efficient Schiff base macrocyclization methods has received much attention in the diverse areas of macrocyclic, metal-catalytic and supramolecular chemistry.<sup>1</sup> Schiff base macrocyclic heteropolydentate ligands are versatile since they are capable of forming mono-, di-, and polynuclear complexes with both transition and non-transition metals and have long been postulated in attempts to explain the function of many biologically important enzymes. Considerable effort has also been devoted in order to develop the potential of chiral Schiff base macrocycles as artificial molecular receptors for cationic, anionic and/or neutral guests, and particularly, for chiral recognition and chiral catalytic applications, using Schiff base-containing salen complexes.

As a result of the potential applications indicated above, there has been a great need during the past two decades for developing convenient methodologies to produce metal-free Schiff base macrocycles starting from various dicarbonyl compounds such as **1** and diamines such as **2** (Scheme 1.1-1). Simple, one-pot Schiff base macrocyclization reactions can produce a mixture of cyclic and macrocyclic products such as the [1+1], [2+2], [3+3] and [4+4] coupled products represented as **3-6**, respectively, as well as linear oligomers such as **7** (Scheme 1.1-1). The undesirable formation of linear oligomers presents the most challenging problem to overcome for this type of simple cyclization chemistry. Some examples of macrocyclic Schiff bases which have been reported to date will be reviewed in the following paragraphs.



**Scheme 1.1-1:** Generalized Schiff base macrocyclization reaction.

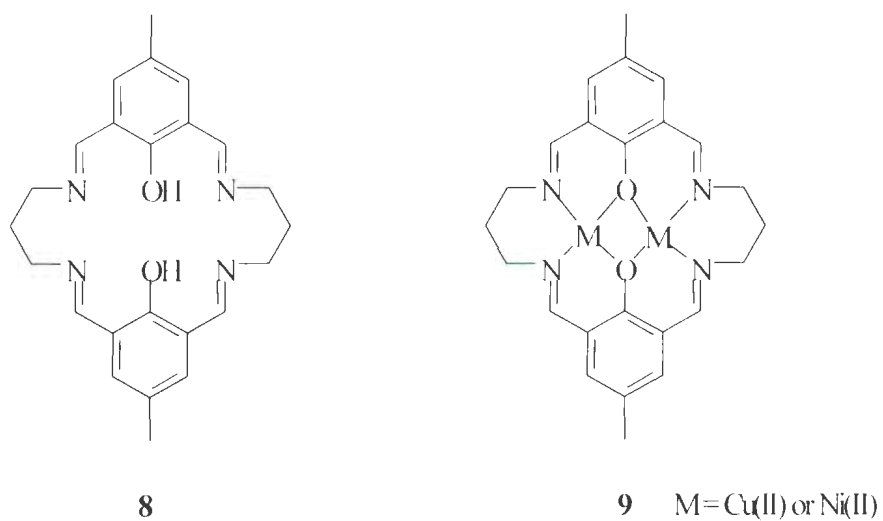


**Figure 1.1-1:** Achiral Robson-type macrocycles.

Robson-type macrocycles such as **8** are well-known examples of Schiff base macrocyclic ligands (Figure 1.1-1). They were first reported by Robson in 1970 using

templated cyclization reactions of 2,6-diformyl-4-methylphenol with 1,3-diaminopropane in the presence of several different first row transition metal ions.<sup>2a</sup> Later on, these same Robson-type macrocycles were prepared as free-metal ligands by reacting the same starting materials in methanol, under highly-diluted and acid-catalyzed conditions.<sup>2b</sup> Robson-type macrocycles are versatile and useful ligands because they can coordinate two metal ions in close proximity to each other, and can form both homo- and hetero-dinuclear complexes.<sup>3</sup> Magnetic properties for different Robson-type metal complexes have been extensively studied. In particular, the di-Ni(II) and di-Cu(II) complexes **9** showed antiferromagnetic properties that depend linearly upon the M-O-M bridge angle as well as upon the intramolecular M---M distance.<sup>4</sup>

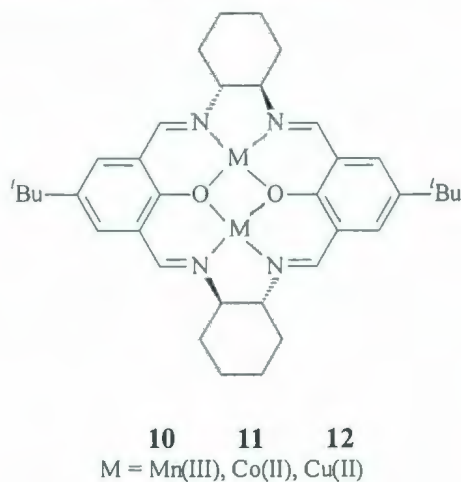
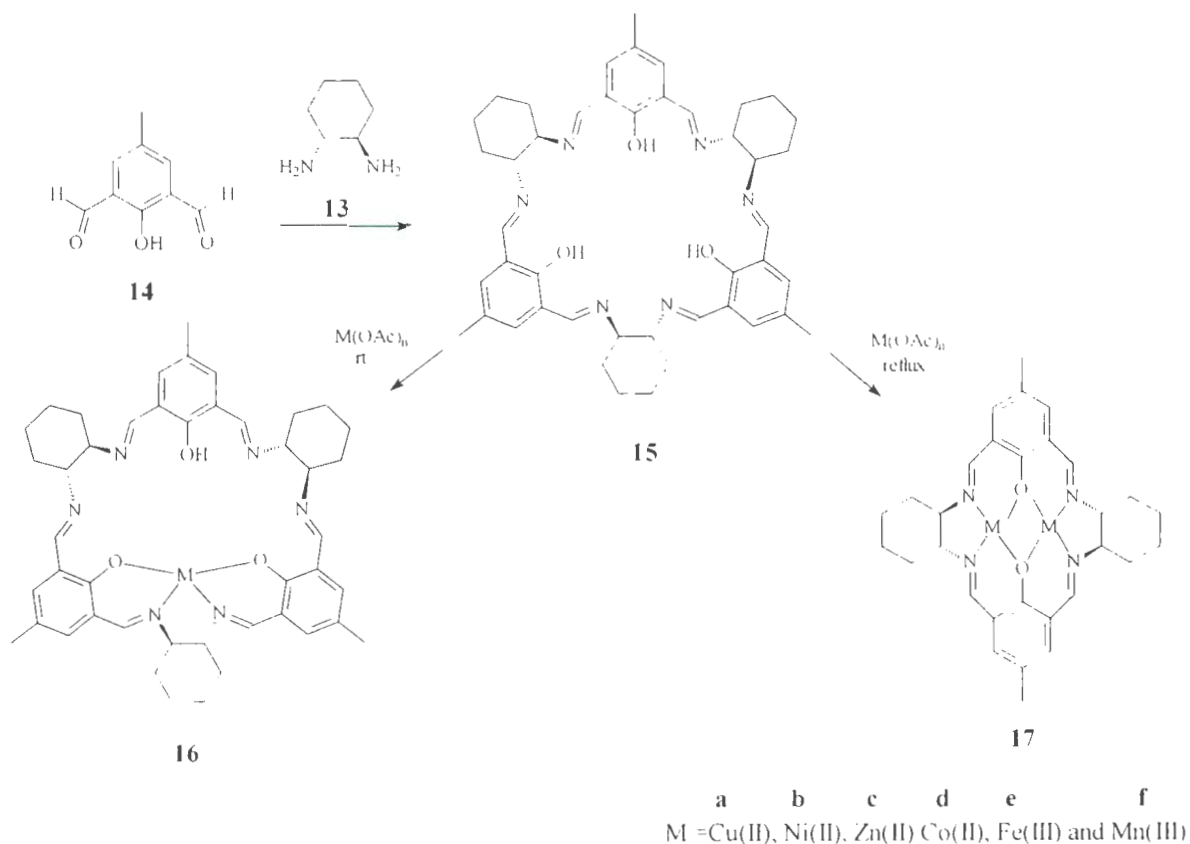


**Figure 1.1-2:** Chiral Robson-type macrocycles.

Chiral Robson-type macrocycles have been effectively used in different asymmetric reactions. The manganese(III) complex **10** (Figure 1.1-2) catalyzed the epoxidation styrene in 71% *ee*, and the Co(II) catalyst **11** induced good enantioselectivity in the reduction of aromatic ketones.<sup>5</sup> For example, the borohydride reduction of

acetophenone in the presence of **11** afforded the corresponding alcohol in 48% *ee*. Furthermore, oxidative coupling of 2-naphthol with the chiral dicopper(II) macrocycle complex **12** gave chiral binaphthol in 86% *ee* and 84% yield.<sup>6</sup>

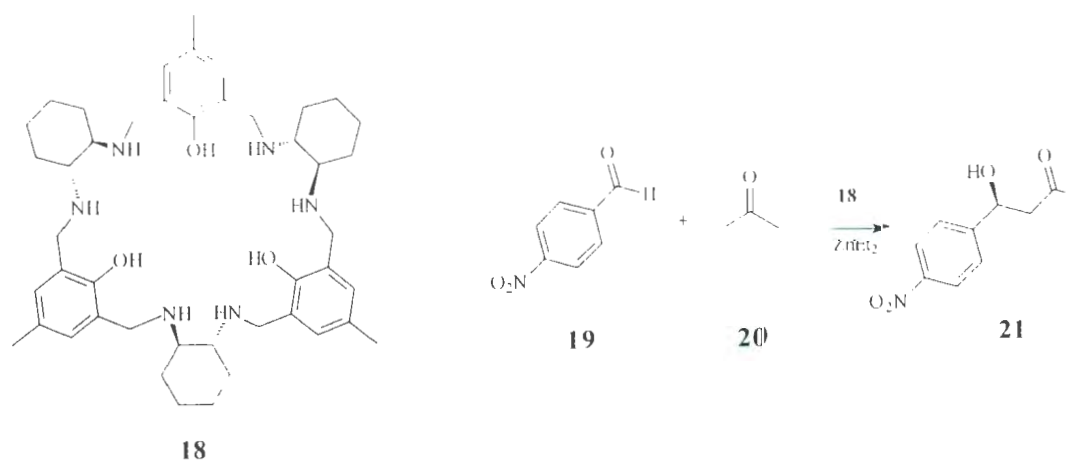


**Scheme 1.1-2:** Formation and complexation reactions of **15**.

The metal-free Schiff base macrocycle **15** has been prepared from the reaction of (1*R*,2*R*)-diaminocyclohexane (**13**) with 2,6-diformyl-4-methylphenol (**14**) under reflux in MeOH (Scheme 1.1-2).<sup>7a</sup> Treating **15** at room temperature with up to 3 molar equivalents of metal ions such as Zn<sup>2+</sup>, Cu<sup>2+</sup>, Ni<sup>2+</sup>, Co<sup>2+</sup>, Fe<sup>2+</sup> or Mn<sup>2+</sup> all failed to give the desired trinuclear complexes, but formed the mono-metal ion-containing complexes **16**, instead. Ligand **15** disproportionated under the reflux complexation reaction with

same metal ions forming the di-metal ionic-salen-dimer complexes **17**. The  $\pi$ -electron delocalization and the crystallization of the Schiff base compounds **15** and **17** in a non-centrosymmetric space group prompted investigations of their non-linear optical properties. The ligand **15** itself and the bimetallic complexes **17c-f** containing Zn(II), Co(II), Fe(III) and Mn(III) ions, respectively, showed modest second harmonic generation (SHG) properties. The bi-metal ionic complexes of Cu(II) **17a** or Ni(II) **17b**, however, did not show any SHG properties.

Reduction of macrocycle **15** gave the hexaaza triphenolic macrocycle **18**, which has striking structural features (Scheme 1.1-3). It is a  $C_3$ -symmetric molecule in which the macrocyclic cavity is defined by 27 atoms and is stabilized by intramolecular (O-H...N; N-H...O and N-H...N) H-bonding.<sup>7b</sup> This chiral cavity makes this class of ligand a very good candidate to utilize for “host-guest” asymmetric catalysis.



**Scheme 1.1-3:** Asymmetric aldol condensation catalyzed by Zn(II) complex of **18**.

The corresponding trinuclear Zn(II) complex of **18** showed high efficiency in catalyzing asymmetric aldol condensations. For example, the  $\beta$ -hydroxyketone **21** was obtained in 95% *ee* from the aldol condensation of acetone (**20**) with *p*-nitrobenzaldehyde (**19**) in the presence of 1 and 3 molar equivalents of **18** and ZnEt<sub>2</sub> respectively.<sup>8</sup> However, the chiral polyaza macrocycle **22** (Figure 1.1-3), which was prepared by reducing the Schiff base macrocycle precursor, was less efficient in its asymmetric catalysis of the aldol condensation of *p*-nitrobenzaldehyde (**19**) and **20**.<sup>9</sup> This aldol condensation in the presence of ZnEt<sub>2</sub> and **22** in DMSO afforded the  $\beta$ -hydroxyketone **21** in only 56% *ee* (Scheme 1.1-3). When compared with chiral **22**, the use of racemic **23** (Figure 1.1-3) formed the same  $\beta$ -hydroxyketone **21** in lower % *ee*. This example illustrates the impact of the chiral environment created by the chiral centers in **22** on the reactants.

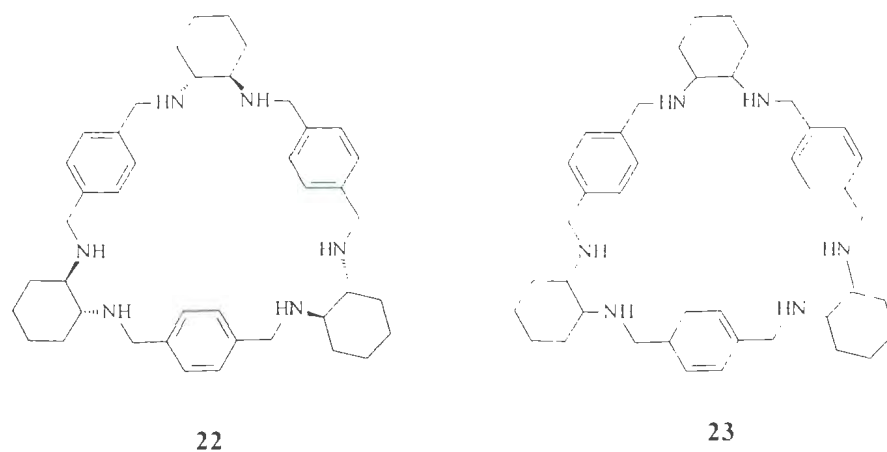
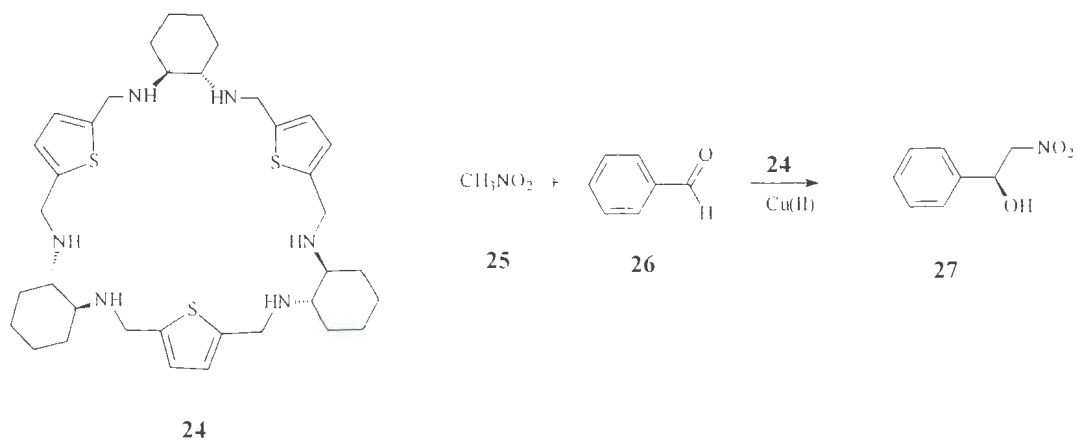
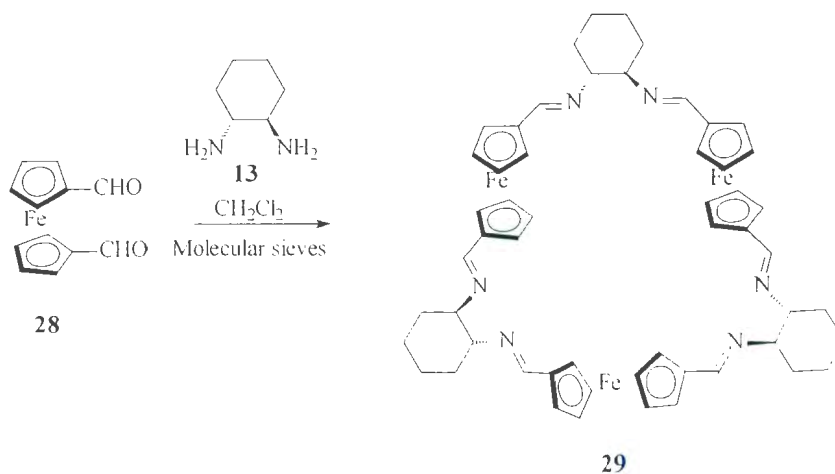


**Figure 1.1-3:** Polyaza macrocycles **22** and **23**.

The thiophene-based polyaza macrocycle **24** is similar in some respects to **22** and **23**<sup>10</sup> and has been evaluated as a catalyst in asymmetric reactions. The alcohol **27** was obtained in 75% *ee* using the Cu(II) complex of **24** as a catalyst in the Henry reaction of nitromethane (**25**) with benzaldehyde (**26**). (Scheme 1.1-4).



**Scheme 1.1-4:** Asymmetric Henry reaction catalyzed by Cu(II) complex of **24**.



**Scheme 1.1-5:** Schiff base reaction of formation of ferrocene-based macrocycle **29**.

The [3+3]-type Schiff base **29** was formed by the reaction of ferrocene dialdehyde (**28**) and (1*R*,2*R*)-diaminocyclohexane (**13**) under non-templated Schiff base

condensation conditions (Scheme 1.1-5).<sup>11</sup> A chiral concave cavity with a rim diameter of 3.6 Å and a depth of 4.7 Å exists in this macrocycle around the *pseudo-C*<sub>3</sub> axis. This chiral cavity allowed **29** to be an excellent receptor for the enantioselective encapsulation of 1,1'-bi-2-naphthol and was effective for its chiral resolution.

In 1994, Brunner reported the synthesis of the chiral bisbinaphthyl macrocycle **30** (Figure 1.1-4) which is an example of a large chiral salen-dimer.<sup>12</sup> Reduction of the imine functional groups in this class of compounds afforded the more stable chiral amine macrocycles such as **31-33** each of which also has a chiral cavity. Compounds **31-33** therefore, have the potential capacity for chiral recognition. Furthermore, because compounds **31-33** have naphthalene moieties, they can also function as fluorescence sensors. Thus, the chiral amine macrocycles **31-33** showed high efficiency in enantioselective fluorescent recognition of  $\alpha$ -hydroxycarboxylic acids.<sup>13,14</sup>

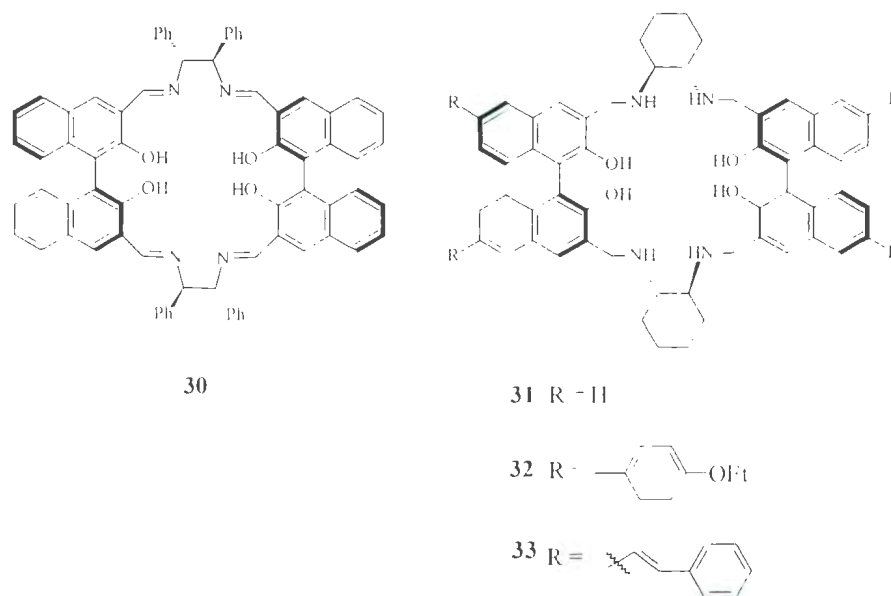


**Figure 1.1-4:** Naphthalene-based tetraimine and tetraamine macrocycles **30-33**.

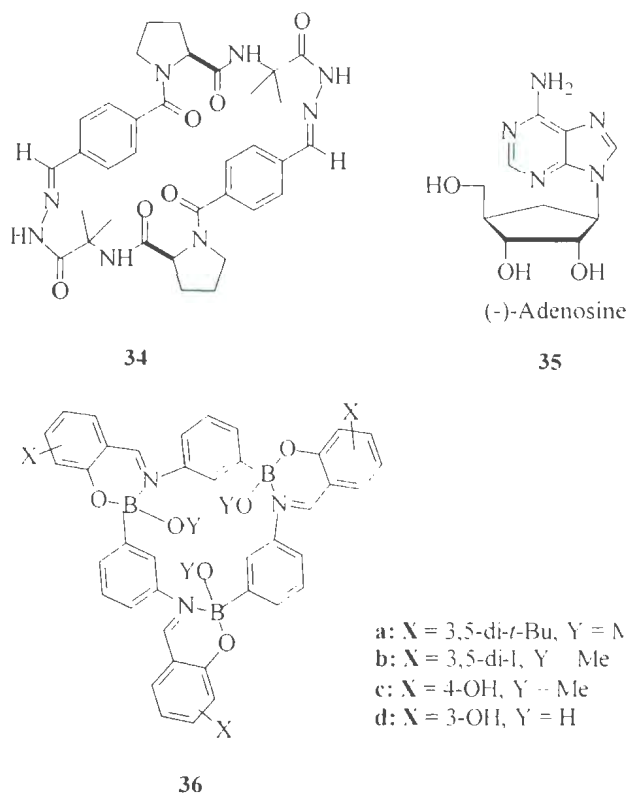


**Figure 1.1-5:** Peptide- and calixarene-like Schiff base macrocycle **34** and **36**.

The “peptide-like” Schiff base macrocycle **34** (Figure 1.1-5) was highly effective as an enantioselective receptor in the recognition of nucleotides such as (-)-adenosine **35**.<sup>15</sup> “Calix-like” oxazaboron Schiff base macrocycles such as **36** (Figure 1.1-5) possess cone-like conformations with  $C_3$  symmetry and deeper cavities than typical calixarenes.<sup>16</sup> Good host-guest complementary relationships were therefore expected with primary alkyl amines such as *e.g.* methyl-, ethyl-, *n*-propyl- and benzylamine, or with their ammonium salts. Host-guest titrations monitored by UV-spectrometry revealed that compounds **36a-d** were indeed modest receptors for alkyl amines and their ammonium salts. Among the *n*-alkyl amines tested, *n*-propylamine gave the highest association constants: with **36c** in

$\text{CHCl}_3$   $K_{\text{assoc}} = 2,828 \pm 329$ . The association constant for **36c** with benzylamine was higher ( $K_{\text{assoc}} = 3,520 \pm 390$ ) which was attributed to  $\pi$ - $\pi$  interactions between the guest and the salicylidene moieties and not to any host-guest size complementary relationship as was postulated for *n*-propylamine. This investigation also showed that receptor **36b** had a very high association constant ( $K_{\text{assoc}} = 5.70 \times 10^9 \pm 3.13 \times 10^8$ ) with benzylammonium chloride in methanol, which was attributed to the formation of additional N-H... $\pi$  interactions.

The *biscalix*[4]arene Schiff bases **37a-e** (Figure 1.1-6) are poor hosts for alkyl ammonium salts.<sup>17</sup> The host-guest properties of these compounds for different bipyridinium salts **38a-d** were investigated using <sup>1</sup>H NMR titration experiments, which suggested that **37a** is the best receptor. Among these compounds, bipyridinium **38d** showed the highest binding constant values ( $K_{\text{assoc}} = 727 \text{ M}^{-1}$ )

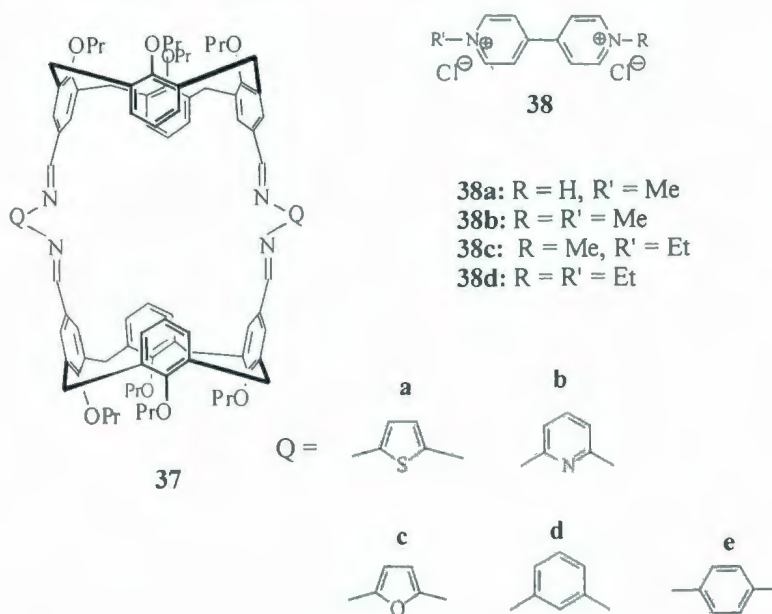


**Figure 1.1-6:** Biscalix[4]arene Schiff base macrocycles **37a-e**.

*Bis*(tripyrrolyl) cryptand **39** was synthesized under [2+3] Schiff base condensation conditions.<sup>18</sup> The compound was designed to encapsulate a guest molecule with the pyrrole nitrogen atoms attracting the guest molecule by hydrogen bonding interactions. Macrocyclic **39** was found to strongly bind 1,2-diaminoethane and 1,2-ethanediol in CHCl<sub>3</sub> solution. The porphyrin macrocycle **40** can include polar molecules, such as ethanol, trifluoroethanol or phenol, inside its cavity *via* hydrogen binding and  $\pi$ - $\pi$  stacking.<sup>19</sup> Using <sup>1</sup>H NMR titration experiments, catechol was shown to bind to receptor **40** with an association constant of around 10<sup>4</sup> M<sup>-1</sup>.

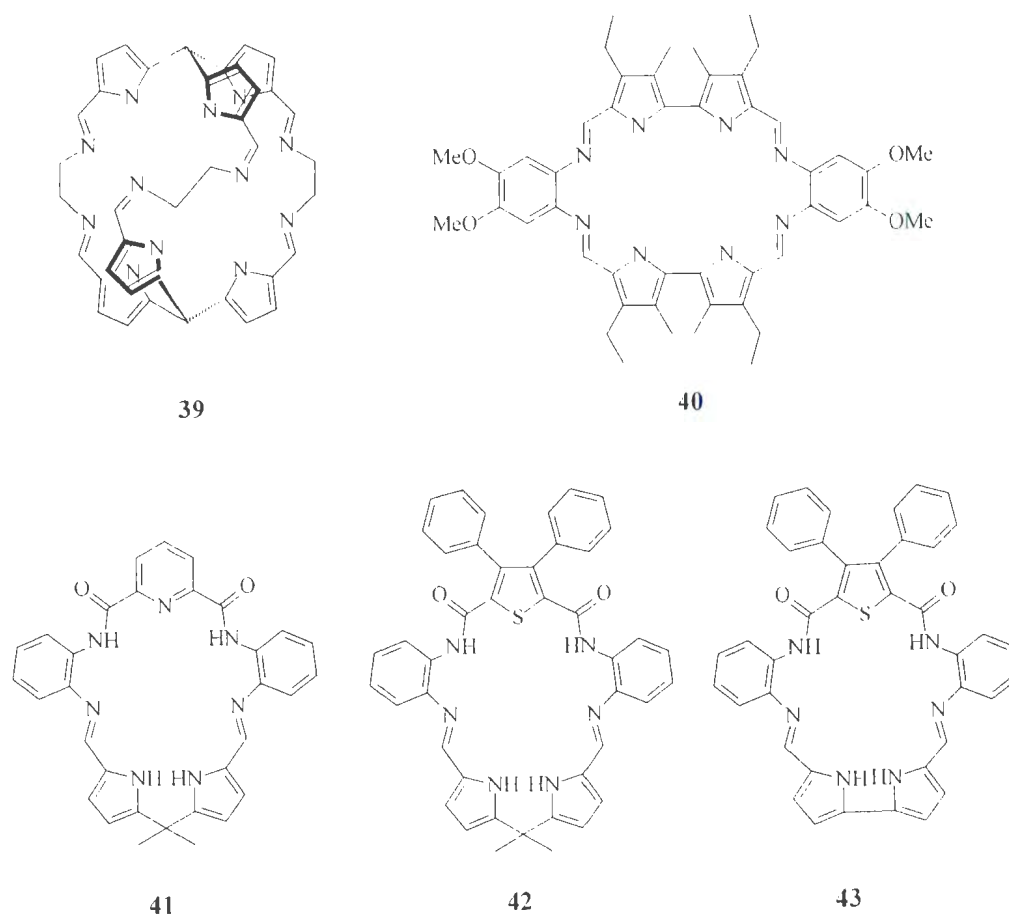
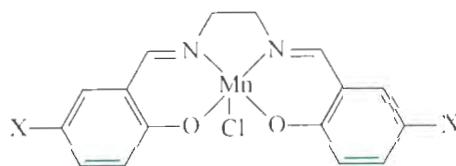


**Figure 1.1-7: Pyrrole-containing macrocycles 39-43.**

Pyrrole-containing macrocycles **41-43** (Figure 1.1-7) showed high binding affinities for anionic guests such as  $\text{Cl}^-$ ,  $\text{Br}^-$ ,  $\text{CH}_3\text{COO}^-$ ,  $\text{HSO}_4^-$  and  $\text{H}_2\text{PO}_4^-$ .<sup>20,21</sup> The 2,6-diamidopyridine-based macrocycle **41** had higher binding constant than **42** and **43**.<sup>21</sup>

### 1.1.2 Mn(III)-salen asymmetric epoxidation catalysis

Enantiopure epoxides are very important because they are useful intermediates in asymmetric organic synthesis and are chiral building blocks for many biologically-active compounds and natural products. The development of methodologies to obtain chiral epoxides with high enantioselectivity has been the focus of many research groups. In 1980, Sharpless developed a titanium-based catalyst for asymmetric epoxidation of allylic alcohols, usually with greater than 90% *ee*, but this methodology has not been demonstrated as suitable for epoxidation of unfunctionalized olefins.<sup>22</sup> Chiral porphyrin-transition metal complexes displayed moderate- to low enantioselectivities and even lower chemical yields.<sup>23</sup>



**44**

X = Cl,  $\text{NO}_2$  and Me

**Figure 1.1-8:** Kochi's achiral Mn(III)-salen.

In the 1980s, Kochi<sup>24</sup> and Burrows<sup>25</sup> reported the non-stereoselective epoxidation of alkenes, using achiral manganese salen complexes such as **44** (Figure 1.1-8) in the presence of iodosylmesitylene as the oxidant. A breakthrough in the field of asymmetric

epoxidation of unfunctionalized alkenes was achieved by Jacobsen<sup>26</sup> and Katsuki<sup>27</sup> in 1990. Jacobsen-type catalysts such as **45-47** (Figure 1.1-9) contain salen units with two chiral centers in the diamine moieties and two bulky groups at the 3 and 3' positions. Katsuki-type complexes such as **48** and **49** (Figure 1.1-9) contain four chiral centers: two at the diamine moiety and another two chiral centers at the 8 and 8' positions. Since then, many chiral Mn(III)-salen catalysts *e.g.* **50-61** (Figure 1.1-10), have been prepared in order to improve the enantioselectivity of epoxidation of unfunctionalized alkenes.<sup>28</sup>

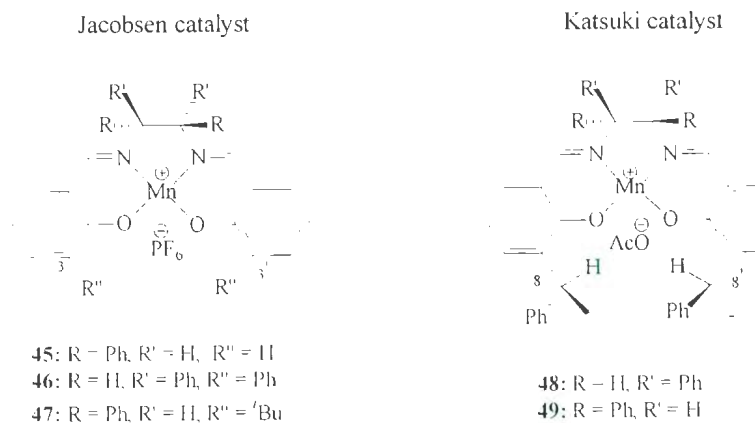


**Figure 1.1-9:** First-generation Jacobsen and Katsuki catalysts.

### 1.1.2.1 The Jacobsen-Katsuki methodology

The epoxidation of unfunctionalized alkenes by Mn(III)-salen based catalysts requires initial oxidation of the metal by a terminal oxidant **63** such as iodobenzene (PhIO),<sup>24,26,27</sup> NaOCl<sup>29</sup> or *m*-chloroperoxybenzoic acid (*m*-CPBA)<sup>30</sup> (Scheme 1.1-6). This oxidation step forms oxo-Mn(IV) intermediate **64**, which is the active species responsible for delivering the oxygen atom to the alkene.<sup>31</sup> Subsequently, the alkene

captures the oxygen atom from the metal oxide to form the radical oxide intermediate **66**<sup>32-34</sup> which collapses to form the desired epoxide **67**.

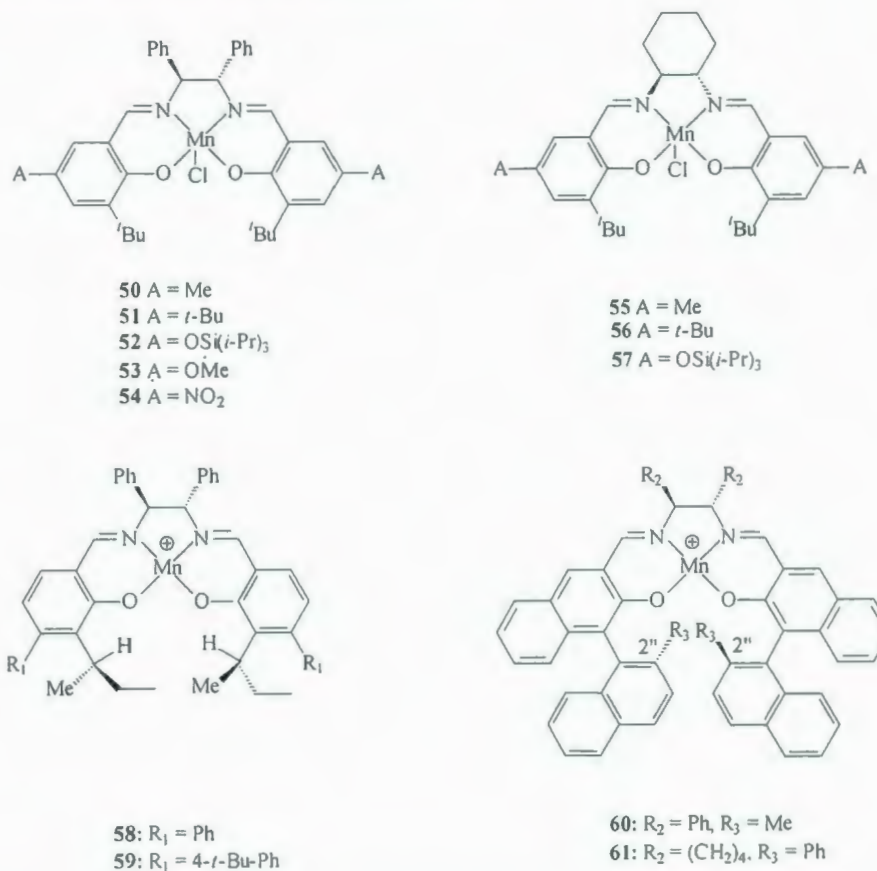
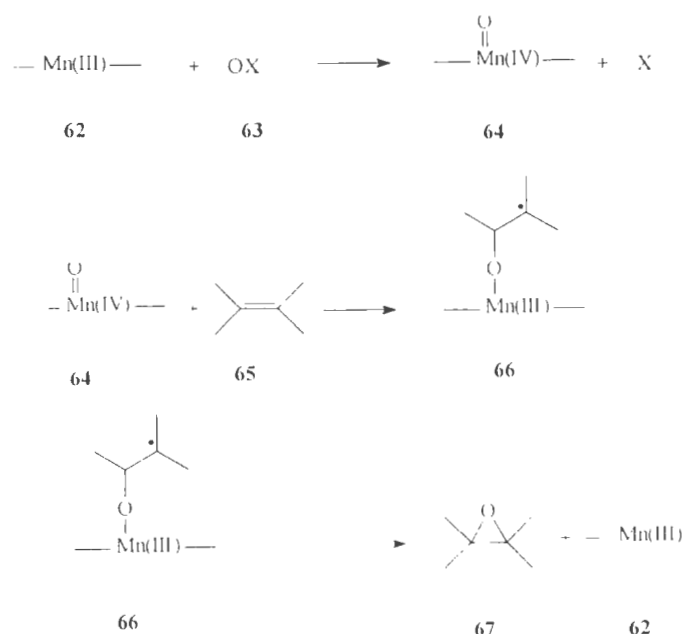


**Figure 1.1-10:** Various examples of Jacobsen- and Katsuki-type Mn(III)-salen catalysts.

### 1.1.2.2 Steric effects of the salen ligand on the enantioselectivity of epoxidation with Jacobsen-Katsuki catalysts

The enantioselectivity seen with the Jacobsen-Katsuki catalysts for epoxidation is thought to result mainly from the steric effects of the substituents on the salen skeleton. Furthermore, the substrate functionalities on the salen unit also orient the approach of the alkene to the oxo-Mn(IV) active species (Scheme 1.1-6). These considerations will be elaborated upon in the following sections.



**Scheme 1.1-6:** General metal-catalyzed epoxidation.

The high enantioselectivities obtained with these catalysts result from the presence of the asymmetric centers in the ethylenediamine units and the nature of the two bulky substituents at the 3 and 3' positions of the salen ligand (Figure 1.1-11). The steric effects of the bulky groups in the 3 and 3' positions direct the alkenes away from approaches **e**, **d** and **d'** and toward the chiral center side of the ethylenediamine-Mn(IV) moiety (approaches **a**, **b** and **b'**).

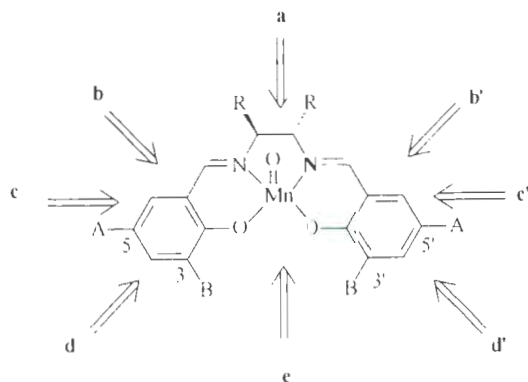


**Figure 1.1-11:** Different approaches for an alkene to attack the oxo-Mn salen species.

Jacobsen ascribed the enantioselectivity found with his catalysts to a “side-on” perpendicular approach of the alkene to the metal-oxo bond (Figure 1.1-12). The incoming alkene follows a pathway in which it faces the least amount of steric interactions with the bulky substituents on the phenyl rings and also with the substituents on the chiral ethylenediamine moieties in **47** and **56**. Jacobsen rationalized that path **c** with **47** and path **a** with **56** in Figure 1.1-11 are the most favorable pathways to produce epoxides in high enantioselectivities from the corresponding unsymmetrical *cis*-disubstituted alkenes.<sup>35</sup>

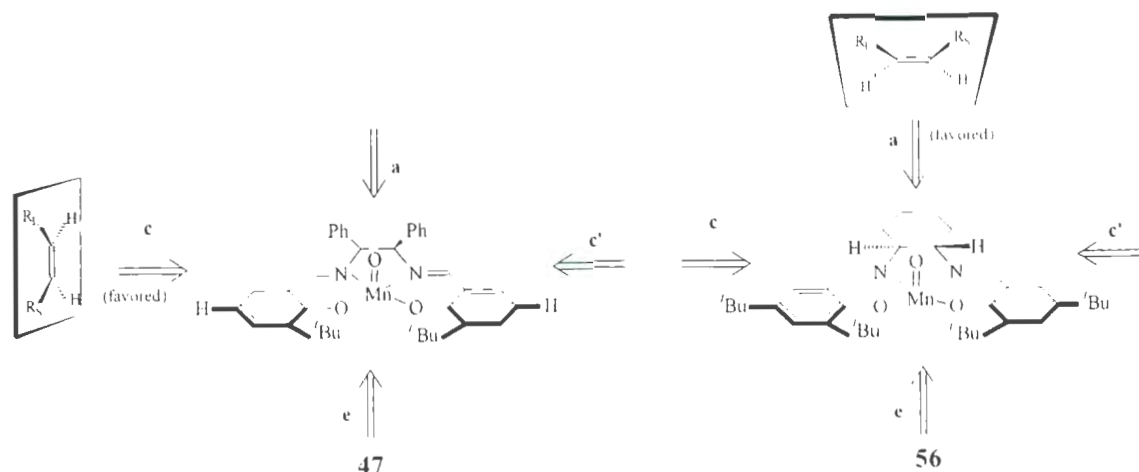


**Figure 1.1-12:** Possible “side-on” approaches to an oxo-Mn-salen intermediate.<sup>35</sup>

In contrast, Katsuki proposed approaches **b** and **b'** (Figure 1.1-11) as the orientation which alkenes follow to capture the oxygen atom from the oxo-Mn species in the catalyst.<sup>36</sup> This argument was based on the idea that the ligand of the oxo-Mn-salen is non-planar (Figure 1.1-13) as confirmed by an X-ray crystallographic structure.<sup>37</sup> Katsuki suggested that the five-membered ring in the oxo-Mn-salen intermediate, which is formed from the chelating ethylenediamine with manganese ion, adopts a half-chair

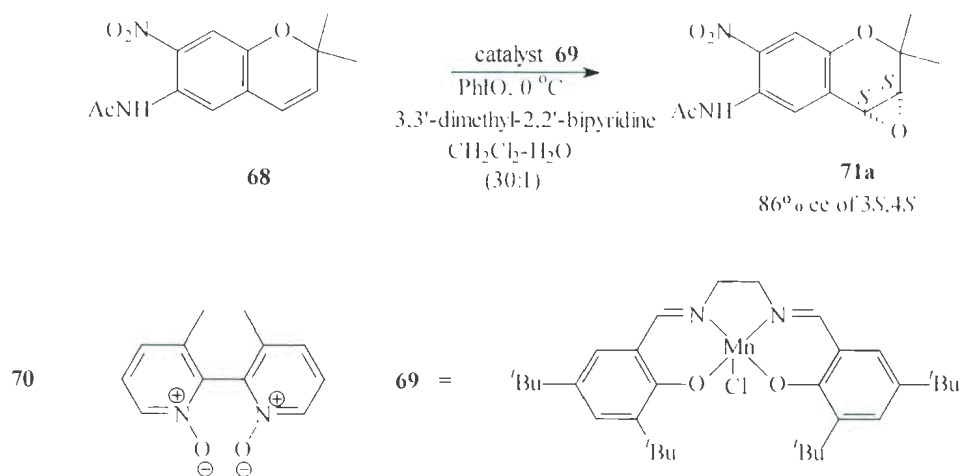
conformation. The two substituents at the ethylenediamine could be organized to be in two axial or two equatorial positions. Therefore, the oxo-Mn-salen intermediate should form two conformers,  $X_{\text{diax}}$  and  $X_{\text{dieq}}$ , in equilibrium (Figure 1.1-13). The equilibrium shifts toward the most stable conformer  $X_{\text{dieq}}$  since the steric interactions between the “R” groups and “L” require the two R substituents on the ethylenediamine to be in *pseudo*-equatorial positions (Figure 1.1-13).



**Figure 1.1-13:** Proposed conformers for oxo-Mn-salen.

Katsuki rationalized that the high enantioselectivity observed in the epoxidation of alkenes with Mn(III)-salen catalysts is attributed to the steric interactions between the alkene skeleton with  $X_{\text{dieq}}$ , and following controlled pathways, **b** and **b'** (Figure 1.1-11), because all the unfavored-pathways (**c**, **c'**, **d**, **d'** and **e**) are blocked by the **A** and **B** substituents. The reaction of an alkene with each conformer  $X_{\text{diax}}$  or  $X_{\text{dieq}}$  can give either the *S*- or *R*-epoxide. The chirality of  $X_{\text{dieq}}$  dictates the enantioselectivity of the resulting epoxide formation. In contrast, shifting the equilibrium towards another conformer  $X_{\text{diax}}$ , should favour formation of the other enantiomer. Thus, using an achiral salen catalyst for epoxidation leads to a racemic mixture since the catalyst is in a 1:1 ratio equilibrium between these two conformers. Katsuki suggested that a shift of this equilibrium toward

one of the two conformers affords one of the epoxide enantiomers in larger yield. Alternatively, the other epoxide enantiomer is produced in smaller yield because the amount of the conformer complex that generates that particular enantiomer is small.



**Scheme 1.1-7:** Epoxidation of 2,2-dimethylchromene by achiral Mn(III)-salen **69** in the presence of a chiral additive.

Katsuki supported this model with experimental results. Catalytic epoxidation of the 2,2-dimethylchromene **68**, using achiral salen **69** in the presence of a chiral axial donor ligand, such as 3,3'-dimethyl-2,2'-bipyridine-*N,N*-dioxide (**70**), afforded epoxide **71a** with high enantioselectivity (86% *ee*) (Scheme 1.1-7).<sup>38-40</sup> A racemic mixture of epoxides is normally produced using the achiral Mn(III)-salen complex alone, since the two conformers  $\mathbf{X}_{\text{diax}}$  and  $\mathbf{X}_{\text{dieq}}$  ( $R = \text{H}$ ) exist in a 1:1 ratio. However, axial coordination of a chiral donor to the metal center of the catalyst leads to a diastereomeric mixture. As a result, the equilibrium shifts towards the conformer which reacts with a greater amount of the alkene to afford the respective epoxide enantiomer in high % *ee*.

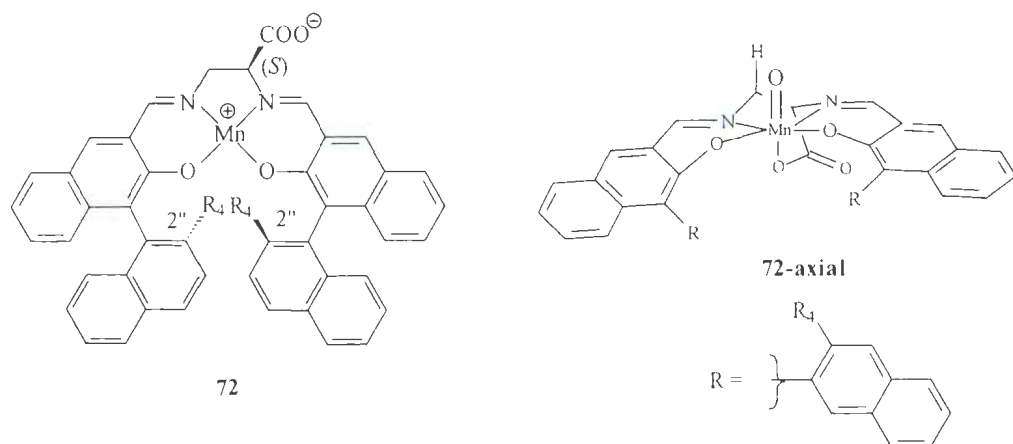
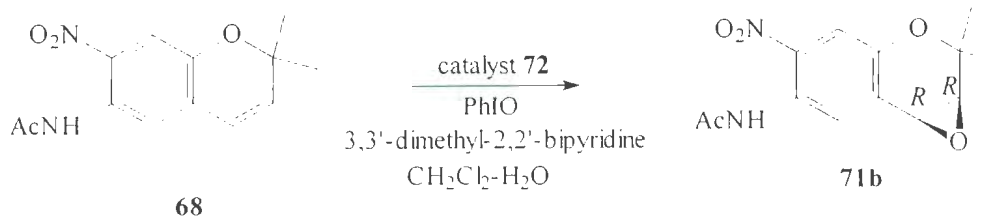


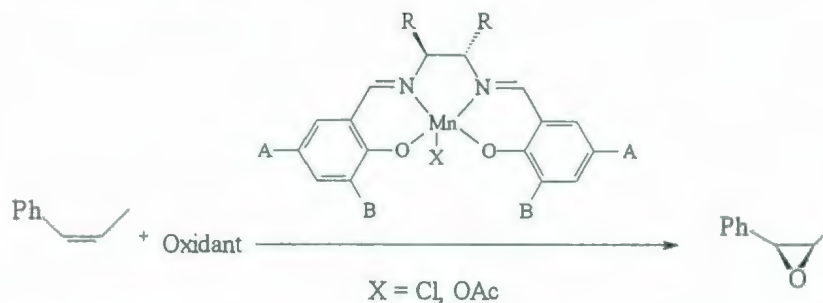
**Figure 1.1-14:** The axial conformer of the oxo-Mn species of the catalyst **72** bearing a carboxylic acid group.



**Scheme 1.1-8:** Reversing the conformation of epoxide **70a** by using catalyst **72** to form the enantiomer **71b**.

Further evidence derives from the reversal of the conformation of the chiral Mn(III)-salen complex **72** bearing a carboxylate group. Axial coordination shifts the equilibrium toward the diaxial conformer **72<sub>axial</sub>** (Figure 1.1-14) resulting in a reversal of the configuration of the resulting epoxide **71b** from 2,2-dimethylchromene (Scheme 1.1-8).<sup>41</sup>

**Table 1.1-1: Asymmetric epoxidation of *cis*- $\beta$ -methylstyrene with different Mn(III)-salen catalysts.**



Entry	R	A	B	oxidant	ee%	Ref.
1	Ph, Ph	H	H	NaOCl	<10	26
2	Ph, Ph	H, Me	<i>t</i> -Bu	NaOCl	84	26
3	Ph, Ph	H	Si( <i>t</i> -Bu)Me <sub>2</sub>	NaOCl	53	33
4	(CH <sub>2</sub> ) <sub>4</sub>	Me	<i>t</i> -Bu	NaOCl	80	42
5	(CH <sub>2</sub> ) <sub>4</sub>	<i>t</i> -Bu	<i>t</i> -Bu	NaOCl	92	42
6	(CH <sub>2</sub> ) <sub>4</sub>	Si( <i>t</i> -Bu)Me <sub>2</sub>	<i>t</i> -Bu	NaOCl	89	43

In considering the steric effects of the substituent groups at the 3 and 3' positions ("B" groups, Figure 1.1-11), it is logical to assume that the more bulky they are, the more they could improve the enantioselectivities shown by these Mn(III)-salen catalysts. Table 1.1-1 shows the results obtained for epoxidation of *cis*- $\beta$ -methylstyrene using various catalysts bearing different B groups. For example, when B = H the corresponding epoxide was obtained with lower than 10% *ee*, but when it is more sterically-hindering, such as when B = *tert*-butyl, the product was obtained with 84% *ee*.

In the Jacobsen-type catalysts, the **B** groups at the 3 and 3' positions are achiral aliphatic groups. However, with the Katsuki-type catalysts they are chiral 2''-alkylphenyl or 2''-arylnaphthyl groups. Catalysts **73** and **74**<sup>44,45</sup> showed improved enantioselectivity. For example, **73** afforded indene oxide from indene with 98% *ee* at 0 °C using commercially-available bleach as the oxidant.<sup>45</sup> This high enantioselectivity was attributed to the  $\pi$ - $\pi$  repulsive interactions between a substituent of the oncoming alkene and the 2-phenylnaphthyl substituent group at the **B** positions (Figure 1.1-11). The salen structure in **73** and **74** regulates the alkene's orientation efficiently to follow the “b” approach, resulting in the formation of epoxides with higher enantioselectivity than what is obtained with Jacobsen-type catalysts having only *tert*-butyl groups at the same positions.

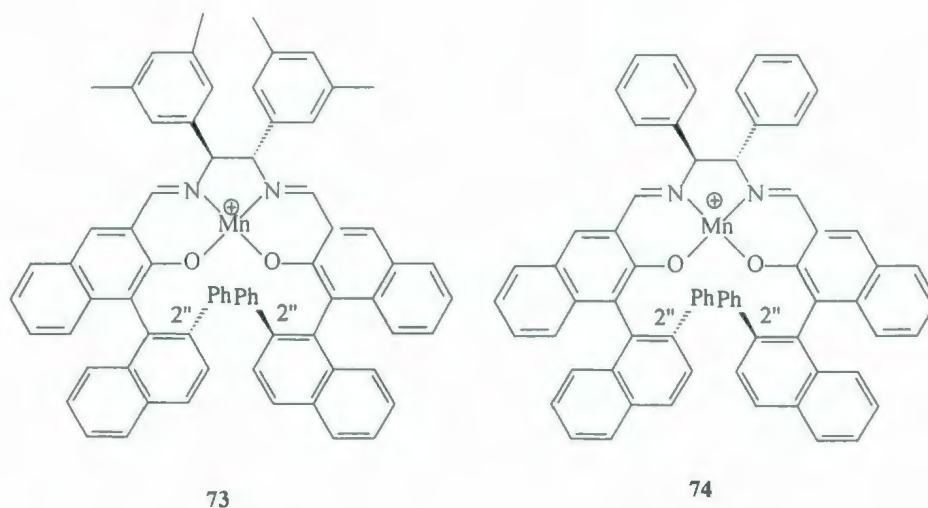


**Figure 1.1-15:** Katsuki catalysts **73** and **74**.

Jacobsen's “side-on” concept failed to explain the poor catalytic results obtained from epoxidation of *trans*-disubstituted alkenes.<sup>35</sup> In contrast, Katsuki catalysts **73** and

74 induced higher % *ee* for epoxidation of *trans* alkenes than Jacobsen-type catalysts 50-54.<sup>45</sup> The low efficiency of epoxidation of *trans* alkenes with a planar oxo-Mn-salen transition state *i.e.* "X" (Figure 1.1-16) is ascribed to the repulsion between one of the two alkene substituents with the salen ligand. This interrupts the desired orientation of the incoming alkene from getting to the oxygen atom, and leads to ineffective interactions between the alkene substituent groups with the chiral center in the oxo-Mn-salen species.

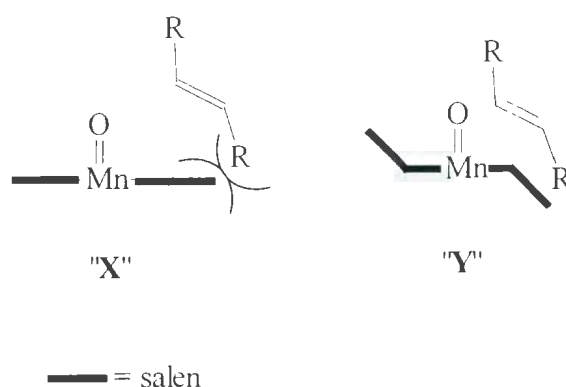


**Figure 1.1-16:** "Planar" and "folded" oxo-Mn-salen species "X" and "Y" respectively, and their interactions with a *trans* alkene.

Katsuki proposed that the "folded" oxo-Mn-salen "Y" transition state is more favoured for epoxidation of this type of olefin because the structure of this species facilitates the approach of the alkene to attack the oxygen atom of the manganese oxide. Furthermore, the skeleton of the folded transition state "Y" offers more effective non-bonding interactions with the alkene which in turn also induces higher enantioselectivity. In catalysts 73 and 74, the two phenyl substituents at the 3 and 3' positions attractively interact with an additional axial ligand such as water, or an alcohol *via*  $\pi$ - $n$  interactions. If this interaction acts synergistically with the interactions between the substituents at the chelating diamine moiety and the axial ligand, the salen ligand will be deeply folded.

Thus, **73** and **74** are good catalysts for epoxidation of *trans* alkenes. The crystal structure of catalyst **61** showed that it is more deeply folded and it showed high efficiency for asymmetric epoxidation of these types of alkenes. For example, the epoxidation of *trans*  $\beta$ -methylstyrene by **61** was attained in 91% *ee*.<sup>46</sup>

The steric effects due to the 5 and 5' groups ("A" groups, Figure 1.1-11) have only small influences on the enantioselectivities observed in the epoxidation of *cis*-disubstituted,<sup>45,35</sup> trisubstituted<sup>36,47</sup> and many tetrasubstituted alkenes.<sup>48</sup> However, poor enantioselectivities were observed (down to only 5% and 1% *ee*) in the epoxidation of highly sterically-hindered tetrasubstituted alkenes when using the bulky 5,5'-substituted Jacobsen catalyst **52** (Figure 1.1-11; A = -OSi(*i*-Pr)<sub>3</sub>).<sup>48</sup>

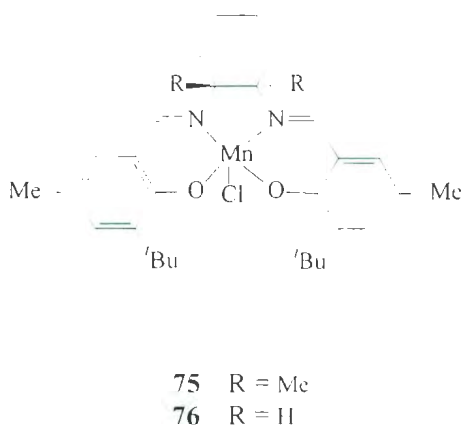


**Figure 1.1-17:** Jacobsen's catalysts **75** and **76**.

The steric effects due to the substituent groups on the diaminocyclohexane unit (Figure 1.1-17) on the enantioselectivities and the yield of epoxides are unclear. The Jacobsen-type catalyst induced low chemical yields and enantioselectivity in the epoxidation of *cis*- $\beta$ -methylstyrene when R was bulky. For example, using catalyst **75** (R

= Me) afforded only a 54% yield of the corresponding epoxide with 49% *ee*. In contrast, using catalyst **76** (R = H), led to the same epoxide in 81% yield with 92% *ee*.<sup>35</sup>

These results were used as evidence to prove that the alkene follows the approach from the side of the diaminocyclohexane moiety (approach **a**, Figure 1.1-11). Therefore, the less sterically-hindered diaminocyclohexane facilitates the alkene approach to the oxo-Mn species and induces higher enantioselectivity. In contrast, a more sterically-hindered catalyst leads to poorer yields and lower optical purities. However, the Katsuki-type catalysts **73** and **74** where the substituents (R = 3,5-(CH<sub>3</sub>)<sub>2</sub>C<sub>6</sub>H<sub>3</sub> and Ph, respectively) are more sterically-hindering, showed high enantioselectivity with many alkenes. For example, the epoxidation of 1,2-dihydronaphthalene using **73** and **74** led to the corresponding epoxide in 92% and 96% *ee*, respectively.<sup>44,45</sup>

### 1.1.2.3 Advances in salen-based Mn catalysis

After Jacobsen and Katsuki developed their Mn(III)-salen methodologies, other groups synthesized different types of chiral Mn(III)-salen complexes. Pedro<sup>49</sup> prepared a less-active Mn(III)-salen complex **77** (Figure 1.1-18) bearing a chiral sesquiterpene-derived component. This catalyst afforded epoxides from various alkenes in high yields by using different oxidants, but the enantioselectivity observed was low (between 5-10% *ee* in all cases) and only 1,2-dihydronaphthalene gave an epoxide with as much as 25% *ee* when iodosylbenzene was used as the oxidant.

In order to control the orientation of the oncoming alkene *via* a chemical recognition process, a salen unit has been attached to a calixarene to form the Mn(III)-salen complex **78** (Figure Figure 1.1-18).<sup>50</sup>

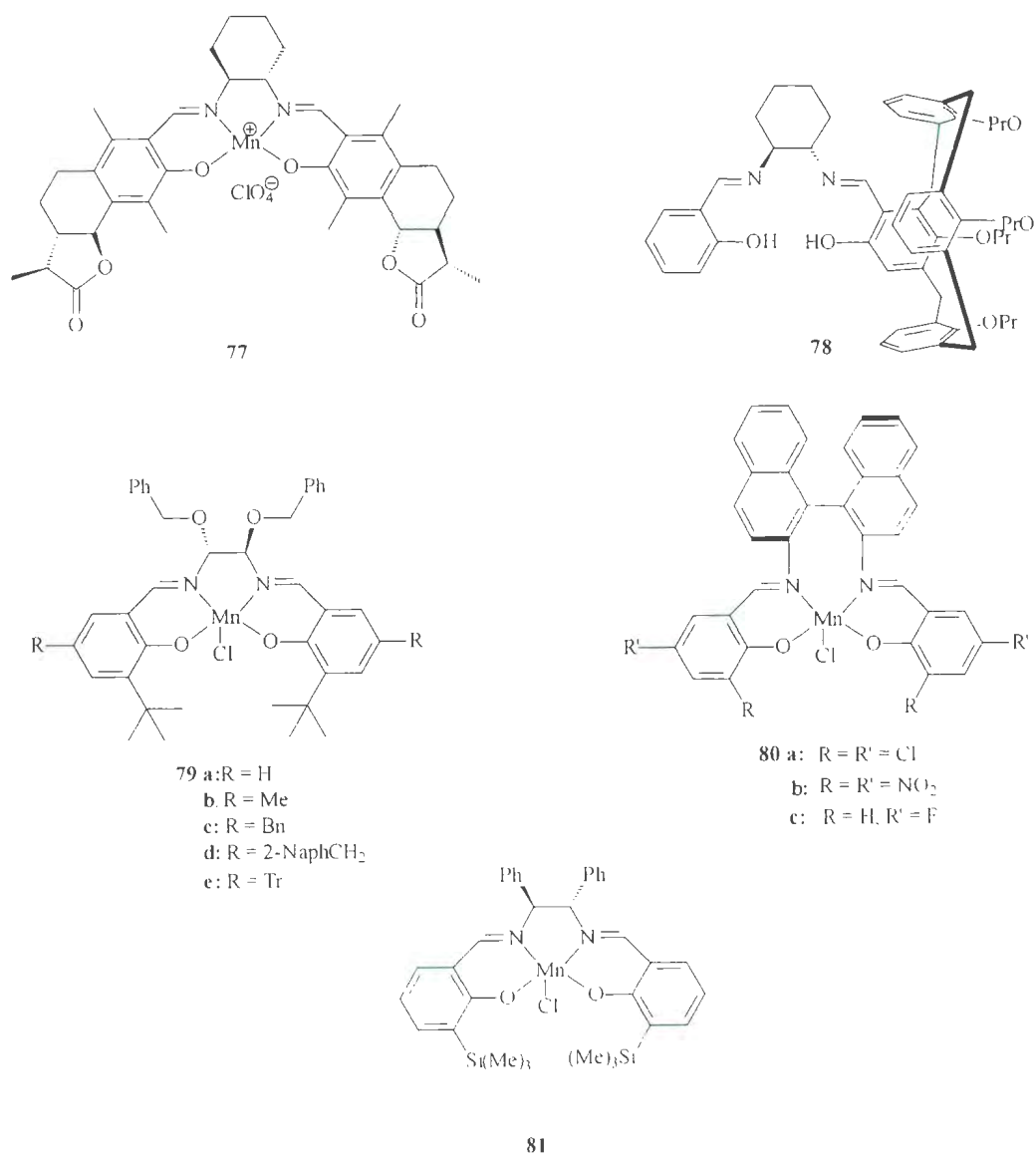


**Figure 1.1-18:** Different types of Mn(III)-Salen catalysts.

It was anticipated that the oncoming alkene would be encapsulated inside the cavity of the calixarene and that the cavity could control the approach of the alkene to become asymmetrically epoxidized by the Mn(III)-salen. However, the results obtained with **78** did not support this prediction. Mosset and Saalfrank synthesized a series of Mn(III)-salen catalysts such as **79a-e** which contained benzyl ether functionalities on the

diamine moiety.<sup>51</sup> These catalysts showed moderate-to-good enantiocontrol for epoxidation of indene and 2,2-dimethylchromene.

Unexpectedly, catalyst **79c** inverted the configuration of the resulting epoxides from the (*R,R*) enantiomer, which Jacobsen's **56** and Katsuki's **58** induced, to (*S,S*). The authors did not provide a clear explanation for this behaviour. Katsuki, however, attributed this phenomenon to the presence of the oxygen atoms on the diamine moiety in the salen unit which makes the complex act analogously to catalyst **72** (Figure 1.1-14). On the other hand, a very low yield and poor enantioselectivity was obtained when the bulky trityl substituted complex **79e** was used with bleach as the oxidant.

Attempted utilization of the chiral influence of a binaphthyl unit in the structure of the Mn(III)-complex **80** to develop the potential chiral catalytic behavior of the salen unit did not show much improvement in stereoselectivity. Epoxidation of *cis*- $\beta$ -methylstyrene by **80a** and **80b** gave only 43% and 54% *ee*, respectively, with high diastereoselectivity for the *cis*-epoxide.<sup>52</sup> However, the difluoro derivative **80c** afforded the epoxide from *trans*- $\beta$ -methylstyrene in 86% *ee* by using *m*-CPBA as the oxidant, at low temperature (-78 °C). This fundamental improvement was ascribed to the strongly electron-withdrawing fluoro substituents.<sup>53</sup> Despite involving larger trimethylsilyl substituents at the 3 and 3' positions, **81** gave low enantioselectivities for the epoxidation of styrene and *cis*- $\beta$ -methylstyrene.<sup>54</sup> This result was ascribed to the length of the C-Si bond which is 20% longer than the C-C bond.<sup>42</sup>

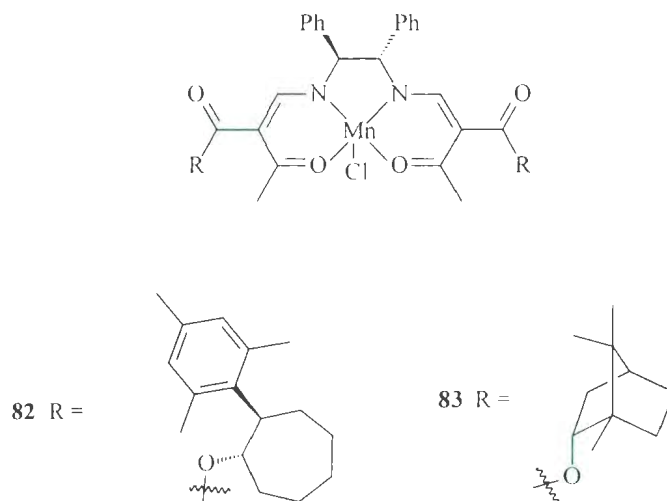


**Figure 1.1-19:**  $\beta$ -Ketoiminato salen **82** and **83** bearing a chiral ester auxiliary.

Mukaiyama developed the non-classical Mn-salen catalysts **82** and **83** bearing a chiral auxiliary group such as cyclooctylester **82**, or (-)-borneol **83** (Figure 1.1-19) from ethylenebis- $\beta$ -ketoiminate.<sup>55</sup> Catalyst **83** afforded the corresponding (3*R*,4*S*)-epoxide from benzocycloheptene with 84% *ee* using O<sub>2</sub>-pivalaldehyde as the oxidant. Changing the terminal oxidant to NaOCl<sub>(aq)</sub> gave the (3*S*,4*R*)-enantiomer with 41% *ee*.

Fluorous biphasic systems (FBS)<sup>56</sup> have been employed in Mn(III)-salen epoxidation methodology to solve the problem of catalyst recovery. Pozzi developed two generations of fluorous Mn(III)-salen catalysts **84-88** (Figure 1.1-20).<sup>57</sup> The first generation perfluorooctanyl Mn(III)-salen catalysts **84**, were soluble in perfluorocarbon solvents but were completely insoluble in commonly used organic solvents like acetonitrile, dichloromethane, or chlorobenzene. Both complexes showed high yields of epoxides from various alkenes, but with very low enantioselectivity, except with indene, where the product was obtained with 90% *ee*.<sup>57a</sup>

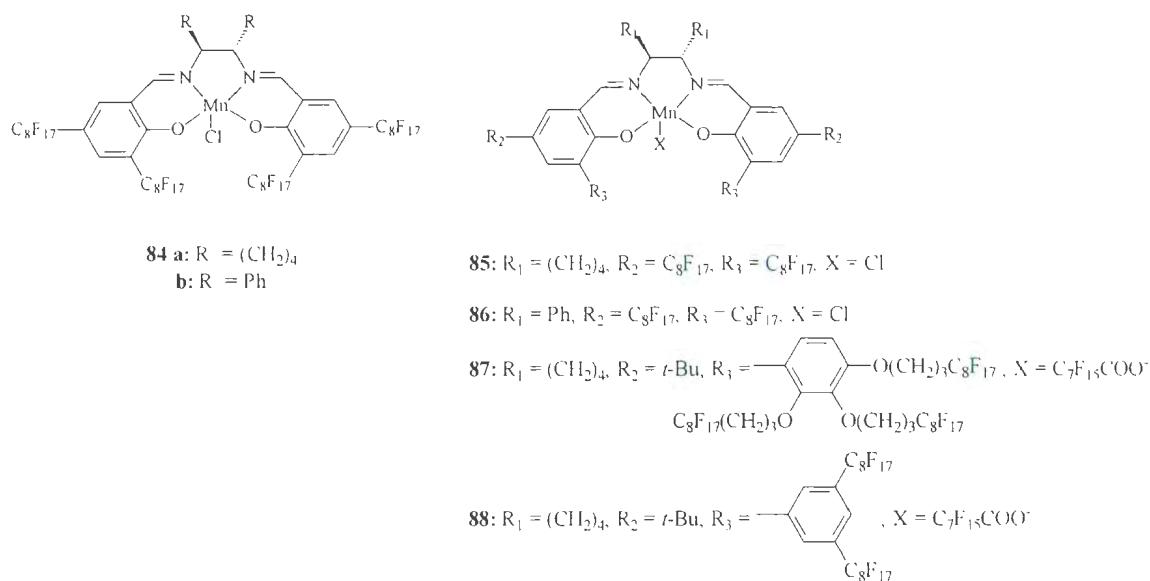


**Figure 1.1-20:** Perfluoroalkyl-substituted Mn(III)-salen complexes.

The second-generation catalysts **85-88** afforded the corresponding epoxides from different alkenes with modest to very good enantioselectivities. For example, catalyst **87** oxidized triphenylethylene to give triphenylethylene oxide in 98% yield and 87% *ee* using PhIO as the oxidant and pyridine N-oxide (PNO) as the additive in a CH<sub>3</sub>CN-perfluorooctane solvent system at 100 °C.<sup>57b</sup>

### 1.1.3 Host-guest catalysis and epoxidation reactions

Host-guest or supramolecular catalysis is an important consideration for the enantioselective catalysis of reactions with hydrocarbon substrates, particularly where there is no functionality on those substrates which can enhance any selectivity. In this type of catalysis, the catalyst is designed to have a cavity in which the active center resides. The reactant molecule is directed towards an active center in the cavity in order to react inside this cavity and give products with high stereoselectivity. This selectivity

arises not just from the steric effects imposed by the environment of the active site upon substrate approach, but also from specific binding at the active site. In host-guest catalysis, molecular recognition is the key to enhancing regio- and stereoselectivity by directing the reactant molecules toward the reactive site.

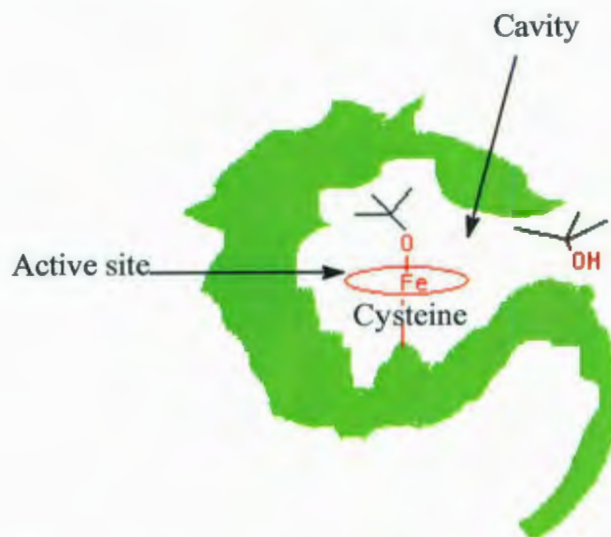


**Figure 1.1-21:** Cytochrome P-450 oxidation model.

Host-guest oxidative catalysis attempts to imitate enzymatic catalysis, especially that of the monooxygenase enzyme of the cytochrome P-450 family,<sup>58</sup> which selectively oxidizes a C-H bond in a hydrocarbon compound making it more water-soluble. The active site in this enzyme is an Fe(III)-porphyrin, the heme unit being coordinated axially to the body of the enzyme by a cysteine thiolate group (Figure 1.1-21).

It is presumed that the oxidation process in cytochrome P-450 goes through the formation of an oxo-ferryl ion species as the active oxygen transfer agent.<sup>59</sup> The enzyme spontaneously rearranges itself to create cavities or clefts around the active site. The regioselectivity in the oxidative behavior of cytochrome P-450 is attributed to the

accessibility of the reactant hydrocarbon molecule to the cavity. Also, binding the reactant substance by the enzyme membrane inside the cavities maximizes the steric interaction between this substance and the skeleton of the porphyrin moiety in the active site, which increases the stereoselectivity of the reaction. The versatility of cytochrome P-450 catalysis has inspired many chemists to design enzyme-mimetic systems for regio- and stereoselective catalysis. These systems can be classified under two types of models: (i) the synthetic complexes with active sites, such as the porphyrin and Schiff base catalysts; (ii) zeolite models.

Zeolites are constructed from  $\text{SiO}_4$  and  $\text{AlO}_4$  tetrahedra linked through oxygen bridges. Each oxygen atom is shared by two silicon or aluminum atoms.<sup>60</sup> The tetrahedral coordination of Si-O and Al-O permits a variety of ringed structures which are joined to form prisms and more complex cages. These cages can act similarly to an enzyme cavity if they have an active site encapsulated inside, such as Mn(III)salen or metal-porphyrin units (Figure 1.1-22). The cavity walls can embrace the alkene substituents and create the steric interactions necessary with the skeleton of the active site to produce epoxides with high enantioselectivity. The structures of zeolites also contain uniformly-sized pores and channels in the range of 4 to 13 Å and are, therefore, able to recognize, discriminate and pre-organize substrate molecules for subsequent reactions. Thus, since zeolites have rigid cages and channels with definite and uniform size, they can induce very interesting properties for designing new and selective supported catalyst.

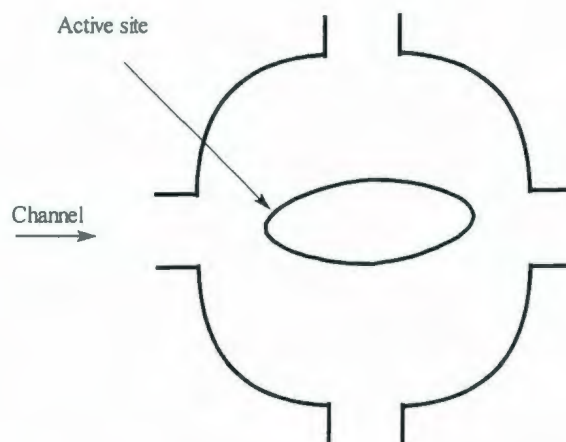
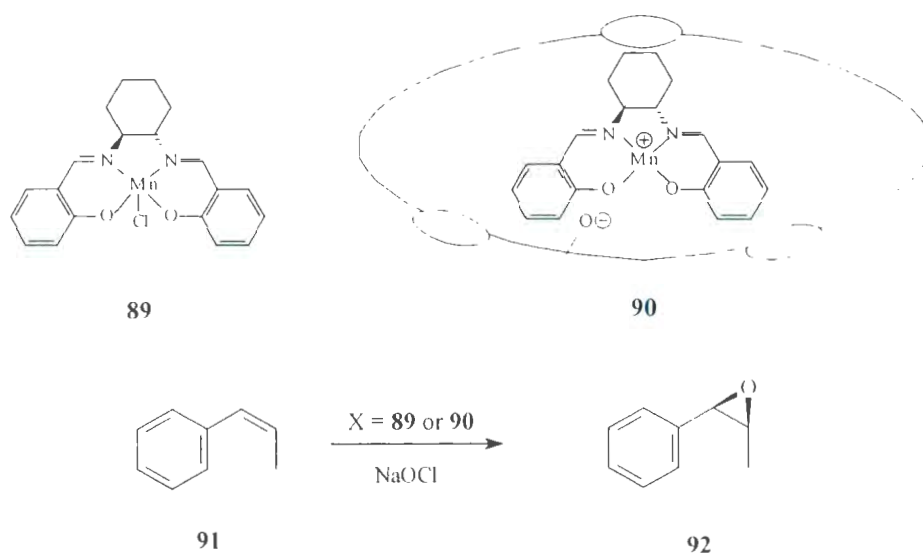


**Figure 1.1-22:** Zeolite catalytic model.

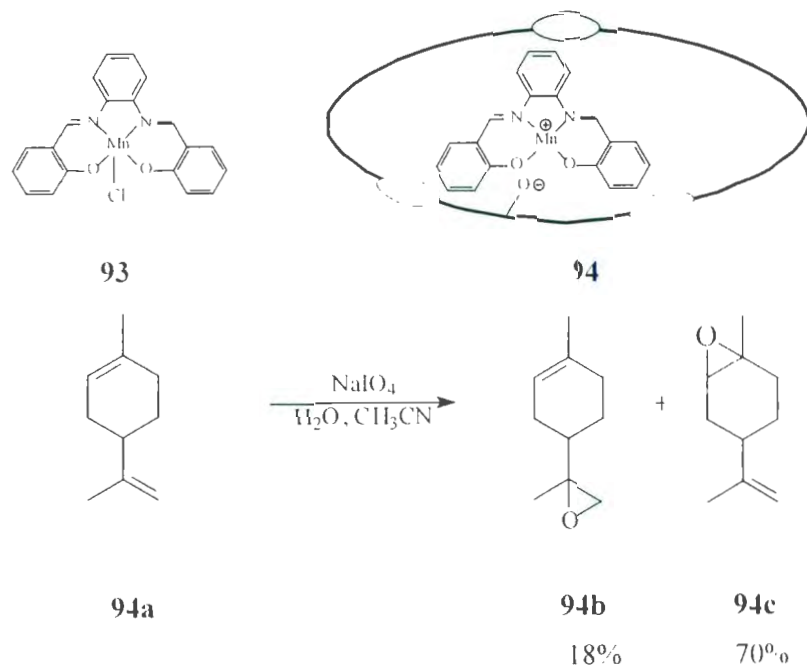
In addition to the host-guest potential capacity of zeolites which can be incorporated into Mn(III)-salen asymmetric epoxidation catalysis, recovery of the catalyst is another crucial objective with this methodology. The use of a zeolite therefore, has also been a target for much research. However, the efficiency of these zeolite-bound Mn(III)-salen complexes in terms of induced enantioselectivity has so far been consistently similar to, or lower than the results obtained using the same unsupported complexes in a homogeneous phase. For example, when chiral Mn(III)-salen complex **90** was encapsulated within zeolite Y (Scheme 1.1-9), which has 13 Å cavities, the highest *ee* that was achieved was 58% for the epoxidation of *cis*- $\beta$ -methylstyrene **91**.<sup>61</sup> On the other hand, when the Jacobsen catalyst **89** was encapsulated inside Al-, Ga-, and Fe-substituted mesoporous silicates,<sup>63</sup> the heterogeneous catalysts showed poorer results compared to the free catalyst **89** under homogenous conditions. In contrast, when the same reaction occurred under the homogeneous conditions of the Jacobsen catalyst **89** pattern, product **92** was obtained in 74% *ee*.



**Scheme 1.1-9:** Chiral Mn(III)-salen catalyst encapsulated within zeolite Y (**90**) for enantioselective epoxidation **91**.

The same catalyst **89** was trapped in the cages of crystalline zeolite EMT, and it showed similar effectiveness as the same free Jacobsen catalyst under homogeneous conditions. However, Mn(III)-salen encapsulated in zeolite EMT exhibited chemoselectivity in the epoxidation of alkenes having bulky substituents.<sup>62</sup> Thus, no epoxidation of cholesterol under the heterogeneous conditions of zeolite EMT up to 18 h of reaction could be detected, whereas 13% of cholesterol epoxide was produced under homogeneous conditions. It was rationalized that the large size of cholesterol prevented it from entering the zeolite pore and reacting with an oxo-Mn(III)-salen unit incorporated therein. This particular reaction illustrated the role that the zeolite pore sizes can play in the chemical recognition of the reactant and suggested that the epoxidation reaction occurred inside the cage. These findings opened the door to the use of zeolites to improve host-guest catalysis.

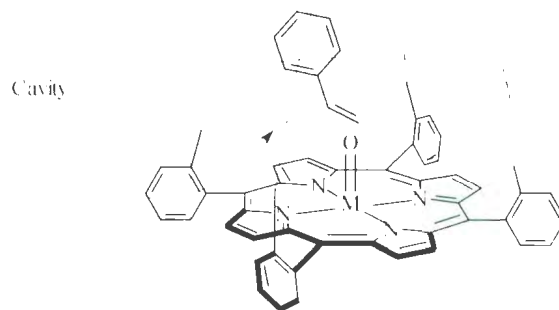
The achiral zeolite-encapsulated Mn(III)-salen **94** catalyst was more efficient than **93** in the epoxidation of a wide range of alkenes (Scheme 1.1-10).<sup>64</sup> All of the epoxides were obtained in higher yields using the heterogeneous catalyst than were obtained under the homogeneous conditions. This provides additional evidence that the epoxidation reaction under heterogeneous conditions occurs inside the zeolite cage. Also, the host-guest mechanism enhanced the reactivity by preventing formation of the unfavorable  $\mu$ -oxo-manganese dimer (Mn-O-Mn) which is a factor in deactivating epoxidation reactions under homogeneous conditions.



**Scheme 1.1-10:** Achiral Mn(III)-salen catalyst encapsulated within zeolite **94** for regio-selective epoxidation.

The observation that the porphyrin moiety is the active site in cytochrome P-450 enzyme has stimulated an extensive area of research into synthetic porphyrin-mimetic enzymatic systems. Porphyrin itself is not efficient in catalytic enantioselective

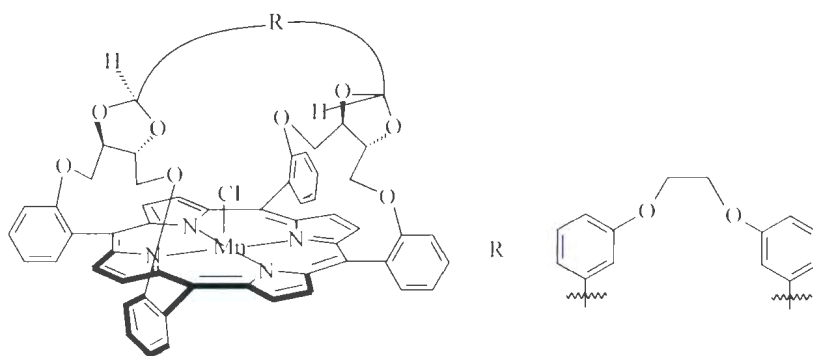




**101**

**Figure 1.1-23:** Porphyrin enzyme mimic system for epoxidation.

Strapped-porphyrins are models of enzyme mimic catalysts bearing straps of chiral moieties at one, or two, faces of a porphyrin (Figure 1.1-24). This class of porphyrin has a chiral cavity that can enhance the enantioselectivity of epoxidation in a supramolecular manner. For example, threitol-strapped Mn(III)-porphyrin complex **102** resulted in high enantioselectivity in the epoxidation of *cis*-disubstituted olefins of up to 88% *ee* and 79% *ee* with monosubstituted olefins.<sup>67</sup>



**102**

**Figure 1.1-24:** “Strapped”-porphyrin **102**.

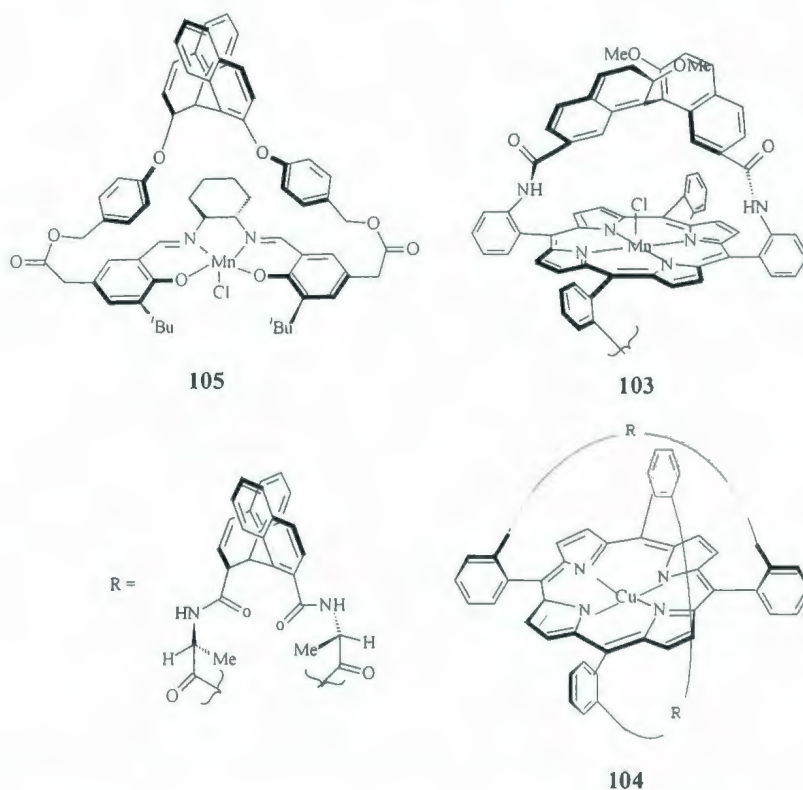
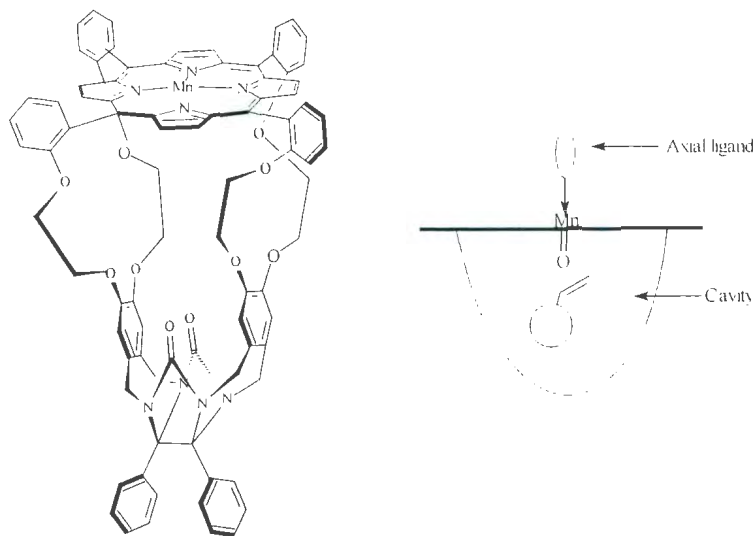


**Figure 1.1-25:** Enantioselective epoxidation catalysts bearing chiral 1,1'-binaphthyl **103-105**.

“Twin-Coronet” porphyrins **104** and **105** (Figure 1.1-25) have been synthesized bearing two chiral 1,1'-binaphthyl groups protecting the two faces of the porphyrin and creating cavities with a chiral environment.<sup>68,23b,c</sup> These catalysts induced high enantioselectivities in the epoxidation of electron-deficient styrenes; for example, up to 96% and 89% *ee* were obtained in the epoxidation of 3,5-dinitro- and 2-nitrostyrene, respectively. This high efficiency was attributed to  $\pi$ - $\pi^*$  interactions between the electron-deficient substrate and electron-rich binaphthyl straps of the catalyst which are believed to orient the approach of the alkene. Murahashi adopted the same idea in the Mn(III)-salen complex **103** (Figure 1.1-25) with a chiral strapping unit. Catalyst **103**

provided the corresponding (3*S*,4*S*)-epoxide with 93% *ee* and in 50% yield from epoxidation of 2,2-dimethylchromene using PhIO as the oxidant and 4-phenylpyridine-*N*-oxide (PPNO) as the axial ligand at -30 °C. Also, epoxidation of *cis*- $\beta$ -methylstyrene was achieved with 82% *ee*.<sup>69</sup>



106

**Figure 1.1-26:** Clip porphyrin **106**.

The “clip” porphyrin **106** was designed to have a metal-porphyrin molecule situated above the receptor cavity (Figure 1.1-26). Its cavity is rigid, relatively closed and well-defined, having a diameter of approximately 9 Å.<sup>70</sup> The clip catalyst **106** is capable of binding an alkene molecule inside the cavity where the epoxidation reaction takes place. However, a strong axial coordination of a ligand to the metal from the outside is crucial to prevent any epoxidation occurring outside of the cavity. Furthermore, oxidizing the metal inside the cavity prevents the formation of undesired  $\mu$ -oxo-metal dimers and prevents deactivation of the catalyst. Indeed, this example of a porphyrin

complex showed high stereoselectivity for the epoxidation of *cis*-stilbene: the *cis*-epoxide was formed in 95% yield and the *trans*-stilbene stereospecifically formed the *trans*-epoxide.

Cyclodextrins (CDs) are interesting natural products which have been intensively investigated as enzyme mimic catalytic model systems. The best-known and best-studied representatives are CDs **107** and **108** (Figure 1.1-27). These CDs are cyclic oligosaccharides which possess relatively rigid shallow bowl-shaped structures consisting of 6 and 7 glucopyranose units, respectively,<sup>71</sup> with an electron-rich, hydrophobic interior. The size of this hydrophobic cavity varies from 0.5 to 0.8 nm depending on the number of glucopyranose units forming the cyclodextrin. As a result of these features, CDs **107** and **108** are efficient water-soluble host molecules for a range of organic guest molecules including aliphatic and aromatic hydrocarbons, alcohols, phenols, ethers, carboxylic acids, esters, amines, etc.

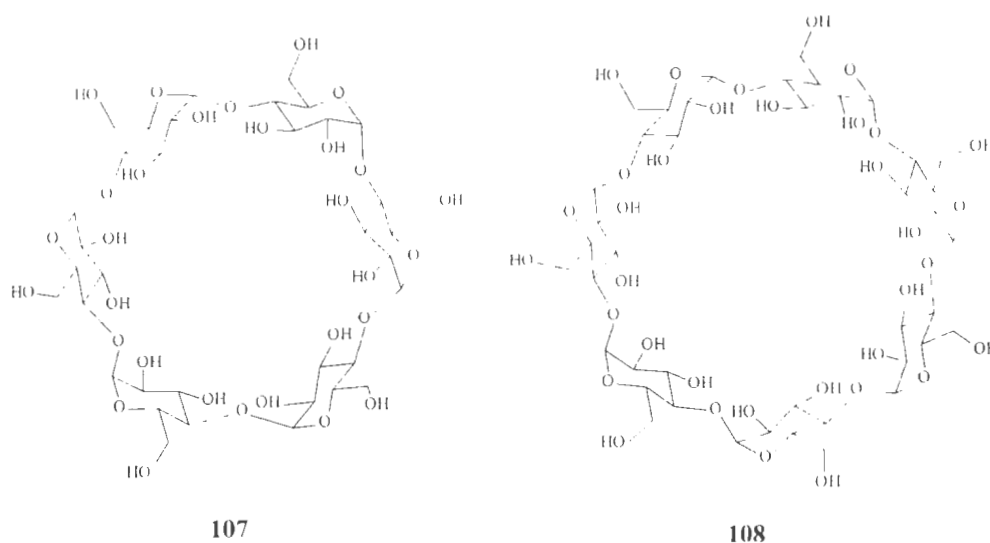
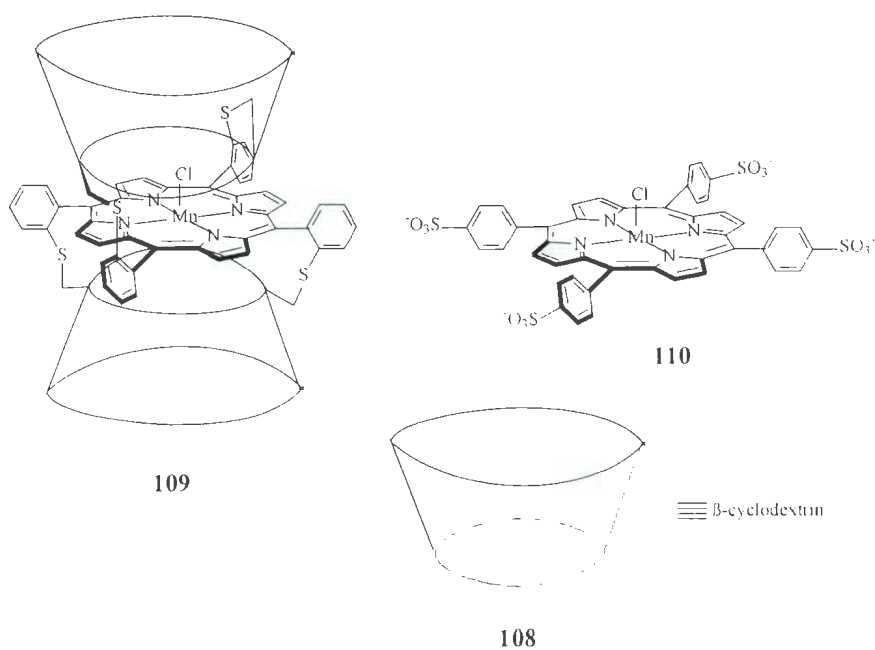


Figure 1.1-27:  $\alpha$ - and  $\beta$ -Cyclodextrins **107** and **108**.

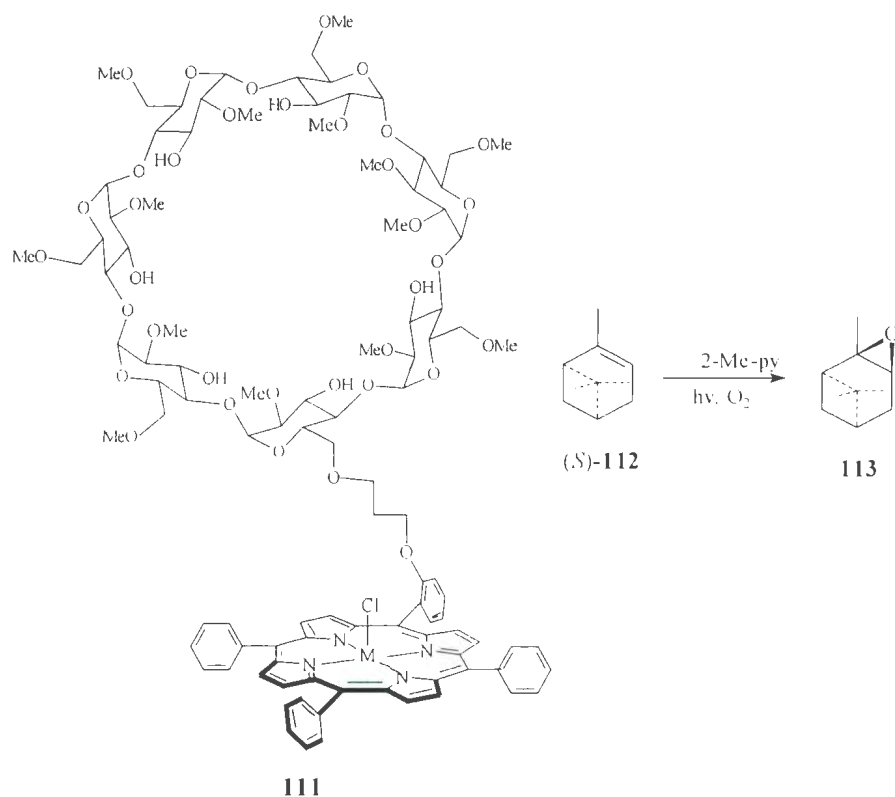
One of the first examples of a CD-enzyme mimic catalyst used for epoxidation is the sandwiched-porphyrin **109** (Figure 1.1-28).<sup>72</sup> Two  $\beta$ -CD **108** rings were attached to the two faces of the porphyrin establishing two binding pockets of cyclodextrins that can recognize various types of hydrophobic organic compounds in an aqueous solution. CD **109** was effective in the epoxidation of cyclohexene in aqueous solution to give the epoxide in 55% yield, while a very low yield was detected when water-soluble porphyrin **110** was used (2%). This result was attributed to effective binding of alkenes in the cyclodextrin cavities. Also, inclusion of the alkene inside the CD ring not only increases alkene solubility in aqueous solution, but also protects the epoxide from decomposition.



**Figure 1.1-28:** Sandwiched-porphyrin **109**.

Another example of a CD employed for catalytic epoxidation is the cyclodextrin-linked porphyrin **111** (Scheme 1.1-12).<sup>73</sup>  $\beta$ -CD was covalently-bonded by a diether

linking group. Moderate results were obtained by photocatalytic oxygenation of chiral  $\alpha$ -pinene **112** in the presence of **111**. The highest *de* obtained was 67% in the presence of 2-methylpyridine.



**Scheme 1.1-12:** Metal-porphyrin complex **111** bearing a  $\beta$ -CD for chiral photocatalytic oxygenation of chiral  $\alpha$ -pinene **112**.

A very useful metal-free epoxidation methodology employs dioxiranes that can be generated *in situ* from the reaction of oxone ( $\text{KHSO}_5$ ) with a catalytic amount of ketone. Attaching CD **108** to a ketone functionality should therefore, in principle, enhance selectivity for epoxidation of unsubstituted alkenes.<sup>74</sup> It was anticipated that CD **114** should chemically recognize and bind the alkene inside its cavity prior to reaction with a dioxirane intermediate, as in **115** (Figure 1.1-29). The best results were achieved in the

epoxidation of styrene to produce styrene oxide in 40% *ee*. It was rationalized that this improvement in styrene epoxide enantioselectivity was a result of inclusion of the styrene aromatic ring within the chiral cavity of the CD. The bridged  $\alpha$ -cyclodextrin **116** was designed to act similarly to **114**. However, **116** gave poorer enantioselectivity in epoxidation of styrene (30% *ee*).

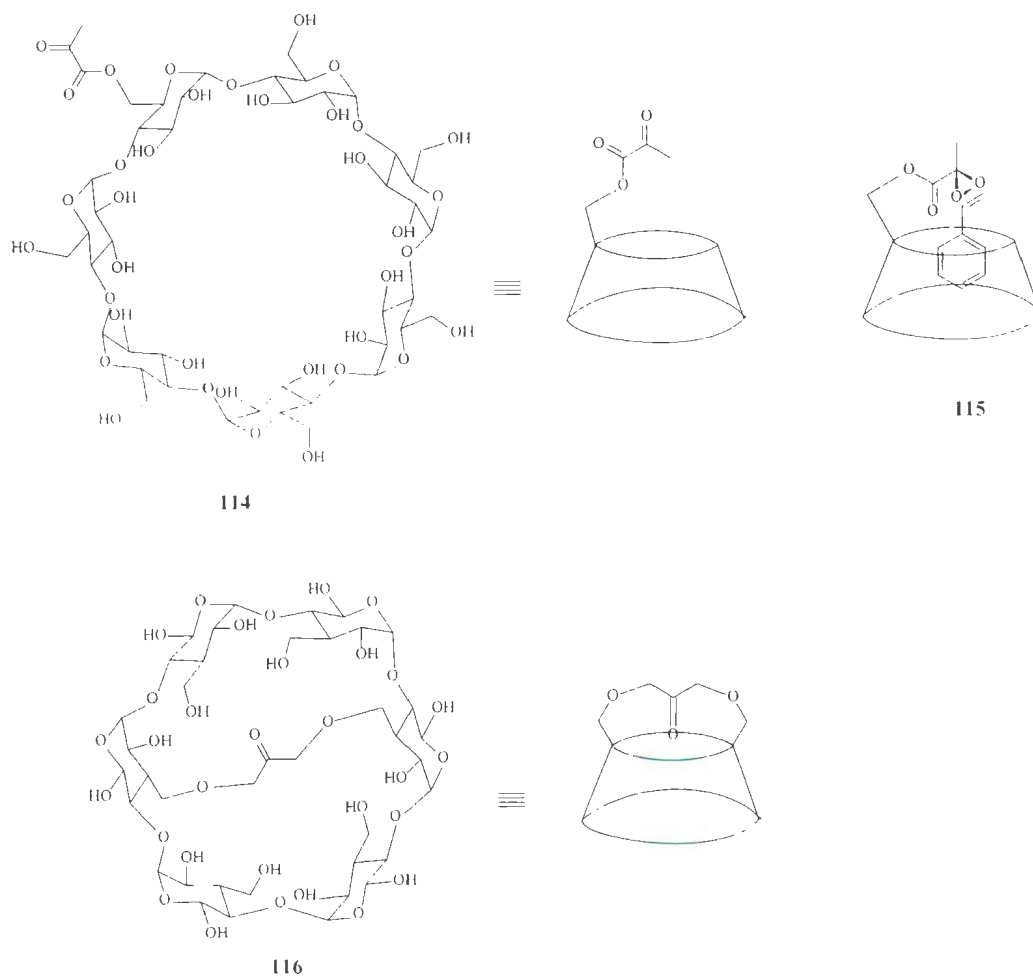


**Figure 1.1-29:** Cyclodextrins **114** and **116** bearing a ketone functionality act as enantioselective catalysts for epoxidation *via* dioxirane intermediates.

### 1.1.4 Development of calixsalen complexes

Jablonski's group developed a series of macrocyclic salen dimer complexes **117**.<sup>76</sup> Since these complexes have calixarene-like structures with an internal chiral cavity, they were named as calix[*n*]salens (Figure 1.1-30). X-ray crystallography of calixsalen **117d** showed it to have a well-defined macrocyclic structure with a large internal cavity (Figure 1.1-31).<sup>77</sup>

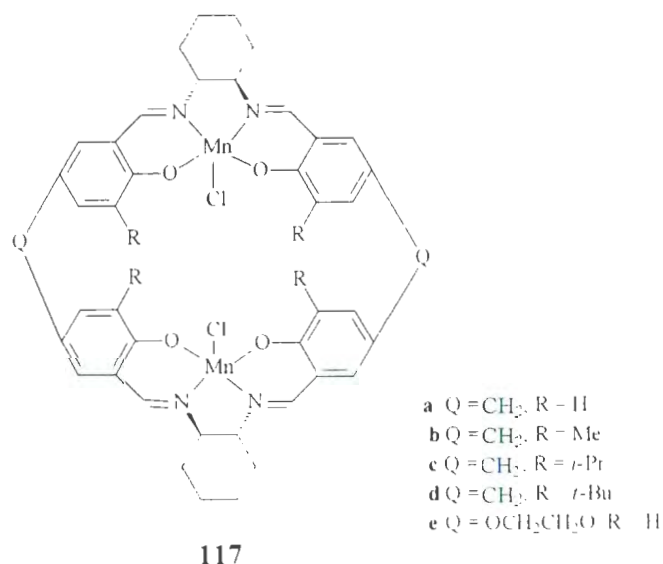


**Figure 1.1-30:** Examples of calix[2]salens **117**.

Calix[*n*]salen complexes are presumed to function as enzyme mimics with oxygen transfer occurring inside the chiral cavity.<sup>78</sup> The main approach in calix[*n*]salen methodology is to direct the alkene to enter the chiral cavity from an unblocked side to capture the oxygen atom from the oxo-Mn species and not from the opposite side which is protected by the alkyl substituent groups (*e.g.*, Me, *i*-Pr or *t*-Bu) (Figure 1.1-32). Also, using relatively large axial donors, such as 4-phenylpyridine-*N*-oxide, to coordinate the manganese atom from outside of the cavity should force alkenes to be epoxidized inside

the cavity. Furthermore, if the alkene epoxidation occurs inside the cavity *via* a radical intermediate, steric interactions within the chiral cavity should minimize bond rotation and lead to higher optical yields.

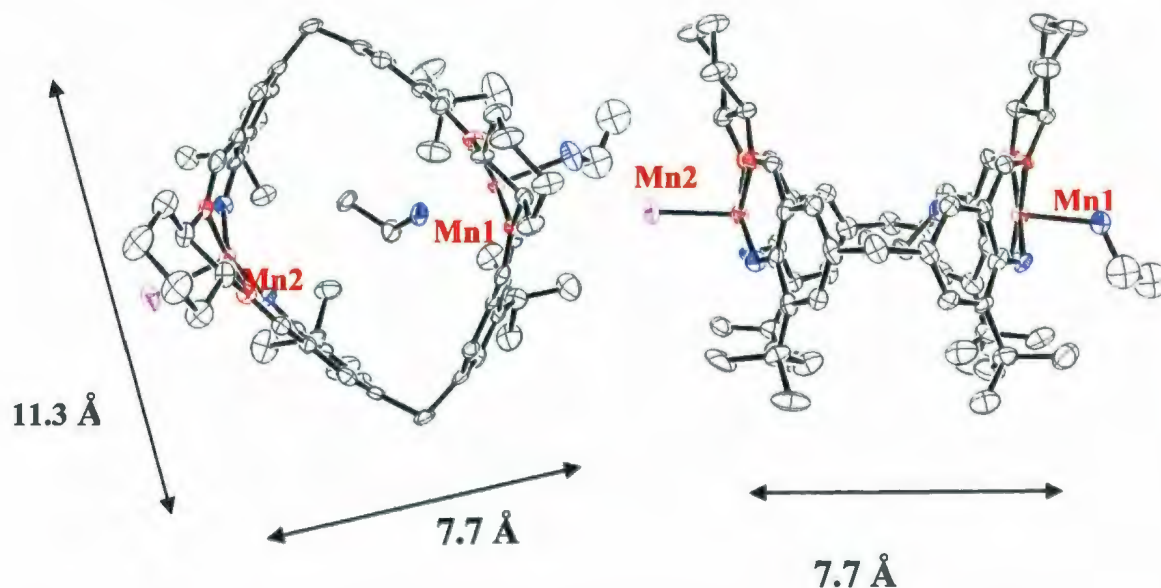


**Figure 1.1-31:** X-ray crystal structure of *syn*-calix[2]salen Mn(III) complex 117d.

It will be recalled that Jacobsen's catalyst **57** generated the epoxide from styrene in 86% *ee*.<sup>30a</sup> It was rationalized that the rotation of the C-C bond in the radical intermediate during the epoxidation process racemizes the product resulting in lower enantioselectivity. Interestingly, epoxidizing styrene with **117d** and *m*-CPBA as the oxidant in the presence of *N*-methylmorpholine-*N*-oxide as the additive at -78 °C, afforded the corresponding epoxide with 98% *ee*.<sup>77</sup> This result is consistent with the envisaged mechanism that has been proposed for this catalyst.

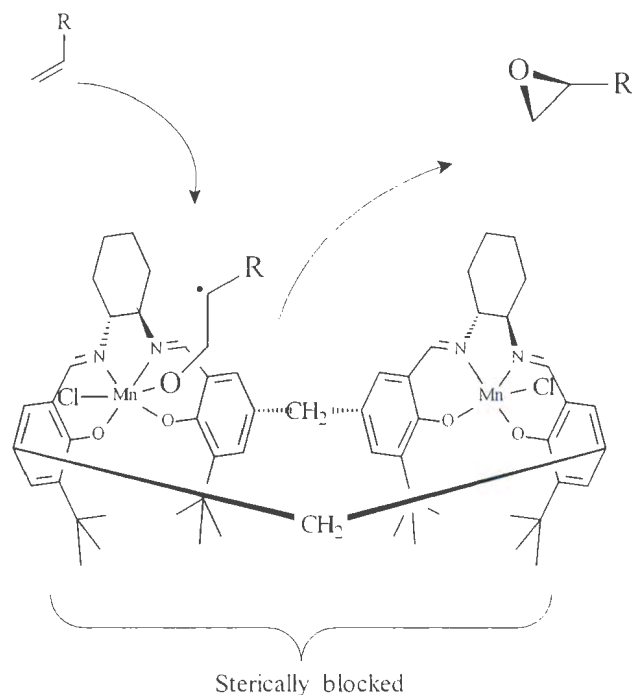
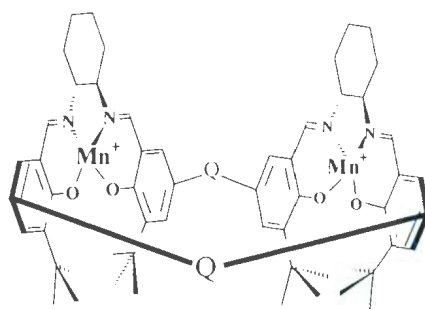


**Figure 1.1-32:** Proposed mechanism of *syn*-calix[2]salen-epoxidation methodology.

Calixsalen **117e** potentially offers a larger ring size than **117d**, however, since the  $-\text{OCH}_2\text{CH}_2\text{O}-$  linker group is flexible, it assumes a conformation driven by  $\pi$ -stacking. Therefore, replacement of the  $-\text{CH}_2-$  linking groups in **117d** by a larger groups such as an *o*-, *m*- or *p*- phenylene, or a disubstituted naphthyl (naphthylene) group for example, should expand the cavity size and keep the structure rigid (Figure 1.1-33). The availability of large ring-sized calixsalens will increase the range of the cavity sizes available and may improve the potential of calix[*n*]salen catalysts for stereoselective epoxidation of larger more sterically-hindered alkenes such as *cis*-stilbene.

The research reported in this thesis involves the synthesis of calix[2]salen ligands of complexes **118** (Figure 1.1-33) generated by linking the salen units to phenylene, naphthylene and anthracylene groups. The synthetic strategy employed various Schiff

base macrocyclization methodologies to prepare the desired salen dimer ligands efficiently from the corresponding dialdehyde systems. Furthermore, the Suzuki-Miyaura coupling reaction was used to efficiently link two salicylaldehyde units to dibromoaryl compounds such as dibromobenzene and dibromonaphthalene. The synthesis of an anthracene-based analogue employed a Ni-catalyzed coupling reaction. All of these approaches will be described and discussed in this thesis.



118

Q = phenylene, naphthylene or anthracylene

**Figure 1.1-33:** Target calixsalens constructed from salen dimer **118**.

In Chapter 2, the synthesis of the bisaldehyde precursors required for the designed Schiff base macrocycles will be described. Chapter 3 contains the description of the synthetic methodologies which were used to form the targeted Schiff base macrocyclic ligands. The second part of this thesis is devoted to research conducted by this author on the chemistry of thiacalixarene, a different macrocyclic system unrelated to the Schiff base macrocycles discussed in Part 1 (Chapters 1-3).

### 1.1.5 References

1. Borisova, N. E.; Reshetova, M. D.; Ustynyuk Y. A. *Chem. Rev.* **2007**, *107*, 46.
2. (a) Pilkington, N. H.; Robson, R. *Aust. J. Chem.* **1970**, *23*, 2225. (b) Atkins, A. J.; Black, D.; Blake, A. J.; Martin-Becerra, A.; Parsons, S.; Ruiz-Ramirez, I.; Schroder, M. *Chem. Commun.* **1996**, 457.
3. (a) Das, R.; Nag, K. *Inorg. Chem.* **1991**, *30*, 2831. (b) Bosnich, B. *Inorg. Chem.* **1999**, *38*, 2554.
4. (a) Nanda, K. K.; Thompson, L. K.; Brisdon J. N.; Nag, K. *J. Chem. Soc., Chem. Commun.* **1994**, 1337. (b) Nanda, K. K.; Das, R.; Thompson, L. K.; Venkatsubramanian, K.; Paul, P.; Nag, K. *Inorg. Chem.* **1994**, *33*, 1188.
5. Kim, G.; Park, D.; Tak, Y. *Catal. Lett.* **2000**, *65*, 127.
6. Gao, J.; Reibenspies, J. H.; Martell, A. E. *Angew. Chem. Int. Ed.* **2003**, *42*, 6008.
7. (a) Korupoju, S. R.; Mangayarkarasi, N.; Ameerunisha, S.; Valente, E. J.; Zacharias, P. S. *J. Chem. Soc., Dalton Trans.* **2000**, 2845. (b) Korupoju, S. R.; Zacharias, P. S. *Chem. Commun.* **1998**, 1267.
8. Gao, J.; Reibenspies, J. H.; Martell, A. E. *Org. Lett.* **2002**, *6*, 2453.
9. Gao, J.; Martell, A. E. *Org. Biomol. Chem.* **2003**, *1*, 2795.
10. Gao, J.; Martell, A. E. *Org. Biomol. Chem.* **2003**, *1*, 2801.
11. Hong, B. K.; Lee, I. S.; Shin, D. M.; Chung, Y. K. *Chem. Commun.* **2004**, 936.
12. (a) Brunner, H.; Schiessling, H. *Angew. Chem. Int. Ed.* **1994**, *33*, 125. (b) Brunner, H.; Schiessling, H. *Bull. Soc. Chim. Belg.* **1994**, *103*, 119.
13. Lin, J.; Zhang, H.; Pu, L. *Org. Lett.* **2002**, *4*, 3297.

14. Li, Z.; Lin, J.; Zhang, H.; Sabat, M.; Hyacinth, M.; Pu, L. *J. Org. Chem.* **2004**, *69*, 6284.
15. Voshell, Sh. M.; Lee, S. J.; Gagne, M. R. *J. Am. Chem. Soc.* **2006**, *128*, 12422.
16. Barba, V.; Villamil, R.; Luna, R.; Godoy-Alcantar, C.; Hopfl, H.; Beltran, H. I.; Zamudio-Rivera, L. S.; Santillan, R.; Farfan, N. *Inorg. Chem.* **2006**, *45*, 2553.
17. Hwang, G. T.; Kim, B. H. *Tetrahedron* **2002**, *58*, 9019.
18. Fox, O. D.; Rolls, T. D.; Drew, M. G. B.; Beer, P. D. *Chem. Commun.* **2001**, 1632.
19. Sessler, J. L.; Mody, T. D.; Lynch, V. *J. Am. Chem. Soc.* **1993**, *115*, 3346.
20. Sessler, J. L.; Roznyatovskiy, V.; Pantos, G. D.; Borisova, N. E.; Reshetova, M. D.; Lynch, V. M.; Khrustalev, V. N.; Ustynyuk, Yu. A. *Org. Lett.* **2005**, *7*, 5277.
21. Sessler, J. L.; Katayev, E. A.; Pantos, G. D.; Scherbakov, P.; Reshetova, M. D.; Khrustalev, V. N.; Lynch, V. M.; Ustynyuk, Yu. A. *J. Am. Chem. Soc.* **2005**, *127*, 11442.
22. Katsuki, T.; Sharpless, K. B. *J. Am. Chem. Soc.* **1980**, *102*, 5974.
23. (a) Groves, J. T.; Nemo, T. E.; Myers, R. S. *J. Am. Chem. Soc.* **1979**, *101*, 1032. (b) Groves, J. T.; Myers, R. S. *J. Am. Chem. Soc.* **1983**, *105*, 5791. (c) Naruta, Y.; Tani, F.; Maruyama, K. *Chem. Lett.* **1989**, 1269. (d) Naruta, Y.; Tani, F.; Ishihara, N.; Murayama, K. *J. Am. Chem. Soc.* **1991**, *113*, 6865. (e) Srinivasan, K.; Michaud, P.; Kochi, J. K. *J. Am. Chem. Soc.* **1986**, *108*, 2309. (f) Samsel, E. G.; Srinivasan, K.; Kochi, J. K. *J. Am. Chem. Soc.* **1985**, *107*, 7606.
24. Srinivasan, K.; Michaud, P.; Kochi, J. K. *J. Am. Chem. Soc.* **1986**, *108*, 2309.
25. Yoon, H.; Burrows, C. J. *J. Am. Chem. Soc.* **1988**, *110*, 4087.

26. Zhang, W.; Loebach, J. L.; Wilson, S. R.; Jacobsen, E. N. *J. Am. Chem. Soc.* **1990**, *112*, 2801.
27. Irie, R.; Noda, K.; Ito, Y.; Matsumoto, N.; Katsuki, T. *Tetrahedron Lett.* **1990**, *31*, 7345.
28. McGarrigle, E. M.; Gilheany, D. G. *Chem. Rev.* **2005**, *105*, 1563.
29. (a) Zhang, W.; Jacobsen, E. N. *J. Org. Chem.* **1991**, *56*, 2296. (b) Deng, L.; Jacobsen, E. N. *J. Org. Chem.* **1992**, *57*, 4320. (c) Hughes, D. L.; Smith, G. B.; Liu, J.; Dezeny, G. C.; Senanayake, C. H.; Larsen, R. D.; Verhoeven, T. R.; Reider, P. J. *J. Org. Chem.* **1997**, *62*, 2222.
30. (a) Palucki, M.; Pospisil, P. J.; Zhang, W.; Jacobsen, E. N. *J. Am. Chem. Soc.* **1994**, *116*, 9333. (b) Palucki, M.; McCormick, G. J.; Jacobsen, E. N. *Tetrahedron Lett.* **1995**, *36*, 5457. (c) Scheurer, A.; Mosset, P.; Spiegel, M.; Saalfrank, R.W. *Tetrahedron* **1999**, *55*, 1063. (d) Adam, W.; Fell, R. T.; Mock-Knoblauch, C.; Saha-Möller, C. R. *Tetrahedron Lett.* **1996**, *37*, 6531.
31. (a) Feichtinger, D.; Plattner, D. A. *Angew. Chem. Int. Ed. Engl.* **1997**, *36*, 1718. (b) Feichtinger, D.; Plattner, D. A. *Chem. Eur. J.* **2001**, *7*, 591. (c) Chipperfield, J. R.; Clayton, J.; Khan, S. A.; Woodward, S. *J. Chem. Soc., Dalton Trans.* **2000**, 1087. (d) Adam, W.; Mock-Knoblauch, C.; Saha-Möller, C. R.; Herderich, M. *J. Am. Chem. Soc.* **2000**, *120*, 9685.
32. (a) Jacobsen, E. N.; Deng, L.; Furukawa, Y.; Martinez, L. E. *Tetrahedron* **1994**, *50*, 323. (b) Lee, N. H.; Jacobsen, E. N. *Tetrahedron Lett.* **1991**, *32*, 6533. (c) Hamada, T.; Irie, R.; Katsuki, T. *Synlett* **1994**, 479. (d) Sasaki, H.; Irie, R.; Katsuki, T. *Synlett*

- 1994, 356. (e) Chang, S.; Lee, N. H.; Jacobsen, E. N. *J. Org. Chem.* **1993**, *58*, 6939.
- (f) Irie, R.; Noda, K.; Ito, Y.; Katsuki, T. *Tetrahedron Lett.* **1991**, *33*, 1055.
33. Irie, R.; Noda, K.; Ito, Y.; Matsumoto, N.; Katsuki, T. *Tetrahedron, Asymmetry* **1991**, *2*, 481.
34. Sasaki, H.; Irie, R.; Katsuki, T. *Synlett* **1994**, 356.
35. Jacobsen, E. N.; Zhang, W.; Muci, A. R.; Ecker, J. R.; Deng, L. *J. Am. Chem. Soc.* **1991**, *113*, 7063.
36. Fukuda, T.; Irie, R.; Katsuki, T. *Synlett* **1995**, 197.
37. Takeda, T.; Irie, R.; Katsuki, T. *Synlett* **1999**, 1166.
38. Hashihayata, T.; Ito, Y.; Katsuki, T. *Synlett* **1996**, 1079.
39. Hashihayata, T.; Ito, Y.; Katsuki, T. *Tetrahedron* **1997**, *53*, 9541.
40. Miura, K.; Katsuki, T. *Synlett* **1999**, 783.
41. Ito, Y. N.; Katsuki, T. *Tetrahedron Lett.* **1998**, *39*, 4325.
42. O'Connor, K. J.; Wey, S. J.; Burrows, C. J. *Tetrahedron Lett.* **1992**, *33*, 1001.
43. Palucki, M.; McCormick, G. J.; Jacobsen, E. N. *Tetrahedron Lett.* **1995**, *36*, 5457.
44. Sasaki, H.; Irie, R.; Hamada, T.; Suzuki, K.; Katsuki, T. *Tetrahedron* **1994**, *50*, 11827.
45. Sasaki, H.; Irie, R.; Katsuki, T. *Synlett* **1994**, 356.
46. Nishikori, H.; Ohta, C.; Katsuki, T. *Synlett* **2000**, 1557.
47. Brandes, B. D.; Jacobsen, E. N. *J. Org. Chem.* **1994**, *59*, 4378.
48. Brandes, B. D.; Jacobsen, E. N. *Tetrahedron Lett.* **1995**, *36*, 5123.
49. Fernandez, I.; Pedro, J. R.; de la Salud, R. *Tetrahedron* **1996**, *52*, 12031.

50. Amato, M. E.; Ballistreri, F. P.; Pappalardo, A.; Tomaselli, G. A.; Toscano, R. M.; Williams, D. J. *Eur. J. Org. Chem.* **2005**, 3562.
51. Scheurer, A.; Mosset, P.; Spiegel, M.; Saalfrank, R. W. *Tetrahedron* **1999**, *55*, 1063.
52. (a) Ho, C. W.; Cheng, W. C.; Cheng, M. C.; Peng, S. M.; Cheng, K. F.; Che, C. M. *J. Chem. Soc., Dalton Trans.* **1996**, 405. (b) Cheng, M. C.; Chan, M. C. W.; Peng, S. M.; Cheung, K. K.; Che, C. M. *J. Chem. Soc., Dalton Trans.* **1996**, 3479.
53. Jacobsen, E. N.; Wu, M. H. "Comprehensive Asymmetric Catalysis", Springer, Berlin, **1999**, Vol. II, 649-693.
54. Zhao, S. H.; Ortiz, P. R.; Keys, B. A.; Davenport, K.G. *Tetrahedron Lett.* **1992**, *37*, 2725.
55. Nagata, T.; Imagawa, K.; Yamada, T.; Mukaiyama, T. *Inorg. Chem. Acta.* **1994**, *220*, 283.
56. (a) Horváth, I. T.; Rábai, J. *Science*, **1994**, *72*. (b) Horváth, I. T. *Acc. Chem. Res.* **1998**, *31*, 641.
57. (a) Pozzi, G.; Cinato, F.; Montanari, F.; Quici, S. *Chem. Commun.* **1998**, 877. (b) Cavizzini, M.; Manfredi, A.; Montanari, F.; Quici, S.; Pozzi, G. *Chem. Commun.* **2000**, 2171.
58. (a) Sato, R.; Omura, T. *Cytochrome P-450*, Kodansha Ltd., Tokyo, **1978**. (b) Dawson, D. H.; Sono, M. *Chem. Rev.* **1987**, *87*, 1255. (c) Gunter, M. J.; Turner, P. *Coord. Chem. Rev.* **1991**, *108*, 115. (d) *Cytochrome P-450, Structure, Mechanism and Biochemistry*, ed. P. R. Ortiz de Montellano, Plenum Press, New York, **1995**.
59. (a) Coon, M. J.; Vermilion, J. L.; Vatsis, K. P.; French, J. S.; Dean, W. L.; Haugen,

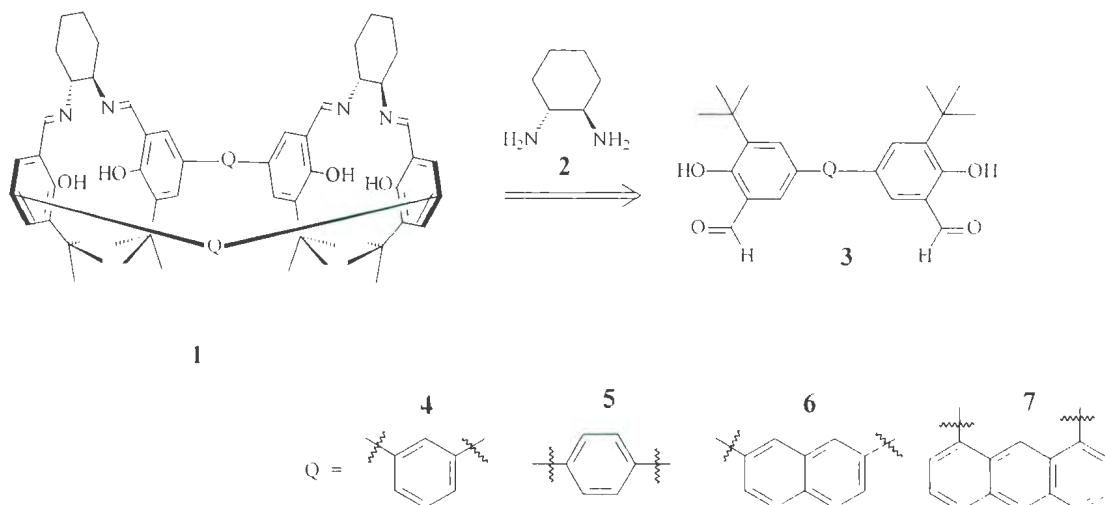
- A. *ACS Symp. Ser.* **1977**, *44*, 46. (b) Peterson, J. A.; Ishimura, Y.; Baron, J.; Estabrook, R. W. "*Oxidases and Related Redox Systems*" University Park Press, Baltimore, **1973**, 565. (c) Pryor, W. A. "*Free Radicals in Biology*", W. A. Pryor, Ed., Academic Press, New York, **1976**, 1. (d) Groves, J. T.; McClusky, G. A.; White, R. E.; Coon, M. J. *Biochem. Biophys. Res. Commun.* **1978**, *81*, 154.
60. (a) Breck, D.W. "*Zeolite Molecular Sieves*", Wiley, New York, **1974**. (b) Barrer, R. M. "*Hydrothermal Chemistry of Zeolites*", Academic Press, New York, **1982**.
61. Sabater, M. J.; Corma, A.; Doménech, A.; Fornés V.; García, H. *J. Chem. Soc., Chem. Commun.* **1997**, 1285.
62. Ogunwumi, S. B.; Bein, T. *J. Chem. Soc., Chem. Commun.* **1997**, 901.
63. Frunza, L.; Kosslick, H.; Landmesser, H.; Hijft, E.; Fricke, R. *J. Mol. Catal. A* **1997**, *123*, 179.
64. Mirkhani, V.; Moghadam, M.; Tangestaninejad, S.; Bahramian, B.; Mallekpoor-Shalamzari, A. *Appl. Catal. A* **2007**, *321*, 49.
65. Groves, J. T.; Haushalter, R. C.; Nakamura, M.; Nemo, T. E.; Evans, B. J. *J. Am. Chem. Soc.* **1981**, *103*, 2884.
66. (a) Mansuy, D.; Battioni, P.; Renaud, J. P.; Guerin, P. *J. Chem. Soc., Chem. Commun.* **1985**, 155. (b) Groves, J. T.; Viski, P. *J. Org. Chem.* **1990**, *55*, 3628. (c) Halterman, R. L.; Jan, S. T. *J. Org. Chem.* **1991**, *56*, 5253. (d) Berkessel, A.; Frauenkron, M. *J. Chem. Soc., Perkin Trans.* **1997**, *1*, 2265. (e) Groves, J. T.; Haushalter, R. C.; Nakamura, M.; Nemo, T. E.; Evans, B. J. *J. Am. Chem. Soc.* **1988**, *103*, 2884.

67. Collman, J. P.; Kellen-Yuen, C. J.; Zhang, X.; Ibers, J. A.; Brauman, J. I. *J. Am. Chem. Soc.* **1995**, *117*, 692.
68. Naruta, Y.; Ishihara, N.; Tani, F.; Maruyama K. *Bull. Chem. Soc. Jpn.* **1993**, *66*, 158.
69. Murahashi, S.; Noji, S.; Komiya, N. *Adv. Synth. Catal.* **2004**, *346*, 195.
70. (a) Elemans, J.; Bijsterveld, E.; Rowan, A. E.; Nolte, R. *Eur. J. Org. Chem.* **2007**, 751. (b) Elemans, J.; Bijsterveld, E.; Rowan, A. E.; Nolte, R. *Chem. Commun.*, **2000**, 2443.
71. Saenger, W.; Jacob, J.; Gessler, K.; Steiner, T.; Hoffmann, D.; Sanbe, H.; Koizumi, K.; Smith S. M.; Takaha, T. *Chem. Rev.* **1998**, *98*, 1787.
72. (a) Khenkin A. M.; Shteinman A. A. *Dokl. Akad. Nauk. SSSR*, **1984**, *279*, 939. (b) Khenkin A. M.; Shteinman, A. A. *Kinet. Katal.* **1989**, *30*, 7. (c) Kuroda, Y.; Hiroshige T.; Ogoshi, H. *J. Chem. Soc., Chem. Commun.* **1990**, 1594.
73. Weber, L.; Imiolczyk, L.; Haufe, G.; Rehorek, D.; Hennig, H. *J. Chem Soc., Chem. Commun.*, **1992**, 301.
74. Chan, W.; Yu, W.; Che, C.; Wong, M. *J. Org. Chem.* **2003**, *68*, 6576.
75. Rousseau, C.; Christensen, B.; Petersen, T. E.; Bols, M. *Org. Biomol. Chem.* **2004**, *2*, 3476.
76. Li, Z.; Jablonski, C. *Chem. Commun.* **1999**, 1531.
77. Wang, L.; Coulter, K.; Jablonski, C. unpublished results.
78. (a) Breslow, R. *Acc. Chem. Res.* **1995**, *28*, 146. (b) van Veggel, F. C. J. M.; Verboom, W.; Reinhoudt, D. N. *Chem. Rev.* **1994**, *94*, 279.

## Chapter 1.2. Synthetic approaches towards the preparation of the bisaldehydes

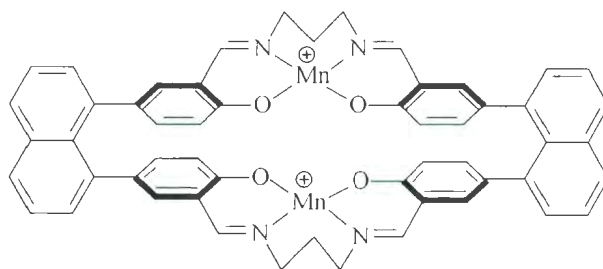
### 1.2.1 Introduction

As described in Chapter 1.1, a new type of highly constrained chiral cavity-containing Mn(III)-calixsalen dimer **117d** (Figure 1.1-30), in which the linking group “Q” is a methylene (CH<sub>2</sub>) group, was highly efficient for the asymmetric epoxidation of alkenes such as styrene and indene.<sup>1</sup> This high efficiency is attributed to structural features which maintain a rigid cavity to facilitate the epoxidation reaction in a chiral and sterically-biased environment. Therefore, in any newly-designed and targeted calixsalen dimer such as **1** (Scheme 1.2-1), replacing the methylene (CH<sub>2</sub>) linking group (“Q” in **117d**, page 43) with larger, and more rigid groups “Q” should increase the cavity size while maintaining the rigid shape of the desired ligands **1**.



**Scheme 1.2-1:** Synthetic strategy for rigid ring-expanded calixsalens **1**.

The strategy employed to construct this new series of Schiff base macrocyclic ligands was to initially prepare bisaldehyde systems such as **3** and then to react them with (1*R*,2*R*)-diaminocyclohexane (**2**) under Schiff base reaction conditions to form the desired salen dimers **1** (Scheme 1.2-1). Bisaldehyde systems (e.g. **3**) were constructed from two alkylsalicylaldehyde units connected by non-flexible linking groups (where Q = **4**, **5**, **6** or **7**) using Suzuki-Miyaura methodology. In this chapter, the synthetic approaches to prepare the bisaldehyde systems **3** will be discussed. Furthermore, an improved Suzuki-Miyaura methodology using a low mol% of the Pd (0) catalyst for coupling of alkyl substituted *p*-methoxyphenyl boronic acid with dibromoaryl systems will be highlighted.



**8**

**Figure 1.2-1:** McAuliffe's Mn(III)-salen dimer.

A similar structure to the targeted Mn(III)-calixsalens was reported in 1994 by McAuliffe, who introduced two 1,8-naphthylene groups in the Mn(III)-salen dimer **8** (Figure 1.2-1).<sup>2</sup> Complex **8** was constructed *in situ* from the reaction of 1,8-bis(3-formyl-4-hydroxyphenyl)naphthalene with 1,3-propanediamine in the presence of Mn(ClO<sub>4</sub>)<sub>2</sub>. The synthesis 1,8-bis(3-formyl-4-hydroxyphenyl)naphthalene was achieved *via* Suzuki-Miyaura coupling of 1,8-naphthalenediboronic acid with 4-bromosalicylaldehyde.

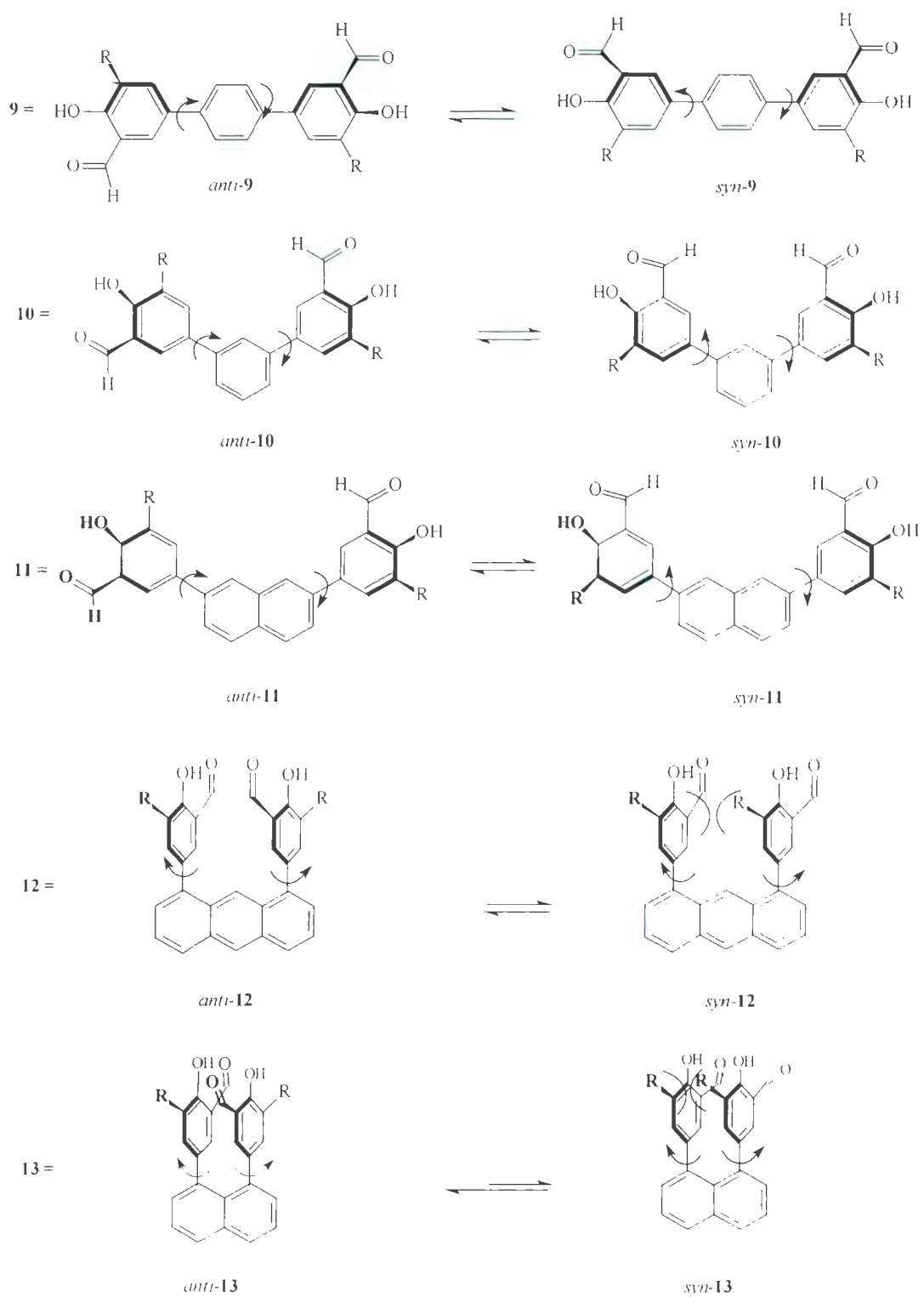
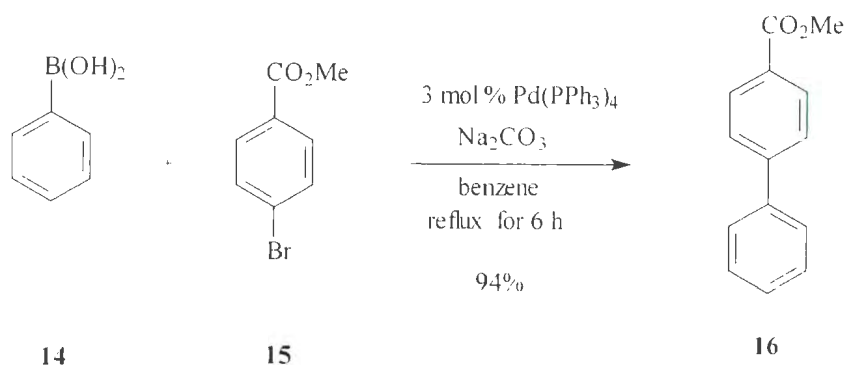


**Figure 1.2-2:** Conformational isomers of bisaldehyde compounds 9-13 (R = H, or alkyl).

In the research reported herein, McAuliffe's strategy was applied using bisaldehydes **9-12** as the linking groups. The *syn* conformers of **9-13** (Figure 1.2-2) would be the required ones to form the desired salen-dimer macrocycles *via* Schiff base macrocyclization reactions. Since the barriers to rotation of the aryl substituted in **9** and **12** are expected to be lower than in **13**, the *syn* conformations of **9-12**, should be better candidates than the 1,8-naphthylene group used by McAuliffe for the objectives envisioned.

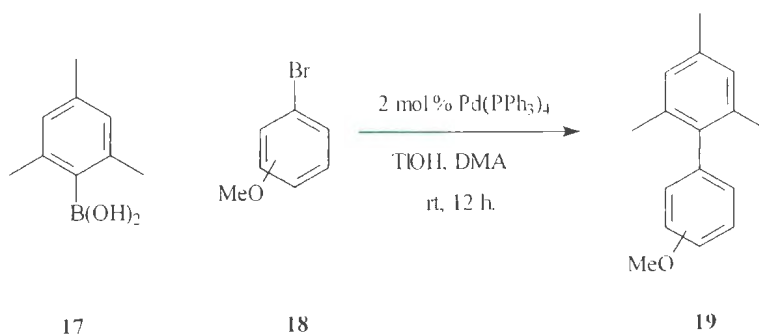


**Scheme 1.2-2:** The first example of Suzuki-Miyaura coupling.

Many methods for aryl-aryl bond formation to build triaryl systems have been reported.<sup>3</sup> Suzuki-Miyaura coupling has been widely used and is remarkably efficient at directly linking two aromatic systems.<sup>4</sup> This methodology utilizes the Pd(0)-catalyzed coupling of an arylboronic acid with an aryl halide under basic conditions. In the first example of this type of coupling, Suzuki isolated biaryl **16** in 94% yield from the reaction of phenylboronic acid (**14**) with methyl 4-bromobenzoate (**15**), under reflux conditions for 6 h in benzene, in the presence of sodium carbonate and 3 mol% of Pd(PPh<sub>3</sub>)<sub>4</sub> catalyst (Scheme 1.2-2).

Despite the fact that boronic acids are not always easily prepared, they have low toxicity, are easier to handle and are environmentally-friendlier than other commonly used organometallic reagents such as aryllithium, arylzinc or Grignard reagents, which are frequently used in other coupling methodologies. Also, Suzuki-Miyaura coupling normally works smoothly with various substituted aryl halides including esters, halides, phenols and other functional groups.

The efficiency of this type of coupling depends on various parameters such as the halide used, the substituted functionality on the aryl halide as well as the boronic acid, and the reaction conditions. As expected, the reactivity of the aryl halides decreases in the order  $I > Br > Cl$ .<sup>5</sup> Investigations of the influence of the base on the coupling reactions of different boronic acids with various aryl halides at ambient temperature, revealed that thallium hydroxide gave the best result in the presence of 2 mol% of  $Pd(PPh_3)_4$  catalyst in dimethylacetamide (DMA) as the solvent (Scheme 1.2-3).<sup>6,7</sup>

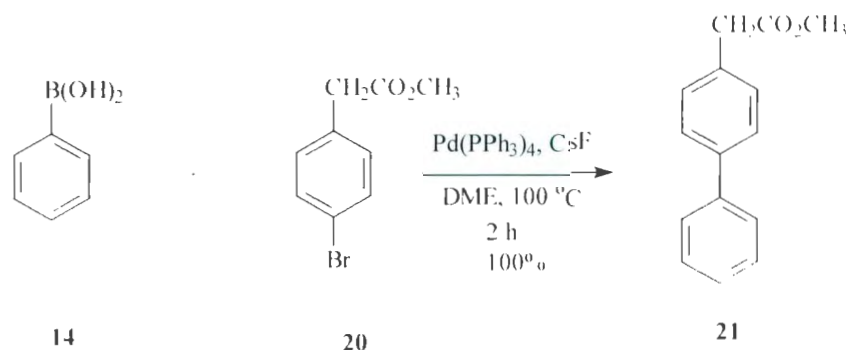


**Scheme 1.2-3:** Efficient ambient temperature conditions for Suzuki-Miyaura coupling.

Snieckus realized from the synthesis of chlorodihydroxybiphenyls, that the efficiency of palladium-catalyzed cross-coupling in the presence of a base, is also facilitated by the nature of the solvent used. Typically, the best results were achieved

with  $\text{Na}_2\text{CO}_3$  as the base and DME as the solvent. However,  $\text{K}_3\text{PO}_4$  activated the reaction remarkably when DMF was used as the solvent.<sup>8</sup>

Fluoride salts reportedly enhanced the rates and yields enormously for Suzuki-Miyaura coupling reactions. In particular, Wright found that cesium fluoride gave the best yield for the product **21** (Scheme 1.2-4).<sup>9</sup>



**Scheme 1.2-4:** Cesium fluoride-catalyzed Suzuki-Miyaura coupling.

### 1.2.2 Strategies and retrosynthetic analysis

As described earlier in this chapter, the synthetic strategy to prepare the targeted salen macrocyclic ligands is based upon transformation of the bisaldehyde adduct **3** to the desired compounds **1** using a Schiff base condensation reaction in the final step (Scheme 1.2-1). At the very beginning of this project, three synthetic routes were proposed to prepare 1,4-bis(3-*tert*-butyl-5-formyl-4-hydroxyphenyl)benzene (**22**) as a representative example of the targeted bisaldehyde systems (Scheme 1.2-5). Each of these pathways was based upon linking two alkyl-substituted salicylaldehyde units to an aromatic ring in

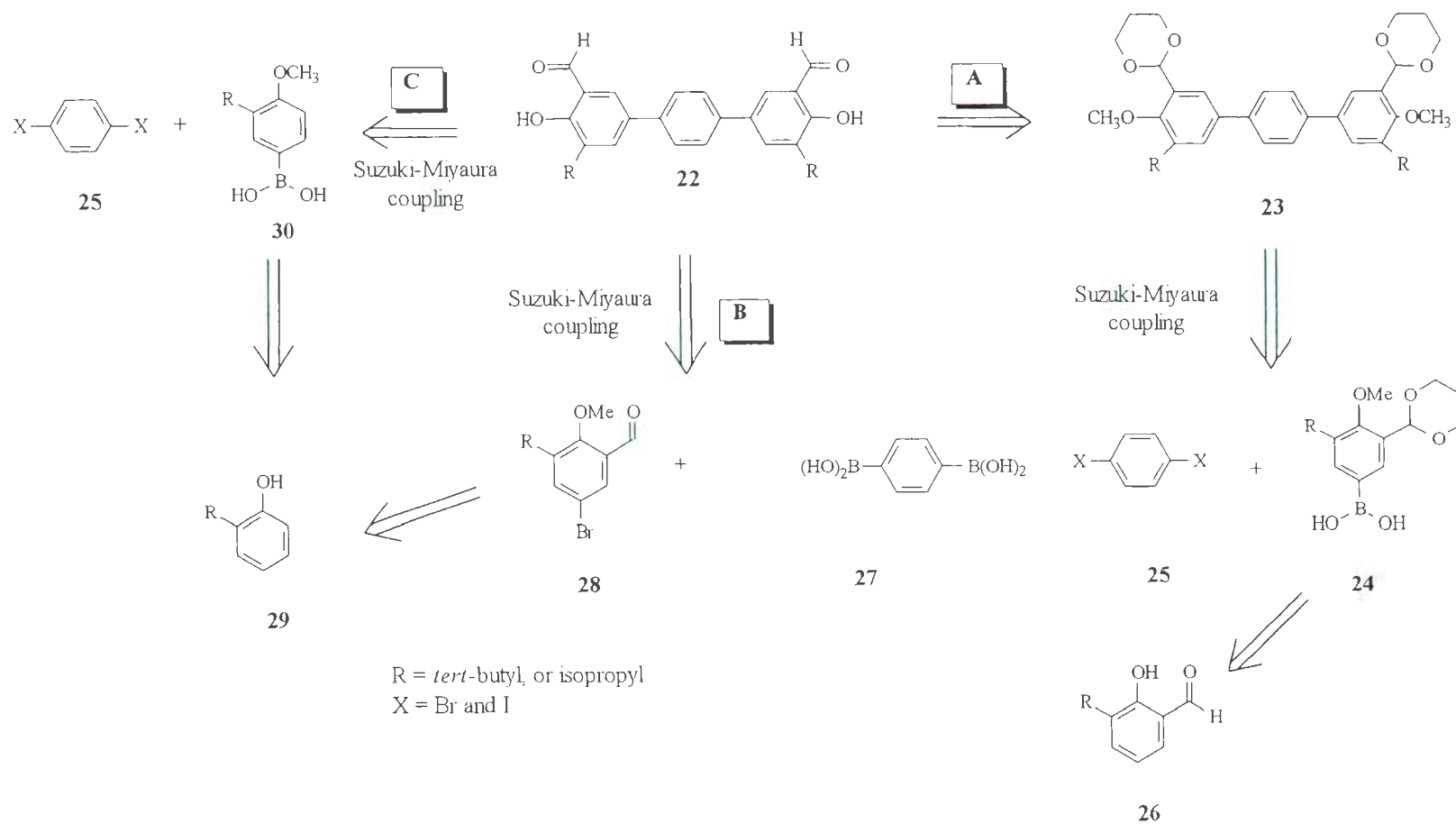
either the *meta*- or *para*- positions using Suzuki-Miyaura coupling as the key reaction step.

### 1.2.2.1 Retrosynthetic Route A

This strategy involves preparation of boronic acid **24** having a protected aldehyde and phenolic hydroxyl group. Reaction of **24** with the dihalobenzene **25** under Suzuki-Miyaura coupling conditions would form **23**. Bisaldehyde **22**, in turn, could be easily synthesized by deprotection of the aldehyde and phenol groups, in **23**. Protection of the aldehyde and phenol groups respectively, in **26**, is crucial for the generation of boronic acid **24** from the corresponding organometallic (lithium or magnesium) reagent.

### 1.2.2.2 Retrosynthetic Route B

This proposed route is more straightforward than the other two since it does not require the use of as many protecting groups. Suzuki-Miyaura coupling of the 1,4-phenylenediboronic acid **27** and 5-bromo-3-*tert*-butyl-2-methoxybenzaldehyde (**28**) leads to bisaldehyde **22** after demethylation. In this route, protection of the aldehyde groups in **28** is not required. Formylation of phenol **29** followed by bromination leads to **28**. Protecting the hydroxy group in **28** however is a crucial step for the envisioned Suzuki-Miyaura coupling reaction.



Scheme 1.2-5: Retrosynthesis of bisaldehyde 22.

### 1.2.2.3 Retrosynthetic Route C

In this pathway, the formylation step is delayed to the end of the synthesis since the aldehyde group is sensitive to nucleophilic organometallic reagents. The transformation from boronic acid **30** to bisaldehyde **22** requires the following series of steps: initial Suzuki-Miyaura coupling of dihalobenzene **25** and boronic acid **30**, deprotection of the phenolic hydroxyl groups, and finally, formylation of the resulting bisphenol terphenyl compound to give **22**. Boronic acid **30** can be prepared from precursor **29** by bromination followed by protection of the hydroxyl group as a required step prior to the generation of the desired boronic acid **30** *via* the corresponding organolithium or Grignard reagent.

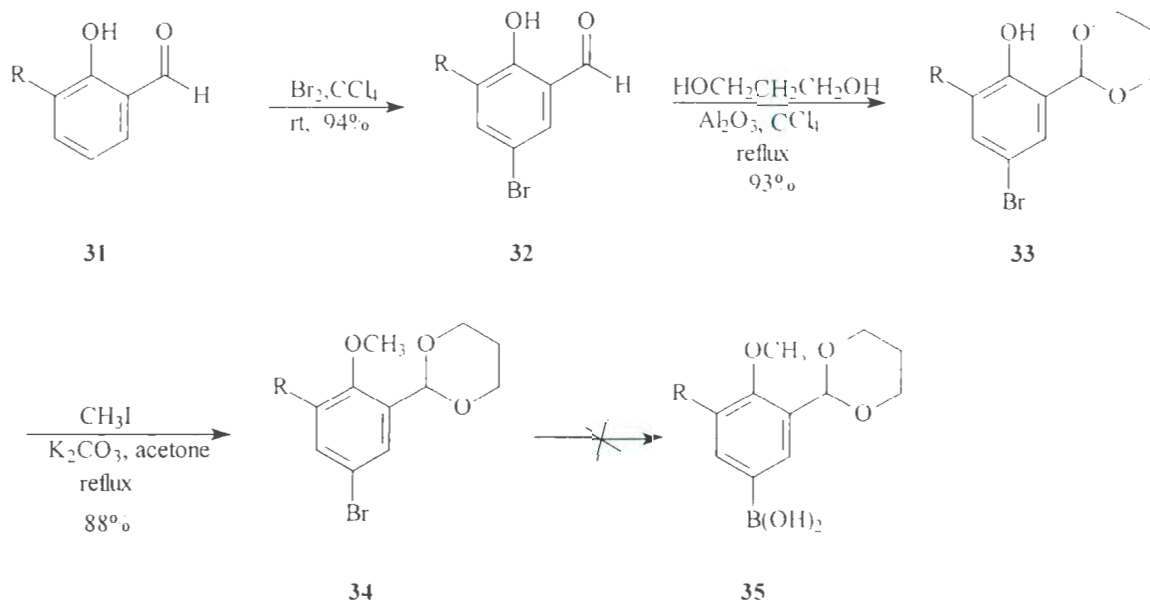
## 1.2.3 Synthesis of Bisaldehydes

### 1.2.3.1 Synthetic Route A

This route (Scheme 1.2-6) was employed to prepare boronic acid **35** with a protected aldehyde group, as a crucial precursor for the Suzuki-Miyaura coupling with a dihalobenzene. 3-Isopropylsalicylaldehyde (**31**), which was previously prepared in our laboratory,<sup>1</sup> was used as the starting material and was brominated to form **32**.

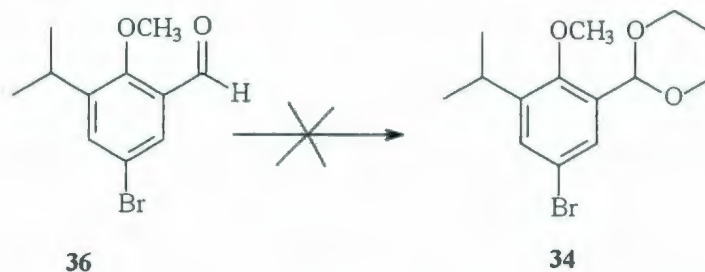
Protection of the aldehyde group in **32** was performed efficiently with 1,3-propanediol under acid-catalyzed conditions in carbon tetrachloride, using acidic alumina, Al<sub>2</sub>O<sub>3</sub> (pH = 4.0), in the presence of sodium sulfate.<sup>10</sup> The reaction mixture was heated at reflux for 60 h, and after work-up, **33** was obtained as a clean crude product in 93% yield. In contrast, using toluene as the solvent led to **33** in lower yield (53%). None of the

desired product however, was obtained when ethylene glycol was employed to form the corresponding dioxolane-protected analogue.



**Scheme 1.2-6:** Synthetic route A (R = isopropyl).

Application of the same alumina-catalyzed methodology used for **33**, to protect the aldehyde group with 1,3-propanediol in the corresponding methoxy derivative **36** (prepared by the reaction of **32** with methyl iodide), surprisingly, was not successful (Scheme 1.2-7). It should be noted that the alumina-catalyzed methodology used to protect aldehyde **32** with 1,3-dihydroxypropane was efficient only in small-scale reactions. When relatively large amounts (more than 3.0 g) of starting materials were used, a sticky solid formed which prevented efficient stirring and led to an intractable product.



**Scheme 1.2-7:** Attempted protection of aldehyde group in **36**.

The  $^1\text{H}$  NMR spectrum of the crude product was consistent for the expected structure of **33**. The acetal hydrogen in the newly-formed 1,3-dioxane ring appeared as a singlet at  $\delta = 7.99$  ppm. The  $^{13}\text{C}$  NMR spectrum showed a new signal at  $\delta = 102.60$  ppm due to the acetal carbon atom, in addition to two high-field signals for the dioxane ring carbons at  $\delta$  67.83 and 25.81 ppm.

Heating a mixture of **33** with methyl iodide in dry acetone at reflux in the presence of anhydrous potassium carbonate afforded **34** in 88% yield.<sup>11</sup> Its  $^1\text{H}$  NMR and  $^{13}\text{C}$  NMR spectra were consistent with the structure of **34**. A singlet at  $\delta = 5.60$  ppm for the phenolic hydrogen in the spectrum of **33** was replaced by a signal at  $\delta = 3.78$  ppm due to the newly introduced methoxy group. In the  $^{13}\text{C}$  NMR spectrum, the corresponding carbon for the methoxy group appeared at  $\delta = 67.72$  ppm. The mass spectrum showed the presence of a molecular ion at  $m/z = 315.0$ , corresponding to **34**.

Subsequently, however, efforts to prepare the corresponding boronic acid **35** from bromide **34** using Grignard or organolithium reagents were terminated because the other routes, particularly route C, proved to be more productive and convenient, since

route **A** still required several more subsequent steps in order to de-protect both the aldehyde and phenolic functional groups.

### 1.2.3.2 Synthetic Route B

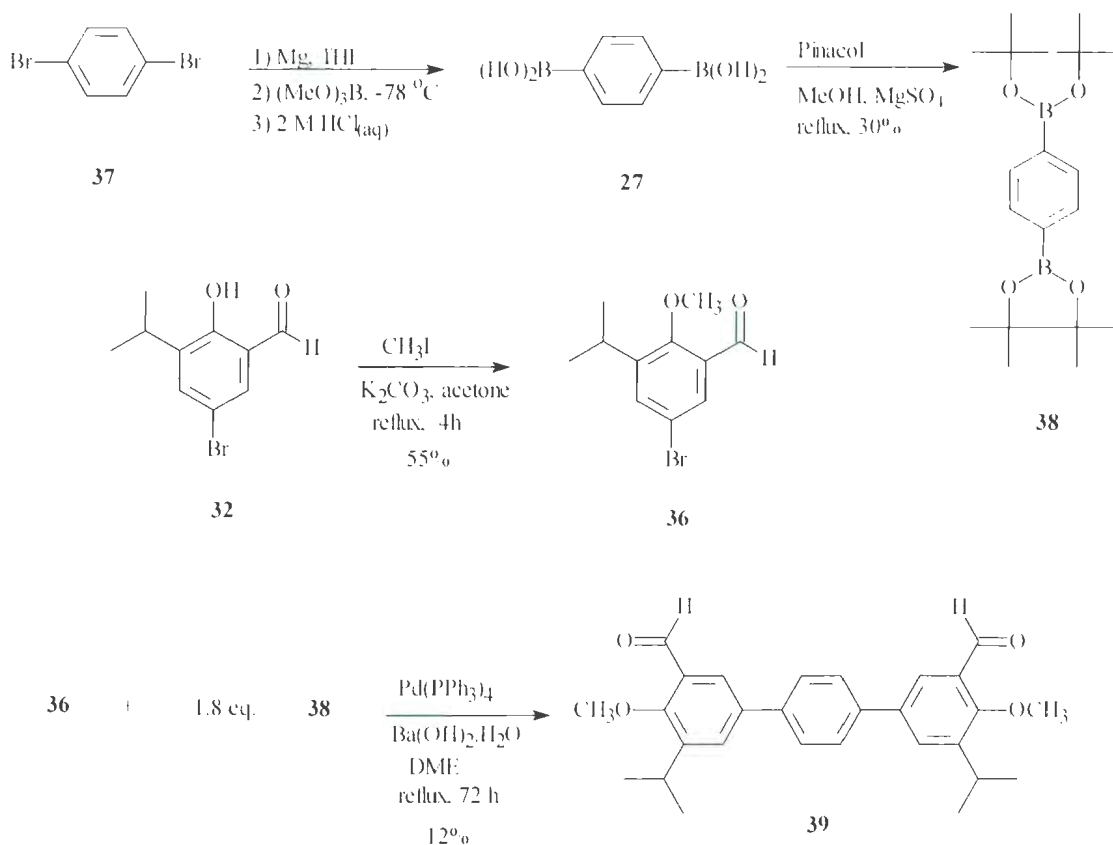
Bisaldehyde **39** was prepared by Suzuki-Miyaura coupling of the diboronic ester **38**, with **36** (Scheme 1.2-8). Reaction of **32** with methyl iodide in acetone in the presence of anhydrous potassium carbonate gave **36** in 55% yield. The  $^1\text{H}$  NMR spectrum of **39** showed a sharp singlet at  $\delta$  3.89 ppm for the methoxy group while the same group appeared at  $\delta$  65.14 ppm in its  $^{13}\text{C}$  NMR spectrum.

Diboronic ester **38** was prepared through a multi-step procedure from 1,4-dibromobenzene (**37**). Quenching the corresponding Grignard reagent formed from **37** with trimethyl borate, followed by hydrolysis of the product with dilute hydrochloric acid, furnished 1,4-benzenediboronic acid (**27**).<sup>12</sup> Heating **27** with pinacol in methanol at reflux afforded the diboronic ester **38** in 30% overall yield for the two steps.

The desired bisaldehyde **39** was obtained, albeit in low yield, from the Suzuki-Miyaura coupling of **38** with bromoanisole **36**. None of the desired product however was obtained when using non-aqueous conditions, that is, toluene under reflux for 24 hours, in the presence of silver carbonate, or cesium carbonate, as the base.<sup>13</sup> In contrast, aqueous barium hydroxide and 1,2-dimethoxyethane (DME) at 80 °C for 24 h, afforded **39** in low yield (12%).<sup>14</sup>

The  $^1\text{H}$  NMR spectrum of compound **39** showed a singlet at  $\delta$  = 7.82 ppm assigned to the four hydrogens of the bridging phenyl ring. Its  $^{13}\text{C}$  NMR spectrum showed the corresponding carbon atoms at  $\delta$  = 127.70 ppm, in addition to the other seven

signals in the aromatic region, an aldehydic carbon at  $\delta = 190.51$  ppm and two isopropyl group carbons at  $\delta = 23.96$  and  $26.43$  ppm. Finally, the mass spectral data showed a molecular ion at  $m/z = 432.2$  which corresponds to **39**.

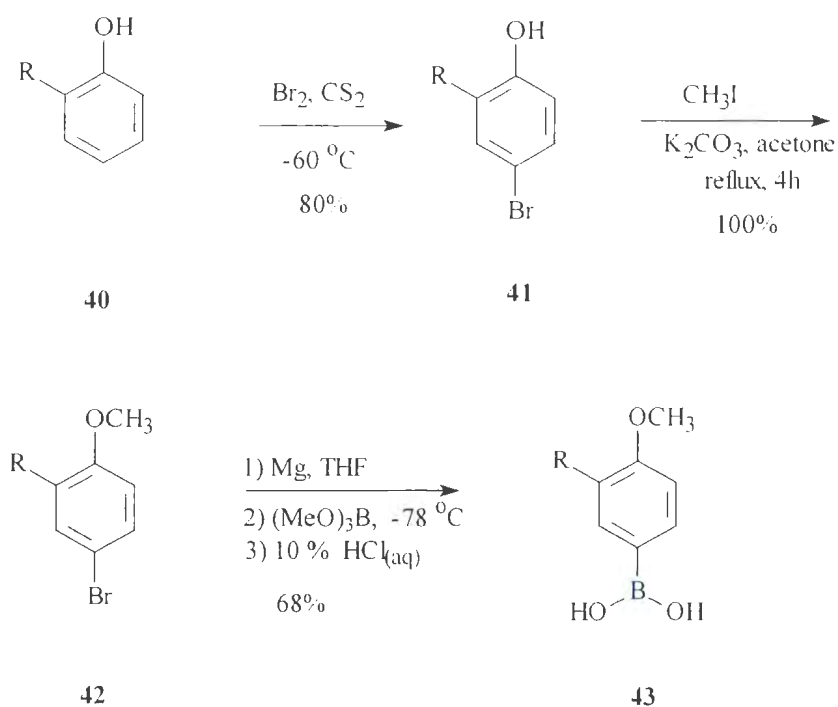


**Scheme 1.2-8: Synthetic route B.**

Although route **B** gave the desired dialdehyde **39**, it was abandoned due to the low yield obtained in the Suzuki-Miyaura step. Also, preparation of other 1,3-phenylenediboronic acids proved more difficult than diboronic acid **27**. Therefore, efforts were focused upon approaches using a monoboronic acid as a precursor, such as **35** (Route **A** in Scheme 1.2-6), or **43** (Route **C** in Scheme 1.2-9).

### 1.2.3.3 Synthetic Route C

This route proved to be easier, more effective, and more versatile than routes **A** or **B**. The key point in this pathway was to build the teraryl systems *via* Suzuki-Miyaura coupling of boronic acid **43**, with either dibromoaryl compounds 1,4-dibromobenzene (**37**), 1,3-dibromobenzene (**44**), or 2,7-dibromonaphthalene (**45**) (Scheme 1.2-10). Subsequent deprotection of the phenolic groups in each of the resulting triaryl systems (Scheme 1.2-13), followed by regioselective formylation of the resulting bisphenolic adducts, afforded the target dialdehyde compounds **57-60** (Scheme 1.2-14).



**Scheme 1.2-9:** Synthetic route **C** to boronic acid **43** ( $\text{R} = \textit{tert}$ -butyl).

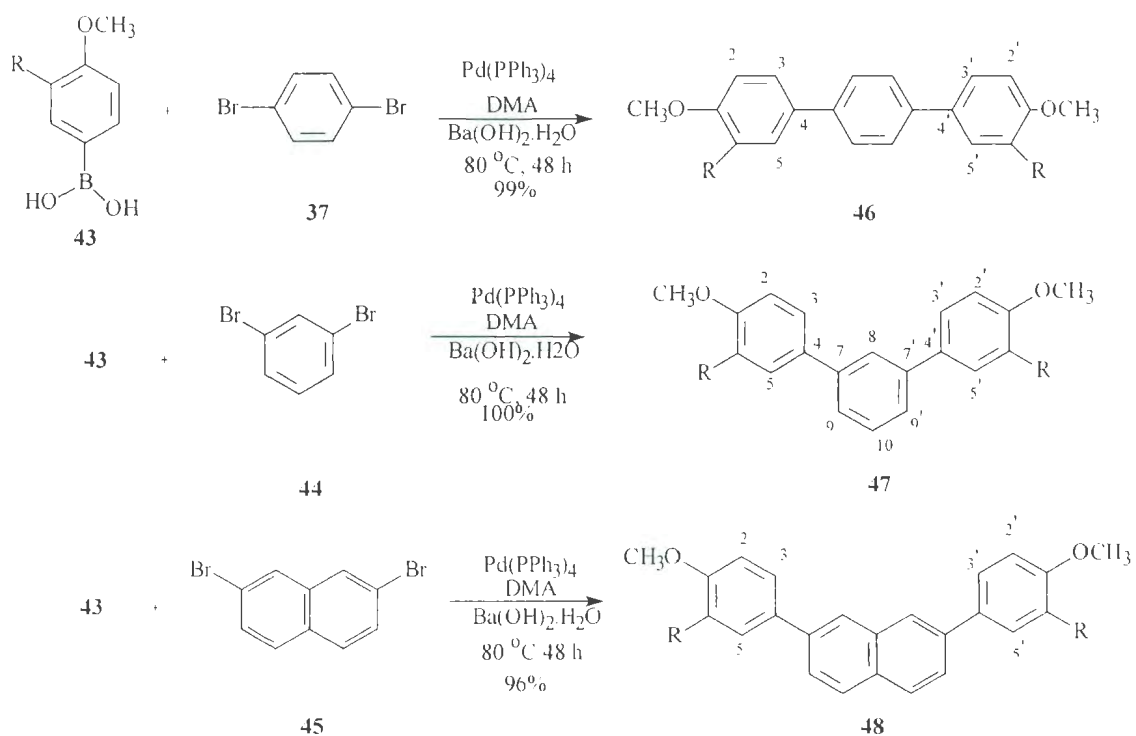
Boronic acid **43** was prepared in several steps from commercially available 2-*tert*-butylphenol (**40**) (Scheme 1.2-9). Bromination of phenol **40** led to a mixture of the corresponding *o*- and *p*-monobrominated isomers. Slow addition of a solution of bromine in CS<sub>2</sub>, under high dilution conditions at low temperature (-60 °C) increased the *para* vs. *ortho* selectivity to give **41** as the major product (80% yield). The <sup>1</sup>H NMR spectrum showed a sharp singlet for the *tert*-butyl group at  $\delta = 1.40$  ppm, a doublet coupled to *ortho*-hydrogen ( $J = 9.0$  Hz) corresponding to the *ortho*-hydrogen to the phenol at  $\delta = 6.56$  ppm and two doublets for the two *meta*-hydrogen atoms at  $\delta = 7.18$  and 7.36 ppm. The <sup>13</sup>C NMR spectrum shows eight peaks: two which were assigned to the *tert*-butyl group, and six to the aromatic carbons.

Methylation of the phenol group in **41** led to 2-*tert*-butyl-4-bromoanisole (**42**) in quantitative yield. Compound **41** was heated overnight at reflux in anhydrous acetone with methyl iodide in the presence of anhydrous potassium carbonate to give, after work-up, **42** as a colourless solid. Its <sup>1</sup>H- and <sup>13</sup>C NMR spectra showed the presence of the methoxy group at  $\delta = 3.83$  and 55.76 ppm, respectively, and its mass spectrum revealed a molecular ion at  $m/z = 244.0$ , consistent with the calculated value for **42**.

Boronic acid **43** was obtained from bromoanisole **42** via the corresponding Grignard reagent, which was generated *in situ* in THF. Quenching with trimethyl borate at low temperature (-78 °C) followed by hydrolysis with aqueous 10% HCl and crystallization from ether:hexane afforded the desired boronic acid **43** as a colourless solid in 68% yield.<sup>15,16</sup> The <sup>1</sup>H- and <sup>13</sup>C NMR spectra of the product showed lower field

aromatic signals when compared with **42**. The molecular ion at  $m/z$  601.3 in its mass spectrum confirmed that the product was the trimer of the desired boronic acid **43**.

### 1.2.3.3.1 Suzuki-Miyaura coupling reactions



**Scheme 1.2-10:** Suzuki-Miyaura coupling reactions of **43** ( $\text{R} = \text{tert-butyl}$ ).

The Suzuki-Miyaura coupling reaction was used to prepare the teraryl products from the reactions of **37**, **44**, and **45** with boronic acid **43** (Scheme 1.2-10).<sup>15</sup> The efficiency of the coupling reaction between boronic acid **43** with **37** and **44**, respectively, depended on the nature of the solvent. The yield of the product obtained from the

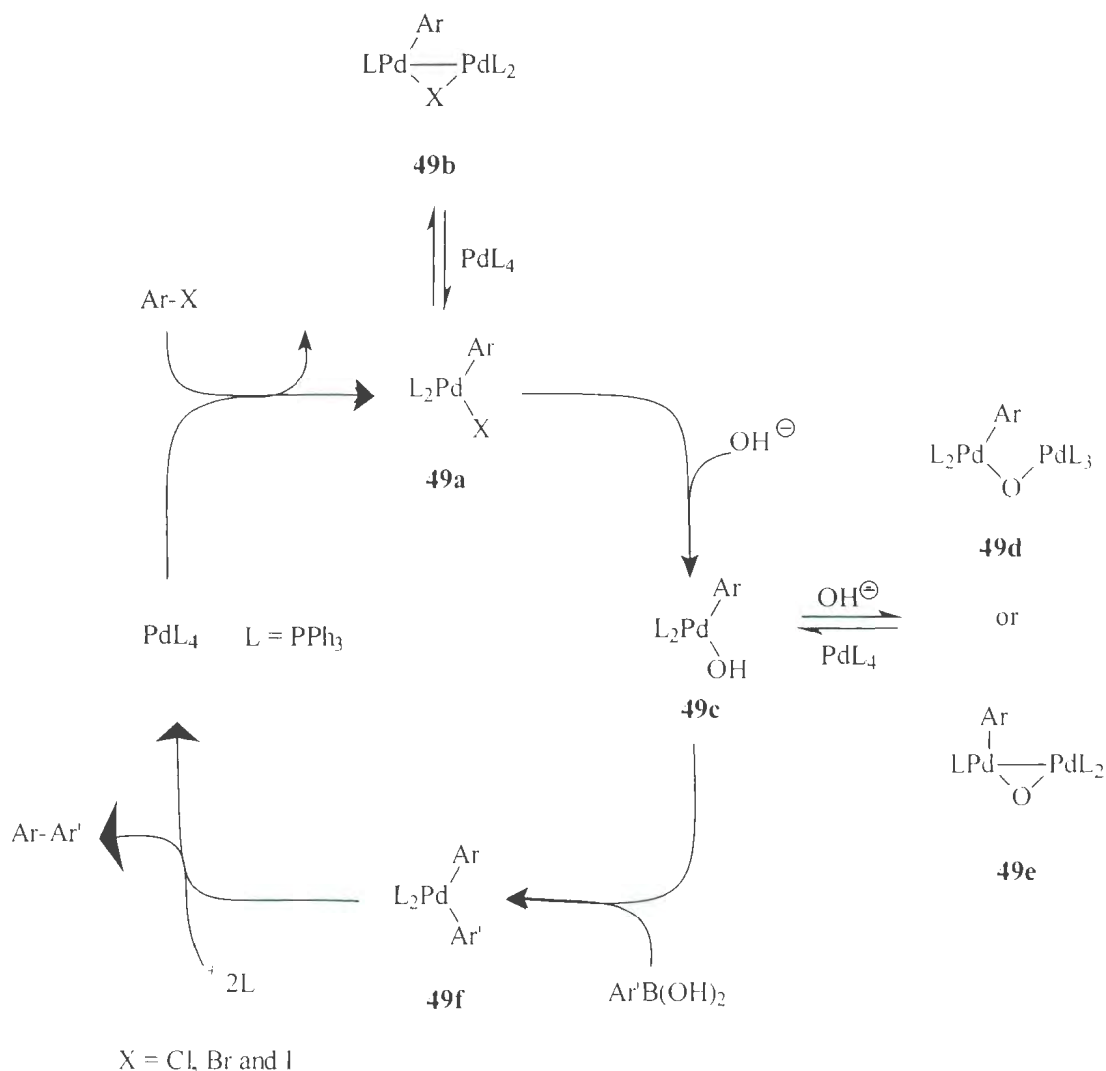
reaction with 1,3-dibromobenzene **44** was found to also depend strongly on the mol% of Pd(0) catalyst used.

**Table 1.2-1: Effect of mol% of catalyst on yields of Suzuki-Miyaura coupling.**

Entry	Starting material	Solvent	Mol% of catalyst	Time of reflux (hr)	Percentage yield (%)
1	<b>37</b>	DME	13	24	76
2	<b>44</b>	DME	13	24	45
3	<b>37</b>	DMA	13	48	98
4	<b>44</b>	DMA	13	48	50
5	<b>44</b>	DMA	1	48	70
6	<b>44</b>	DMA	0.5	48	82
7	<b>44</b>	DMA	0.025	48	100
8	<b>45</b>	DMA	0.025	48	96

As shown in Table 1.2-1, the use of dimethyl ethylene glycol (DME) as the solvent at 80 °C for 24 h, in the presence of barium hydroxide, water and 13.0% Pd(PPh<sub>3</sub>)<sub>4</sub> as the catalyst led to products **46** and **47** in 76% and 45% yields from the reaction of **43** with **37** and **44**, respectively. In the case of **37**, mono-coupling products were also detected by <sup>1</sup>H NMR monitoring of the reaction. In contrast, changing the solvent to *N,N*-dimethylacetamide (DMA), with the same mol% of the Pd catalyst, considerably improved the yield of **46** to 99%. However, using the same conditions with 1,3-dibromobenzene (**44**) afforded **47** in only 50% yield and decreasing the reaction times did not improve its yield. Decreasing the mol% of Pd catalyst from 13.0% to

0.025% and using DMA as the solvent at 80 °C for 48 h with **44**, however, significantly improved the yield of **47** from 50% to quantitative (Table 1.2-1).<sup>17</sup>



**Scheme 1.2-11:** Suzuki-Miyaura coupling mechanism.

It was rationalized that at higher concentrations Suzuki-Miyaura coupling is diminished as a result of  $\text{Pd}(\text{PPh}_3)_4$  self-coupling to form a species such as **49b** (Scheme 1.2-11).<sup>16</sup> At high  $\text{Pd}(\text{PPh}_3)_4$  concentration the effective  $[\text{Pd}(\text{PPh}_3)_4]$  available for the

Suzuki-Miyaura catalytic cycle is reduced. In contrast, at low concentrations, catalyst leakage by this process is effectively diminished. As shown in Scheme 1.2-11, the formation of intermediate **49a** is crucial for the coupling reaction. The high efficiency of this type of palladium-catalyzed reaction is attributed to the generation of species **49c** which is more reactive than intermediate **49a**. It is logical to expect that species **49b** and/or **49e** could be formed at high catalyst concentrations because Pd-Pd dimer complexes are well-known to be stable. These two species (*e.g.* **49b** and **49e**) are inactive in this catalytic cycle. At low Pd(PPh<sub>3</sub>)<sub>4</sub> concentration, therefore, reaction deactivation *via* formation of the inactive species **49b** and **49e** is diminished. The recognition of these factors in the Suzuki-Miyaura coupling reaction was very helpful. Use of decreased, rather than higher, mol% of Pd(PPh<sub>3</sub>)<sub>4</sub> catalyst with **44** also makes this class of reaction less expensive. Additionally, the crude product **47** obtained under the low mol% catalyst conditions was cleaner, as revealed by its <sup>1</sup>H NMR spectrum, and crystallized as large colourless crystals directly from the DMA reaction solution on standing overnight.

Teraryl compound **46** derived from reaction of **37** with **43** gave satisfactory analytical data. Its <sup>1</sup>H NMR spectrum showed that the aromatic peaks were shifted upfield compared to those of boronic acid **43**. Additionally, a singlet at  $\delta = 7.62$  ppm was observed and corresponds to the four equivalent aromatic hydrogens due to 1,4-phenylene group in **46**. The methoxy group showed as a singlet peak at  $\delta = 3.93$  ppm. The hydrogens at C-2,2'; C-3,3' and C-5,5' appeared as a doublet, a doublet of doublets and doublet at  $\delta = 7.01$  (*ortho*,  $J = 9.0$  Hz), 7.51 (*meta*,  $J = 2.0$  and *ortho*,  $J = 8.5$  Hz),

7.62 (*meta*,  $J = 2.5$  Hz), respectively. The  $^{13}\text{C}$  NMR spectrum confirmed the structure of **46**. The spectrum consisted of eight aromatic signals, including the characteristic sharp signal of the 1,4-phenylene group at  $\delta = 127.34$  ppm; three signals at higher field, corresponding to the methoxy groups at  $\delta = 55.61$  ppm, and those at  $\delta = 30.25$  and  $35.46$  ppm due to the *tert*-butyl substituent groups.

The  $^1\text{H}$  NMR spectrum of **47** in  $\text{C}_6\text{D}_6$  also was consistent with its structure. The central 1,3-phenylene group was observed as a triplet at  $\delta = 7.39$  ppm (*ortho*,  $J = 7.5$  Hz), a doublet of doublets at  $\delta = 7.60$  (*meta*,  $J = 2.0$  Hz and *ortho*,  $J = 7.8$  Hz) and a triplet at  $\delta = 8.07$  ppm (*meta*,  $J = 1.8$  Hz). The *p*-methoxyphenyl moiety showed up in the  $^1\text{H}$  NMR spectrum as a doublet at  $\delta = 6.82$  ppm (*ortho*,  $J = 8.0$  Hz) for the hydrogens at C-2,2' (Scheme 1.2-10), a doublet of doublets for the hydrogens at C-3,3' at  $\delta = 7.48$  (*meta*,  $J = 3.0$  Hz and *ortho*,  $J = 8.0$  Hz) and a doublet for the hydrogens at C-5,5' at  $\delta = 7.81$  ppm (*meta*,  $J = 2.5$  Hz). The methoxy and the *tert*-butyl groups appeared as two singlets at  $\delta = 1.69$  and  $3.36$  ppm, respectively. The  $^{13}\text{C}$  NMR spectrum revealed ten aromatic signals due to the six carbons for the *p*-methoxyphenyl moiety (with the characteristic signal for the methoxy-substituted carbon at  $\delta = 158.77$  ppm) and the other four due to the carbons of the central 1,3-phenylene group. The signal at  $\delta = 142.63$  ppm was attributed to the *p*-methoxyphenyl-substituted carbons (C-7,7'). Of the three signals at high field, two are assigned to the *tert*-butyl groups at  $\delta = 30.36$  and  $35.57$  ppm and the third at  $\delta = 55.69$  ppm to the methoxy group carbons.

The Suzuki-Miyaura coupling reaction of **45** with **43** under the same conditions that were used optimally with **45** afforded the desired disubstituted naphthalene **48** in

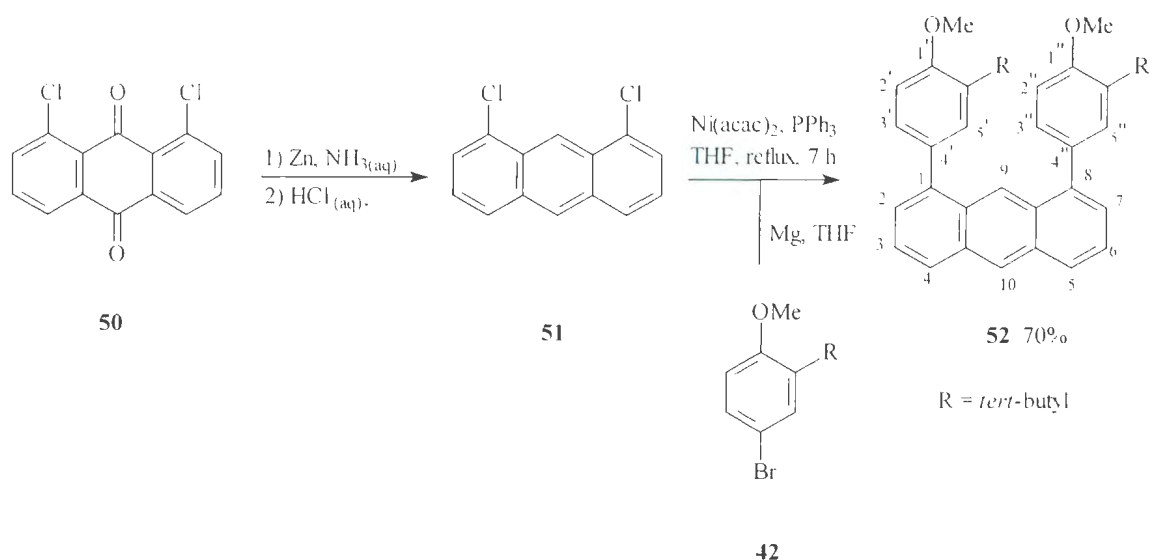
96% yield (Scheme 1.2-10). 2,7-Dibromonaphthalene (**45**) was prepared by the substitution reaction of 2,7-dihydroxynaphthalene with bromine at 340 °C in the presence of PPh<sub>3</sub>.<sup>18a</sup> The <sup>1</sup>H NMR spectrum of the product, **48** in CDCl<sub>3</sub>, revealed a doublet of doublets at  $\delta = 7.73$  ppm (*meta*,  $J = 1.5$  Hz and *ortho*,  $J = 8.5$  Hz), a doublet at  $\delta = 7.91$  ppm (*ortho*,  $J = 8.5$  Hz), and a singlet at  $\delta = 8.05$  ppm due to the 2,7-naphthylene group. The <sup>1</sup>H NMR signals of the *p*-methoxyphenyl substituent groups were similar to those in **47**. The hydrogens at C-2,2'; C-3,3' C-5,5' (Scheme 1.2-10) appeared as a doublet, a doublet of doublets and a doublet at  $\delta = 7.03$  ppm (*ortho*,  $J = 8.5$  Hz), 7.59 ppm (*meta*,  $J = 3.0$  Hz and *ortho*,  $J = 8.8$  Hz) and 7.70 ppm (*meta*,  $J = 3.0$  Hz), respectively. The singlet at  $\delta = 3.93$  ppm was assigned to the methoxy groups. The <sup>13</sup>C NMR spectrum was also consistent with **48**, and revealed twelve signals in the aromatic region. Six of these signals are due to the *p*-methoxyphenyl substituent groups and six are assigned to the 2,7-naphthylene group. Furthermore, three additional signals showed at high field for the *tert*-butyl and methoxy groups. As shown in Table 1.2-2, all of the compounds **46-48**, showed accurate mass measurements for their respective structural formulas.

**Table 1.2-2: Exact molecular mass analysis of Suzuki-Miyaura products.**

Compound No	Structural formula	Found	Calculated
<b>46</b>	C <sub>28</sub> H <sub>34</sub> O <sub>2</sub>	402.25577	402.25508
<b>47</b>	C <sub>28</sub> H <sub>34</sub> O <sub>2</sub>	402.25780	402.25508
<b>48</b>	C <sub>32</sub> H <sub>36</sub> O <sub>2</sub>	452.27160	452.27153

The anthracene-based compound **52**, which could also serve as a different linker towards a calixsalen, was also targeted for synthesis. It was considered to potentially be

better than the naphthalene-based linker used by McAuliffe<sup>2</sup> in **8**, for several reasons. Foremost, a larger cavity size was anticipated. Also, since the two aryl groups on the anthracene scaffold at C-1 and C-8 are further apart from each other than they are in the naphthalene ring-based precursors for **8**, there would be less of a barrier to free rotation of these groups. This should therefore facilitate the desired macrocyclization process over any potential oligo- or polymerization in the Schiff base formation step.



**Scheme 1.2-12:** Preparation of 1,8-bis(3-*tert*-butyl-4-methoxyphenyl)anthracene (**52**).

The 1,8-diaryl-substituted anthracene, **52**, was obtained by Ni-catalyzed coupling of 1,8-dichloroanthracene (**51**) with the corresponding Grignard reagent generated *in situ*, in THF, from bromoanisole (**42**) (Scheme 1.2-12).<sup>18b</sup> The Grignard reagent derived from **42** was added to a solution of **51** and Ni(acac)<sub>2</sub> in the presence of PPh<sub>3</sub>. Using 3 equivalents of **42** afforded the desired product in 70% yield. 1,8-Dichloroanthracene itself was obtained from 1,8-dichloroanthraquinone (**50**) *via* two steps involving

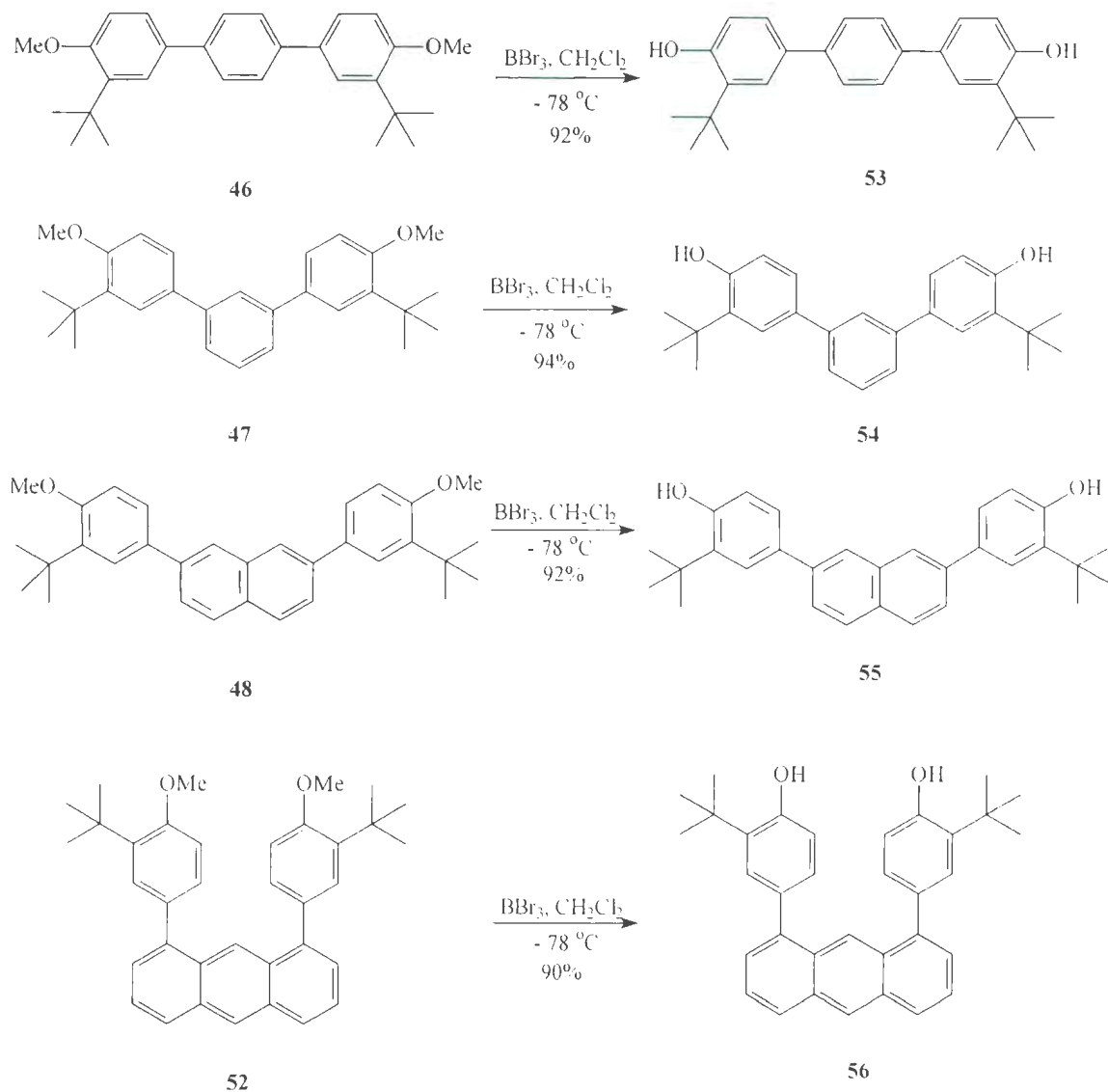
reduction by zinc in aqueous ammonia (30%), followed by hydrolysis using a solution of hydrochloric acid in propanol.<sup>18b</sup>

The <sup>1</sup>H NMR spectrum of **52** was consistent with the proposed structure. Two singlet peaks at  $\delta = 8.55$  and  $8.90$  ppm were assigned to the hydrogens at C-9 and C-10 (Scheme 1.2-12) and two doublets at  $\delta = 7.39$  (*ortho*,  $J = 6.5$  Hz) and  $8.02$  ppm (*ortho*,  $J = 8.5$  Hz) were assigned to the hydrogens at C-2,7 and C-4,5, respectively. The two hydrogens at C-3,6 in the anthracene moiety appeared as pair of doublets at  $\delta = 7.52$  ppm (*ortho*,  $J = 6.5$  Hz) and  $7.53$  ppm (*ortho*,  $J = 7.5$  Hz). The signals assigned to the *p*-methoxyphenyl substituent groups at C-2',2"; C-5',5" and C-3',3", were respectively, as follows: a doublet at  $\delta = 6.93$  ppm (*ortho*,  $J = 8.0$  Hz), another doublet at  $\delta = 7.31$  ppm (*meta*,  $J = 2.5$  Hz) and a doublet of doublets at  $\delta = 7.43$  ppm (*meta*,  $J = 2.3$  Hz and *ortho*,  $J = 8.3$  Hz). The <sup>13</sup>C NMR spectrum, revealed fourteen signals in the aromatic region: six signals are due to the *p*-methoxyphenyl moiety and eight signals are due to the anthracene ring, the two to *p*-methoxyphenyl-substituted carbons 1 and 8 being at  $\delta = 141.22$  ppm.<sup>16</sup> Two signals at  $\delta = 29.87$  and  $34.95$  ppm are due to the *tert*-butyl group, and a third at  $\delta = 55.00$  ppm, is due to the methoxy group. An exact mass measurement for the predicted structural formula C<sub>36</sub>H<sub>38</sub>O<sub>2</sub> further supported the structure **52**.

Finally, the relatively simple <sup>1</sup>H- and <sup>13</sup>C NMR spectra of **46-48** and **52** for each compound provide additional evidence that these compounds are symmetrical structures having C<sub>2v</sub> symmetry.

### 1.2.3.3.2 Demethylation of phenol groups

The methoxy groups in **46–48** and **52** were demethylated using boron tribromide in dry dichloromethane to afford the corresponding phenolic products **53–56** in excellent yields.



**Scheme 1.2-13:** Demethylation reactions of compounds **46–48** and **52**.

(Table 1.2-3 and Scheme 1.2-13).<sup>19</sup> The demethylation step for these compounds was crucial for the subsequent formylation step. Treating **46** with boron tribromide afforded a product which was purified by silica gel column chromatography, to afford the corresponding phenol **53** in 92% yield. Demethylation of **47** gave **54** in 94% yield which was also purified by silica gel column chromatography. However, it proved sufficient to simply wash the crude products from the demethylation reactions of **48** and **52** with hot hexane to obtain clean products **55** and **56** in 92% and 90% yields, respectively.

**Table 1.2-3: Yields and <sup>1</sup>H-, <sup>13</sup>C NMR (CDCl<sub>3</sub>) summary analysis of 53-56.**

Compound No	Yield %	<sup>1</sup> H NMR of resulting OH(ppm)	<sup>13</sup> C NMR of the phenolic carbon (ppm)	<sup>1</sup> H NMR of removed OCH <sub>3</sub> (ppm)	<sup>1</sup> H NMR of removed OCH <sub>3</sub> (ppm)
<b>53</b>	92	4.85	154.00	3.93	55.61
<b>54</b>	94	4.82	154.06	3.36	55.42
<b>55</b>	92	4.84	154.11	3.93	55.42
<b>56</b>	90	4.79	153.75	3.87	55.00

The data presented in Table 1.2-3 shows that the corresponding <sup>1</sup>H- and <sup>13</sup>C NMR signals due to the methoxy groups of the starting materials **46-48** and **52** (ca.  $\delta \approx 3.4 - 3.9$  and 55 ppm, respectively) had disappeared and were replaced by characteristic singlet signals for the newly introduced phenolic hydrogens ( $\delta \approx 4.8$  and 154 ppm, respectively) for compounds **53-56**.

As shown in Table 1.2-4, all of the bisphenolic compounds **53-56** had accurate mass measurements consistent with their corresponding structural formulas.

**Table 1.2-4: Exact molecular masses for compounds 53-56.**

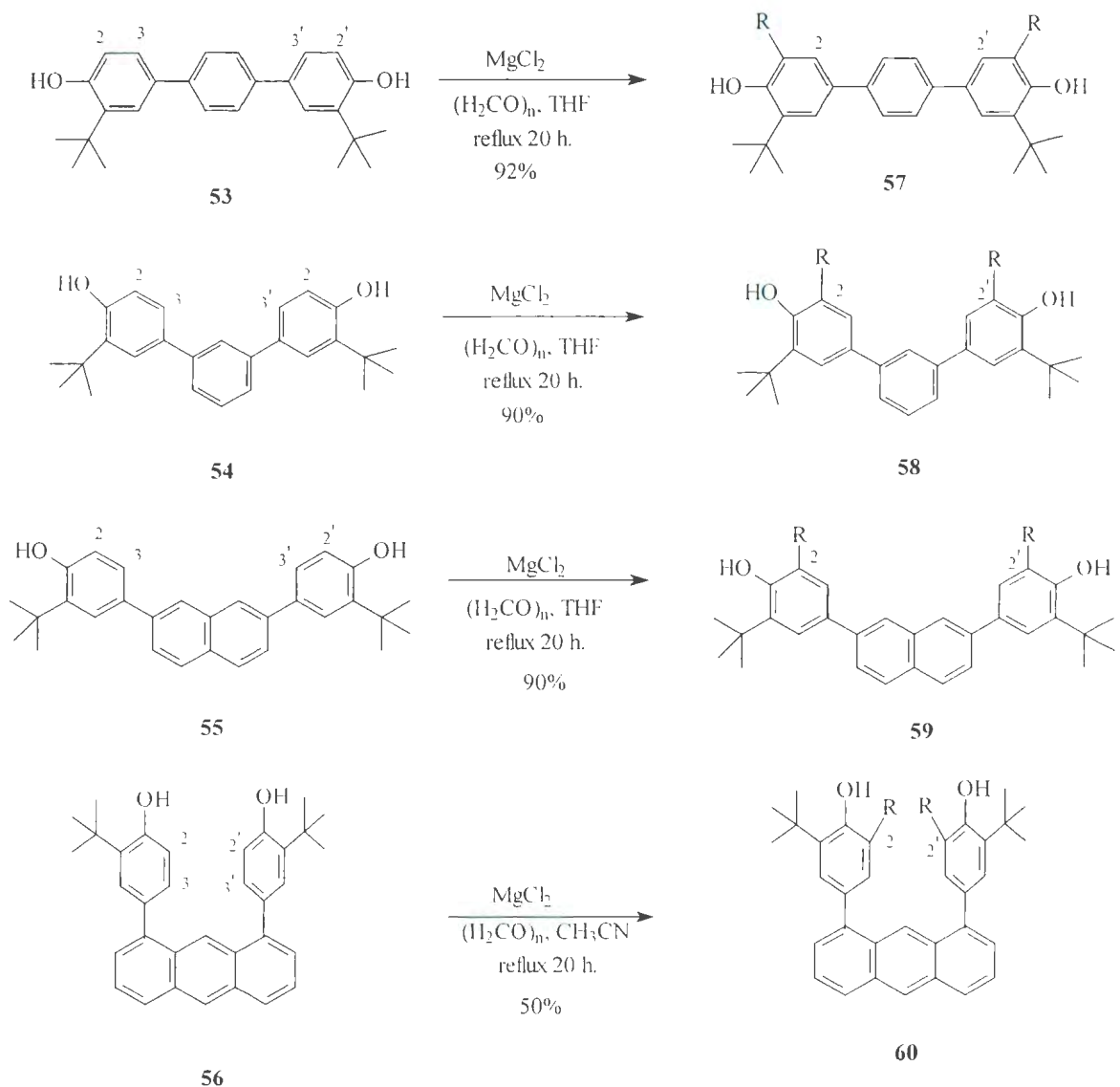
Compound No	Structural formula	Found	calculated
53	C <sub>26</sub> H <sub>30</sub> O <sub>2</sub>	374.22744	374.22458
54	C <sub>26</sub> H <sub>30</sub> O <sub>2</sub>	374.22614	374.22458
55	C <sub>30</sub> H <sub>32</sub> O <sub>2</sub>	424.24190	424.24020
56	C <sub>34</sub> H <sub>34</sub> O <sub>2</sub>	474.25690	474.25590

### 1.2.3.3.3 *Ortho*-regioselective formylation of the bisphenols 53-56.

Regioselective *ortho*-formylation was used to generate the desired dialdehyde compounds 57-60. This was achieved by refluxing bisphenols 53-56 with anhydrous magnesium chloride and paraformaldehyde in either anhydrous acetonitrile,<sup>20</sup> or THF,<sup>21</sup> in the presence of triethylamine (Scheme 1.2-14). Anhydrous conditions are crucial requirements for these reactions. The mild conditions of magnesium chloride as a Lewis acid in this reaction proved to be very effective.

**Table 1.2-5: Formylation reaction yields in THF and acetonitrile.**

Entry	Starting material	Solvent	Time	Yield %
1	53	CH <sub>3</sub> CN	20	52
2	54	CH <sub>3</sub> CN	20	87
3	55	CH <sub>3</sub> CN	48	65
4	56	CH <sub>3</sub> CN	72	50
5	53	THF	20	92
6	54	THF	20	90
7	55	THF	20	90



**Scheme 1.2-14:** Formylation reactions of phenols **57-60** ( $\text{R} = \text{CHO}$ ).

Using THF as the solvent afforded the desired products in high yields and as "cleaner" crude products than when acetonitrile was used (Table 1.2-5). The crude product from the reaction of **56** was a mixture. Using silica gel column chromatography, several different solvent systems were tried but were unsuccessful in purifying this

mixture. Nevertheless, one of the products was eventually isolated by simple precipitation from CH<sub>2</sub>Cl<sub>2</sub> solution as a fairly clean product in 50% yield.

The <sup>1</sup>H- and <sup>13</sup>C NMR spectra were consistent for the structures of **57-60**. The <sup>1</sup>H NMR spectra of **57-60** showed that the phenolic hydrogen atoms appeared at low fields at  $\delta \approx 11.8$  ppm (Table 1.2-6). The aldehydic hydrogen atoms appeared as singlet peaks around  $\delta \approx 10$  ppm and the <sup>13</sup>C NMR spectra showed signals at around  $\delta \approx 197.6$  ppm due to the aldehydic carbons.

**Table 1.2-6: <sup>1</sup>H-, <sup>13</sup>C NMR summary analysis of 57-60.**

Compound No	<sup>1</sup> H NMR of -CHO	<sup>13</sup> C NMR of -CHO	<sup>1</sup> H NMR of -OH	<sup>13</sup> C NMR of -OH
<b>57</b>	10.00	197.45	11.83	161.60
<b>58</b>	10.00	197.41	11.86	161.23
<b>59</b>	10.02	197.39	11.87	161.01
<b>60</b>	9.87	196.94	11.79	160.83

Furthermore, the hydrogens at C-2 and C-2' (Table 1.2-7) in the starting materials **53-56** (Scheme 1.2-14), which appeared as doublet signals at  $\delta = 6.77$  ppm (*ortho*,  $J = 8.0$  Hz), disappeared from the <sup>1</sup>H NMR spectra of the products **57-60**. Also, the carbon signals for C-2,2' were shifted downfield from  $\delta \approx 117$  ppm to 138-139 ppm. The chemical shifts of the hydrogens at C-3,3' in **53-60**, which usually appeared as doublets of doublets at  $\delta \approx 7.35-7.47$  ppm (*meta*,  $J = 2.5-1.0$  Hz and *ortho*, 8.5-8.0 Hz), were shifted to lower field in **57-60** appearing at  $\delta = 7.56-7.95$  ppm (*meta*,  $J = 1.5-2.0$  Hz).

**Table 1.2-7: <sup>1</sup>H- and <sup>13</sup>C NMR summary analysis of 53-60.**

Compound No	<sup>1</sup> H NMR of H-C-2,2' (ppm)	<i>o</i> - <i>J</i> of H-C-2,2' (Hz)	<sup>13</sup> C NMR of C-2,2' (ppm)	<sup>1</sup> H NMR of H-C-3,3' (ppm)	<i>J</i> of H-C-3,3' (Hz)
53	6.76	8.5	117.17	7.35	2.5, 8.0
54	6.77	8.0	117.16	7.35	2.3, 9.4
55	6.80	8.5	117.27	7.47	2.3, 8.0
56	6.72	8.5	116.82	7.23	2.3, 7.3
57	-	-	139.35	7.82	1.5
58	-	-	139.17	7.84	2.0
59	-	-	138.22	7.95	1.5
60	-	-	138.22	7.56	2.0

**Table 1.2-8: Exact molecular masses for compounds 57-60.**

Compound No	Structural formula	Found	calculated
57	C <sub>28</sub> H <sub>30</sub> O <sub>4</sub>	430.21431	430.21443
58	C <sub>28</sub> H <sub>30</sub> O <sub>4</sub>	430.21280	430.21443
59	C <sub>32</sub> H <sub>32</sub> O <sub>4</sub>	480.22990	480.23006
60	C <sub>36</sub> H <sub>34</sub> O <sub>4</sub>	530.24570	530.24571

As shown in Table 1.2-8, the compounds **57-60**, gave satisfactory accurate mass measurement values for the proposed structural formulas.

### 1.2.4 Summary

The target bisaldehyde systems **57-60** were successfully synthesized in ~ 46, 46, 44 and 26% overall yields, respectively, in six steps starting with 2-*tert*-butylphenol **40**. The strategy of performing the regioselective formylation step at the end of the synthesis, after building the terphenyl systems *via* Suzuki-Miyaura coupling was very efficient. This synthetic route was shortened by avoiding several steps required for protection and deprotection of the aldehyde groups. Furthermore, this strategy used only one stable, and easy to make, boronic acid. Route **B** involved preparation of different diboronic acids, most of which have not been reported in the literature. The Suzuki-Miyaura coupling reaction afforded the desired terphenyls **46-48** in high yield (99, 100 and 96%, respectively) and its efficiency was attributed to the use of low mol percentages of the Pd(PPh<sub>3</sub>)<sub>4</sub> catalyst in DMA as the solvent. All the compounds thus produced were characterized by <sup>1</sup>H NMR, <sup>13</sup>C NMR and accurate mass spectrometry.

## 1.2.5 Experimental Section

### Materials

Chemical reagents and solvents were purchased from Sigma-Aldrich and were used as received. THF used for synthesizing the bisaldehyde systems was further purified by distillation over sodium. Dichloromethane was dried over phosphorus pentoxide and then distilled over calcium hydride.

### Methods

All reactions for the syntheses of bisaldehyde systems were conducted under argon or nitrogen. Nitrogen gas was purified by passing through a series of columns containing DEOX (Alpha) catalyst heated to 120 °C, granular P<sub>4</sub>O<sub>10</sub>, and activated 3 Å molecular sieves. Organic solvents were evaporated under reduced pressure using a rotary evaporator. Flash chromatography was performed on SAI silica gel, particle size 32-63 µm, pore size 60 Å. Preparative thin-layer chromatography plates (PLC) were made from SAI F-254 silica gel for TLC (particle size 5-15 µm). Thin-layer chromatography was performed using percolated SAI F-254 silica gel plates layer thickness 200 µm.

### Instrumentation

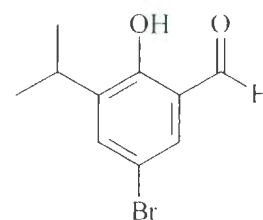
Melting points (mp) were determined on a MEL-TEMP II apparatus and are uncorrected. Mass spectra of compounds were obtained using LCMS (HP series 1100) or GCMS (HP 5972 series II). Unless otherwise specified, all <sup>1</sup>H- and <sup>13</sup>C NMR were

recorded on a GE-300 MHz spectrometer or on a Bruker AM-500 Fourier Transform spectrometer using  $\text{CDCl}_3$  containing  $\text{Me}_4\text{Si}$  as an internal standard. Chemical shifts for the  $^1\text{H}$  NMR spectra are relative to the internal standard at 0.00 ppm. Data were reported as follows: chemical shift, multiplicity (s = singlet, d = doublet, dd = doublet of doublets, t = triplet, b = broad, h = heptet, m = multiplet), coupling constant ( $J$ , Hz), integration and assignment ( $m\text{H-x}$ , where  $m$  denotes the number of protons at position  $x$  in the molecule).  $^1\text{H}$ - and  $^{13}\text{C}$  NMR spectra were processed using "Nuts" software. Chemical shifts for  $^{13}\text{C}$  NMR spectra are relative to the solvent 77.23 ppm for  $\text{CDCl}_3$ .

### Syntheses:

#### 4-Bromo-6-formyl-2-isopropylphenol (32).

A solution of bromine (9.74 g, 0.0610 mol) in  $\text{CCl}_4$  (50 mL) was added dropwise over 1 h to a solution of 5-formyl-2-isopropylphenol (10.0 g, 0.0610 mol) in  $\text{CCl}_4$  (100 mL) at room temperature. The reaction mixture was stirred for 4 h. The solvent was evaporated under vacuum to give a product with a

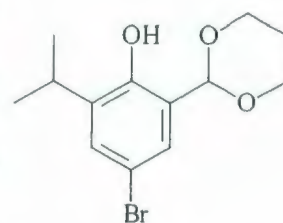


32

clean  $^1\text{H}$  NMR spectrum (13.7 g, 94%): mp 75-77 °C;  $^1\text{H}$  NMR ( $\text{CDCl}_3$ )  $\delta$  1.25 (d,  $J = 7.0$  Hz, 6H), 3.35 (h, 1 H), 7.52 (d,  $J = 2.0$  Hz, 2H), 7.53 (d,  $J = 2.5$  Hz, 2H), 9.83 (s, 2H), 11.30 (s, 1H);  $^{13}\text{C}$  NMR ( $\text{CDCl}_3$ )  $\delta$  22.28, 26.67, 111.63, 121.50, 133.21, 136.66, 140.18, 158.50, 195.95. ; MS (ESMS)  $m/z$  243.2 ( $\text{M}^+$ ), calcd for  $\text{C}_{10}\text{H}_{11}\text{BrO}_2$  243.0.

### 2-[5-Bromo-3-isopropyl-2-hydroxyphenyl]-1,3-dioxane (33).

In a 50 mL round-bottom flask, a stirred mixture of **32** (2.00 g, 8.20 mmol), 1,3-propanediol (1.25 g, 16.0 mmol), sodium sulfate (2.00 g) and alumina (pH = 4, 2.00 g) in dry  $\text{CCl}_4$  (10 mL) was heated at reflux for 60 h. The reaction mixture was cooled and the product was extracted with dichloromethane (3 x 25 mL),

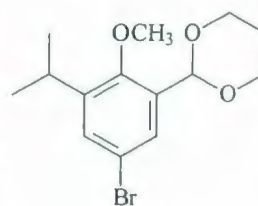


**33**

then filtered. The filtrate was washed with water (2 x 20 mL) then dried over  $\text{MgSO}_4$  and filtered. The solvent was evaporated to give a colourless solid having a clean  $^1\text{H}$  NMR spectrum (2.30 g, 93%): mp 92-94 °C  $^1\text{H}$  NMR ( $\text{CDCl}_3$ ):  $\delta$  1.22 (d,  $J = 6.5$  Hz, 6H), 2.18-2.31 (m, 2H), 3.30 (h,  $J = 6.5$  Hz, 1H) 3.98-4.04 (m, 2H), 4.30-4.33 (m, 2 H), 5.59 (s, 1 H), 7.17 (d,  $J = 2.5$  Hz, 1 H), 7.27 (d,  $J = 2.5$  Hz, 1H), 7.99 (s, 1H);  $^{13}\text{C}$  NMR ( $\text{CDCl}_3$ )  $\delta$  22.58, 25.81, 26.99, 67.83, 102.60, 111.815, 123.66, 127.92, 130.21, 139.05, 151.82; MS (ESMS)  $m/z$  300.0 ( $\text{M}^+$ ), calcd for  $\text{C}_{13}\text{H}_{17}\text{BrO}_3$  301.18.

### 2-[5-Bromo-3-isopropyl-2-methoxyphenyl]-1,3-dioxane (34).

A mixture of phenol **33** (1.57 g, 5.23 mmol), anhydrous  $\text{K}_2\text{CO}_3$  (3.60 g, 26.0 mmol) and iodomethane (7.41 g, 52.4 mmol) in dry acetone (22 mL) was stirred overnight under reflux. After the reaction mixture was cooled to room temperature, the acetone was evaporated under vacuum. The residue was dissolved in



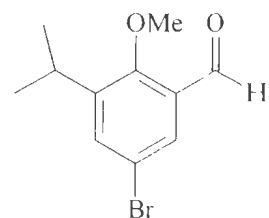
**34**

dichloromethane (20 mL) and filtered. The solvent was evaporated under vacuum to give **34** as a colourless solid (1.45 g, 88%): mp 108-110 °C;  $^1\text{H}$  NMR ( $\text{CDCl}_3$ )  $\delta$  1.21 (d,  $J = 6.9$  Hz, 9 H), 2.20-2.29 (m, 2 H), 3.29 (h,  $J = 6.9$  Hz, 1 H), 3.78 (s, 3 H), 3.97-4.02 (m, 2

H), 4.23-4.27 (m, 2 H), 5.77 (s, 1H), 7.35 (d,  $J = 2.5$  Hz, 1 H), 7.61 (d,  $J = 2.5$  Hz, 1H);  $^{13}\text{C}$  NMR ( $\text{CDCl}_3$ )  $\delta$  23.85, 25.894, 26.54, 63.22, 67.72, 97.27, 117.95, 128.22, 130.70, 134.11, 144.38, 154.03; ESMS ( $m/z$ ) 316 (M+H), calcd for  $\text{C}_{14}\text{H}_{19}\text{BrO}_3$  315.2.

### 5-Bromo-3-isopropyl-2-methoxybenzaldehyde (**36**).

A mixture of phenol **32** (3.00 g, 0.0123 mol), anhydrous  $\text{K}_2\text{CO}_3$  (8.51 g) and iodomethane (17.44 g, 0.123 mol) in dry acetone (51 mL) was stirred overnight under reflux. Cooling the reaction mixture to room temperature was followed by evaporation of acetone under vacuum. The residue was

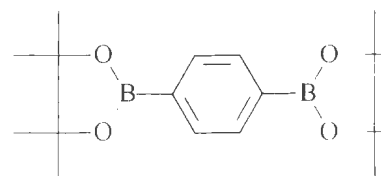


**36**

dissolved in hexane (50 mL), filtered and then purified by silica gel column chromatography using 5% ethyl acetate:hexane to afford **36** as a colourless liquid (1.76 g, 55.3%):  $^1\text{H}$  NMR ( $\text{CDCl}_3$ )  $\delta$  1.25 (d,  $J = 6.9$  Hz, 6H), 3.34 (h,  $J = 6.9$  Hz, 1H), 3.89 (s, 3H), 7.60 (d,  $J = 2.5$  Hz, 2H), 7.79 (d,  $J = 2.5$  Hz, 2H), 10.29 (s, 2H);  $^{13}\text{C}$  NMR ( $\text{CDCl}_3$ )  $\delta$  23.68, 26.31, 65.14, 116.90, 129.30, 130.51, 136.25, 153.67, 160.06, 189.08; MS (ESMS)  $m/z$  256.0 ( $\text{M}^+$ ), calcd for  $\text{C}_{11}\text{H}_{13}\text{BrO}_2$  257.1.

### 1,4-Benzenediboronic acid, dipinacol ester (**38**).

A dry 250 mL round-bottom flask was charged with magnesium turnings (1.22 g), a crystal of iodine and dry THF (50 mL). A few drops of a solution of 1,4-dibromobenzene (6.00 g, 2.55 mmol)



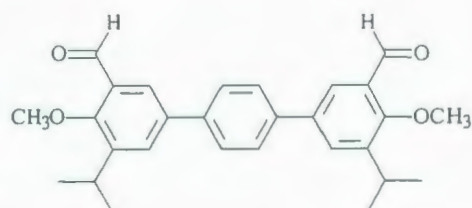
**38**

in THF (50 mL) were added under nitrogen atmosphere and the mixture was heated until

the reaction initiated. After the rest of the 1,4-dibromobenzene (**37**) solution was added dropwise, the reaction was heated at reflux for 8 h. The reaction mixture was cooled to  $-78\text{ }^{\circ}\text{C}$  and the Grignard reagent was treated by dropwise addition of trimethyl borate (15.9 g, 0.153 mol). After warming to room temperature the mixture was stirred overnight. The reaction was quenched with aqueous HCl solution (50 mL, 1.0 M), and the mixture was stirred for 30 min. The organic layer was separated and the product was extracted with ethyl ether (2 x 40 mL). The organic layer was dried over  $\text{MgSO}_4$ , filtered and the solvent was evaporated to give **27** (1.54 g) as a colourless solid. The crude product was heated at reflux for 12 h in a 50 mL-round bottom flask with pinacol (5.32 g, 0.045 mol) and anhydrous  $\text{Na}_2\text{SO}_4$  (1.00 g) in 20 mL of toluene. The reaction was cooled and dichloromethane (30 mL) was added. The mixture was washed with water (2 x 30 mL) and the combined separated organic layers was dried over  $\text{MgSO}_4$ , filtered and the solvent was evaporated. The product was purified by silica gel column chromatography using 30% ethyl ether:hexane eluent to afford **38** (2.53 g, 30.0%) as a colourless solid: mp  $230\text{--}232\text{ }^{\circ}\text{C}$  (Lit:  $234\text{--}236\text{ }^{\circ}\text{C}$ ,<sup>22</sup> and  $226\text{ }^{\circ}\text{C}$ <sup>23</sup>);  $^1\text{H}$  NMR ( $\text{CDCl}_3$ )  $\delta$  1.36 (s, 24H), 7.82 (s, 4H);  $^{13}\text{C}$  NMR ( $\text{CDCl}_3$ )  $\delta$  25.08, 84.05, 134.09; MS (ESMS)  $m/z$  330.3 ( $\text{M}^+$ ), calcd for  $\text{C}_{18}\text{H}_{28}\text{B}_2\text{O}_4$  330.0.

#### 1,4-Bis[4-(5-formyl-3-isopropyl-4-methoxyphenyl)benzene (**39**).

A mixture of **38** (0.141 g, 0.904 mmol), 5-bromo-3-isopropyl-2-methoxybenzaldehyde (**36**) (0.420 g, 1.63 mmol), barium hydroxide

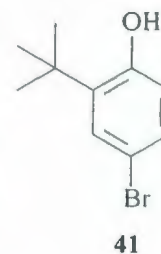


**39**

monohydrate (1.35 g, 7.20 mmol), 1,2-dimethoxyethane (8.0 mL), H<sub>2</sub>O (1 mL), and Pd(PPh<sub>3</sub>)<sub>4</sub> (0.022 g, 0.018 mmol), was heated at 80 °C for 24 h under nitrogen. The resulting mixture was cooled and benzene (25 mL) was added. The mixture was washed with water (2 x 20 mL) and the organic layer dried over MgSO<sub>4</sub> and then filtered. The benzene was evaporated under vacuum and the product was crystallized from 5% ethyl acetate:hexane to afford **39** (0.042 g, 12%) as a colourless solid: mp 180-181 °C; <sup>1</sup>H NMR (CDCl<sub>3</sub>) δ 1.35 (d, *J* = 6.5 Hz, 6 H), 3.47 (h, 1 H) 3.97 (s, 3 H) 7.80 (s, 4H), 7.81 (d, *J* = 2.5 Hz, 2H), 7.98 (d, *J* = 2.0 Hz, 2H), 10.46 (s, 2H); <sup>13</sup>C NMR (CDCl<sub>3</sub>) δ 23.96, 26.43, 65.10, 125.10, 127.70, 129.64, 131.97, 137.36, 139.39, 143.83, 160.48, 190.51; MS (APCI) (*m/z*) 431.2 (M<sup>+</sup>+H), calcd for C<sub>28</sub>H<sub>30</sub>O<sub>4</sub> 430.5.

#### 4-Bromo-2-*tert*-butylphenol (**41**).

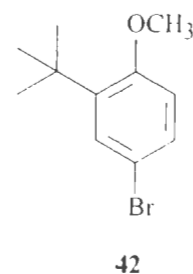
A solution of bromine (21.3 g, 0.133 mol) in 50 mL CS<sub>2</sub> was added dropwise over 3 h to a solution of 2-*tert*-butylphenol **40** (20.0 g, 0.133 mol) in 100 mL of CS<sub>2</sub> kept at -60 °C. The solvent was evaporated and the product was purified by silica gel column chromatography,



initially by using hexane, then with 20:80 ethyl acetate:hexane eluent. The product was dried on a vacuum line for 24 h to give **41** (24.8 g, 80%): <sup>1</sup>H NMR (CDCl<sub>3</sub>) δ 1.40 (s, 9H), 4.82 (s, 1H), 6.56 (d, *J* = 9.0 Hz, 1H), 7.18 (dd, *J* = 2.0, 9.0 Hz, 1H), 7.36 (d, *J* = 2.0 Hz, 1H); <sup>13</sup>C NMR (CDCl<sub>3</sub>) δ 29.78, 35.18, 113.39, 118.59, 130.01, 130.60, 139.00, 153.71; MS (APCI) *m/z* 227.0 [M-H], calcd for C<sub>10</sub>H<sub>13</sub>BrO 228.0.

#### 4-Bromo-2-*tert*-butylanisole (**42**).

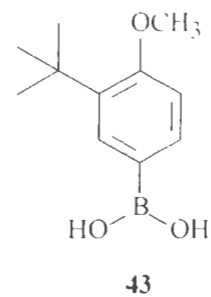
A mixture of phenol **41** (12.0 g, 0.0520 mol), anhydrous K<sub>2</sub>CO<sub>3</sub> (43.0 g) and iodomethane (74.0 g, 0.524 mol) in dry acetone (300 mL) was stirred overnight under reflux. The reaction mixture was cooled to



room temperature and the solvent removed under vacuum. The crude product was dissolved in 50 mL of hexane and filtered. Evaporation of the solvent under vacuum afforded **41** as a colourless solid (12.7 g, 100%), mp 31-32 °C (Lit.<sup>24</sup> ~ 30 °C); <sup>1</sup>H NMR (CDCl<sub>3</sub>) δ 1.37 (s, 9H), 3.83 (s, 3H), 6.75 (d, *J* = 9.0 Hz, 1H), 7.29 (dd, *J* = 2.5, 8.5 Hz, 1H), 7.37 (d, *J* = 2.5 Hz, 1H); <sup>13</sup>C NMR (CDCl<sub>3</sub>) δ 29.94, 35.43, 55.65, 113.32, 113.60, 129.91, 130.10, 130.19, 141.06, 158.00; MS (APCI) *m/z* = 244.1 (M<sup>+</sup>+H), calcd for C<sub>11</sub>H<sub>13</sub>BrO 243.0.

#### 3-*tert*-Butyl-4-methoxyphenylboronic acid (**43**).

A dry round-bottom flask was charged with magnesium turnings (0.979 g, 0.0400 mol), a crystal of iodine and dry THF (100 mL). A few drops of the solution of **42** (8.50 g, 0.037 mol) in THF (50 mL) was added under nitrogen atmosphere and the mixture heated until



the reaction initiated. Once initiation occurred, the reaction was maintained at reflux by the dropwise addition of the remainder of the solution of 4-bromoanisole. The resulting grey solution was heated under reflux for a further 2 h, prior to cooling to -78 °C. To the resulting Grignard reagent was then added dropwise, trimethyl borate (8.3 mL, 0.070 mol) and the mixture was allowed to warm to room temperature overnight. The reaction was

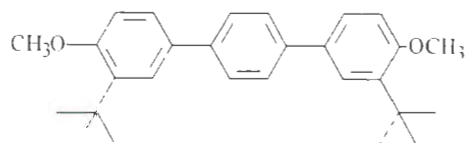
quenched with aqueous of 10% HCl (10 mL), and the mixture was concentrated under vacuum, and partitioned between equal volumes of diethyl ether and aqueous 10% HCl (150 mL). The organic phase was dried over MgSO<sub>4</sub>, filtered and evaporated, to yield a lightly-coloured solid which was crystallized from diethyl ether-hexane to give **43** as colourless solid (5.0 g, 69 %): mp 172-174 °C; <sup>1</sup>H NMR (CDCl<sub>3</sub>) δ 1.48 (s, 9H), 3.94 (s, 3H), 7.02 (d, *J* = 8.5 Hz, 1H), 8.08 (dd, *J* = 1.5, 8.0 Hz, 1H), 8.21 (d, *J* = 1.5 Hz, 1H); <sup>13</sup>C NMR (CDCl<sub>3</sub>) δ 30.09, 35.28, 55.35, 111.36, 134.54, 135.87, 137.83; MS (APCI) *m/z* 601.3 (3M-H<sub>2</sub>O) C<sub>33</sub>H<sub>48</sub>B<sub>3</sub>O<sub>8</sub> 601.4.

#### **Suzuki-Miyaura coupling reactions. General procedure:**

A mixture of the respective dibromoaryl compounds **37**, **44** or **45** (0.756 g, 3.21 mmol), boronic acid **43** (1.46 g, 7.40 mmol), barium hydroxide monohydrate (2.42 g, 0.0128 mol), *N,N*-dimethylacetamide (25 mL) and H<sub>2</sub>O (5 mL) was thoroughly degassed by a nitrogen stream before the addition of Pd(PPh<sub>3</sub>)<sub>4</sub> (2.0 mg, 0.00160 mmol). The mixture was then heated at 80 °C for 48 h under nitrogen. The resultant mixture was cooled and dichloromethane (25 mL) added. The organic phase was separated and washed with 10% hydrochloric acid (25 mL x 4) and dried over MgSO<sub>4</sub>. The solution of the product in the remaining reaction solvent (DMA) was concentrated after evaporating of dichloromethane under reduced pressure. The following coupling products were obtained:

### 1,4-Bis(3-*tert*-butyl-4-methoxyphenyl)benzene (**46**).

The product was crystallized from the reaction solvent after adding methanol (10 mL) to give **46** as a colourless solid in 99% yield: mp



**46**

218-220 °C;  $^1\text{H}$  NMR ( $\text{CDCl}_3$ )  $\delta$  1.50 (s, 18H),

3.93 (s, 6H), 7.01 (d,  $J = 9.0$  Hz, 2H), 7.51 (dd,  $J = 2.0, 8.0$  Hz, 2H), 7.62 (d,  $J = 2.5$  Hz,

2H), 7.62 (s, 4H);  $^{13}\text{C}$  NMR ( $\text{CDCl}_3$ )  $\delta$  30.00, 35.21, 55.37, 112.10, 125.62, 125.81,

127.43, 133.11, 138.71, 139.96, 158.36; MS (APCI)  $m/z$  403.3 ( $\text{M}^+\text{+H}$ ), calcd for

$\text{C}_{28}\text{H}_{34}\text{O}_2$  402.3.

### 1,3-Bis(3-*tert*-butyl-4-methoxyphenyl)benzene (**47**).

The product crystallized from the reaction solvent DMA on standing overnight. The colourless crystals were purified by column chromatography and eluted by 5%



**47**

dichloromethane-hexane to give **47** as a colourless solid in 100% yield: mp 106-108 °C;

$^1\text{H}$  NMR ( $\text{C}_6\text{D}_6$ )  $\delta$  1.69 (s, 18H), 3.36 (s, 6H), 6.82 (d,  $J = 8.0$  Hz, 2H), 7.39 (t,  $J = 7.5$  Hz,

1H), 7.48 (dd,  $J = 2.5, 8.0$  Hz, 2H), 7.60 (dd,  $J = 2.0, 7.8$  Hz, 2H), 7.81 (d,  $J = 2.5$  Hz,

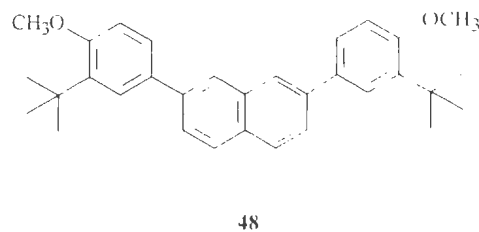
2H), 8.07 (t,  $J = 1.8$  Hz, 1H);  $^{13}\text{C}$  NMR ( $\text{CDCl}_3$ )  $\delta$  30.00, 35.21, 55.35, 112.08, 125.43,

125.90, 126.01, 126.21, 129.19, 133.65, 138.71, 142.28, 158.43; MS (APCI)  $m/z$  403.1

( $\text{M}^+\text{+H}$ ), calcd for  $\text{C}_{28}\text{H}_{34}\text{O}_2$  402.3.

### 2,7-Bis(3-*tert*-butyl-4-methoxyphenyl)naphthalene (**48**).

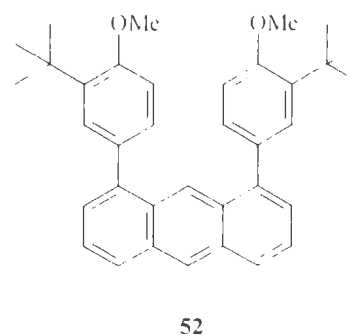
The product solution was concentrated and the methanol (15 mL) was added. The product **48** crystallized from the reaction solvent DMA and methanol as a colourless solid in 96 % yield: mp



210-212 °C; <sup>1</sup>H NMR (CDCl<sub>3</sub>) δ 1.49 (s, 18H), 3.93 (s, 6H), 7.03 (d, *J* = 8.5 Hz, 2H), 7.59 (dd, *J* = 3.0, 8.8 Hz, 2H), 7.70 (d, *J* = 3.0 Hz, 2H), 7.73 (dd, *J* = 1.5, 8.5 Hz, 2H), 7.91 (d, *J* = 8.5 Hz, 2H), 8.05 (s, 2H); <sup>13</sup>C NMR (CDCl<sub>3</sub>) δ 30.01, 35.26, 55.42, 112.17, 125.42, 125.63, 126.06, 126.12, 128.19, 131.30, 133.35, 134.34, 138.84, 139.44, 158.50; MS (APCI-) *m/z* [M-H], calcd for C<sub>32</sub>H<sub>36</sub>O<sub>2</sub> 452.3.

### 1,8-Bis(3-*tert*-butyl-4-methoxyphenyl)anthracene (**52**).

A dry round-bottom flask was charged with magnesium turnings (0.979 g, 0.0400 mol), a crystal of iodine and dry THF (60 mL). A few drops of a solution of 4-bromoanisole (**42**) (5.90 g, 24.2 mmol) in THF (30 mL) was added under nitrogen atmosphere and the mixture



was heated until the reaction initiated. Once initiation occurred, the reaction was maintained at reflux for 2 h by the dropwise addition of the remainder of the solution of 4-bromoanisole. After cooling to room temperature, the reaction solution was concentrated to a volume of approximately 65 mL by nitrogen gas blow-down. The Grignard reagent solution was then added, dropwise and with stirring over 1 h, to a solution of dichloride **51** (2.00 g, 8.07 mmol), nickel(II) acetylacetonate (21 mg, 0.084

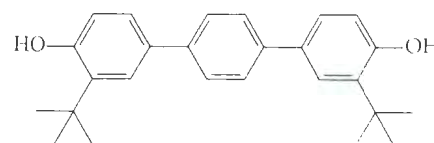
mmol) and  $\text{Ph}_3\text{P}$  (43.0 mg, 0.164 mmol) of in of THF (21 mL). The resulting black (colloidal Ni) mixture was heated at reflux for 7 h and after cooling to room temperature was then poured aqueous solution of hydrochloric acid (25 mL, 3.0 M). The crude product was extracted by  $\text{CH}_2\text{Cl}_2$  (3 x 30 mL). The combined organic extract was dried over  $\text{MgSO}_4$  and filtered. The solvent was evaporated and the product was crystallized from hexane to give **52** (2.29 g, 56%) as a colourless solid. The rest of the product was purified by silica gel column chromatography using hexane as the eluent to give an additional amount of **52** (0.57 g, 14% yield). The combined yield of **52** was 70% yield: mp 181-183; °C;  $^1\text{H}$  NMR  $\delta$  1.23 (s, 18H), 3.87 (s, 6H), 6.93 (d,  $J = 8.0$  Hz, 2H) 7.31 (d,  $J = 2.5$  Hz, 2H), 7.34 (dd,  $J = 2.3, 8.3$  Hz, 2H), 7.39 (d,  $J = 6.5$  Hz, 2H) 7.52 (d,  $J = 6.5$  Hz, 1H), 7.53 (d,  $J = 7.5$  Hz, 1H), 8.02 (d,  $J = 8.5$  Hz, 2H), 8.55 (s, 1H), 8.90 (s, 1H);  $^{13}\text{C}$  NMR ( $\text{CDCl}_3$ )  $\delta$  29.87, 34.95, 55.00, 111.50, 124.452, 125.49, 126.09, 126.88, 128.17, 128.93, 130.61, 132.18, 132.54, 137.63, 141.22, 158.00; MS (APCI)  $m/z$  503.3  $[\text{M}^+ + \text{H}]$ , calcd for  $\text{C}_{36}\text{H}_{38}\text{O}_2$  502.4.

#### General demethylation procedure:

Boron tribromide (0.51 mL, 5.4 mmol) was added dropwise to the solution of anisole, **46-48** or **52**, (2.5 mmol) in 15 mL of dry dichloromethane under nitrogen in a 50-mL round-bottom flask which was cooled in a dry ice-isopropanol bath (-78 °C). The cooled bath was removed and the mixture was stirred for 2 hr, poured into ice water with 10% hydrochloric acid, stirred for 0.5 h, then saturated with salt, and extracted with dichloromethane. The extract was dried ( $\text{MgSO}_4$ ) and concentrated. The following products were obtained:

### 1,4-Bis(3-*tert*-butyl-4-hydroxyphenyl)benzene (**53**).

The product was purified by silica gel column chromatography using 30% ethyl ether-hexane eluent to give **53** as a colourless solid in 92% yield: mp 237-



**53**

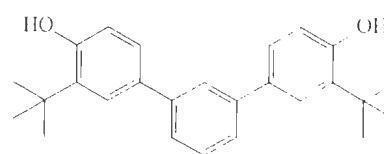
239 °C;  $^1\text{H NMR}$  ( $\text{CDCl}_3$ )  $\delta$  1.48 (s, 18H), 4.85(s, 2H)

6.76 (d,  $J = 8.5$ , 2H), 7.35 (dd,  $J = 2.5$ , 8.0 Hz, 2H), 7.55 (d,  $J = 2.5$ , 2H) 7.58 (s, 4H);

$^{13}\text{C NMR}$  ( $\text{CDCl}_3$ )  $\delta$  29.85, 34.93, 117.39, 125.69, 126.30, 127.31, 133.59, 136.60, 139.90, 154.00.; MS (APCI)  $m/z$  373.1 (M-H), calcd for  $\text{C}_{36}\text{H}_{38}\text{O}_2$  374.2.

### 1,3-Bis(3-*tert*-butyl-4-hydroxyphenyl)benzene (**54**).

The product was purified by silica gel column chromatography using 6:4 dichloromethane:hexane eluent to give **54** as a colourless solid in 94% yield: mp



**54**

146-147 °C;  $^1\text{H NMR}$  ( $\text{CDCl}_3$ )  $\delta$  1.48 (s, 18H), 4.82 (s,

2H), 6.77 (d,  $J = 8.0$  Hz, 2H), 7.35 (dd,  $J = 2.3$ , 9.4 Hz, 2H), 7.46-7.48 (m, 3H), 7.55 (d,

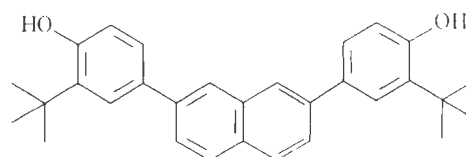
$J = 2.0$  Hz, 2H), 7.69 (s, 1H);  $^{13}\text{C NMR}$  ( $\text{CDCl}_3$ )  $\delta$  29.85, 34.93, 117.16, 125.45, 125.81,

125.96, 126.56, 129.19, 134.11, 136.60, 142.17, 154.07; MS (APCI)  $m/z$  373.1 (M-H)

calcd for  $\text{C}_{36}\text{H}_{38}\text{O}_2$  374.2.

### 2,7-Bis(3-*tert*-butyl-4-hydroxyphenyl)naphthalene (**55**).

The product was purified by washing with hot hexane to give **55** as a colourless solid in 92% yield: mp 212-213.5 °C;  $^1\text{H NMR}$  ( $\text{CDCl}_3$ )  $\delta$  1.53

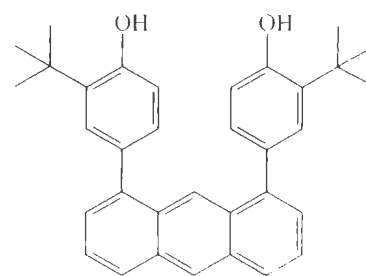


**55**

(s, 18H), 4.84 (s, 2H) 6.80 (d,  $J = 8.5$  Hz, 2H), 7.47 (dd,  $J = 2.5, 8.0$  Hz, 2H), 7.67 (d,  $J = 2.5$  Hz, 2H), 7.71 (dd,  $J = 2.3, 9.0$  Hz, 2H), 7.91 (d,  $J = 9.0$  Hz, 2H), 8.03 (s, 2H);  $^{13}\text{C}$  NMR ( $\text{CDCl}_3$ )  $\delta$  29.90, 34.98, 117.27, 125.41, 125.61, 126.13, 126.63, 128.22, 131.33, 133.86, 134.315, 136.71, 139.35, 154.11; MS (APCI-)  $m/z$  423.3 [M-H], calcd for  $\text{C}_{30}\text{H}_{32}\text{O}_2$  424.6.

### 1,8-Bis(3-*tert*-butyl-4-hydroxyphenyl)anthracene (**56**).

The product was purified by washing with hot hexane to give **56** as a colourless solid in 90% yield: mp 238.5-239.5 °C;  $^1\text{H}$  NMR ( $\text{CDCl}_3$ )  $\delta$  1.30 (s, 18H), 4.79 (s, 2H) 6.72 (d,  $J = 8.5$  Hz, 2H), 7.23 (dd,  $J = 2.3, 7.3$  Hz, 2H).



**56**

7.32 (d,  $J = 1.0$  Hz, 2H), 7.38 (d,  $J = 6.0, 2\text{H}$ ), 7.51 (dd,  $J = 6.5, 6.5$  Hz, 2H), 8.01 (d,  $J = 9.0$  Hz, 2H), 8.55 (s, 1H), 8.90 (s, 1H);  $^{13}\text{C}$  NMR ( $\text{CDCl}_3$ )  $\delta$  29.81, 34.71, 116.82, 124.19, 125.50, 126.19, 127.00, 127.37, 128.32, 129.41, 129.48 130.56, 132.17, 133.02, 135.76, 141.01, 153.75; MS (APCI-)  $m/z$  473.4 (M-H), calcd for  $\text{C}_{34}\text{H}_{34}\text{O}_2$  474.6.

### General formylation procedure:

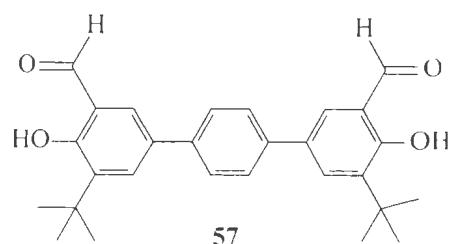
A dry round-bottom flask was charged with the respective phenolic compounds (**53-56**) (58 mmol), dry paraformaldehyde (0.59 g, 19.45 mmol), anhydrous  $\text{MgCl}_2$  (0.041g, 6.9 mmol), dry triethylamine (1.47 mL, 10.5 mmol) and dry THF 20.0 mL. The reaction mixture was heated at reflux for 22 h under nitrogen and then cooled to room temperature. The product was extracted with dichloromethane (50 mL). The organic

extract was washed with 2.0 M hydrochloric acid (3 x 50 mL). The organic extract was dried over MgSO<sub>4</sub>, filtered and the solvent was evaporated under vacuum.

#### 1,4-Bis(3-*tert*-butyl-5-formyl-4-hydroxyphenyl)benzene (**57**).

The product was washed with hexane to give **57** as a yellow solid in 92% yield: mp 264.5-266 °C:

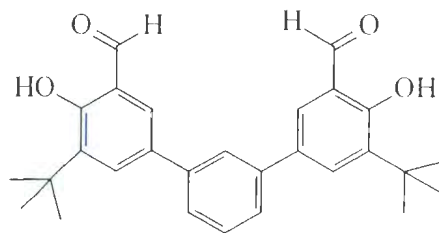
<sup>1</sup>H NMR (CDCl<sub>3</sub>) δ 1.51 (s, 18H), 7.65 (s, 4H), 7.66 (d, *J* = 3.0 Hz, 2H), 7.82 (d, *J* = 1.5 Hz, 2H), 10.00 (s,



2H), 11.83 (s, 2H); <sup>13</sup>C NMR (CDCl<sub>3</sub>) δ 29.49, 35.31, 121.05, 127.42, 130.14, 132.05, 133.23, 139.17, 139.23, 161.00, 197.45; MS (APCI) *m/z* 429.1 (M-H), calcd for C<sub>28</sub>H<sub>30</sub>O<sub>4</sub> 430.2.

#### 1,3-Bis(3-*tert*-butyl-5-formyl-4-hydroxyphenyl)benzene (**58**).

The product was purified by silica gel column chromatography and eluted with 6:4 dichloromethane-hexane to give **58** as a solid in 90% yield: mp 231-233 °C: <sup>1</sup>H NMR (CDCl<sub>3</sub>) δ 1.52



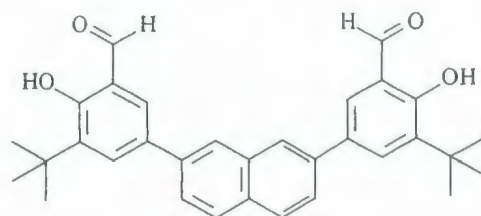
(s, 18H), 7.54 (m, 3H), 7.66 (d, *J* = 2.5 Hz, 2H),

7.69 (s, 1H), 7.82 (d, *J* = 2.0 Hz, 2H), 10.00 (s, 2H), 11.84 (s, 2H); <sup>13</sup>C NMR (CDCl<sub>3</sub>) δ 29.47, 35.30, 121.00, 125.46, 125.91, 129.74, 130.39, 132.65, 133.47, 139.19, 141.26, 161.04, 197.41; MS (APCI) *m/z* 429.1 (M-H), calcd for C<sub>28</sub>H<sub>30</sub>O<sub>4</sub> 430.2.

### 2,7-Bis(3-*tert*-butyl-5-formyl-4-hydroxyphenyl)naphthalene (59).

The product was purified by silica gel column chromatography and eluted with 35% diethyl ether-hexane to give **59** as yellow solid in 90% yield: mp 190-192 °C; <sup>1</sup>H NMR (CDCl<sub>3</sub>) δ 1.53 (s, 18H), 7.73 (dd, *J* = 1.8, 9.3 Hz, 2H), 7.76 (d, *J* = 1.5 Hz, 2H),

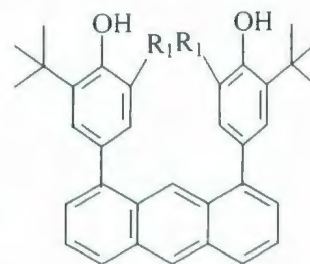
7.95 (d, *J* = 3.0 Hz, 2H), 7.97 (d, *J* = 8.0 Hz, 2H), 8.08 (s, 2H), 10.02 (s, 2H), 11.85 (s, 2H); <sup>13</sup>C NMR (CDCl<sub>3</sub>) δ 29.52, 35.34, 121.08, 125.46, 126.48, 128.65, 130.53, 131.71, 132.38, 133.47, 134.22, 138.28, 139.19, 161.01, 197.39; MS (APCI) *m/z* 479.1 (M-H), calcd for C<sub>32</sub>H<sub>32</sub>O<sub>4</sub> 480.2.



**59**

### 1,8-Bis(3-*tert*-butyl-5-formyl-4-hydroxyphenyl)anthracene (60).

A dry round-bottom flask was charged with bisphenol **56** (0.55 g, 1.58 mmol), paraformaldehyde (0.590 g, 19.5 mmol), anhydrous MgCl<sub>2</sub> (0.041 g, 6.9 mmol), dry triethylamine (1.47 mL, 10.5 mmol) and dry acetonitrile (11.0 mL). The reaction mixture was heated at reflux for 24 h under nitrogen and then another portion of dry



**60** R<sub>1</sub> = CHO

paraformaldehyde (0.590 g, 19.5 mmol) was added. The reaction was heated at reflux for a further 48 h, then cooled down to room temperature. The product was extracted with dichloromethane (50 mL). The organic extract was washed with hydrochloric acid (2.0 M,

3 x 50 mL). The organic phase was dried over MgSO<sub>4</sub> and filtered. The solvent was removed under vacuum, the crude product was dissolved in CH<sub>2</sub>Cl<sub>2</sub> (5 mL) from which a yellow solid precipitated. This precipitation process was repeated three times yielding **60** (0.308 g, 50% yield): 286-287 °C; <sup>1</sup>H NMR (CDCl<sub>3</sub>) δ 1.21 (s, 18H), 7.42 (d, *J* = 8.5 Hz, 2H), 7.53 (s, 4H), 7.55 (s, 1H), 7.56 (d, *J* = 6.5 Hz 1H), 7.57 (d, *J* = 6.5 Hz 1H), 8.08 (d, *J* = 8.5 Hz, 2H), 8.60 (s, 1H), 9.87 (s, 2H), 11.79 (s, 2H); <sup>13</sup>C NMR (CDCl<sub>3</sub>) δ 29.25, 34.99, 120.94, 123.06, 125.62, 126.49, 127.51, 128.12, 130.48, 131.62, 132.14, 132.55, 136.30, 138.22, 139.39, 160.83, 196.94; MS (APCI-) (*m/z*) 529.2 [M-H], calcd for C<sub>36</sub>H<sub>34</sub>O<sub>4</sub> 530.2.

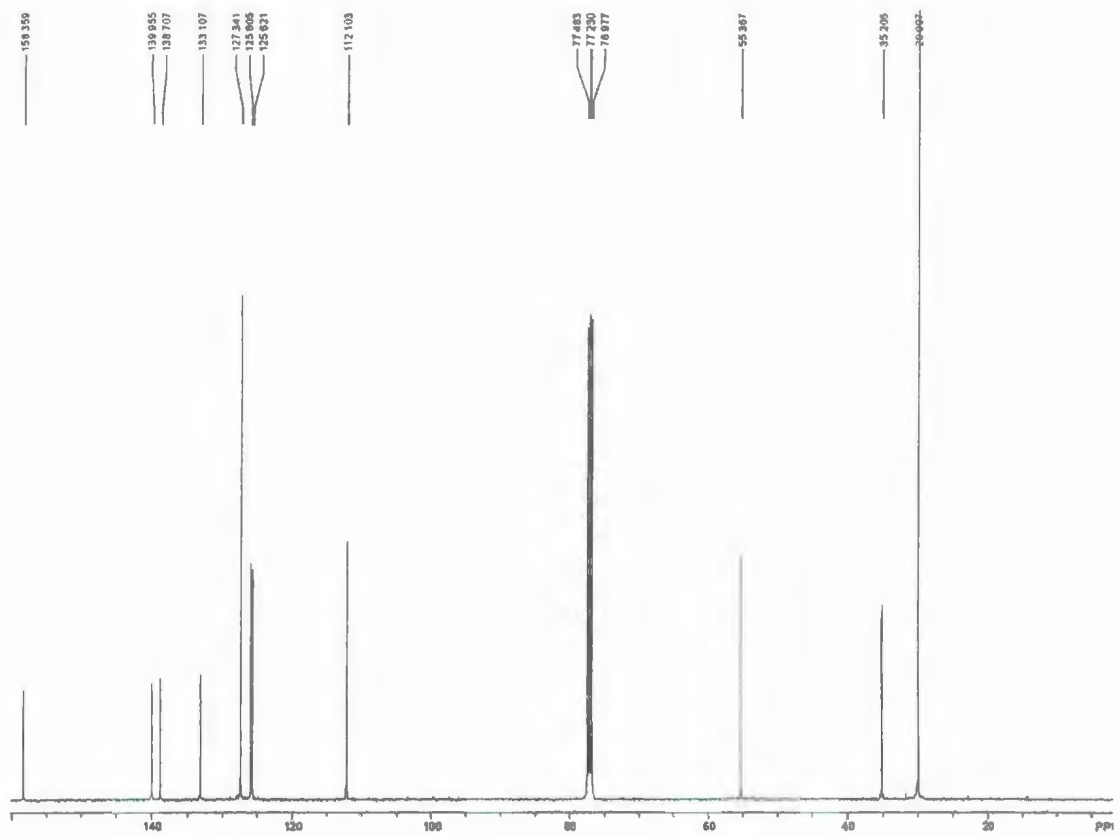
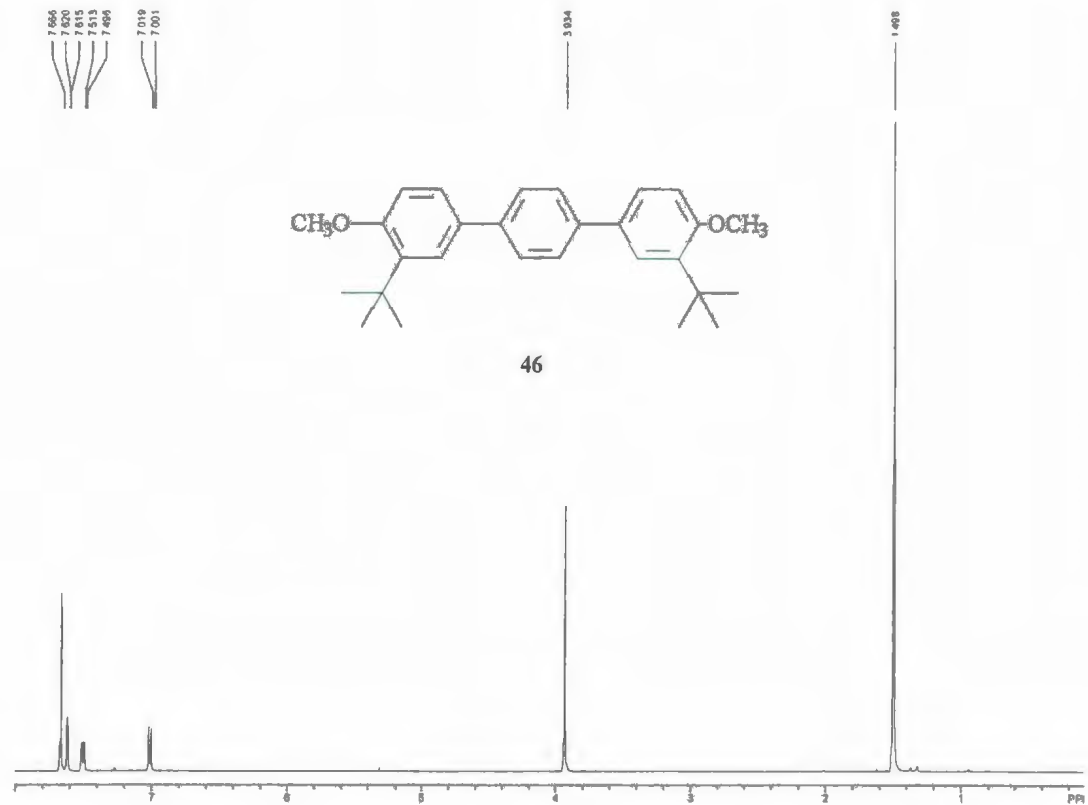
## 1.2.6 References

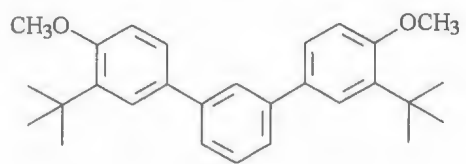
1. Li, Z. ; Jablonski, C. *Chem. Commun.* **1999**, 1531. (b) Wang, L.; Coulter, K.; Jablonski, C. *unpublished results*.
2. Wastkinson, M.; Whiting, A.; McAuliffe, C. A. *J. Chem. Soc., Chem. Commun.* **1994**, 2141.
3. Hassan, J.; Sevignon, M.; Gozzi, C.; Schulz, E.; Lemaire, M. *Chem. Rev.* **2002**, *102*, 1359.
4. Miyaura, N.; Yanagi, T.; Suzuki, A. *Synth. Commun.* **1981**, *11*, 513.
5. Fitton, P.; Rick, E. A. *J. Organomet. Chem.* **1971**, *28*, 287.
6. Anderson, J. C.; Namli, H. *Synlett* **1995**, 765.
7. Anderson, J. C.; Namli, H.; Roberts, C. A. *Tetrahedron* **1997**, *53*, 15123.
8. Nerdinger, S.; Kendall, C.; Marchhart, R.; Riebel, P.; Johnson, M. R.; Yin, C. F.; Eltis, L. D.; Snieckus, V. *J. Chem. Soc., Chem. Commun.* **1999**, 2259.
9. Wright, S. W.; Hageman, D. L.; McClure, L. D. *J. Org. Chem.* **1994**, *59*, 6095.
10. Kamitori, Y.; Jojo, M.; Masuda, R.; Yoshida, T. *Tetrahedron Lett.* **1985**, *26*, 4767.
11. Mackenzie, A. R.; Moody, C. J.; Rees, C. W. *Tetrahedron* **1986**, *42*, 3259.
12. Lightowler, S.; Hird, M. *Chem. Mater.* **2004**, *16*, 3963.
13. Waas, J. R.; Sidduri, A.; Knochel, P. *Tetrahedron Lett.* **1992**, *33*, 3717.
14. Watanabe, T.; Miyaura, N.; Suzuki, A. *Synlett* **1992**, 207.
15. Steele, M.; Watkinson, M.; Whiting, A. *J. Chem. Soc., Perkin. Trans. 1* **2001**, 588.
16. (a) Leoni, P.; Pasquali, M.; Pieri, G.; Albinati, A.; Pregosin, P. S.; Rügger, H. *Organometallics* **1995**, *14*, 3143. (b) Leoni, P.; Pasquali, M.; Sommovigo, M.; Laschi,

- F.; Zanello, P.; Albinati, A.; Lianza, F.; Pregosin, P. S.; Ruegger, H. *Organometallics* **1993**, *12*, 1702. (c) Leoni, P.; Pasquali, M.; Sommovigo, M.; Albinati, A.; Lianza, F.; Pregosin, P. S.; Ruegger, H. *Organometallics* **1993**, *12*, 4503.
17. The suggestion for using lower mol% of Pd(0) was initially provided by Dr. Graham J. Bodwell, Department of Chemistry, Memorial University of Newfoundland.
18. (a) Neenan, T. X.; Whitesides, G. M. *J. Org. Chem.* **1988**, *53*, 2489. (b) House, H.; Hrabie, J. A.; VanDerveer D. *J. Org. Chem.* **1986**, *51*, 921.
19. Vickery, E. H.; Pahler, L. F.; Eisenbraun, E. J. *J. Org. Chem.* **1979**, *44*, 4444.
20. Hofsløkken, N. U.; Skattebøl, L. *Acta Chem. Scand.* **1999**, *53*, 258.
21. Hansen, T. V.; Skattebøl, L. *Org. Synth.* **2005**, *82*, 64.
22. Chaumeil, H.; Le Drian, C.; Defoin, A. *Synthesis* **2002**, 757.
23. Wasgindt, M.; Klemm, E. *Synth. Commun.* **1999**, *29*, 103.
24. Charpentier, B.; Bernardon, J.; Eustache, J.; Millois, C.; Martin, B.; Michel, S.; Shroot, B. *J. Med. Chem.* **1995**, *38*, 4993.

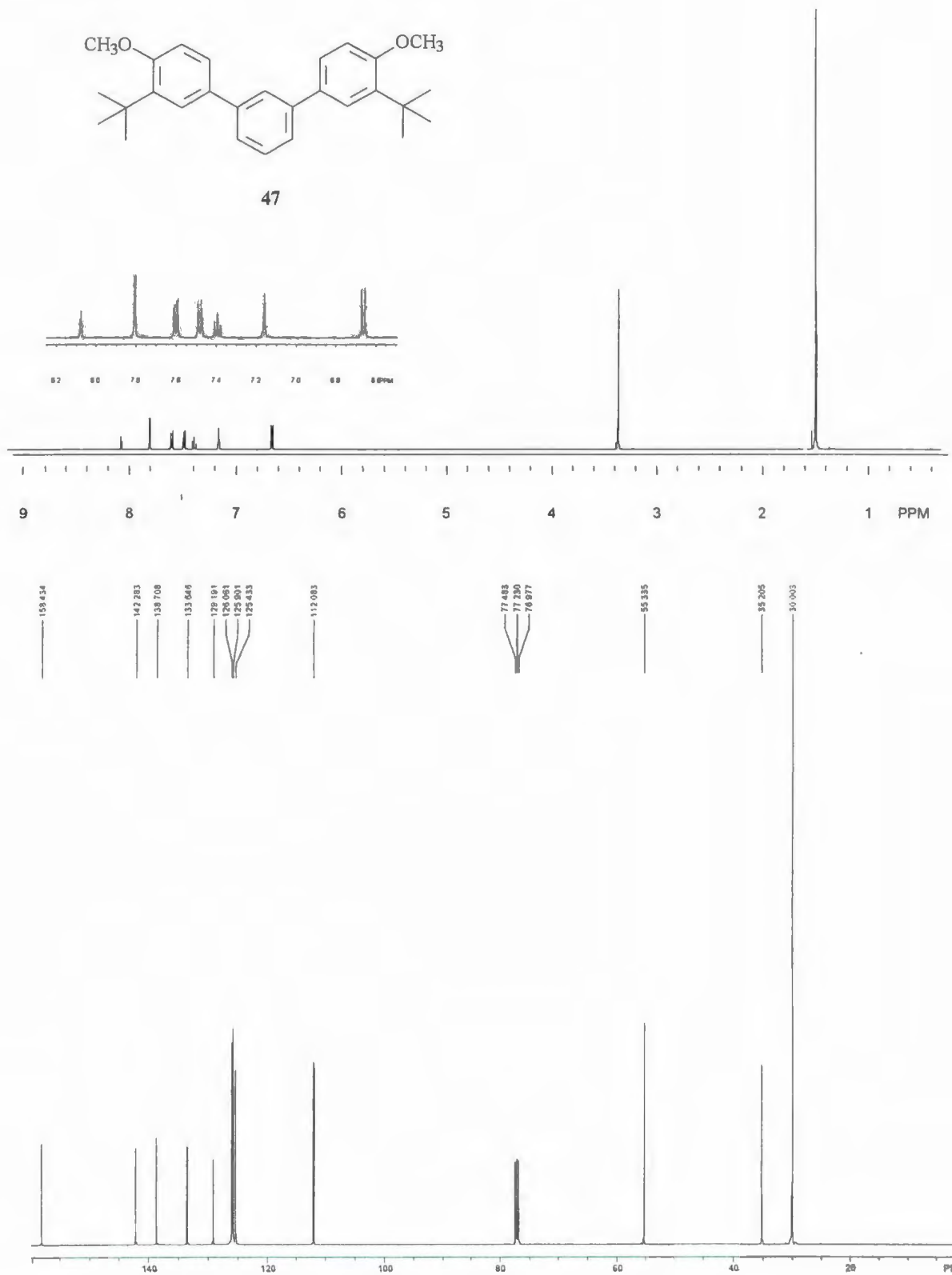
## **Appendix A**

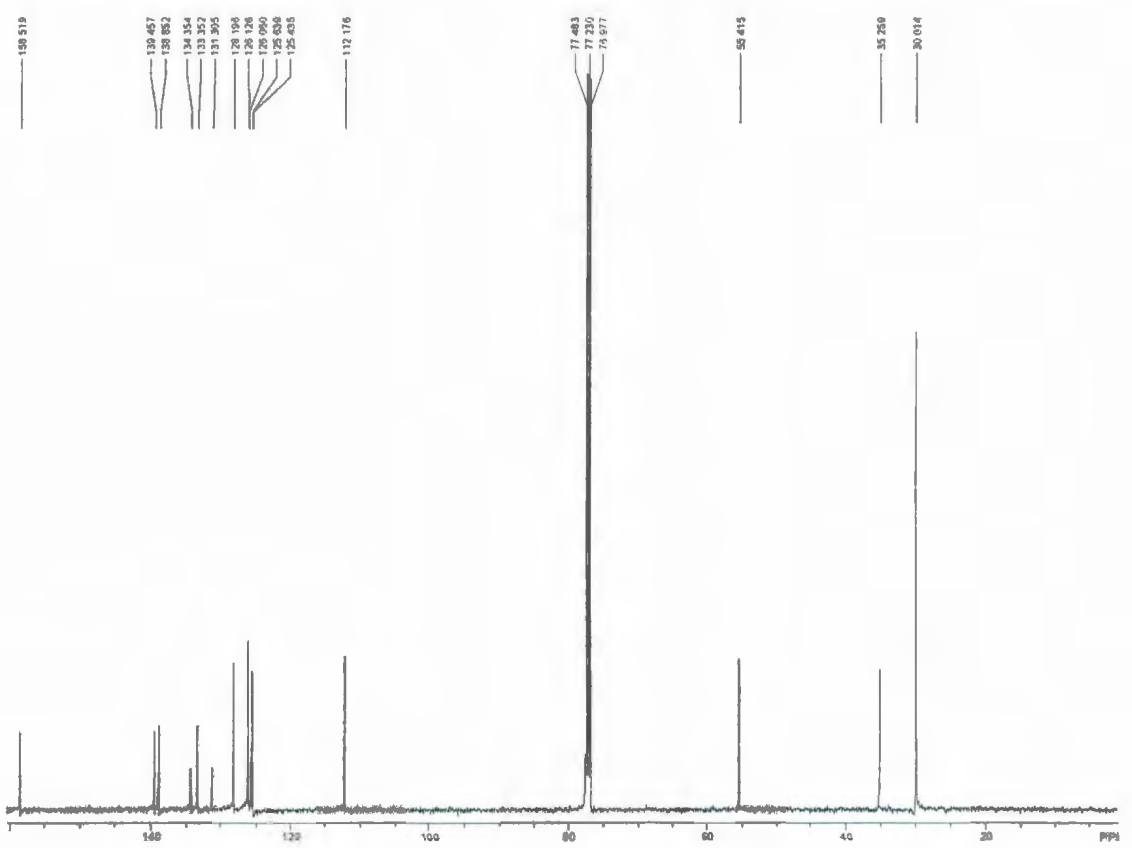
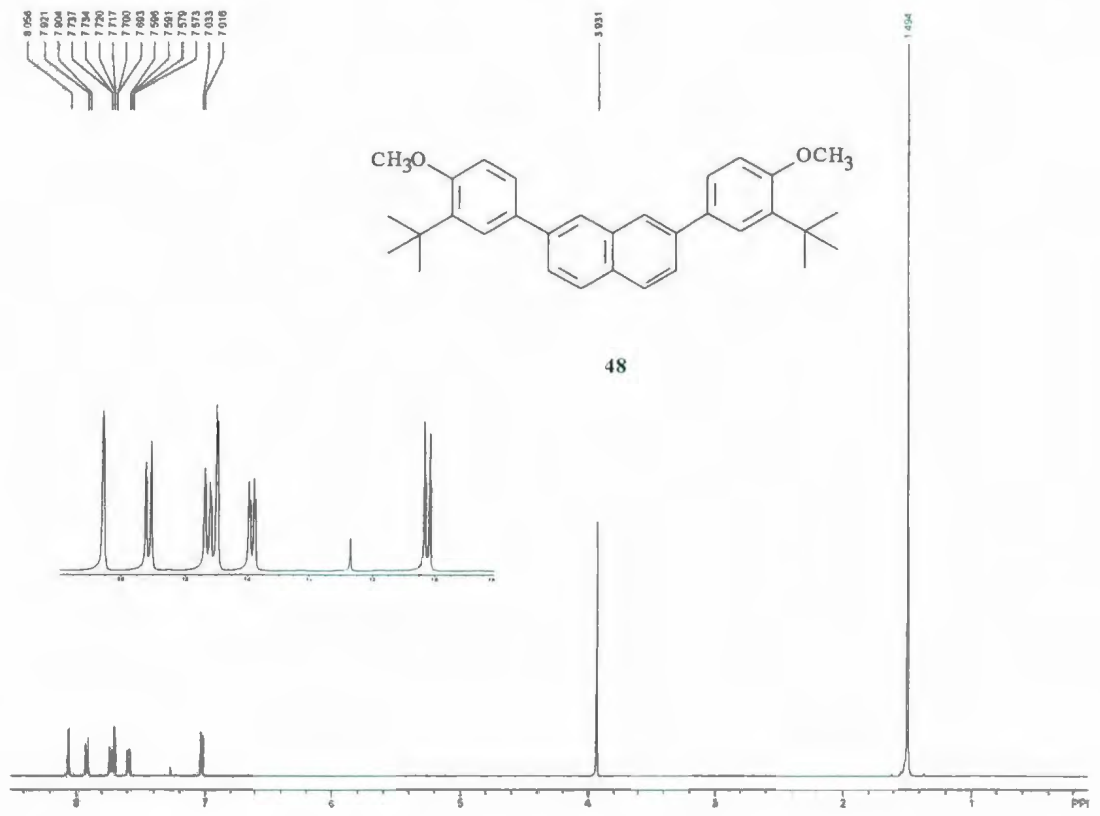
**Selected NMR spectra for synthesized compounds  
described in Chapter 1.2**

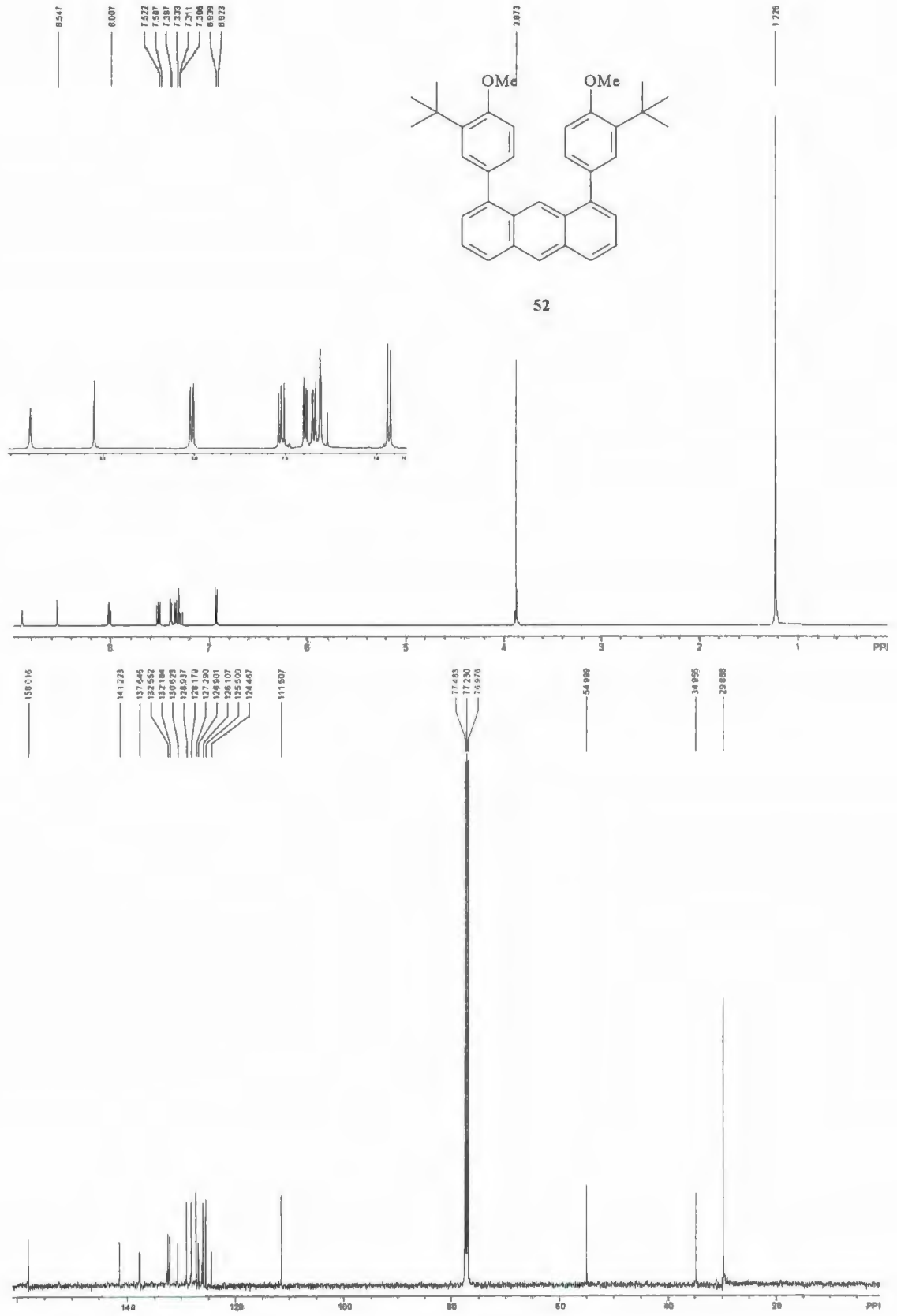


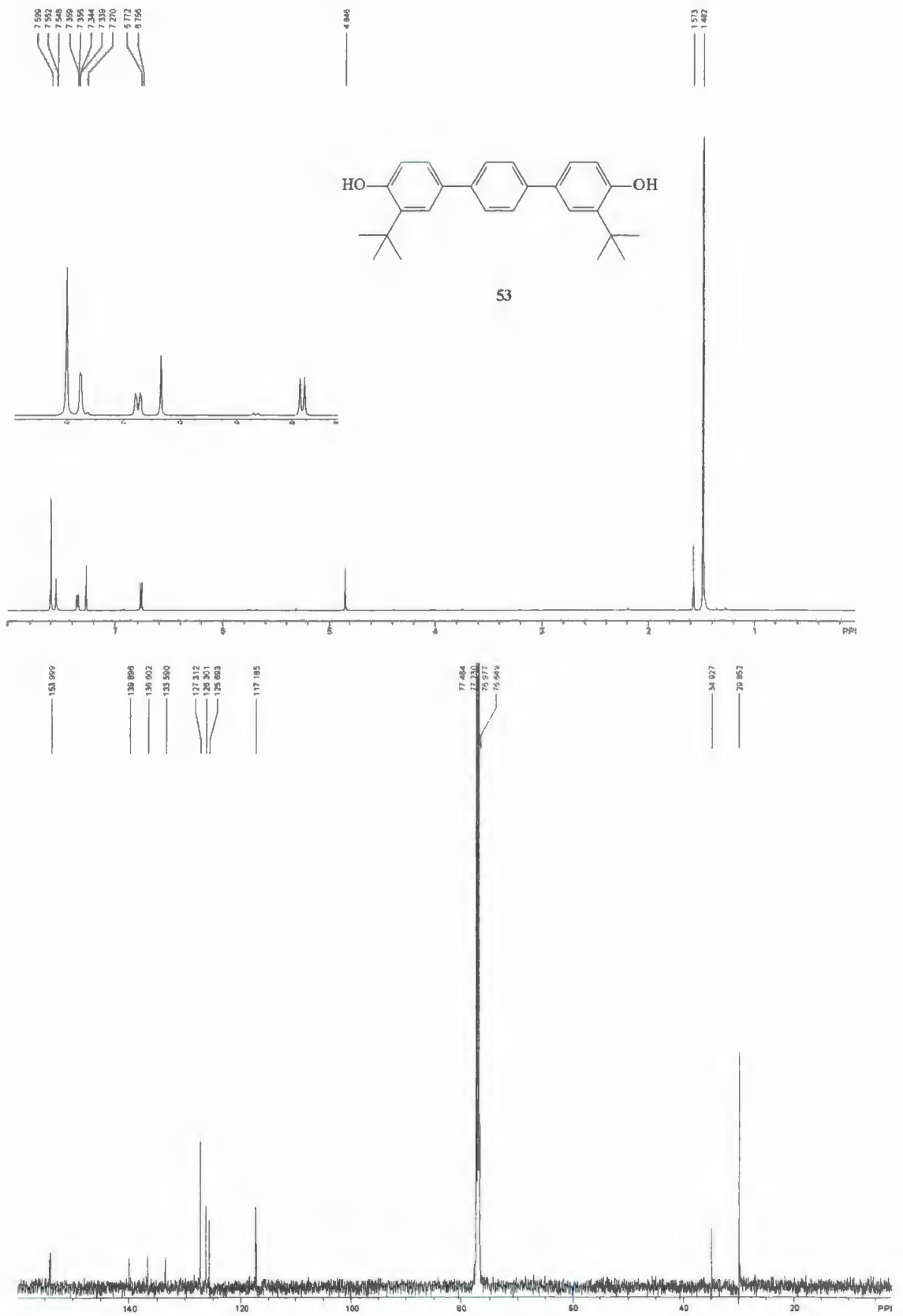


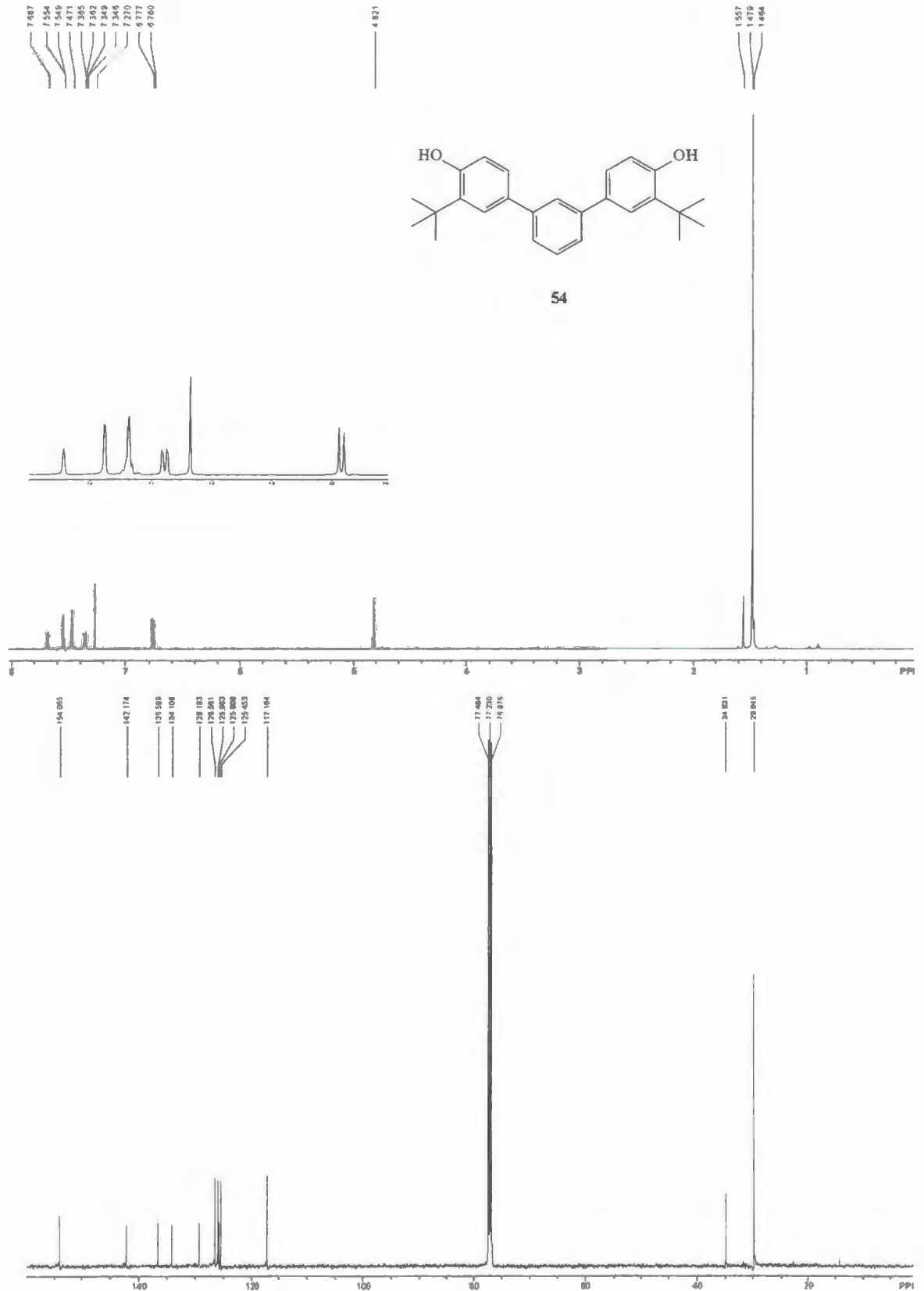
47







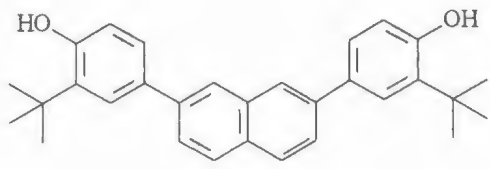




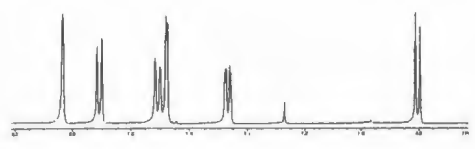
8.034  
7.938  
7.898  
7.777  
7.714  
7.700  
7.687  
7.680  
7.675  
7.478  
7.474  
7.465  
7.457  
6.851  
6.795

4.877

15.25

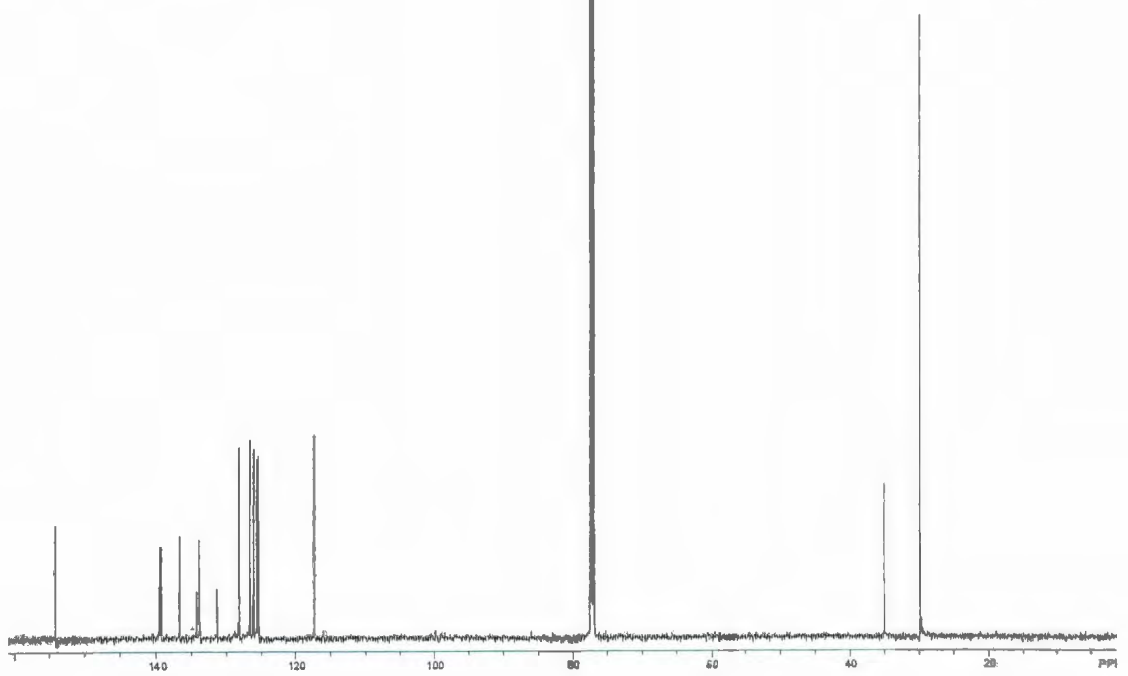


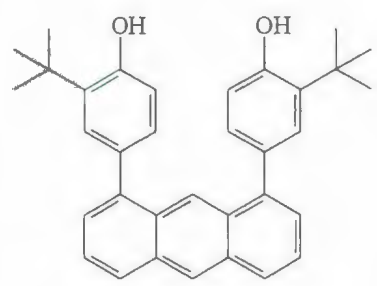
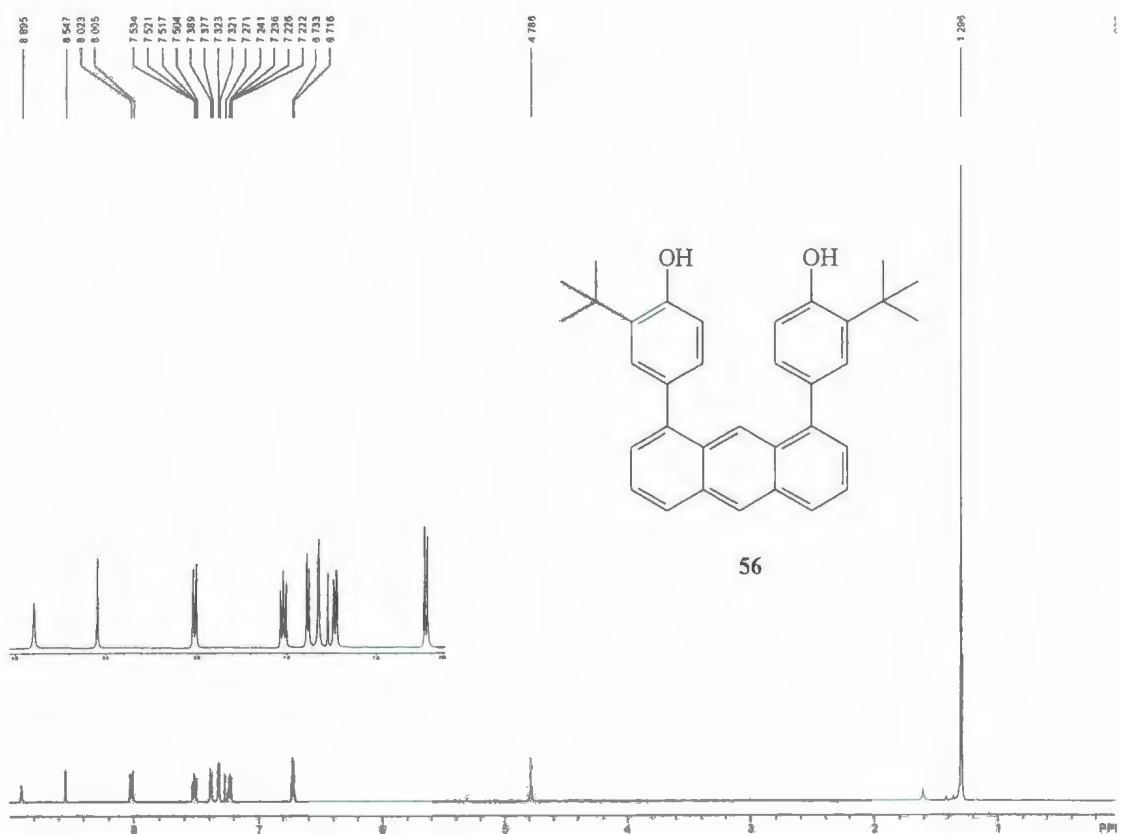
55



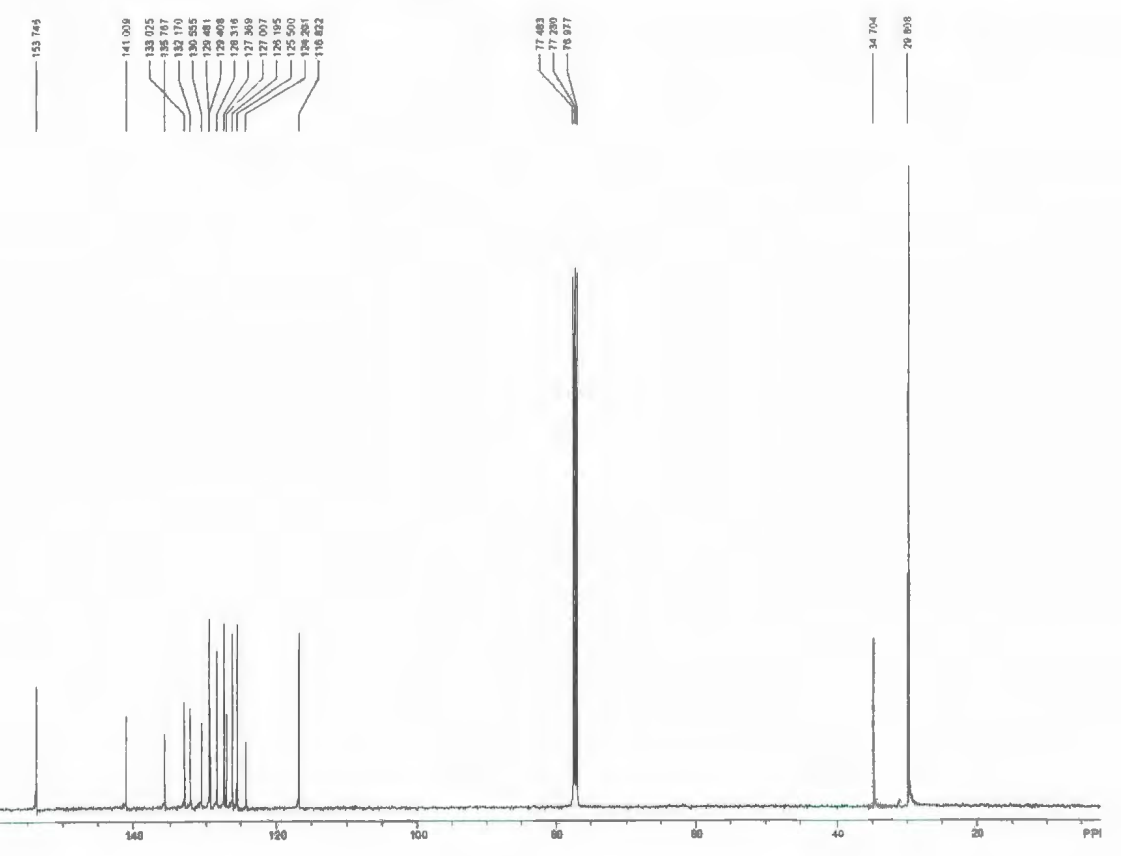
154.133  
139.361  
138.716  
138.552  
133.852  
131.334  
128.224  
126.631  
126.127  
125.605  
125.494  
117.272

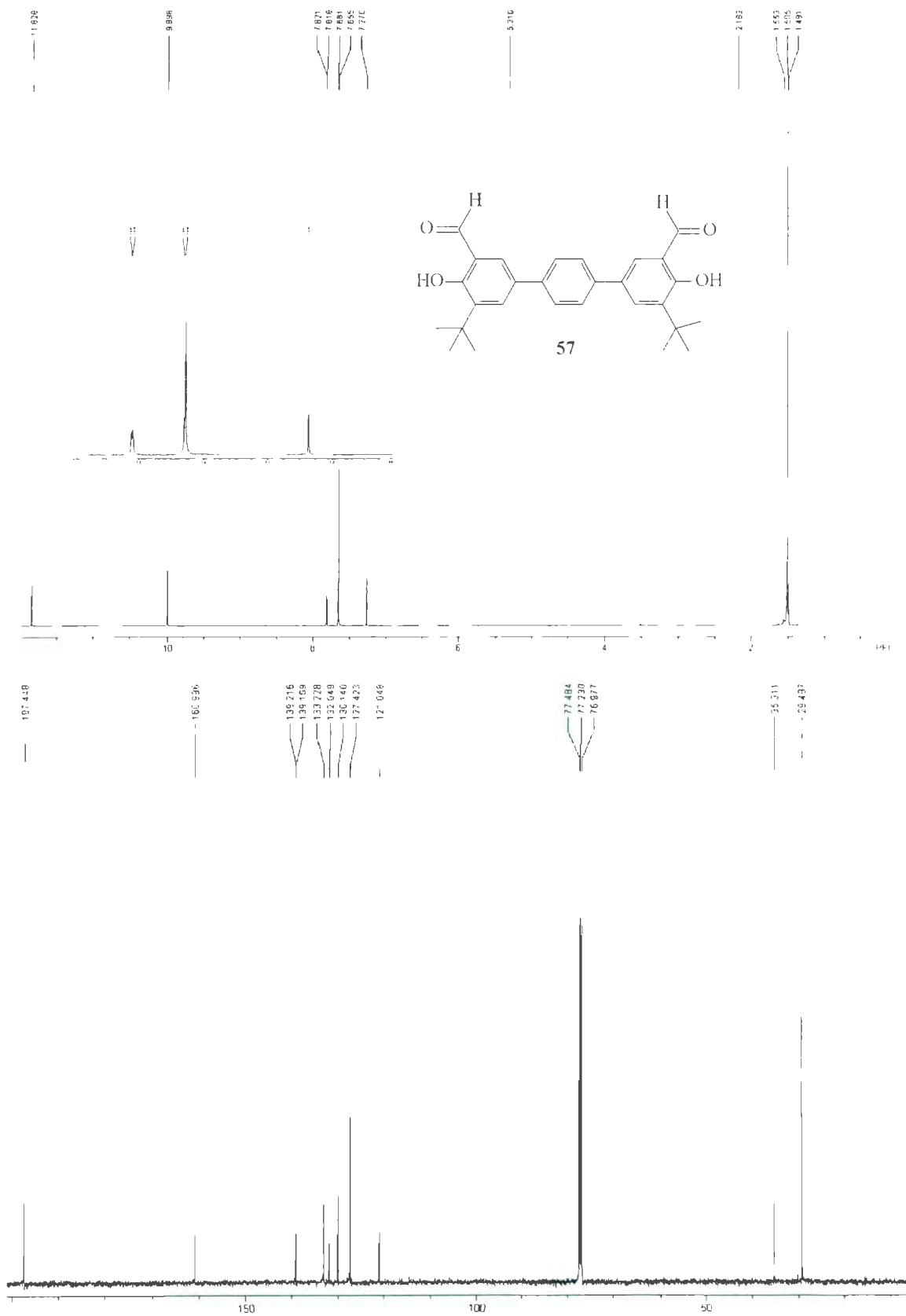
34.978  
29.882

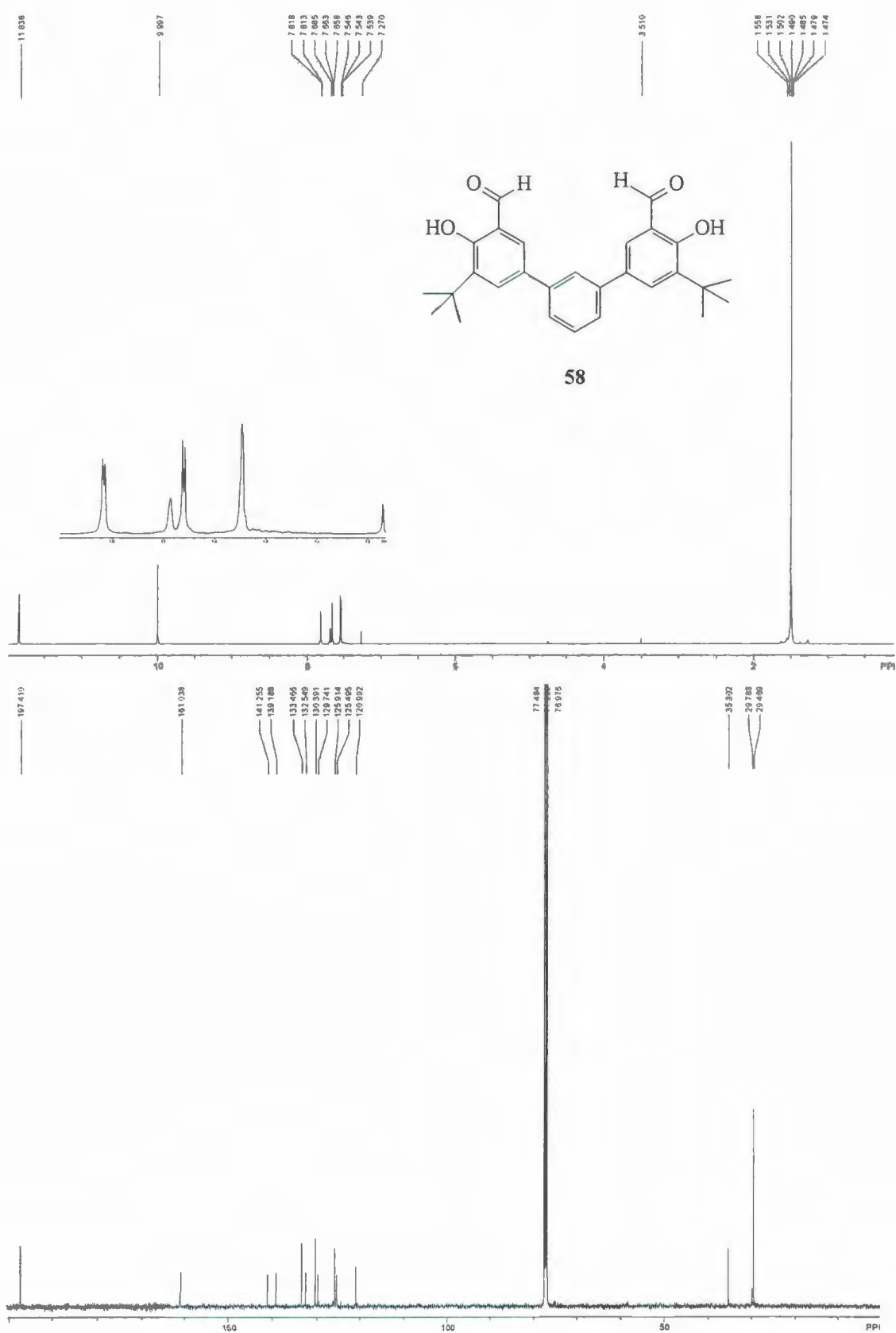




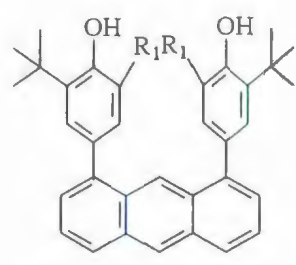
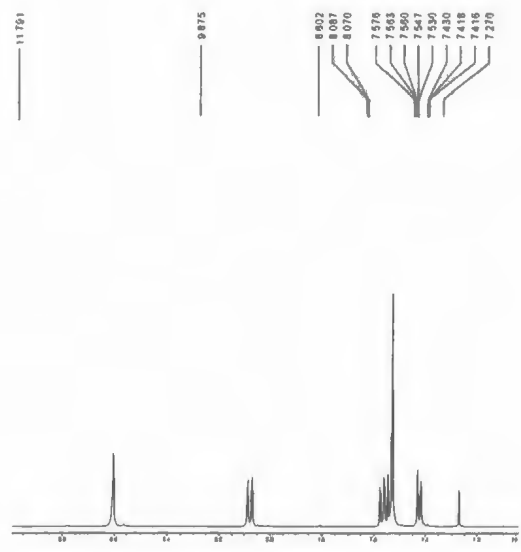
56



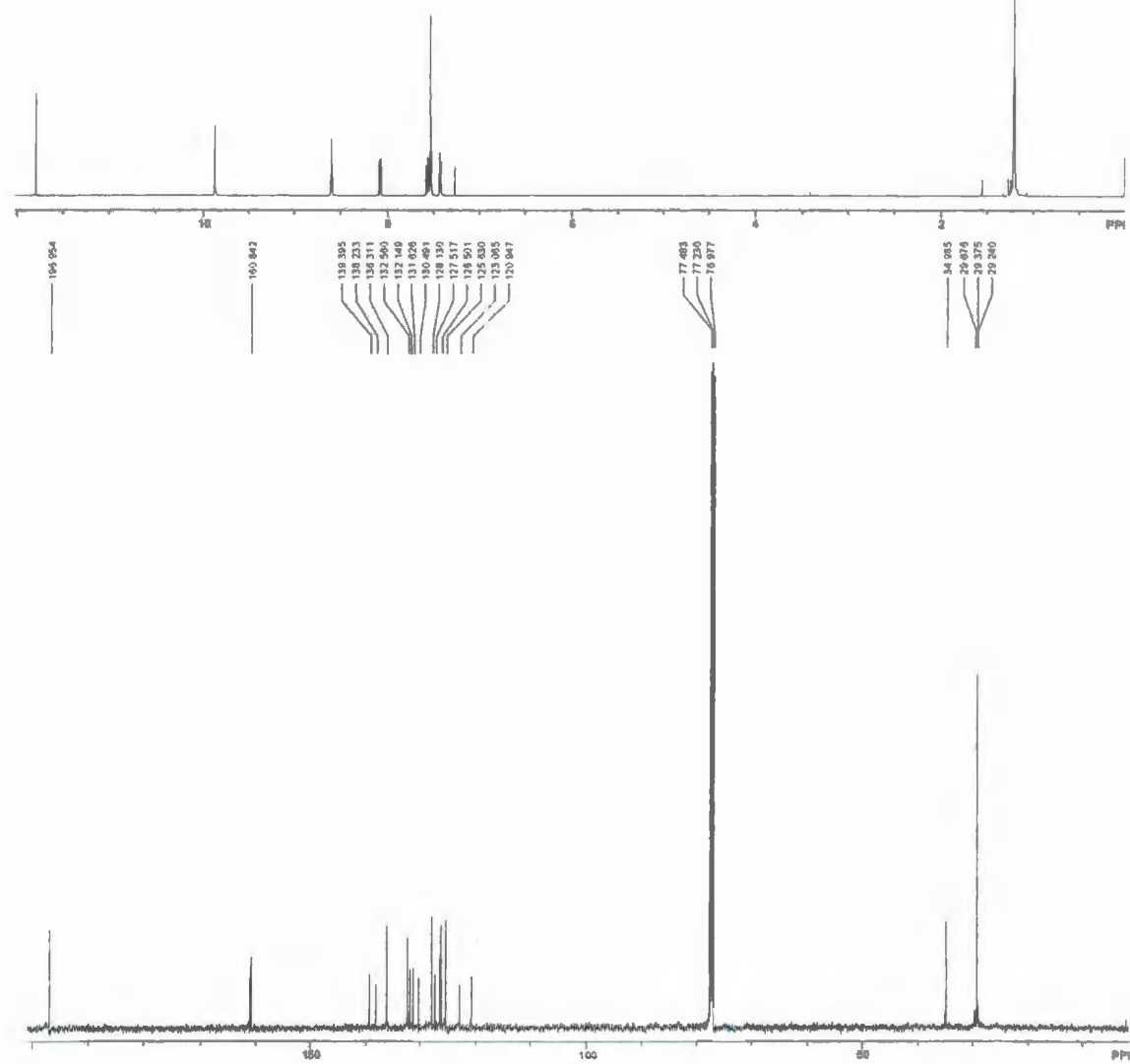








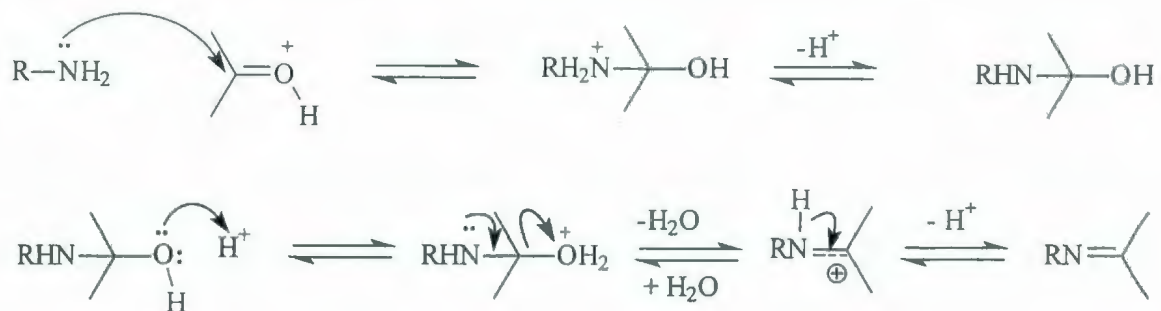
**60** R<sub>1</sub> = CHO



## Chapter 1.3 Synthesis and characterization of calixsalens

### 1.3.1 Macrocyclization methodologies

Since Hugo Schiff<sup>1</sup> discovered the condensation reaction of a primary amine with a carbonyl group in 1864, this reaction, which has been named in his honour, has been widely used in the preparation of a broad variety of azomethines. The acid catalyzed Schiff base reaction is efficient, gives high yields of imine products, and its mechanism is well-understood (Scheme 1.3-1).



**Scheme 1.3-1:** General outline for the Schiff base condensation reaction.

Chiral Schiff bases have been extensively used for the synthesis of chiral diimine ligands from a variety of aromatic aldehydes. In addition, metal complexes of these ligands have been used as efficient catalysts for asymmetric epoxidation, aziridination,<sup>2</sup> nucleophilic epoxide ring opening,<sup>3</sup> Michael addition,<sup>4</sup> Diels-Alder reactions,<sup>5</sup> cyanohydrin<sup>6</sup> and imine formation (Jacobsen-Katsuki catalysts)<sup>7</sup> as well as for the construction of supramolecular structures.<sup>8</sup> In particular, optically-active *trans*-1,2-diaminocyclohexane derivatives and their complexes have been employed as catalysts for asymmetric synthetic organic reactions.<sup>9</sup>

As described in Chapter 1, much effort has been focused on the development of a reliable and convenient macrocyclization methodology built on Schiff base chemistry. This is due to the fact that Schiff base macrocyclic compounds have important applications such as in chemical sensors, catalysts, fluorescent substances and supramolecular applications.<sup>10-18</sup>

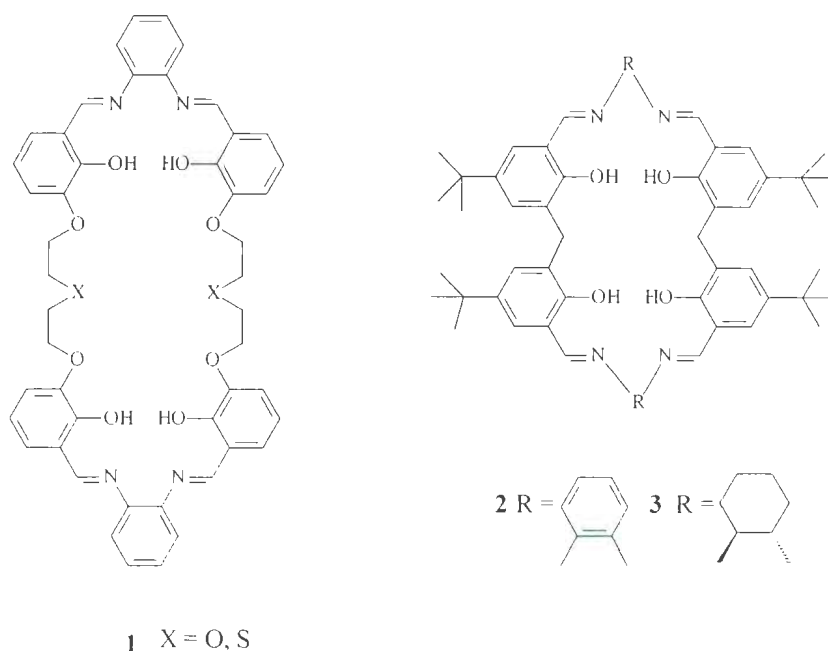
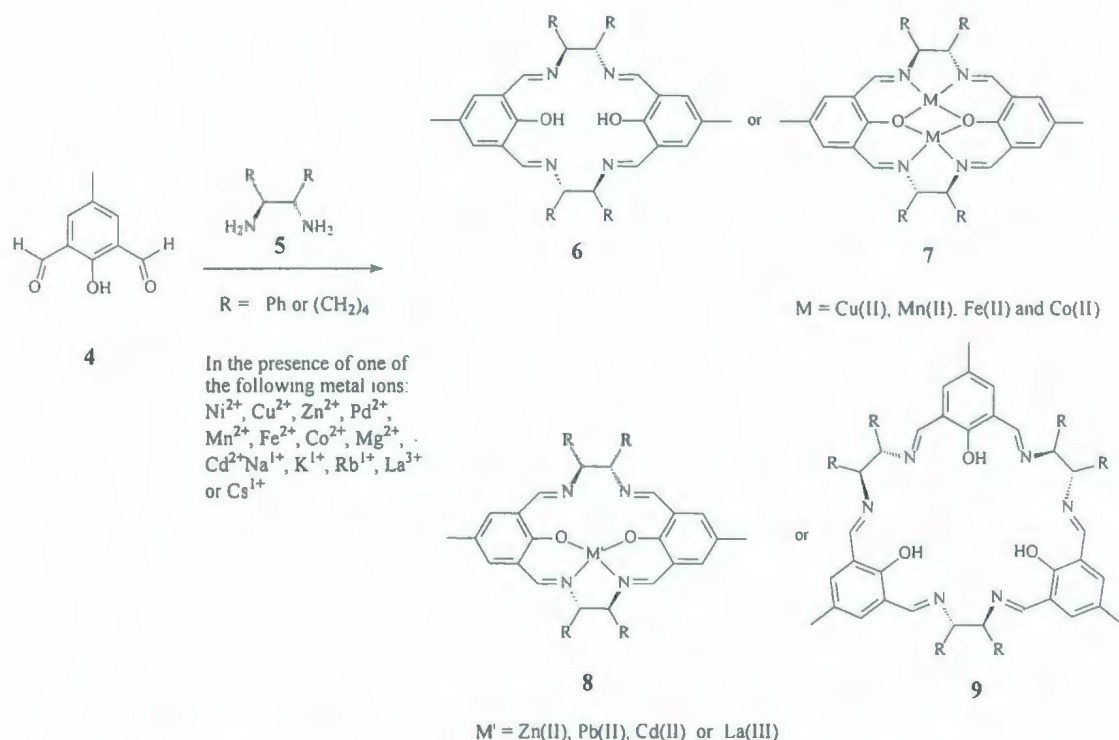


**Figure 1.3-1:** [2+2]-Condensation products of metal-templated Schiff base macrocyclization reactions.

In general, Schiff base macrocyclization reactions take place efficiently between dialdehydes or bisaldehydes and diamine compounds, under dilute conditions, in the presence of a Lewis acid template. However, these types of reaction conditions often require long reaction times. Hisaeda employed boric acid as the template in a solution of 1:1 MeOH:CH<sub>2</sub>Cl<sub>2</sub> to afford the desired calix[2]salens, **2** and **3**, in yields of 88% and

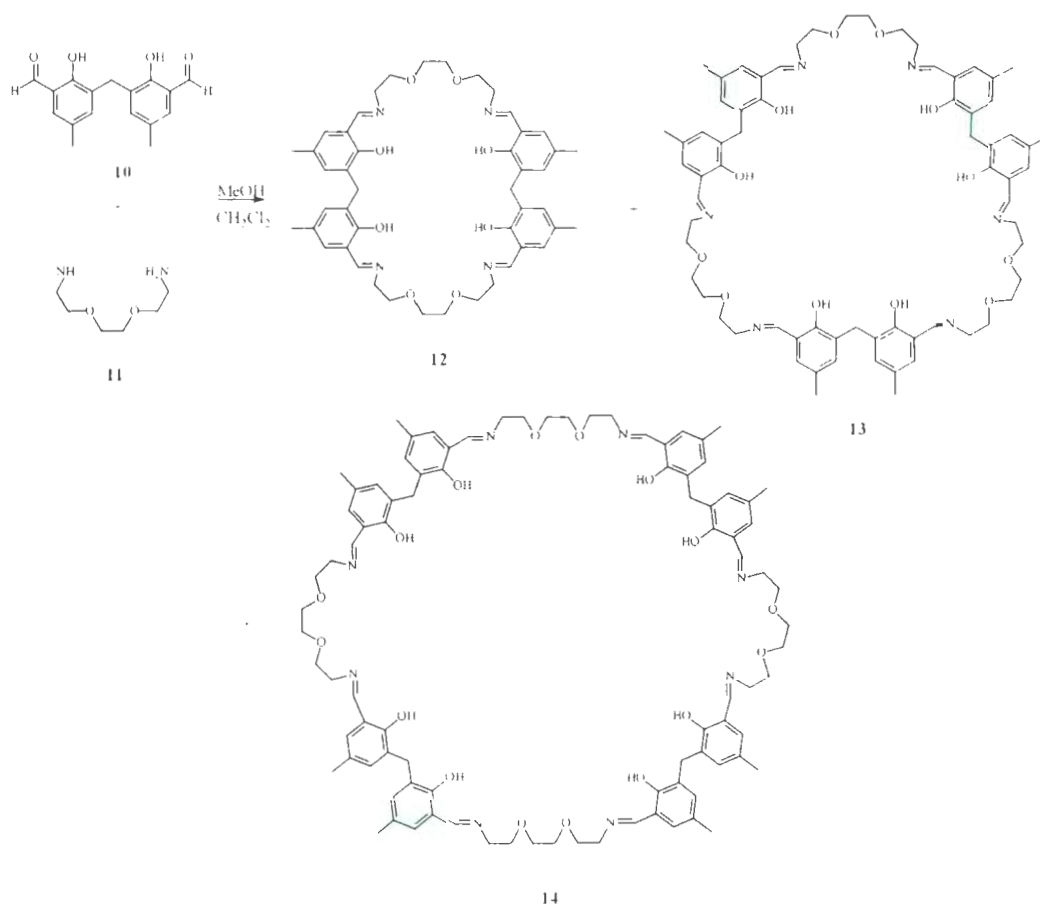
89%, respectively (Figure 1.3-1).<sup>19</sup> The [2+2] salen crown ether **1** (Figure 1.3-1) was synthesized from the corresponding bisaldehyde and 1,2-diaminobenzene were heated in methanol at reflux in the presence of Ba(CF<sub>3</sub>SO<sub>3</sub>)<sub>2</sub> or Cs(CF<sub>3</sub>SO<sub>3</sub>) as a template.<sup>20</sup>



**Scheme 1.3-2:** Templated Schiff base macrocyclization reactions.

The effects of metal templates (*e.g.* Ni<sup>2+</sup>, Cu<sup>2+</sup>, Zn<sup>2+</sup>, Pb<sup>2+</sup>, Mn<sup>2+</sup>, Fe<sup>2+</sup>, Co<sup>2+</sup>, Mg<sup>2+</sup>, Na<sup>+</sup>, K<sup>+</sup>, Rb<sup>+</sup>, La<sup>3+</sup> and Cs<sup>+</sup>) on the Schiff base macrocyclization reaction of the chiral diamines **5** and the dialdehyde **4** were investigated by Gao *et al.* (Scheme 1.3-2).<sup>21</sup> Interestingly, Ni<sup>2+</sup>-templated reactions at 45 °C in MeOH and CH<sub>3</sub>CN led to the [2+2] macrocycles **6** (R = Ph or (CH<sub>2</sub>)<sub>4</sub>) in high yields (> 90%). Employing, Cu<sup>2+</sup>, Mn<sup>2+</sup>, Fe<sup>2+</sup> and Co<sup>2+</sup> as the template ions, however, afforded the corresponding dimetallic complexes, **7**, instead, in good yields. In contrast, the mono-metal complexes **8** were

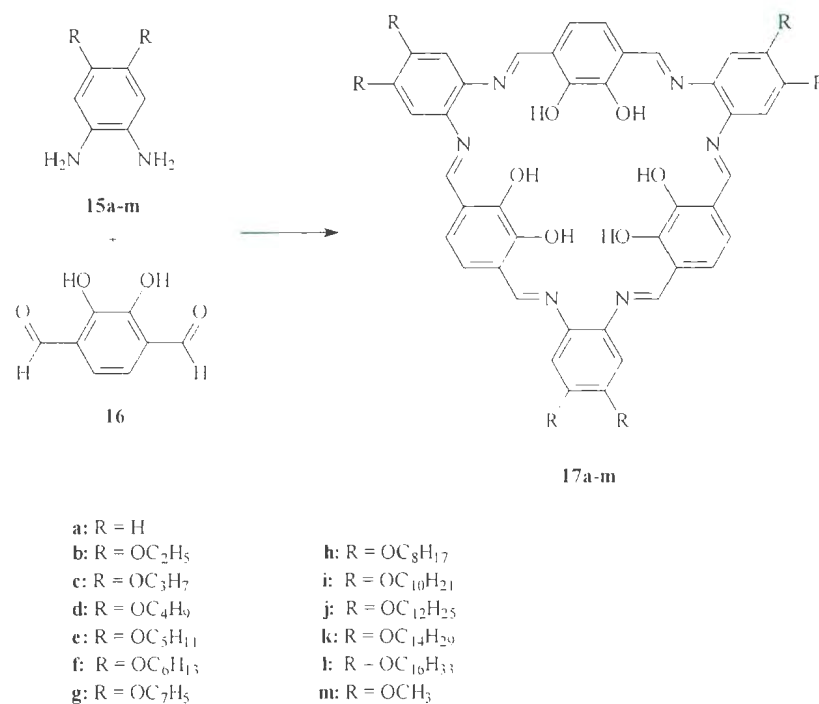
obtained under  $Zn^{2+}$ ,  $Pb^{2+}$ ,  $Cd^{2+}$  and  $La^{3+}$ -templated conditions. Other cations including  $Na^+$ ,  $K^+$ ,  $Rb^+$ , and  $Cs^+$ , however, did not show metal templating effects in this macrocyclization reaction. The [3+3] macrocycles **9** were obtained when excess  $Ni(ClO_4)_2$  was employed and allowing slow evaporation of the solvent 1:1  $MeOH:CH_2Cl_2$  from the reaction solution.



**Scheme 1.3-3:** [2+2] macrocycle **12**, [3+3] macrocycle **13** and [4+4] macrocycle **14** formed under non-templated Schiff base macrocyclization.

Non-templated and high-dilution conditions usually give lower yields of macrocycles than the template-controlled conditions (Scheme 1.3-3). For example, the

Schiff base macrocyclization reaction of 1,2-bis(2-aminoethoxy)ethane (**11**) and methylenebis(4,4'-methyl-6,6'-salicylaldehyde) (**10**) under high-dilution conditions with 1:1 MeOH:CH<sub>2</sub>Cl<sub>2</sub> solvent furnished a mixture of the [2+2], [3+3] and [4+4] macrocycles **12**, **13** and **14**, in 14, 7 and 4% yields, respectively.<sup>22</sup>

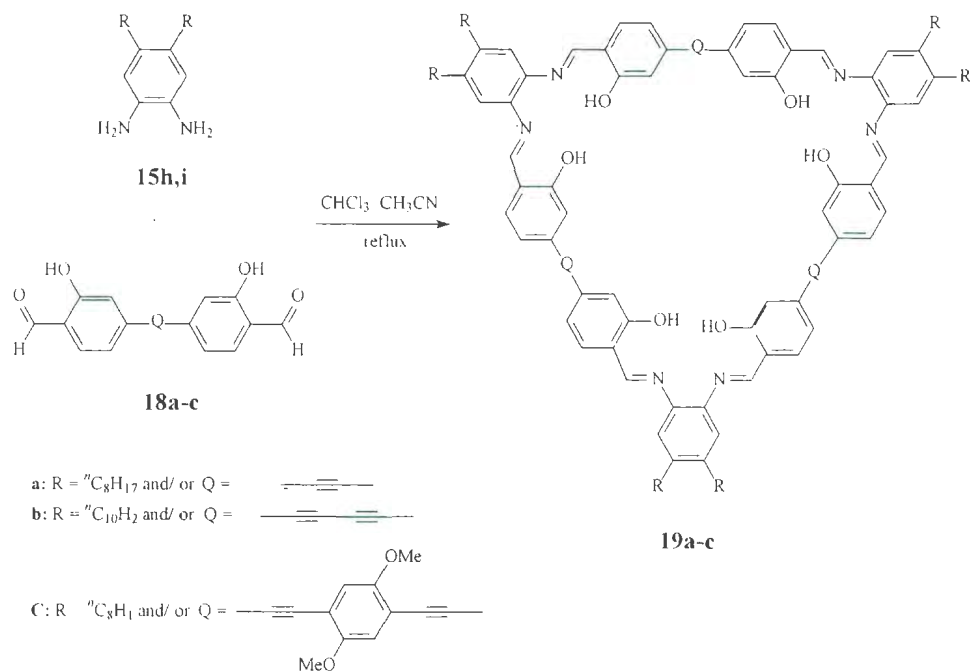


**Scheme 1.3-4:** Template-free macrocyclization reactions to produce conjugated Schiff base macrocycles **17a-m**.

Nabeshima prepared the conjugated [3+3] Schiff base macrocycle **17a** under template-free conditions in 92% yield (Scheme 1.3-4).<sup>2,3a</sup> This high yield was achieved when **15a** and **16** ( $4 \times 10^{-2}$  M) were allowed to react in acetonitrile, at room temperature, for two weeks. The macrocycle **17a** precipitated out directly from the reaction solution. However, a lower yield (19%) was obtained and a longer reaction time (one month) was required when the reaction was conducted under more dilute conditions ( $2.5\text{--}4.0 \times 10^{-3}$  M). It was rationalized that the driving force of the reaction to produce **17a** in high yield was

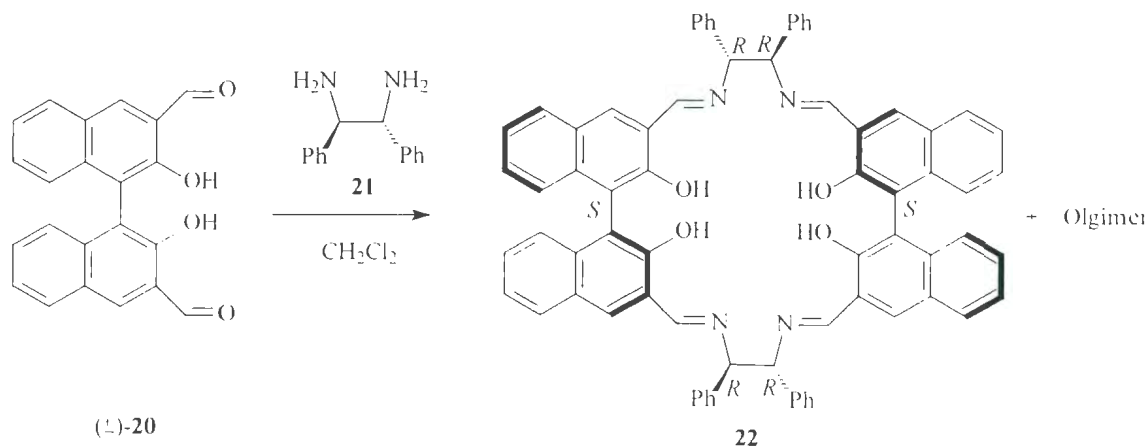
its precipitation from the reaction solution as soon as it was being formed. MacLachlan modified the solubility of **17a** by functionalizing the phenylenediamine with alkoxy groups, to form **17b-m** (Scheme 1.3-4).<sup>23b,c</sup> The dialkoxyphenylenediamines **15b-m** were reacted with dialdehyde **16** to form **17b-m** in different yields. Those macrocycles having the larger alkoxy substituents *e.g.*, **17l** and **17k** were formed in only 18% and 34% yields, respectively, whereas those having the shorter alkoxy groups, *e.g.* **17h** and **17f**, were obtained in much higher yields (87% and 75%, respectively). Furthermore, the reactions leading to the formation of the macrocycles having the larger alkoxy substituents were slower: for example, the formation of **17f** (R = OC<sub>6</sub>H<sub>13</sub>) required 1-3 h to complete, but for **17l** (R = OC<sub>16</sub>H<sub>33</sub>), more than 12 h was required, and only a 34% yield was obtained. MacLachlan suggested that the larger alkoxy group-containing phenylenediamine reactants required a longer time to aggregate in the reaction solvent (1:1 CHCl<sub>3</sub>:MeCN), and thus are less reactive than their shorter alkoxy group-containing phenylenediamine counterparts.

The same template-free methodology was employed in the macrocyclization reactions of bis(salicylaldehydes) **18a-c** (Scheme 1.3-5). These macrocycles are flexible since there can be free rotation between the phenyl-alkyne bonds as compared with **16** which has fixed geometry, to form **19a-c** in good yields (68, 62 and 40%, respectively).<sup>23d</sup>



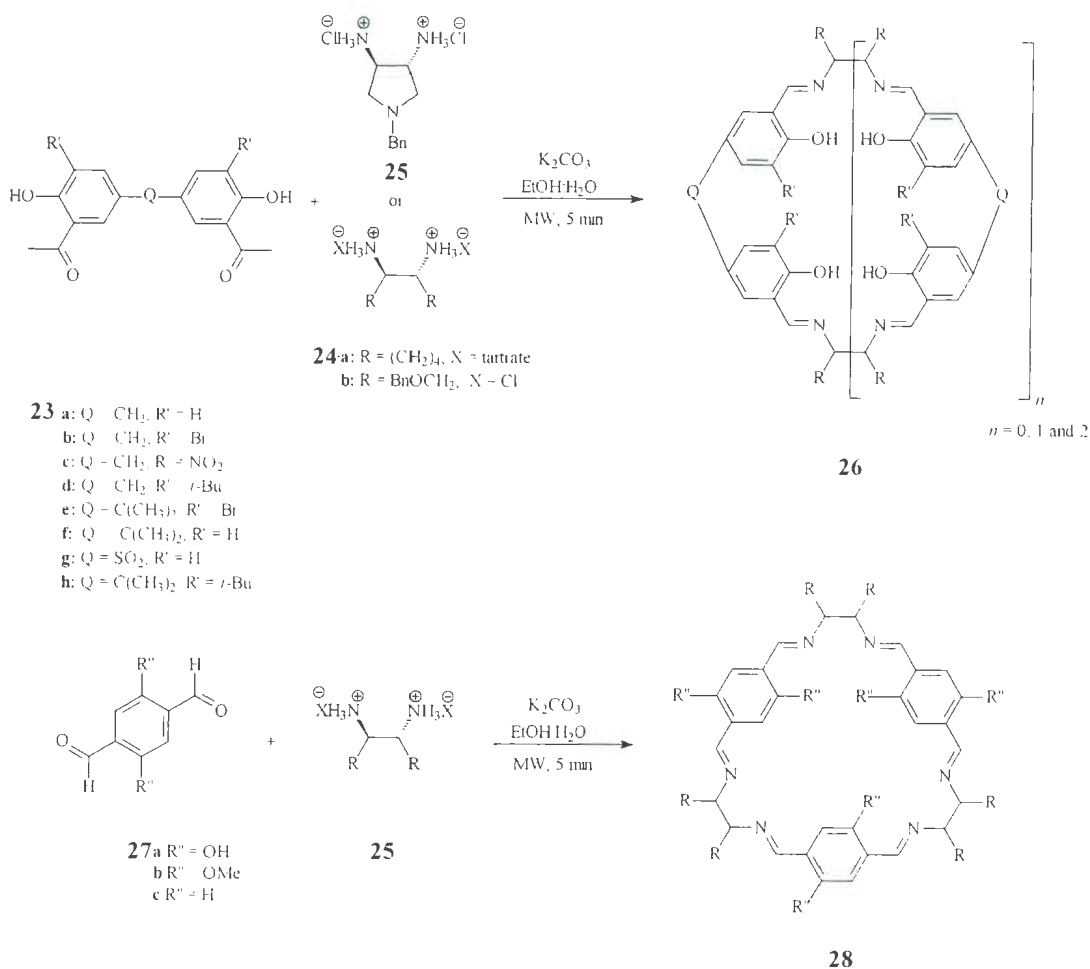
**Scheme 1.3-5:** Template-free macrocyclization reactions to produce Schiff base macrocycles **19a-c**.

It should be noted that in some cases, the yield of [2+2] macrocycles formed under non-templated conditions are relatively higher than those obtained in the examples cited previously, in Scheme 1.3-3. For example, the reaction of racemic 3,3'-diformyl-2,2'-binaphthol (**20**) and (*R,R*)-1,2-diamino-1,2-diphenylethane (**21**) under high-dilution conditions in dichloromethane furnished the optically pure 24-membered macrocycle **22** in 45% yield from the Schiff base condensation reaction of (*S*)-3,3'-diformyl-2,2'-binaphthol with **21** (Scheme 1.3-6). The other enantiomer, ((*R*)-3,3'-diformyl-2,2'-binaphthol), afforded only an enantiomerically-pure polyimine product.<sup>24</sup>



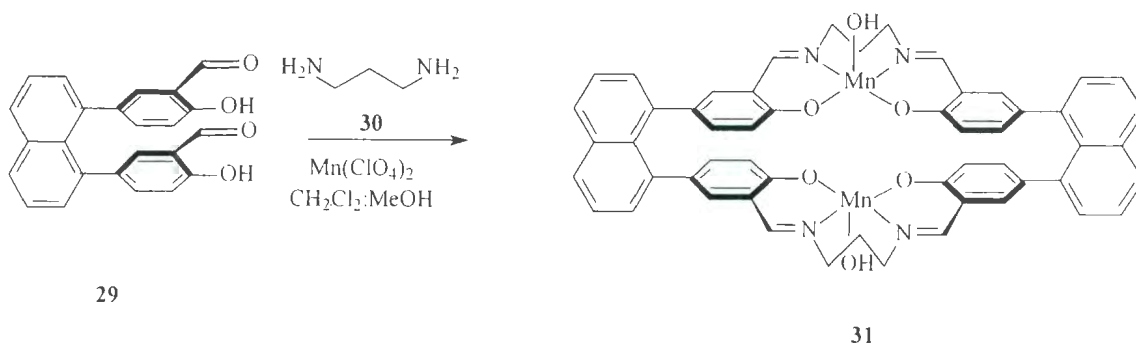
**Scheme 1.3-6:** Schiff base macrocyclization reaction of racemic mixture of 3,3'-diformyl-2,2'-binaphthol (**20**) with (*R,R*)-1,2-diamino-1,2-diphenylethane (**21**).

Macrocyclization of bisaldehydes **23a-g** (Scheme 1.3-7) with a series of chiral diamines such as **24** and **25** using very short (5 min) microwave irradiation times, successfully afforded mixtures of calix[*n*]salens such as **26** in moderate yields.<sup>25</sup> However, the desired macrocycle(s) **26** were contaminated with linear oligo- or polymeric imines in the reaction mixtures. Furthermore, some of the resulting mixtures, such as that from the condensation reaction of bisaldehyde **23a** with diamine **24a**, could not be purified. In contrast, the thermal condensation reaction of the bisaldehyde **23h** with diamine **24a** led to a polyimine product.<sup>26</sup> As well, under microwave irradiation conditions the reaction of phenyl dialdehydes such as **27a-c** with diamine **25** furnished the trimer **28** also in high yields.<sup>25</sup>



**Scheme 1.3-7:** Schiff base macrocyclization under microwave irradiation conditions.

McAuliffe employed Mn(ClO<sub>4</sub>)<sub>2</sub> as a template to form the Mn(III)-salen dimer **31** (Scheme 1.3-8, discussed earlier in Chapter 2), *in situ* from the corresponding ligand.<sup>27</sup>

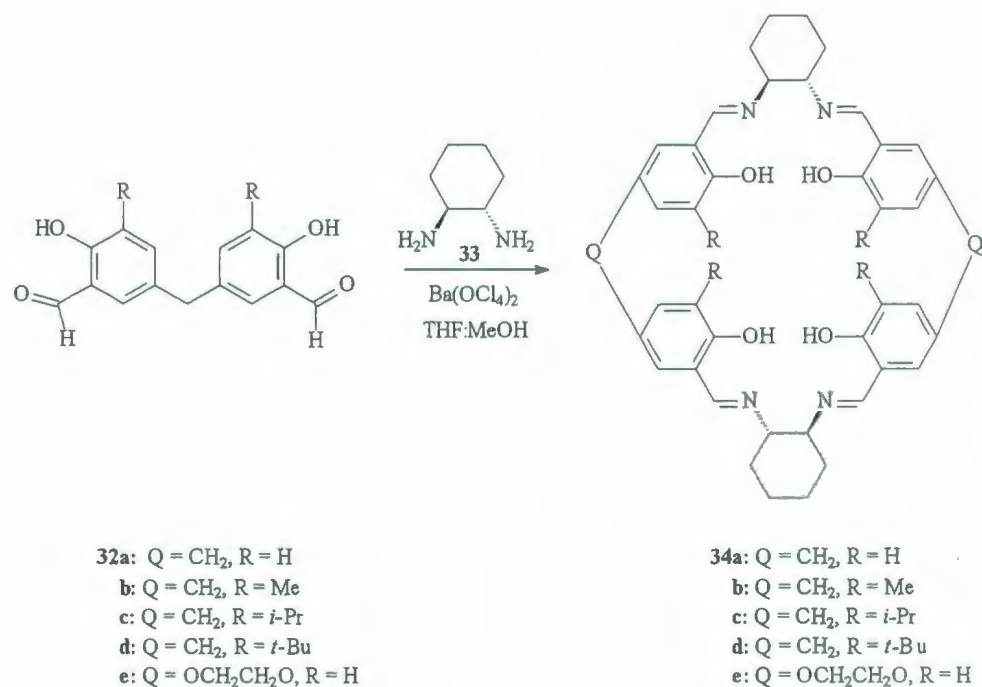


**Scheme 1.3-8:** McAuliffe's Mn(III)-salen dimer **31**.

Li first synthesized novel chiral calix[*n*]salens (Scheme 1.3-9) using Ba(ClO<sub>4</sub>)<sub>2</sub>-templated Schiff base macrocyclization with dialdehydes **32** with **33** under high dilution conditions in THF, and in MeOH.<sup>28</sup> In addition to the [3+3] and [4+4] macrocycles, the [2+2] salen products **34** were obtained as mixtures of different conformers.<sup>29</sup> It is notable that the condensation reactions of bisaldehydes **32a-c** afforded product mixtures of the [2+2] and [4+4] macrocycles in higher yields than those obtained with the bisaldehyde **32d** which contains *tert*-butyl groups. Furthermore, the product mixtures from **32d** consisted of only small amounts of the [2+2] macrocycle **34d**, and mainly of presumed polymeric products and the [4+4] macrocycle. This finding was presumed to be a result of the steric requirements of **32d**, which favored formation of resinous oligomers or polymers over the more highly-strained and thermodynamically less stable macrocyclic products. Ligand **34d** reacted with a stoichiometric amount of Mn(OAc)<sub>3</sub> · 2H<sub>2</sub>O at room temperature to give the corresponding [Mn(III)]<sub>2</sub>-calix[2]salen complex (compound **117d**, Figure 1.1-30, Section 1.1.4) in 80% yield.<sup>29</sup> This complex induced high enantioselectivity in the epoxidation of styrene and indene. For example, styrene oxide was produced in 97% *ee* by using *m*-CPBA as the oxidant at -78 °C and indene oxide was obtained in 97% *ee* in the presence of NaOCl as oxidant at 0 °C. In contrast, *trans*-stilbene was epoxidized in very low yield (4.0%).

A rationalization for these results is that it is too difficult for bulky olefins such as *trans*-stilbene to fit in the cavity (whose diameter is approximately 7.7 Å) in order to approach the active centre. This was an indication that the epoxidation of olefins catalyzed by Mn(III)-calixsalen complexes proceeds *via* an internal host-guest pathway.

This finding prompted the synthesis of a new generation of calix[2]salens having larger cavity dimensions which would be crucial to fully explore the catalytic potential of calixsalens such as **34a-e** (Scheme 1.3-9).



**Scheme 1.3-9:** Ba(ClO<sub>4</sub>)<sub>2</sub>-templated Schiff base macrocyclization reactions.

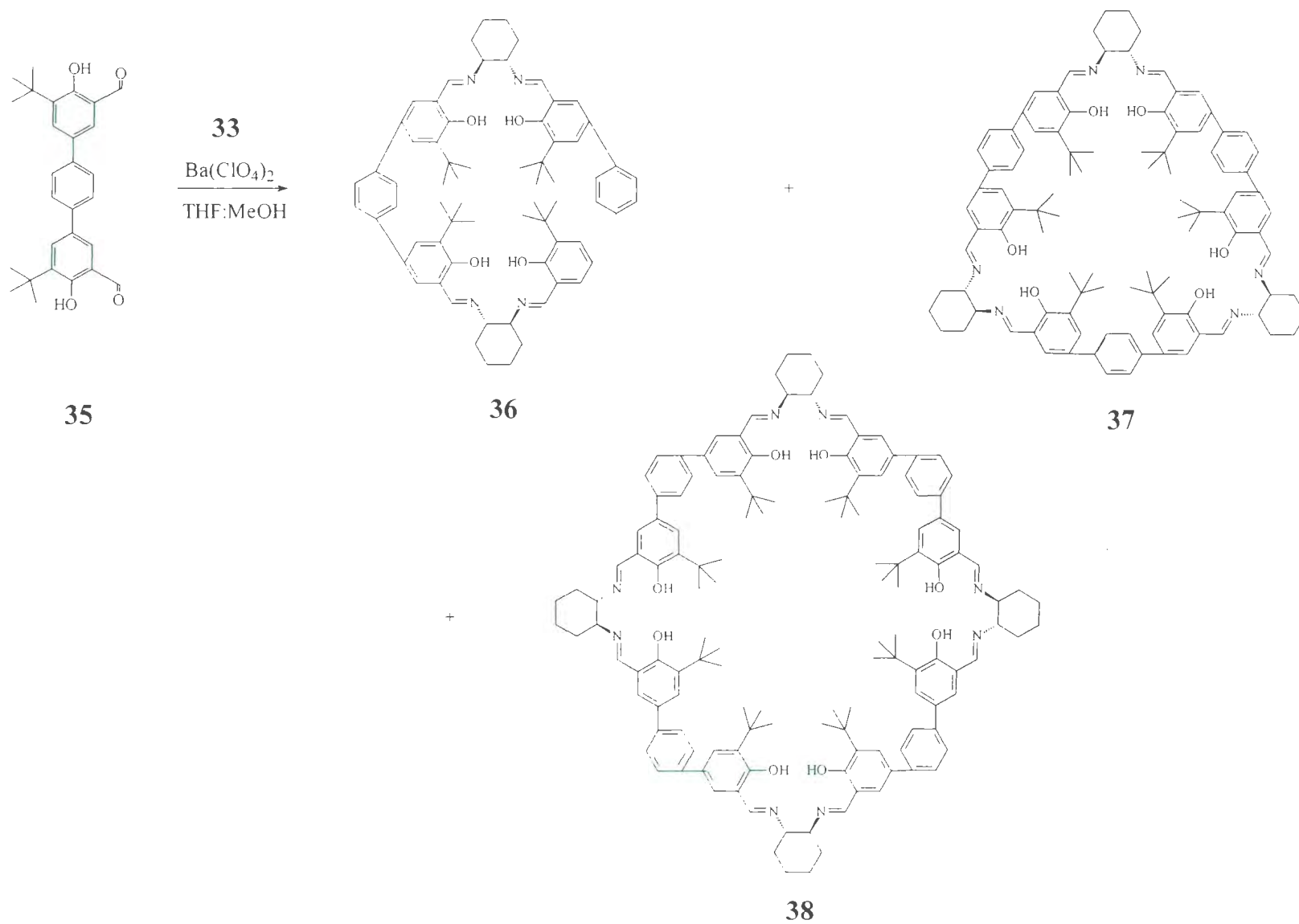
Calix[*n*]salens with rigid linker groups are basket-shaped and could also have a chiral internal cavity. Increasing the cavity size could also increase the scope for such compounds to act as chiral receptors *via* host/guest interactions and therefore, besides asymmetric catalytic epoxidation, could also potentially improve resolution of some chiral guests. In addition, development of a new method for Schiff base macrocyclization would be a useful approach in organic synthesis because the Schiff base methodology is a common step in many synthetic routes of supramolecular systems. The research aims

described in this chapter are: (i) The synthesis and characterization of a new series of calix[*n*]salens with larger cavities based on rigid phenylene linking groups; and (ii) the development of convenient and reliable methodologies for the Schiff base reaction as an efficient macrocyclization technique.

## 1.3.2 Results and discussion

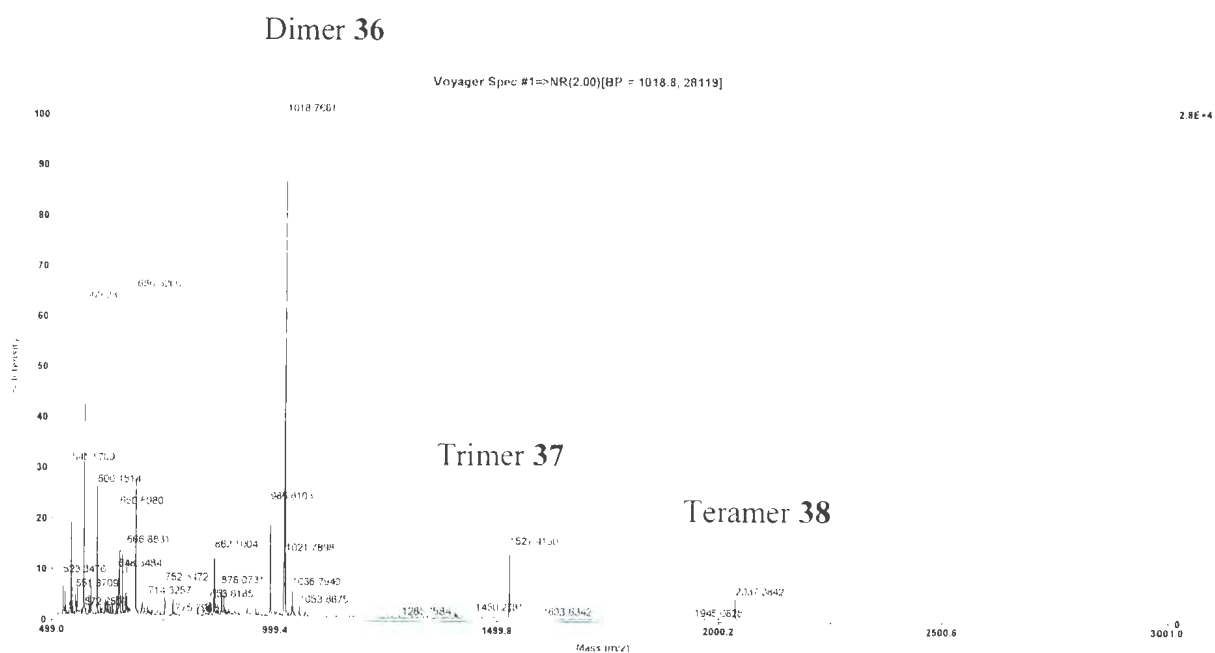
### 1.3.2.1 Schiff base condensation of bisaldehyde **35**

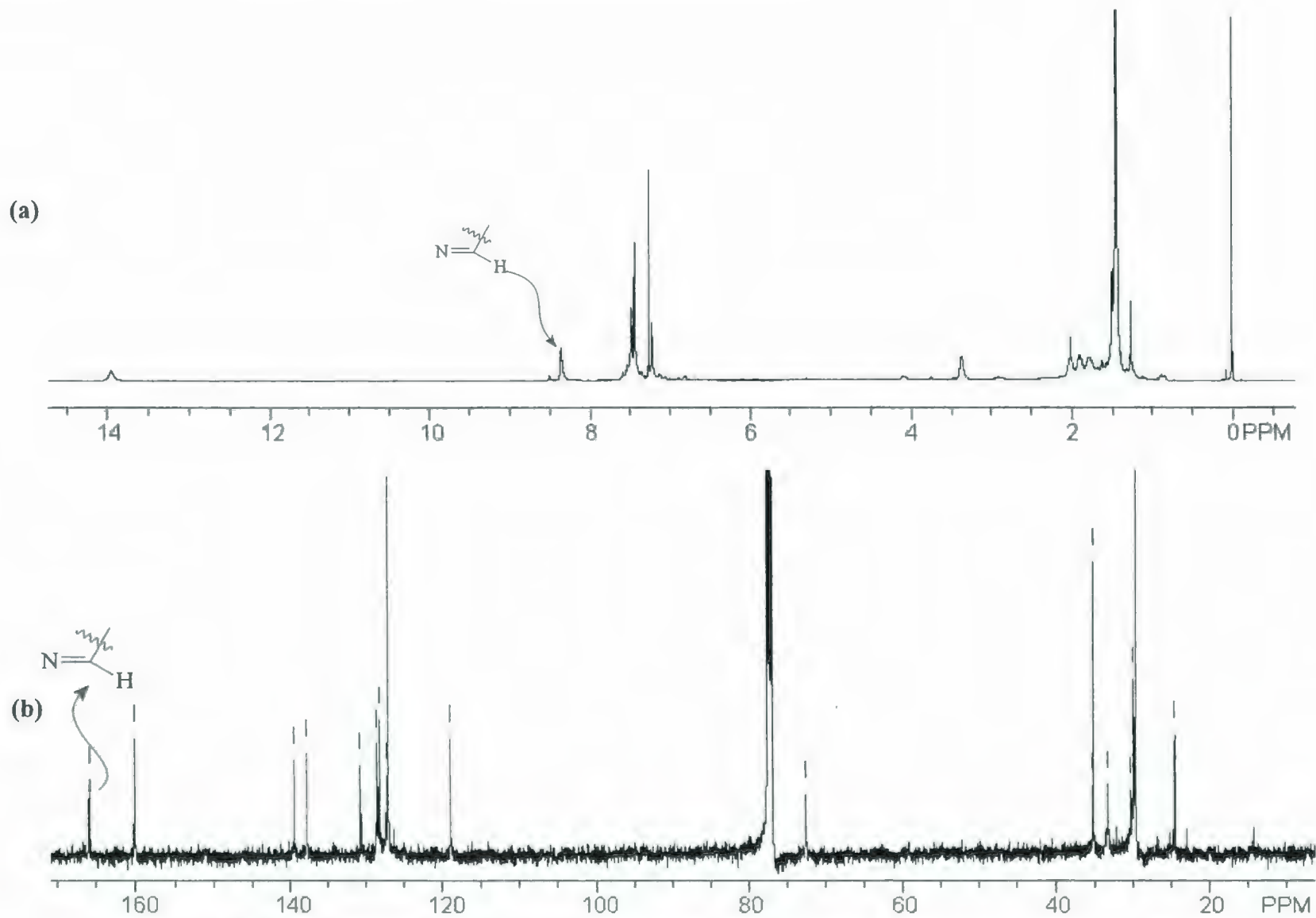
The condensation reaction of 1,4-bis(3-*tert*-butyl-5-formyl-4-hydroxyphenyl)-benzene (**35**) with (*S,S*)-*trans*-1,2-diaminocyclohexane (DACH) (**33**) was accomplished under the same conditions that were previously reported by Jablonski's group, using Ba(ClO<sub>4</sub>)<sub>2</sub> as the template (Scheme 1.3-10).<sup>28</sup> Solutions of **35** in THF (0.0256 M) and diamine **33** in MeOH (0.0256 M) were simultaneously added to the solution of Ba(ClO<sub>4</sub>)<sub>2</sub> in (1:1) THF:MeOH over 24 h. The reaction solution initially changed to a yellow-green colour. The <sup>1</sup>H NMR spectrum of the crude product obtained by evaporation of the reaction solvent, was consistent with a mixture of Schiff base products. No remaining starting materials were detected, but three sharp Schiff base signals appeared at  $\delta = 8.38, 8.50$  and  $8.52$  ppm, along with two broad, overlapping phenolic signals at  $\delta = 14.00$  and  $13.97$  ppm. The aromatic region in the <sup>1</sup>H NMR spectrum was very complicated although a sharp singlet at  $\delta = 7.60$  ppm assigned to the *p*-disubstituted phenyl linking group could be discerned. The MALDI-TOF mass spectrum of the crude



**Scheme 1.3-10:** The Schiff base macrocyclization reaction of bisaldehyde **35**.

product showed three peaks which are assigned to the molecular ions of [2+2] macrocycle **36**, [3+3] macrocycle **37** and [4+4] macrocycle **38** (Scheme 1.3-10, Figure 1.3-2).





The  $^1\text{H}$  NMR spectra of the fractions collected consistently showed aldehyde signals owing to imine hydrolysis. These results suggested that the desired salen macrocycles **36** and **37** are likely strained and that only a small amount of energy is sufficient to cause ring opening under the slightly acidic environment of silica gel. Fortunately, crystallization proved to be a better method for separating the components of this mixture. Different binary solvent systems were employed including MeOH:hexane, diethyl ether:hexane,  $\text{CH}_2\text{Cl}_2$ :methanol and THF:acetonitrile. The THF:acetonitrile (1:2.5) system turned out to be the best solvent to use and resulted in precipitation of a product in 38% yield. This product had  $^1\text{H}$ - and  $^{13}\text{C}$  NMR spectra, which were consistent with structures of the salen macrocycles **36** (Figure 1.3-3).

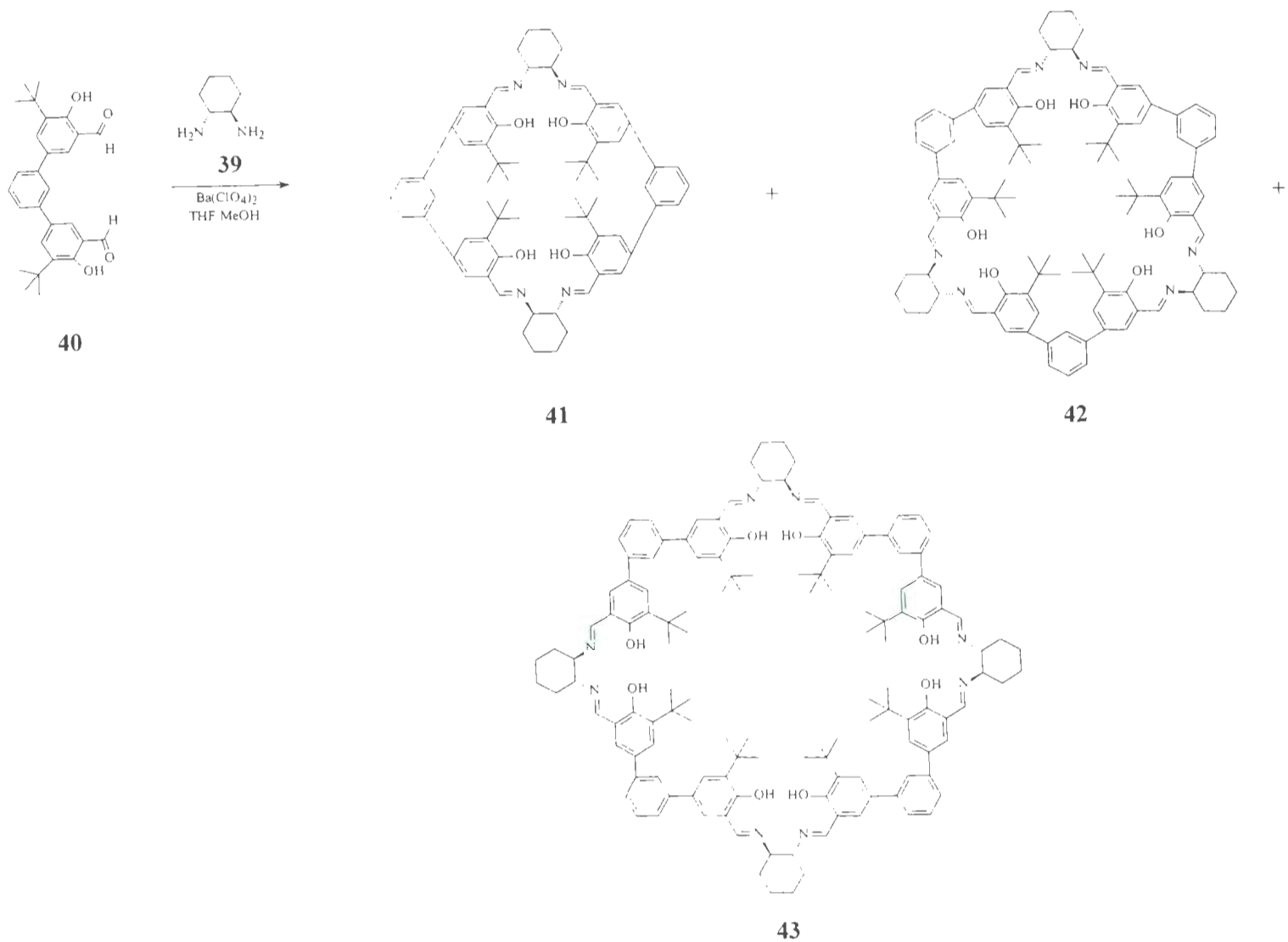
The  $^1\text{H}$  NMR spectrum revealed the Schiff base imine protons as a singlet at  $\delta = 8.36$  ppm, a broad phenolic peak at  $\delta = 13.95$  ppm (Figure 1.3-3a), a sharp singlet at  $\delta = 7.49$  ppm corresponding to the four hydrogens of the 1,4-phenylene groups, and two singlets at  $\delta = 7.22$  and  $7.54$  ppm, which were assigned to the two hydrogens of the salicylaldehyde moiety. In the upfield region, a multiplet appeared at  $\delta = 1.90$  ppm due to the hydrogens of the cyclohexyl group and a sharp singlet at  $\delta = 1.45$  ppm corresponding to the hydrogens of the four *tert*-butyl groups. The  $^{13}\text{C}$  NMR spectrum (Figure 1.3-3b) showed a characteristic signal at  $\delta = 165.88$  ppm for the Schiff base imine-carbons and another phenolic carbon at  $\delta = 160.13$  ppm in addition to eight signals in the aromatic region, all of which are consistent with the structure of the desired cyclic salen-dimer **36**. Three high-field signals assigned to the cyclohexyl group were observed at  $\delta = 24.51$ ,  $29.73$  and  $72.61$  ppm. The *tert*-butyl group showed signals at  $\delta = 29.61$  and  $35.25$  ppm.

The MALDI-TOF mass spectrum of this product was similar to that of the crude mixture (Figure 1.3-2). It showed a strong peak corresponding to dimer **36** and another two weaker signals which were related to trimer **37** and tetramer **38**. Monitoring this product by  $^1\text{H}$  NMR spectrometry showed that it was not stable in  $\text{CDCl}_3$  solution. Over a one-week period, three new Schiff base related signals were observed at  $\delta = 7.91$ ,  $8.24$  and  $8.35$  ppm. In addition, the  $^1\text{H}$  NMR spectrum in the aromatic region was more complex. Since the spectrum did not show a signal corresponding to an aldehyde group, the changes observed were presumed to be due to the presence of one, or more, different conformers, or interconversion between the dimer, trimer and tetramer macrocycles.

### **1.3.2.2 Schiff base condensation of *meta*-bisaldehyde **40****

#### **1.3.2.2.1 Schiff base macrocyclization of **40** in methanol:THF**

The  $\text{Ba}^{2+}$ -templated conditions used previously for the Schiff base macrocyclization of bisaldehyde **35** and (*S,S*)-DACH **33** in THF:methanol was employed for the reaction of **40** and **39** (Scheme 1.3-11). The  $^1\text{H}$  NMR spectrum of the crude product mixture showed mainly three Schiff base singlet signals at  $\delta = 8.37$ ,  $8.40$  and  $8.30$  ppm, along with two lower intensity singlets at  $\sim \delta = 8.38$  ppm and  $\delta = 8.39$  ppm. No starting materials were detected in the spectrum of the crude product. The MALDI-TOF mass spectrum for this mixture was similar to that of the product mixture from the macrocyclization reaction of bisaldehyde **35** (Figure 1.3-2). There were three peaks at  $m/z$  1018.7, 1528.3 and 2036.9 which are consistent with the calculated masses for the dimer **41**, trimer **42** and tetramer **43**, respectively.



Scheme 1.3-11: Schiff base macrocyclization reaction of bisaldehyde **40**.

Purification of the crude product mixture using silica gel flash column chromatography and several different eluents, failed to separate the mixture. Most of the products appeared to have undergone hydrolysis on the silica gel. With dichloromethane, a fraction, whose mass amounted to 52% of the total mass of the crude product, was eluted. Its  $^1\text{H}$  NMR spectrum was similar to that of the crude product, and its MALDI-TOF mass spectrum showed the presence of compounds **41-43**. A second fraction was eluted with 10% methanol in dichloromethane, however, its  $^1\text{H}$  NMR spectrum showed many signals which were due to imine group-containing oligomeric or polymeric products, with **41** being only a minor component.

Since silica gel chromatography failed to separate the components of the mixture obtained, attempts to purify the crude product by crystallization were conducted but were also unsuccessful. An acetone-insoluble solid, whose mass was approximately 23% of the mass of the total crude product, was separated by filtration. Its  $^1\text{H}$  NMR spectrum revealed broad and poorly-resolved signals, and only a very weak  $^{13}\text{C}$  NMR spectrum. The MALDI-TOF mass spectrum also did not show any significant features, except for a very weak signal corresponding to presumably a small amount of **41**. All of these results suggested that the acetone-insoluble product was most likely a mixture of oligomeric and/or polymeric imines. The THF:methanol macrocyclization protocol, apparently facilitated the formation of oligo-, or, polyimines. Therefore, in order to reduce polymerization and to produce the target dimer **41** in better yields, other solvent systems were evaluated.

### 1.3.2.2.2 Schiff base macrocyclization of **40** in methanol

The reaction to form the Schiff base by the slow addition of dilute solutions of **40** and (*R,R*)-DACH **39** in methanol, at room temperature, in the presence of barium perchlorate, furnished a crude mixture whose  $^1\text{H}$  NMR spectrum did not show any starting materials remaining. Furthermore, the  $^{13}\text{C}$  NMR spectrum of this product showed very weak signals, even when the sample was relatively concentrated (28 mg/mL). Attempts to dissolve the crude product in acetone left an insoluble material which constituted  $\sim 42\%$  of the total product, and whose  $^1\text{H}$  NMR and  $^{13}\text{C}$  NMR spectra were poorly-resolved and weak, respectively. Also, its MALDI-TOF mass spectrum did not show any evidence of either macrocycles **41-43**. This suggests that the acetone-insoluble product was again probably a mixture of oligo- or polyimines. The remaining crude product was purified on silica gel TLC, using 15% ethyl acetate in hexane as the eluent. Four bands were extracted. Isolation of the most mobile band afforded a yellow solid, in  $\sim 10\%$  yield, which was assigned as trimer **42**. Its MALDI-TOF mass spectrum revealed a very strong peak at  $m/z$  1527.2 corresponding to **42**, in addition to two smaller peaks related to **41** and **43** at  $m/z$  1018.6 and 2035.8, respectively (Figure 1.3-4). The  $^1\text{H}$  NMR spectrum in benzene- $d_6$  revealed one major Schiff base peak at  $\delta = 7.95$  ppm (Figure 1.3-5a), and its  $^{13}\text{C}$  NMR spectrum contained a Schiff base peak at  $\delta = 165.71$  ppm, in addition to ten signals in the aromatic region and three signals at  $\delta = 72.60$ , 33.24 and 24.45 ppm assigned to the cyclohexane ring (Figure 1.3-5b). The  $^1\text{H}$  NMR spectra of the extracted compounds from the other three bands, indicated that these compounds were

resulting from hydrolysis on the silica gel. Thus, **42** appears to resist hydrolysis on silica gel better than **41**.

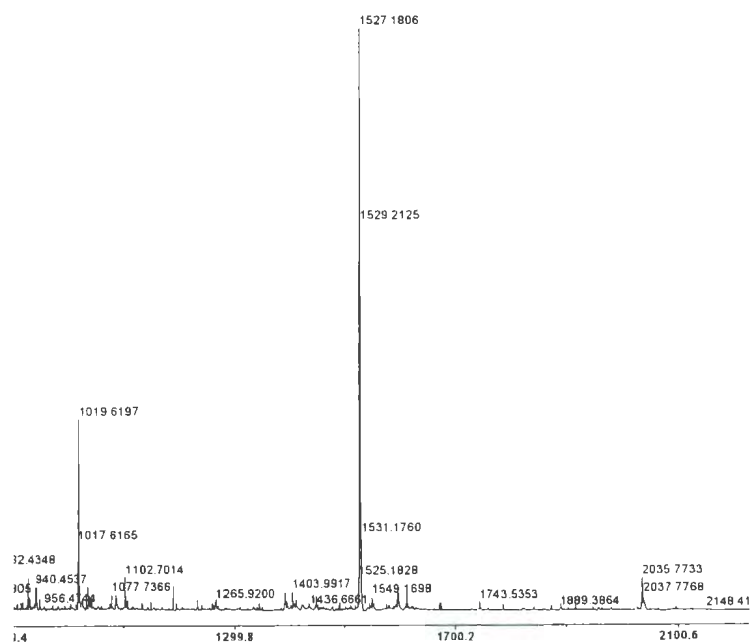
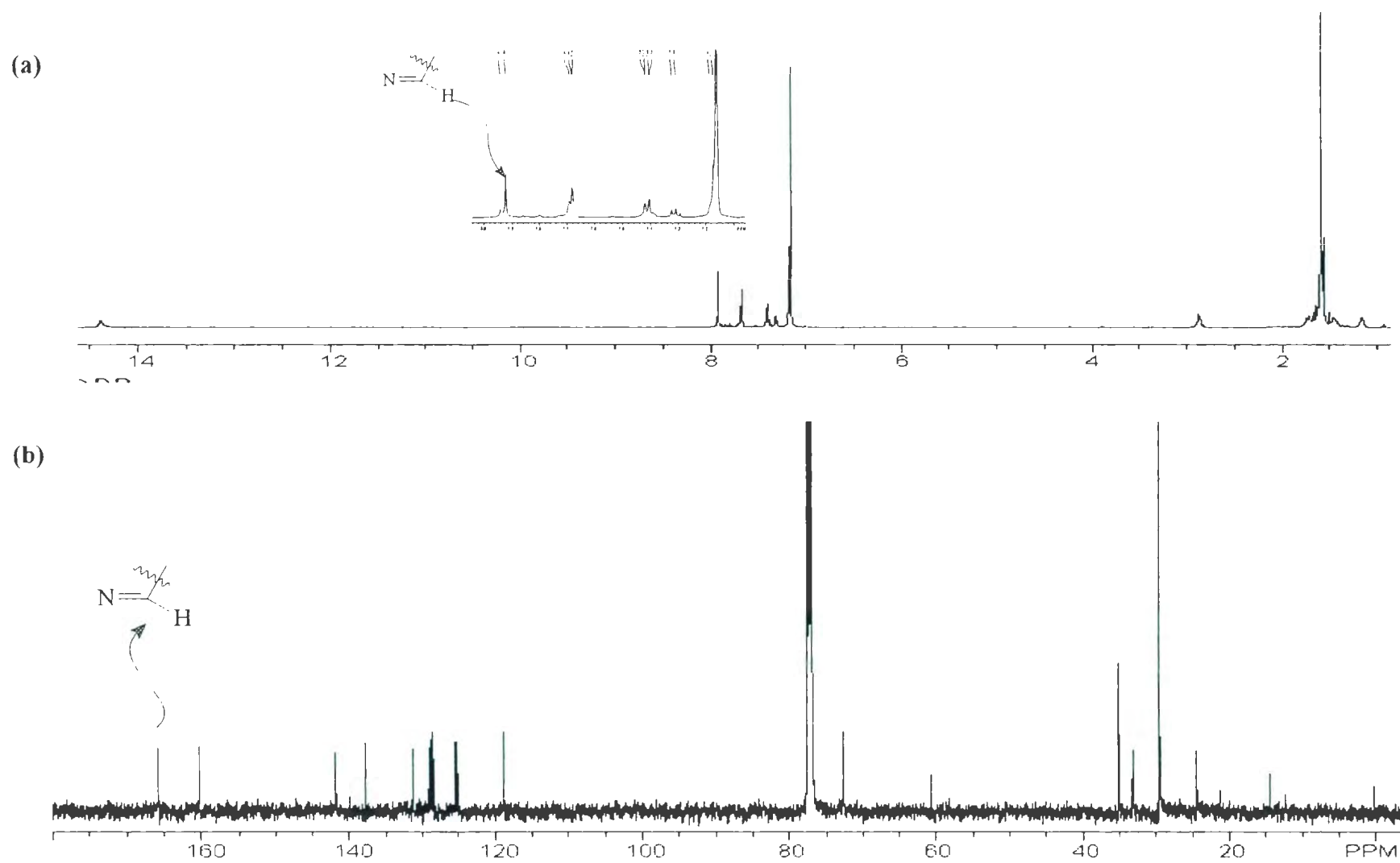


**Figure 1.3-4:** MALDI-TOF mass spectrum of the cyclized imine isolated by silica gel TLC.

In conclusion, using methanol as the solvent in the Schiff base reaction of bisaldehyde **40** afforded a product mixture of cyclized imines and a large quantity of oligo- or polyimines. This methodology, therefore, was not suitable to optimally produce the targeted cyclized Schiff base imines.



### 1.3.2.2.3 Schiff base macrocyclization of **40** in THF

As discussed in Sections 1.3.2.2.1 and 1.3.2.2.2, the use of methanol alone, or with THF, enhanced the formation of polyimines in the Schiff base reaction. Figure 1.3-6 shows two possible conformations of the bisaldehyde **40**. As determined by molecular mechanics modeling (MMM),<sup>30</sup> the *anti*-bisaldehyde **40a** is approximately only 1.5 kJ/mol lower in energy than the *syn*-bisaldehyde conformer **40b**. This MMM calculated energy difference alone is insufficient to account for the preferential formation of polyimines from **40a**, in the case of methanol or methanol/THF solvent. Nor is it sufficient to account for the preferential formation of macrocycles from **40b** in the polar aprotic solvents THF, acetonitrile or dichloromethane. Additional discussion on the effect of solvent upon the macrocyclization reaction will be presented in Section 1.3.2.2.3.

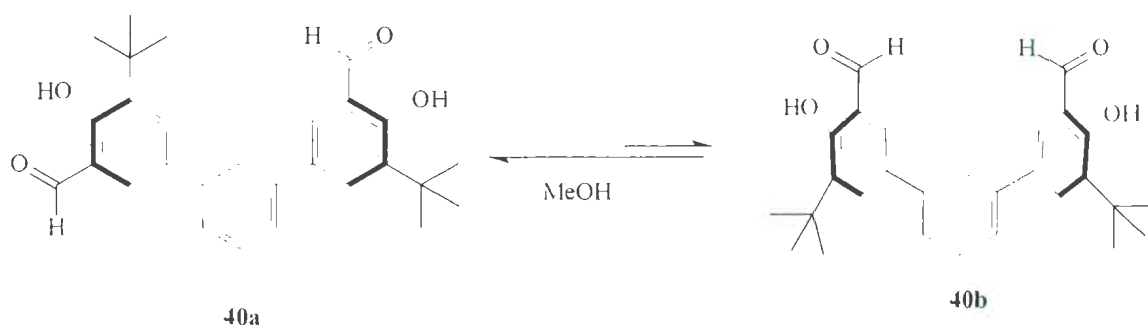


**Figure 1.3-6:** *Syn* and *anti* conformations of bisaldehyde **40**.

The use of THF alone as the solvent in the Schiff base reaction of **40**, under the same conditions that were used in the THF:methanol procedure, provided a different product mixture. The <sup>1</sup>H NMR spectrum (Figure 1.3-7a) of the crude product showed a peak at  $\delta = 8.54$  ppm corresponding to a major product. However, the addition of sodium

carbonate to the reaction of **40** with (*R,R*)-DACH **39** afforded an imine mixture whose  $^1\text{H}$  NMR spectrum (Figure 1.3-7b) revealed a major Schiff base peak at  $\delta = 8.30$  ppm which could be assigned to dimer **41**. In the presence of, and in the absence of sodium carbonate, the Schiff base reactions occurred efficiently, and no remaining starting materials were detected. However, the reactions carried out in the presence of the drying agent were slower; and required 7 days for completion, whereas only 24 hours were required for the reaction without any drying agent present. The  $^{13}\text{C}$  NMR spectra of the crude products showed a major Schiff base peak at  $\delta = 165.55$  ppm in both cases.

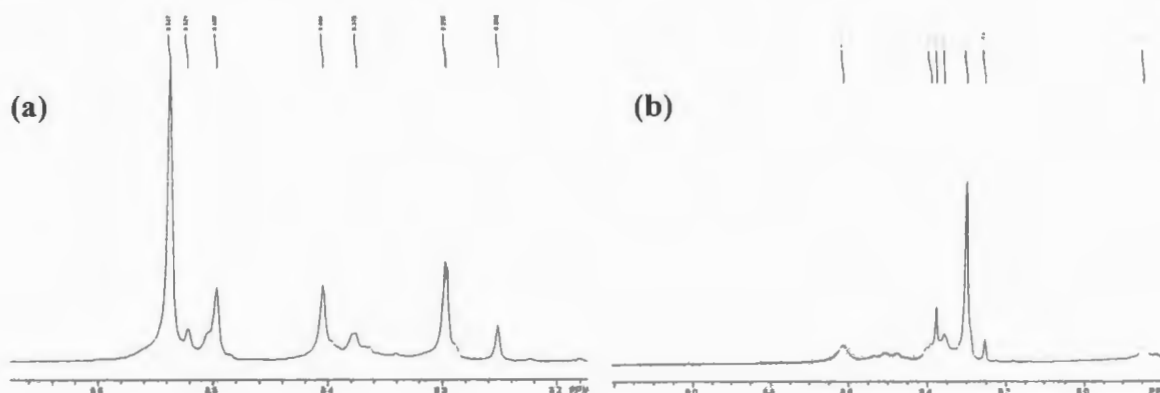


**Figure 1.3-7:**  $^1\text{H}$  NMR Schiff base signals for the crude product from the reaction of **40** in THF solvent: (a)  $\text{Na}_2\text{CO}_3$ -free-reaction; (b) in the presence of  $\text{Na}_2\text{CO}_3$ .

The MALDI-TOF mass spectra of the crude products obtained from both conditions were similar (Figure 1.3-8). The strongest peak which appeared at  $m/z$  1018.3 corresponds to dimer **41**. A weaker peak at  $m/z$  1526.7 is assigned to trimer **42** and the weakest peak at  $m/z$  2036.0 is assigned to tetramer **43**.

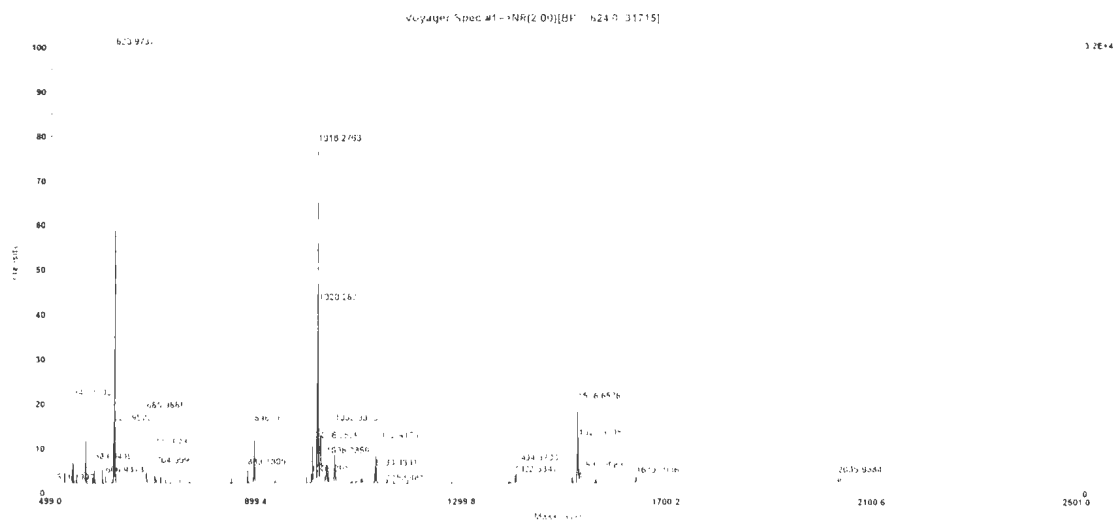


**Figure 1.3-8:** The MALDI-TOF mass spectrum product of Schiff base reaction of **40** THF solvent.

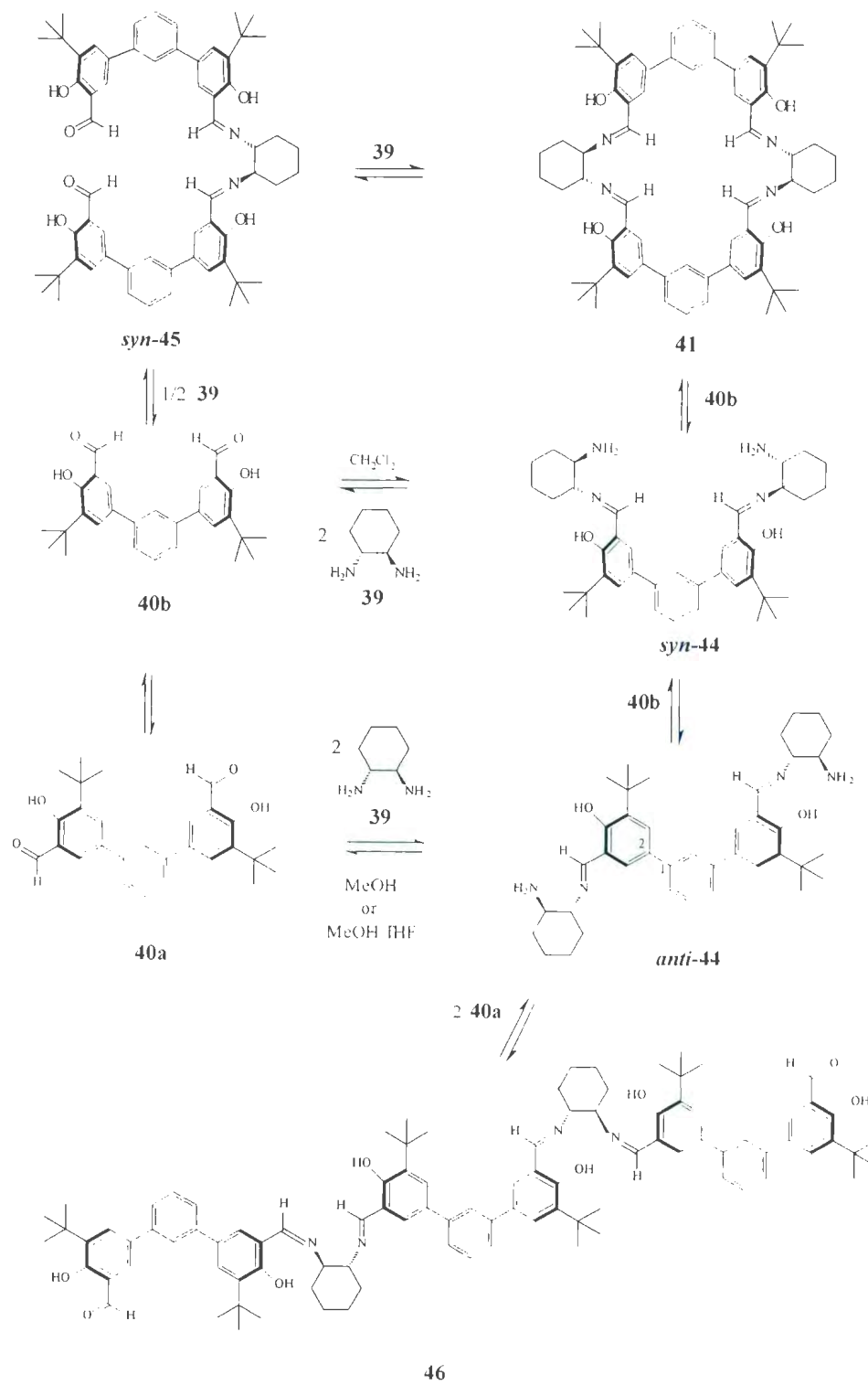
Attempts to purify the two mixtures from the Schiff base reactions in THF failed to give pure cyclized imine. However, using THF diminished the amount of acetone-insoluble polyimine byproduct to 14%. Silica gel TLC purification of the crude product from the sodium carbonate reaction conditions afforded four distinct bands. The second mobile band, had spectroscopic properties consistent with dimer **41**: a base peak at  $\delta = 8.25$  ppm and MALDI-TOF mass spectrum peaks at  $m/z$  1018.4 and 896.3 in 2.3% yield. The other mobile bands comprised only 2.3% of the crude reaction product, and all this material appeared to have been hydrolyzed on the silica gel.

In summary, using THF as the solvent for the Schiff base reaction of bisaldehyde **40** with (*R,R*)-DACH **39** diminished the polymerization process and afforded more of the cyclized imines **41-43**, as a mixture, with **41** as the major product. However, these mixtures of cyclized imine were inseparable and appeared to be easily hydrolyzed on silica gel. As well, the Schiff base reactions were sensitive the presence of any moisture in the THF.

#### 1.3.2.2.4 Schiff base macrocyclization of **40** in dichloromethane

In the preceding sections, it was described that the use of an aprotic solvent such as dichloromethane for the Schiff base macrocyclization reaction of **40** with (*R,R*)-DACH **39** reduced the extent of product hydrolysis. Using dichloromethane as the solvent, the reaction was not complicated by the formation of oligo- or polyimine by-products and afforded a clean mixture of cyclized Schiff base imines **41-43** from which pure **41** could be isolated. The acetone-soluble crude product mixtures gave sharp  $^1\text{H}$  NMR signals and produced strong  $^{13}\text{C}$  NMR spectra, even in low concentration conditions indicating that little, or no, oligo- or polymers had been produced.

The Schiff base reactions in methanol and methanol:THF were much faster than when dichloromethane was used as a solvent. A proposed abbreviated pathway for the reaction is conjectured and is shown in Scheme 1.3-12. The Schiff base reactions between the bisaldehyde **40a** in two steps with and two molecules of diamine **39** forms the diamino product, *anti*-**44**. This precursor could react at either amine terminal with the bisaldehyde molecules to form for example, the linear oligomer **46**. However, rotation about the C1-C2 bond would form *syn*-**44** which would lead to the desired macrocycle **41** *via* a subsequent reaction with a molecule of **40b** *via* two distinct Schiff base condensation steps. On the other hand, a polyimine product is produced from intermediate *anti*-**44** if the C1-C2 bond rotation to form *syn*-**44** is slower, or is prevented.



**Scheme 1.3-12:** Proposed polymerization and cyclization process in the Schiff base reaction of 40.

In dichloromethane, Schiff base reactions are slower, requiring a period of 3 to 8 days at room temperature for all of the starting materials to be consumed. (Scheme 1.3-12). Under these conditions, dimer **41** could be formed *via* reaction of an intermediate *syn-44* with **40b**, and/or *via* reaction of intermediate such as *syn-45* with **40b**. The stereochemistry in both compounds *syn-44* and **45** can be favored to some extent, by intramolecular hydrogen bonding.<sup>23</sup> In contrast, when methanol is employed as the solvent for this reaction, intramolecular hydrogen bonding is possibly diminished or weakened as a result of the stronger intermolecular hydrogen bonding possible between the methanol molecules and **44**. It is postulated that intermediate *anti-44*, which is the precursor for the formation of non-cyclic oligomers, becomes the predominant one over the *syn-44* conformer.

The <sup>1</sup>H NMR spectrum in CDCl<sub>3</sub>, of the crude product mixture showed that the aldehydic hydrogen signal at  $\delta = 10.00$  ppm had disappeared and was replaced with a major Schiff base signal at  $\delta = 8.30$  ppm, and other, minor signals, at  $\delta = 8.39$  ppm and  $\delta = 8.60$  ppm. The <sup>13</sup>C NMR spectrum had one Schiff base peak at  $\delta = 165.55$  ppm. The MALDI-TOF mass spectrum showed three characteristic peaks corresponding to the respective molecular masses of macrocycles **41-43**.

Variable-temperature <sup>1</sup>H NMR spectra recorded at 25, 30, 35, 50 and 80 °C showed no changes in either signal shapes or chemical shifts. Also, a low-temperature <sup>1</sup>H NMR spectrum recorded at -50 °C showed no changes in either the positions, or the intensities of the signals. This implies the presence of a mixture of different compounds,

or atropisomers whose rotational motions were limited due to the steric interactions between the *tert*-butyl groups.

When the crude product was re-dissolved in dichloromethane, the initial homogenous solution slowly became turbid upon standing. Filtration furnished a yellow solid whose MALDI-TOF mass spectrum showed only major peak, at  $m = 1018.6$  consistent with the molecular mass for the dimer **41** (Figure 1.3-9). Dimer **41** was isolated with a total yield of 30% from the filtrate by repeated crystallizations from dichloromethane.

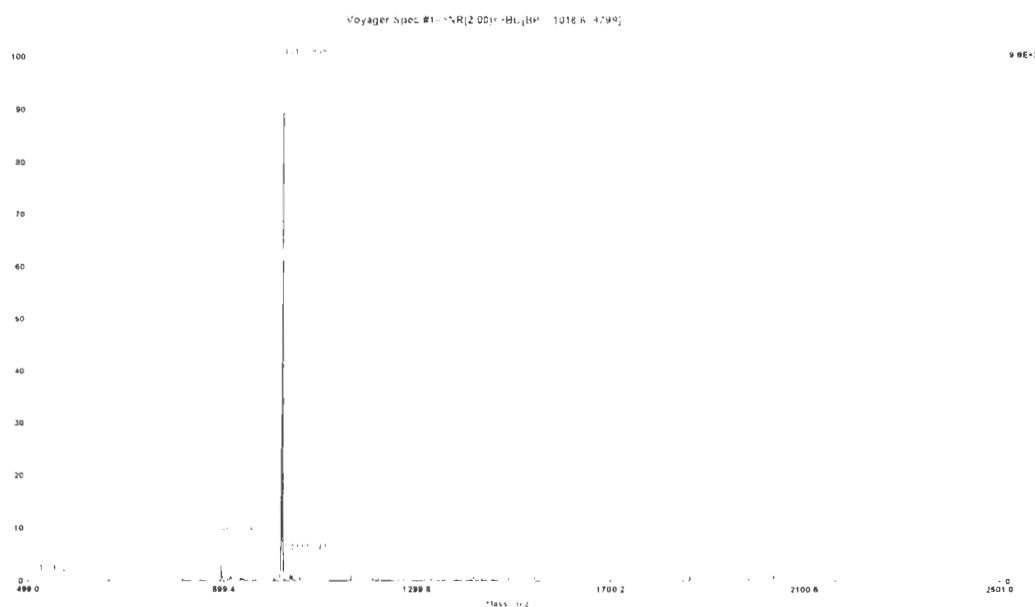


**Figure 1.3-9:** MALDI-TOF mass spectrum of the dimer **41**.

The  $^1\text{H}$  NMR spectrum (benzene- $d_6$ ) of this yellow solid showed it to be dimer **41** (Figure 1.3-10), as characterized by a sharp Schiff base singlet peak at  $\delta = 7.81$

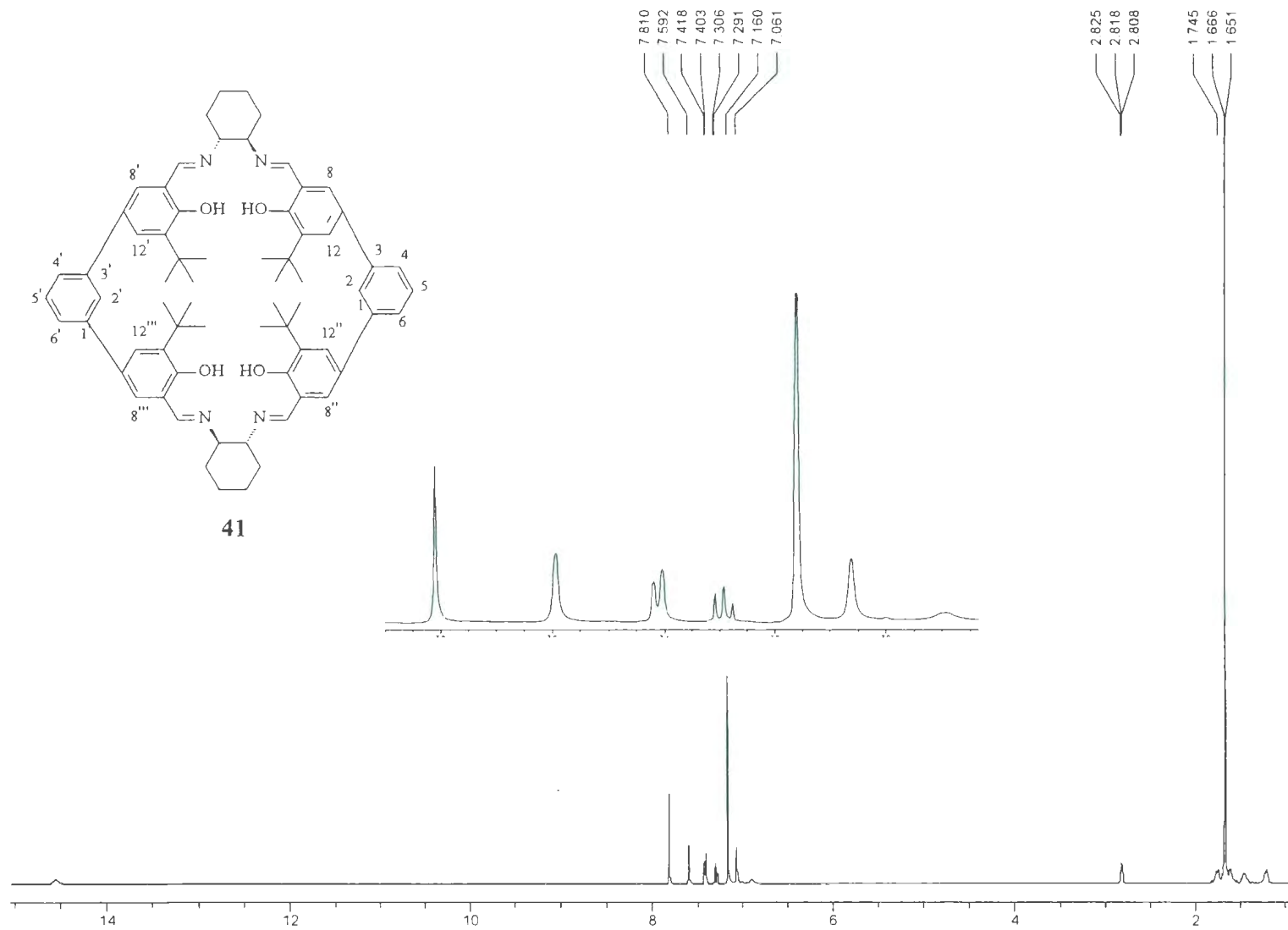


Figure 1.3-10: The  $^1\text{H}$  NMR spectrum of dimer **41** in  $\text{C}_6\text{D}_6$

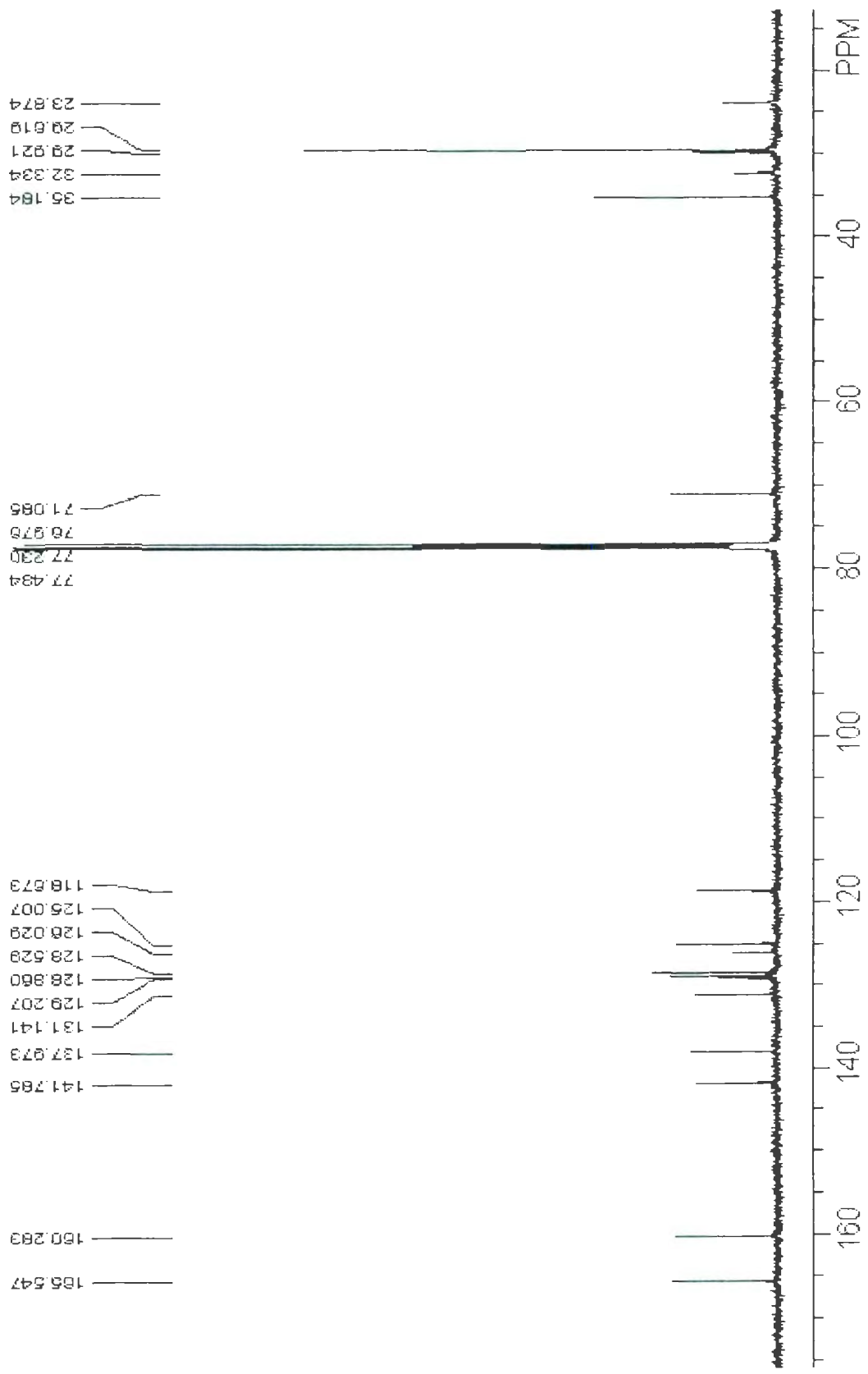


Figure 1.3-11: The  $^{13}\text{C}$  NMR spectrum of 41 in  $\text{CDCl}_3$

ppm (8.30 ppm in CDCl<sub>3</sub>) and a broad phenolic singlet at  $\delta = 14.56$  ppm. The linking phenylene group protons at C-2,2', C-4,4' and C-5,5' appeared as a doublet, a doublet of doublets and a triplet at  $\delta = 7.59$  ppm (*meta*,  $J = 2.5$  Hz), 7.41 ppm (*meta*,  $J = 2.5$  Hz and *ortho*,  $J = 8.0$  Hz) and 7.31 ppm (*ortho*,  $J = 8.0$  Hz), respectively. Also, the C-12,12',12'',12''' hydrogens appeared as a singlet signal at higher field, at  $\delta = 7.06$  ppm, while the C-8,8',8'',8''' hydrogens appeared as a singlet at  $\delta = 7.16$  ppm (which is buried under the benzene-*d*<sub>6</sub> signal). Three characteristic signals were observed for the cyclohexane ring at  $\delta = 71.09$ , 32.33 and 23.87 ppm and two signals at  $\delta = 35.18$  and 29.62 ppm corresponding to the *tert*-butyl group, confirmed the structure assignment for **41**.

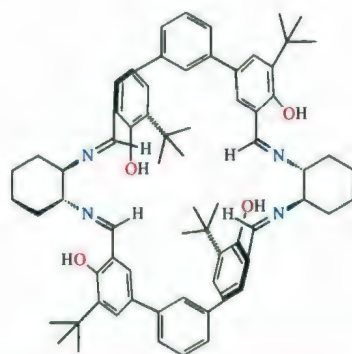
The <sup>13</sup>C NMR spectrum in CDCl<sub>3</sub> showed one Schiff base peak at  $\delta = 165.55$  ppm, one phenolic signal at  $\delta = 160.28$  ppm and nine (plus one overlapped) signals in the aromatic region, due to four nonequivalent carbon atoms of the phenyl linking groups and the six non-equivalent salen unit carbon atoms (Figure 1.3-11). Five high-field signals were observed: two were assigned for the *tert*-butyl groups at  $\delta = 29.62$  and 35.18 ppm, and three for the cyclohexyl rings at 23.87, 32.33 and 71.09 ppm. The <sup>1</sup>H NMR and <sup>13</sup>C NMR spectra confirm that **41** has C<sub>2</sub> symmetry. This compound, a "calix[2]salen", **41** gave an accurate mass measurement ( $m/z = 1016.6229$ ) for the structural formula C<sub>68</sub>H<sub>80</sub>O<sub>4</sub> (requires  $m/z = 1016.6180$ ).

All efforts to produce an X-ray viable single crystal for calix[2]salen **41** failed. Therefore, a molecular mechanics modeling (MMM) calculation study using the MMFF94 force field, was conducted on optimized conformations of **41**. These were based on conformations defined by the relative positions of the *tert*-butyl substituent

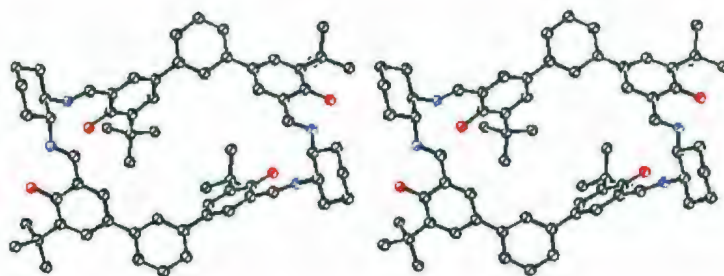
groups,<sup>30</sup> and are analogous to those major conformations which are usually defined in calixarene conformational analysis, as namely *cone*, *partial cone*, *1,2-alternate* and *1,3-alternate* and *saddle* (or *boat*) conformations.

The calculations suggested that the most stable conformer (Figure 1.3-12a) is the *saddle/boat*, the free energy of which is 276.2 kcal/mol. The *partial-pinched-cone* conformer (Figure 1.3-12b) is less stable by 1.3 kcal/mol. In this conformer, one of the *tert*-butyl groups lies in the opposite direction to the others. The *cone* conformer (Figure 1.3-12c) has higher energy (278.2 kcal/mol) than either the *saddle/boat* or the *partial-pinched-cone* conformers and has a structure in which all of the *tert*-butyl groups are *syn*. In the *1,3-alternate* conformer (305.9 kcal/mol) (Figure 1.3-12d), each of the proximal pairs of *tert*-butyl groups are *anti* to each other. In the *1,2-alternate* conformer (Figure 1.3-12e), which has highest free energy (315.4 kcal/mol), two of the *tert*-butyl groups linked *via* the same salen units are *syn* to each other, but are *anti* to the other pair of *tert*-butyl groups. The <sup>1</sup>H NMR spectrum of **41** is consistent with the anticipated spectra for the *cone* or *saddle/boat* conformations, however it should be borne in mind that the MMM calculations are for gas phase, isolated structures, whereas the NMR spectra are in solution and are subject to intermolecular interactions and solvation effects.

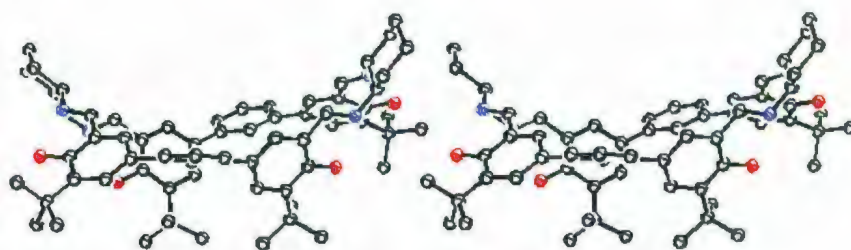
The MMM calculations reveal that *cone-41* conformer possesses a well-defined cavity whose widths are approximately 12.4 Å between the distal imine hydrogens of the salen units, and 6.3 Å between the phenyl linking groups.



Structure of the *boat* conformer of **41**.



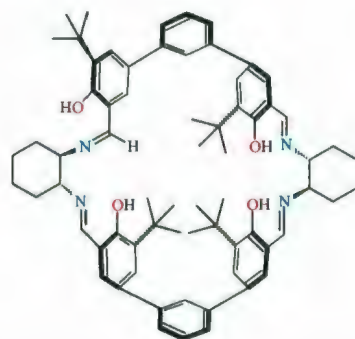
Stereoview of the *boat* conformer of **41** showing  
*tert*-butyl groups below the plane.



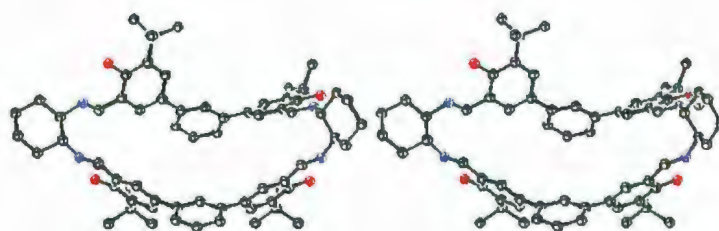
Stereoview of the side-view of *boat* conformer of **41**.

$$E = 276.2 \text{ kcal/mol}$$

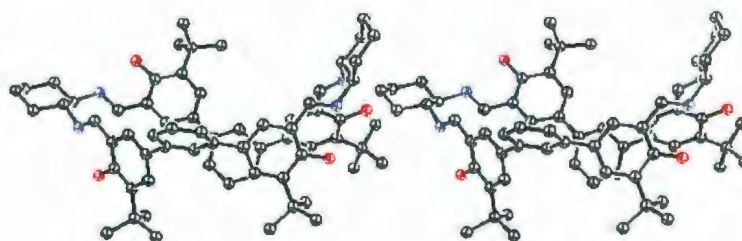
**Figure 1.3-12a:** Structure and free energy of the MMM-generated *boat* conformer of **41**.



Structure of the *partial-pinched-cone* conformer of **41**



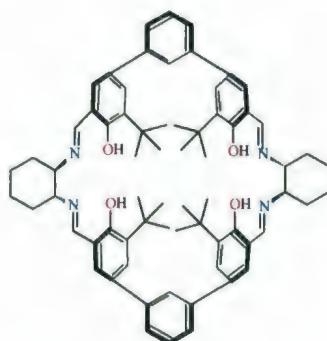
Stereoview of the *partial-pinched-cone* conformer of **41** showing  
*tert*-butyl groups below the plane



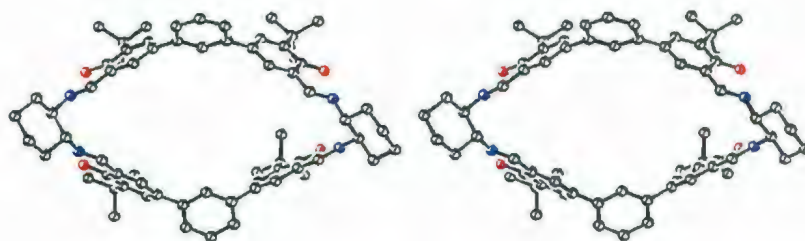
Stereoview of the side- view of the *partial-pinched-cone* conformer of **41**.

$$E = 277.5 \text{ kcal/mol}$$

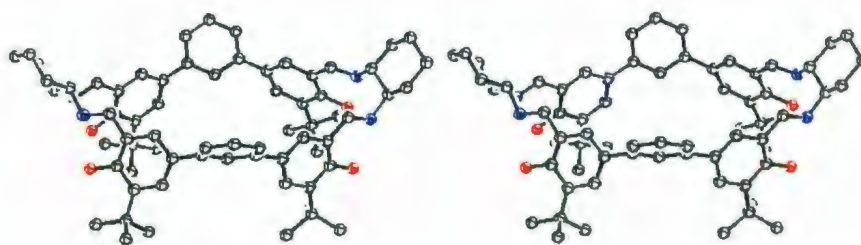
**Figure 1.3-12b:** Structure and free energy of the MMM-generated *partial-pinched-cone* conformer of **41**.



Structure of the *cone* conformer of **41**.



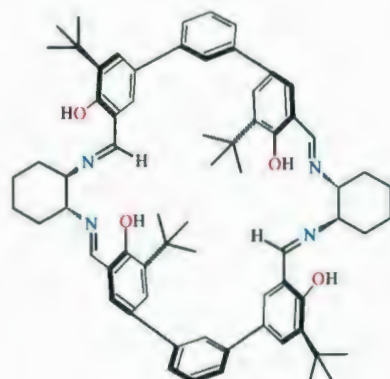
Stereoview of the *cone* conformer of **41** showing  
*tert*-butyl groups below the plane.



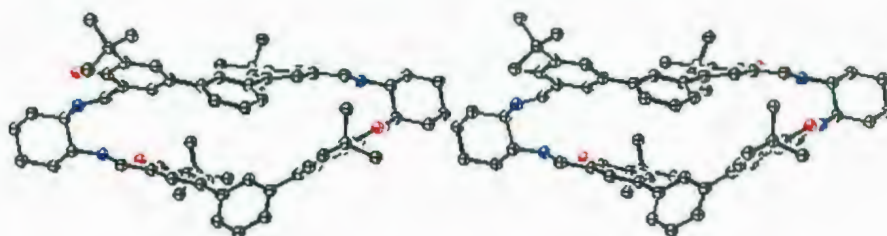
Stereoview of the side-view of the *cone* conformer of **41**.

$$E = 278.2 \text{ kcal/mol}$$

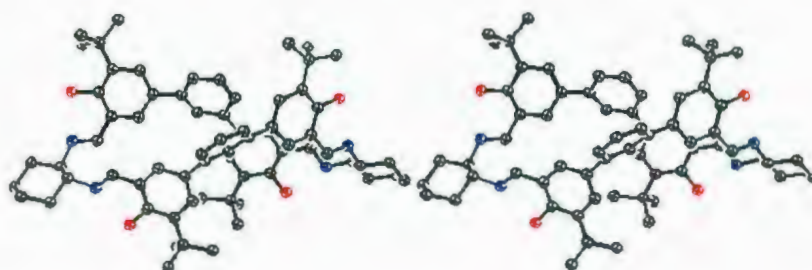
**Figure 1.3-12c:** Structure and free energy of the MMM-generated *cone* conformer of **41**.



Structure of the 1,3-*alternate* conformer of **41**



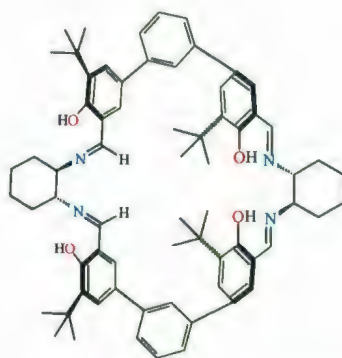
Stereoview of the 1,3-*alternate* conformer of **41** showing  
*tert*-butyl groups below the plane



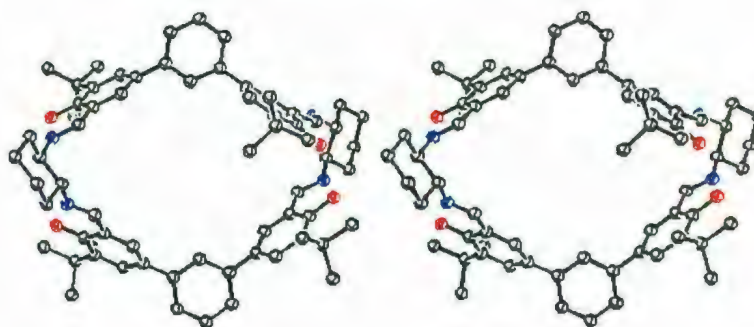
Stereoview of the side-view of the 1,3-*alternate* conformer of **41**.

$$E = 305.9 \text{ kcal/mol}$$

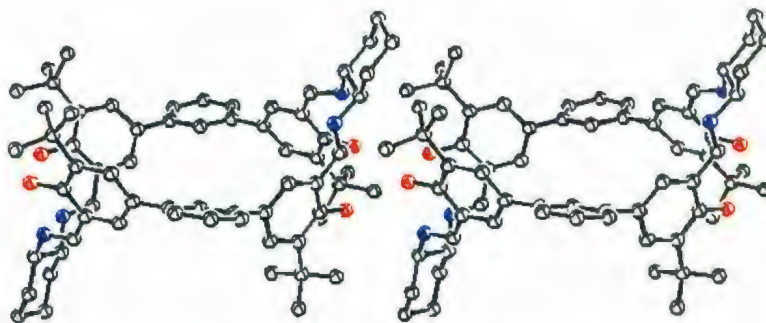
**Figure 1.3-12d:** Structure and free energy of the MMM-generated 1,3-*alternate* conformer of **41**.



Structure of the 1,2-*alternate* conformer of **41**



Stereoview of the 1,2-*alternate* conformer of **41** showing  
*tert*-butyl groups below the plane



Stereoview of the side-view of 1,2-*alternate* conformer of **41**

$$E = 315.4 \text{ kcal/mol}$$

**Figure 1.3-12e:** Structure and free energy of the MMM-generated 1,2-*alternate* conformer of **41**.

**Table 1.3-1: Effect of concentration on the yields of 41.**

Entry	Concentration of 40 in CH <sub>2</sub> Cl <sub>2</sub> (g/L)	yield % dimer 41
1	0.944	-
2	0.475	30%
3	0.218	70%

As shown in Table 1.3-1, dilution of the reaction solution clearly affected the yield of the dichloromethane-insoluble dimer **41** isomer. At higher concentration (0.944 g/L), **41** could not be isolated. However, when the reaction was run under more dilute conditions (0.218 g/L), the MALDI-TOF mass spectrum of the isolated crude product showed a single peak at *m/z* 1018.8 and pure **41** could be isolated in 70% yield.

The Schiff base reactions leading to **41** were found to also be sensitive to the method of purification of the dichloromethane used as the reaction solvent. A different crude product was obtained from solvent which had only been distilled over calcium hydride before use, than that afforded with dichloromethane which had first been dried more rigorously over P<sub>2</sub>O<sub>5</sub>, and then distilled over CaH<sub>2</sub>. In the former case, the <sup>1</sup>H NMR spectrum of the crude product, contained a major Schiff base peak at δ = 8.53 ppm. Its <sup>13</sup>C NMR spectrum showed a single Schiff base signal at δ = 165.51 ppm and the MALDI-TOF mass spectrum showed a strong dimer **41** ion peak, and two smaller peaks corresponding to the trimer **42** and **43**.

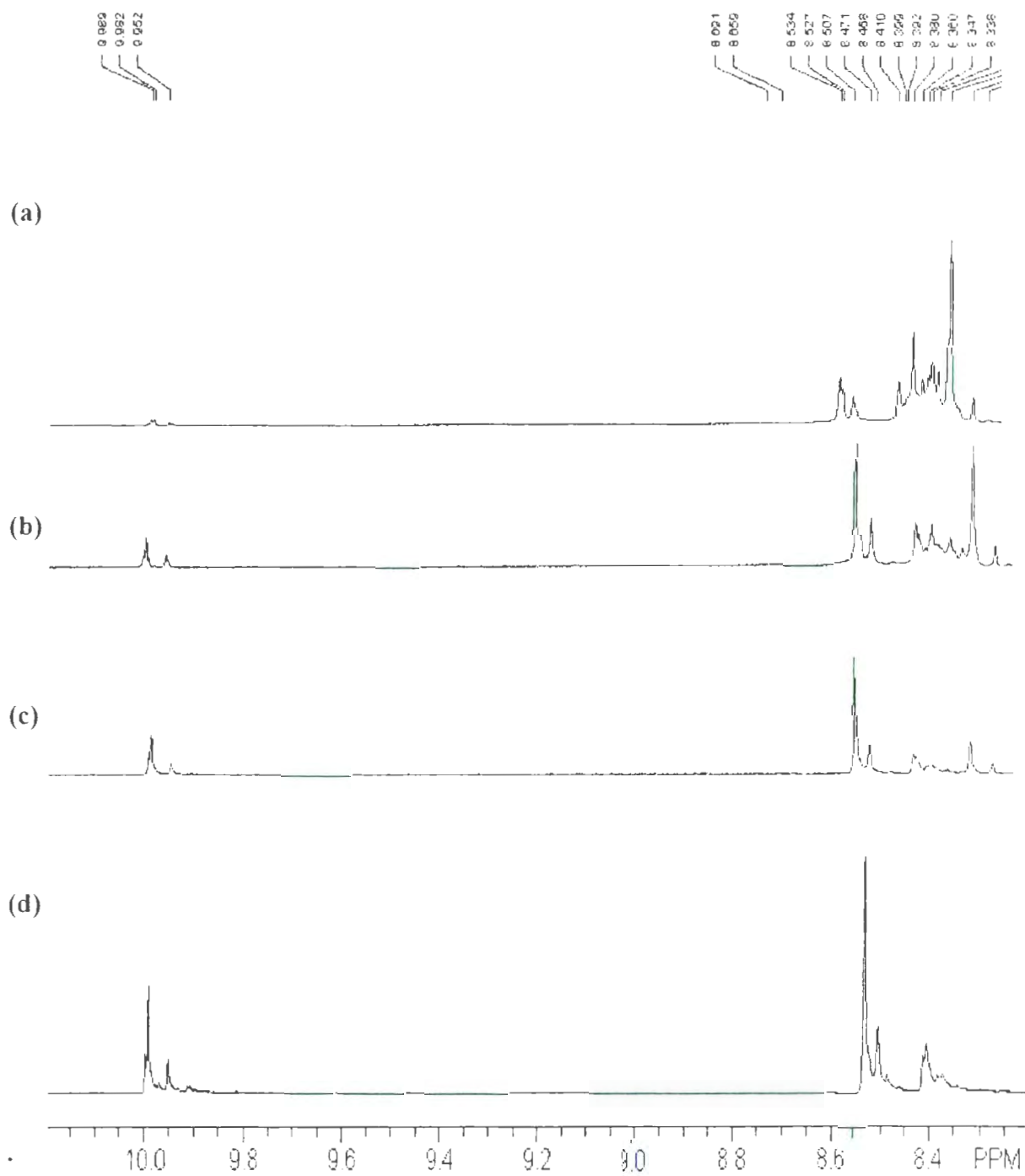


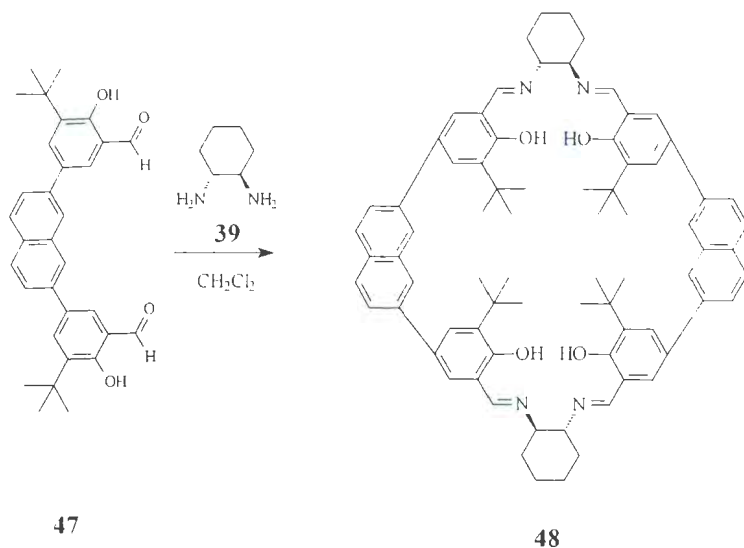
**Figure 1.3-13:**  $^1\text{H}$  NMR spectra showing the Schiff base reaction of **40** in dichloromethane solvent at ambient temperature after: (a) 5 d; (b) 4 d; (c) 2 d; (d) 1 h.

The reaction of **40** with diamine **39** in dichloromethane which had been dried over  $P_2O_5$  and then distilled over  $CaH_2$  was monitored by  $^1H$  NMR spectroscopy (Figure 1.3-13). In the first hour, the reaction rapidly formed imine product having a Schiff base proton signal at  $\delta = 8.53$  ppm, assigned to a kinetically-favored isomer of **41** which initially formed, then became slower after the first day. It is presumed that this was as result of water being produced during the reaction. After two days, **41** began to form, as evidenced by its characteristic Schiff base proton signal at  $\delta = 8.30$  ppm, presumably of the thermodynamically more stable isomer of **41**, while the intensity of the  $\delta = 8.53$  ppm signal decreased. After 5 days, **41** became the major product.

### 1.3.2.3 Schiff base condensation of bisaldehyde **47**

The 2,7-naphthylene-bridged bisaldehyde **47** has the same basic structural features as **40** and as a result, the same conditions that successfully gave the desired macrocyclic **41** were employed. (*R,R*)-DACH **39** was stirred with bisaldehyde **47** in dichloromethane (dried over  $P_2O_5$  then distilled over  $CaH_2$ ) solution under high-dilution (250.0 mg/L) conditions (Scheme 1.3-13). The reaction required 30 days to completely consume the starting material **47**. The  $^1H$  NMR spectrum (in  $CDCl_3$ ) of the crude product mixture showed that the aldehydic proton signal at  $\delta = 10.00$  ppm had disappeared and was replaced with Schiff base signals at  $\delta = 8.15$  ppm (major product) and  $\delta = 8.422$  and  $8.420$  ppm (minor products).

The MALDI-TOF mass spectrum of the crude product showed one peak which could be assigned to the target dimer **48**, at  $m/z$  1116.6 (calculated: 1116.6 g/mol). After standing overnight, pure **48** precipitated out as a yellow solid, in 30% yield, from a concentrated solution of dry  $\text{CHCl}_3$  (dried over  $\text{Na}_2\text{CO}_3$ ).



**Scheme 1.3-13:** Macrocyclization reaction of bisaldehyde **47**.

The  $^1\text{H}$  NMR spectrum of **48** (Figure 1.3-14) in  $\text{CD}_2\text{Cl}_2$  showed a single sharp Schiff base singlet at  $\delta = 8.18$  ppm and another at  $\delta = 1.59$  ppm for the *tert*-butyl groups. The signals due to the phenolic protons were at  $\delta = 14.27$  ppm. The hydrogens of the naphthalene linking group appeared as three signals: a doublet of doublets at  $\delta = 7.47$  ppm coupled to the *ortho*- and *meta*-hydrogens ( $J = 8.0$  and  $1.5$  Hz, respectively); a doublet at  $\delta = 7.75$  ppm coupled to an *ortho*-hydrogen ( $J = 8.0$  Hz), and a doublet at  $\delta = 7.61$  ppm (*meta*,  $J = 1.5$  Hz). The hydrogens of the phenyl groups showed as doublets at  $\delta = 7.07$  and  $7.61$  ppm (*meta*,  $J = 2.0$  Hz). The  $^{13}\text{C}$  NMR spectrum in  $\text{CD}_2\text{Cl}_2$  (Figure 1.3-15) showed a characteristic Schiff base signal at  $\delta = 167.26$  ppm, a phenolic carbon

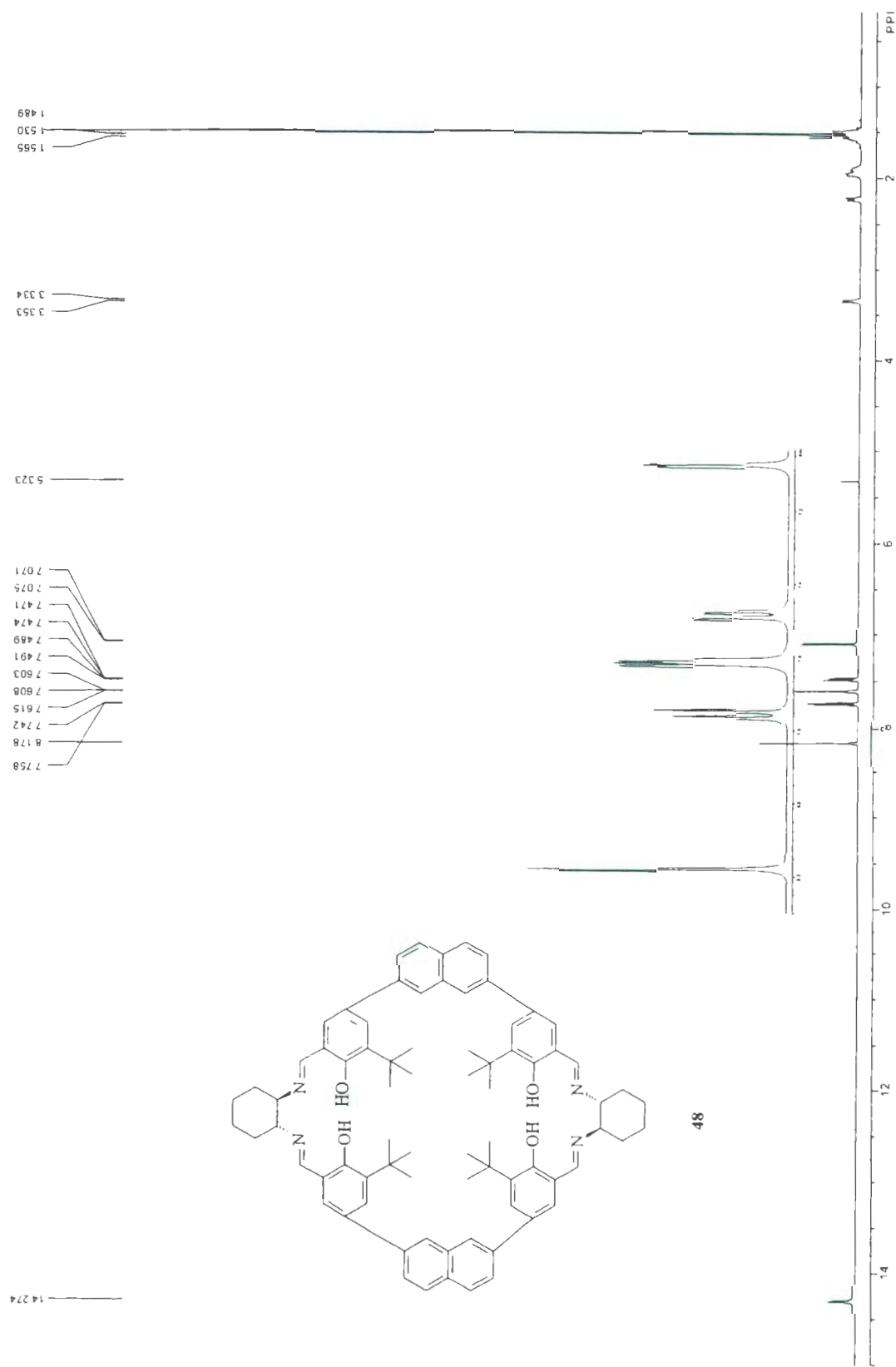


Figure 1.3-14: The <sup>1</sup>H NMR spectrum of dimer 48 in CD<sub>2</sub>Cl<sub>2</sub>.

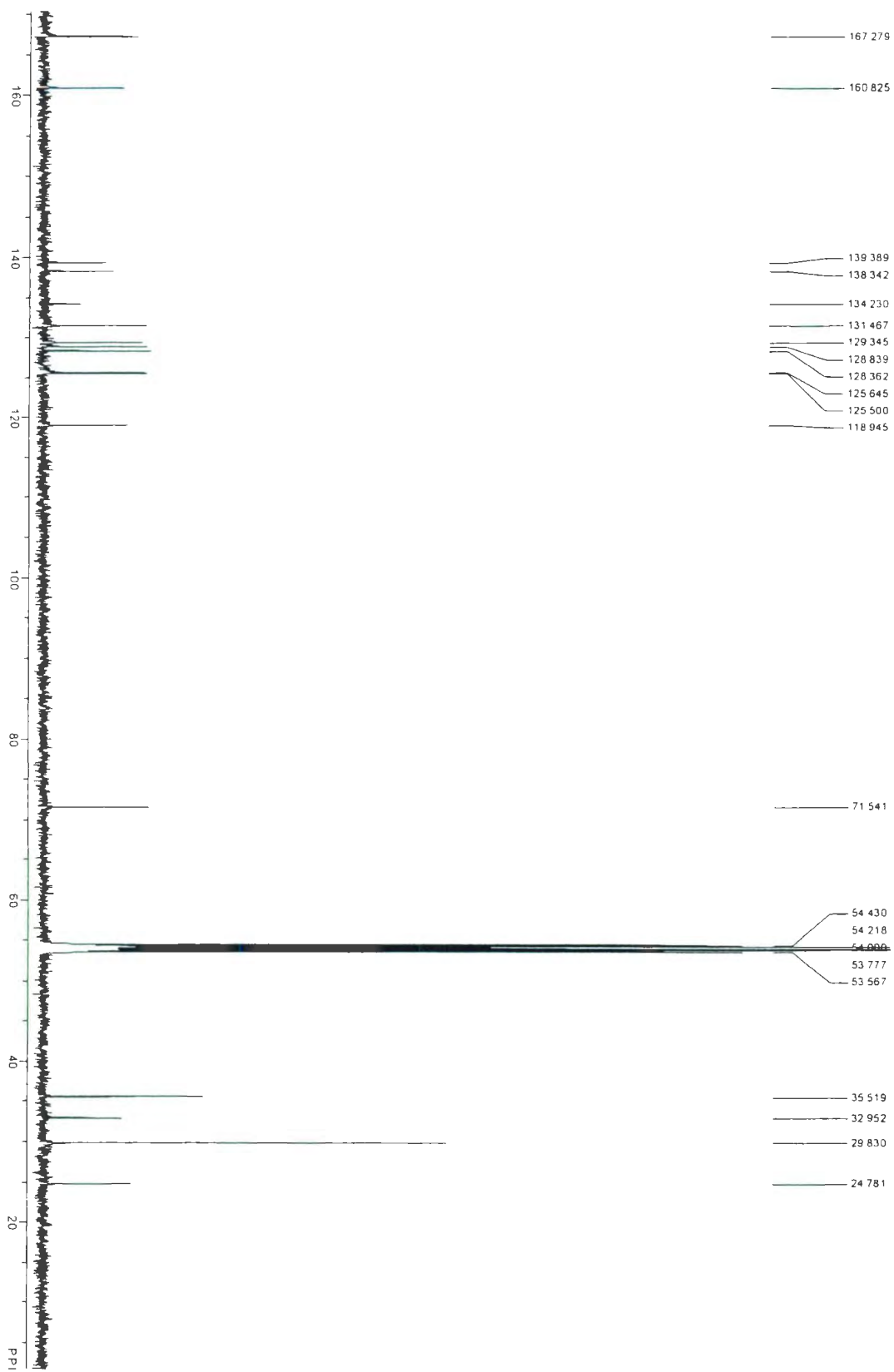
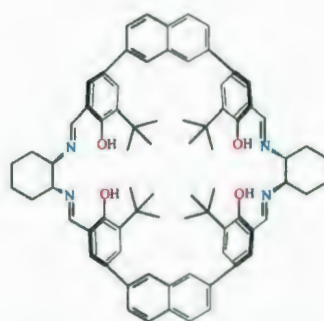


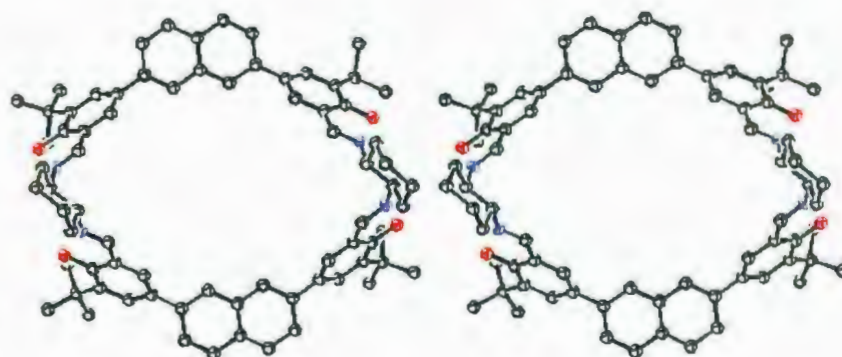
Figure 1.3-15: The  $^{13}\text{C}$  NMR spectrum of 48 in  $\text{CD}_2\text{Cl}_2$

signal at  $\delta = 160.82$  ppm, and twelve additional signals due to aromatic carbon atoms: six are assigned to the phenyl groups and the remaining signals to the six nonequivalent carbon atoms of the 2,7-naphthylene group. The MALDI-TOF mass spectrum confirmed structure **48** by showing a peak at  $m/z$  1116.7 consistent with a [2+2] dimer.

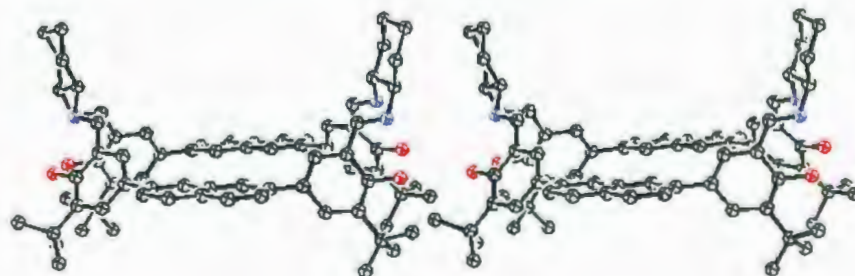
Attempts to produce an X-ray-viable single crystal for **48** failed. However, MMM<sup>30</sup> studies were undertaken, similar to what was conducted on **41**, using the MMFF94 force field. It was suggested that calix[2]salen **48** can also adopt conformations similar to **41**,<sup>30</sup> as in Figures 1.3-16a-d, e.g. *partial-pinched-cone* (Figure 1.3-16d), *1,3-alternate* (Figure 1.3-16c), *cone* (Figure 1.3-16a), and *1,2-alternate* (Figure 1.3-16b). The *partial-pinched-cone* was found to be the most stable conformer, and the *1,2-alternate* the least stable. The <sup>1</sup>H NMR spectrum of **48** was not consistent with a static *partial-pinched-cone* or *1,3-alternate* structure, but rather with both the *cone* (Figure 1.3-16a) and *1,2-alternate* (Figure 1.3-16b) conformers, or, a flexible structure that populates all accessible conformers rapidly on the NMR time scale. The *cone* conformer is calculated to be more stable than the *1,2-alternate* isomer by 3.8 kcal/mol. MMM of the *cone-48* conformer, however, suggested that it has a clearly defined cavity with a maximum width of approximately 15 Å between the two salen units and 7 Å between the two 1,8-naphthylene groups. It is therefore a good candidate to act as a receptor for many hydrocarbons, aromatics or molecules with hydrogen bonding capabilities.



Structure of the *cone* conformer of **48**.



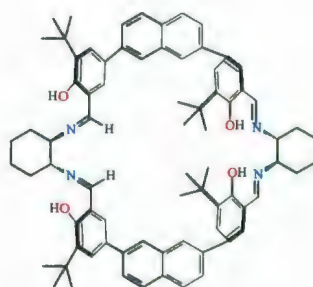
Stereoview of the *cone* conformer of **48** showing  
*tert*-butyl groups below the plane.



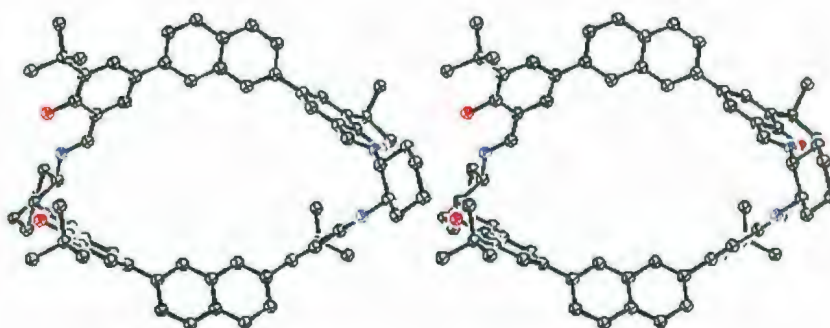
Stereoview of the side-view of the *cone* conformer of **48**.

$E = 326.8$  kcal/mol

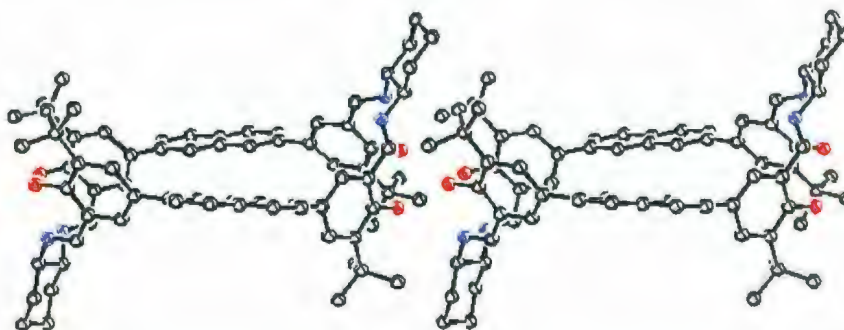
**Figure 1.3-16a:** Structure and free energy of the MMM-generated *cone* conformer of **48**.



Structure of the 1,2-*alternate* conformer of **48**



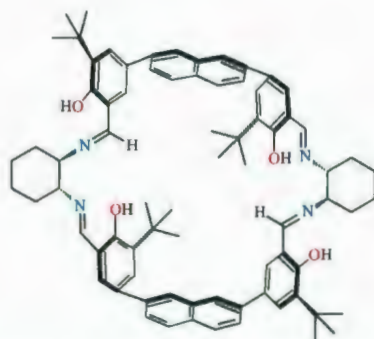
Stereoview of the 1,2-*alternate* conformer of **48** showing  
*tert*-butyl groups below the plane



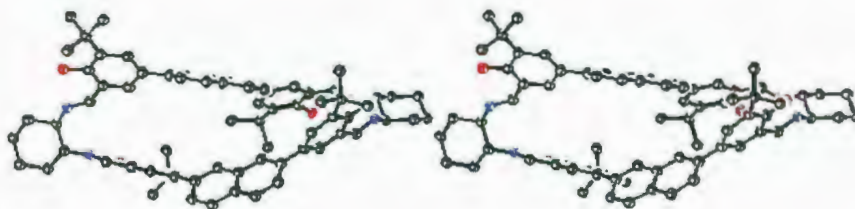
Stereoview of the side-view of the 1,2-*alternate* conformer of **48**

$$E = 330.6 \text{ kcal/mol}$$

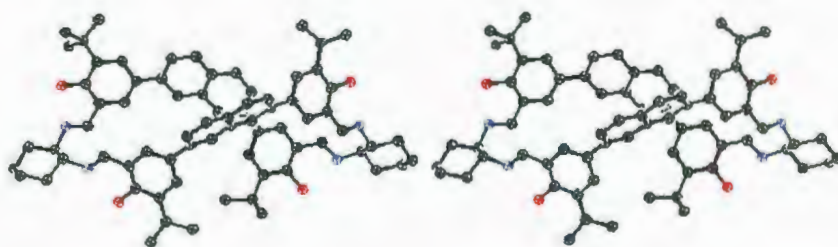
**Figure 1.3-16b:** Structure and free energy of the MMM-generated 1,2-*alternate* conformer of **48**.



Structure of the 1,3-*alternate* conformer of **48**



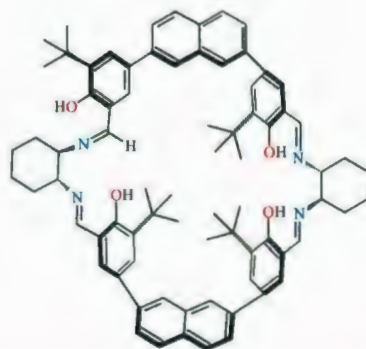
Stereoview of the 1,3-*alternate* conformer of **48** showing  
*tert*-butyl groups below the plane



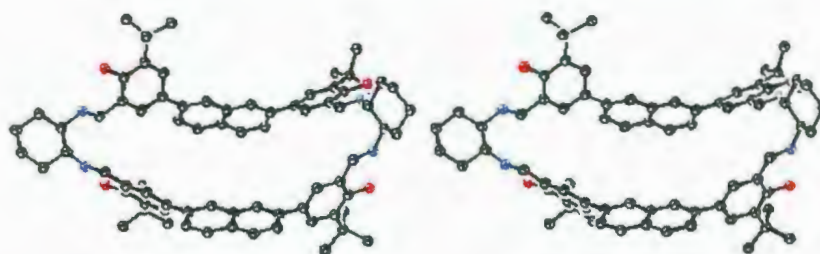
Stereoview of the side-view of the 1,3-*alternate* conformer of **48**.

$E = 326.0$  kcal/mol

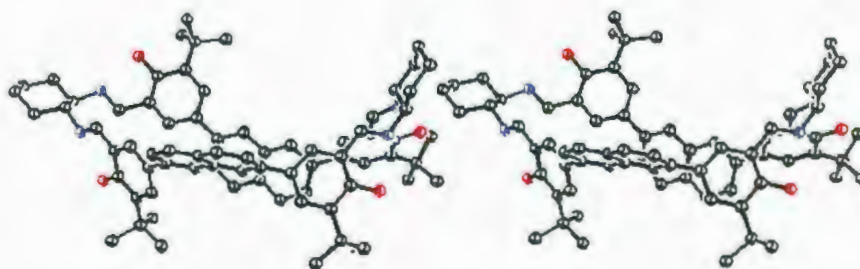
**Figure 1.3-16c:** Structure and free energy of the MMM-generated 1,3-*alternate* conformer of **48**.



Structure of the *partial-pinched-cone* conformer of **48**.



Stereoview of the *partial-pinched-cone* conformer of **48** showing  
*tert*-butyl groups below the plane.

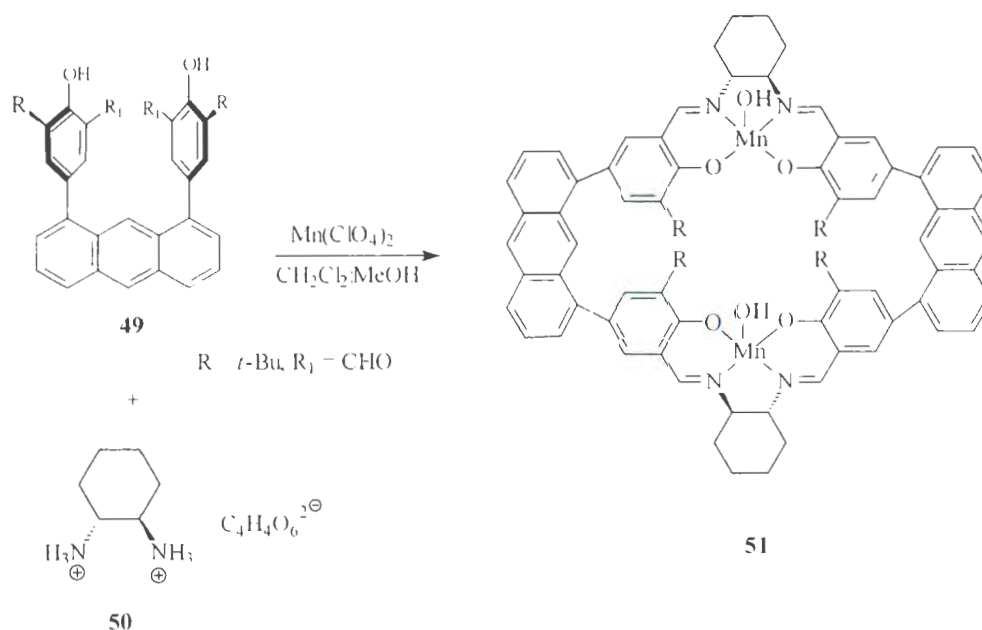


Stereoview of the side-view of the *partial-pinched-cone* conformer of **48**.

$E = 320.0 \text{ kcal/mol}$

**Figure 1.3-16d:** Structure and free energy of the MMM-generated *partial-pinched-cone* conformer of **48**.

### 1.3.2.4 Schiff base condensation of bisaldehyde **49**



**Scheme 1.3-14:** Mn(II) template-assisted construction of the macrocyclic complex **51**.

The same methodology used successfully to prepare macrocycles **41** and **48** was also employed for the Schiff base macrocyclization reaction with the anthracene-based bisaldehyde linking group. Bisaldehyde **49** was stirred with (*R,R*)-DACH **39** in dichloromethane (dried over  $\text{P}_2\text{O}_5$  then distilled over  $\text{CaH}_2$ ) at room temperature, under high-dilution conditions, over a 30 day period. The  $^1\text{H}$  NMR spectrum of the crude product mixture showed mainly Schiff base-related broad signals at  $\delta \sim 8.60$  ppm. The MALDI-TOF mass spectrum of the crude product showed a very weak peak at  $m/z$  1217.8, which was assigned to the target dimer, **51**. This weak mass spectrum and the broad  $^1\text{H}$  NMR signals are indicative of extensive polyimine formation.

The methodology, therefore, was changed in an attempt to synthesize the Mn(III) complex **51** directly, using a McAuliffe's Mn(II) template-assisted approach (Scheme

1.3-14).<sup>27</sup> Bisaldehyde **49** was stirred for one week, in 1:1 dichloromethane:methanol solution, with (1*R*,2*R*)-*trans*-cyclohexanediammonium tartrate (**50**), in the presence of Mn(ClO<sub>4</sub>)<sub>2</sub>. A dichloromethane-soluble brown solid was isolated and was purified on a short silica gel column, using 5% methanol:dichloromethane as the eluent.

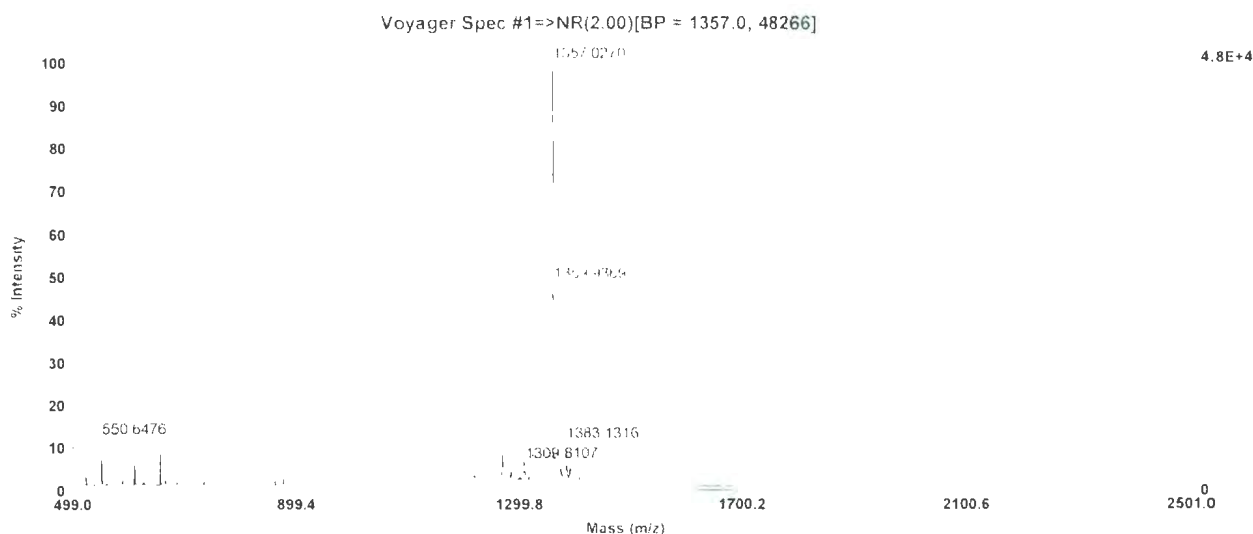


**Figure 1.3-17:** The MALDI-TOF MS of Mn(II) complex **51**.

The MALDI-TOF mass spectrum of the product isolated from this mixture showed a very strong peak at  $m/z$  1357.0 which was assigned to the target complex **51** (Figure 1.3-17). The Mn(II) was presumably oxidized *in situ* by perchlorate to form the Mn(III).<sup>27</sup> Structure **51** was assumed, by analogy, with McAuliffe's complex, **31** (Scheme 1.3-8).

In the absence of a crystal structure, a MMM study was also carried out on **51** to determine its lowest energy conformations. The results suggested that this 34-membered macrocycle has a *syn* disposition of the two salen units and a well-defined rectangular-shaped cavity with a width of around 11.3 Å between the distal intrannular carbon atoms

of two 1,8-anthracylene groups, and 9.2 Å between the two manganese ions (Figure 1.3-18).

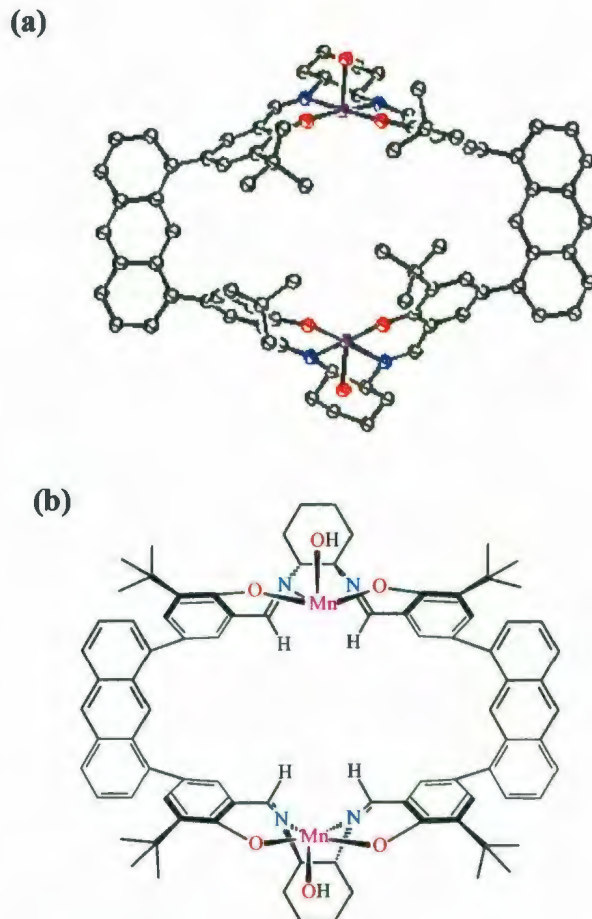
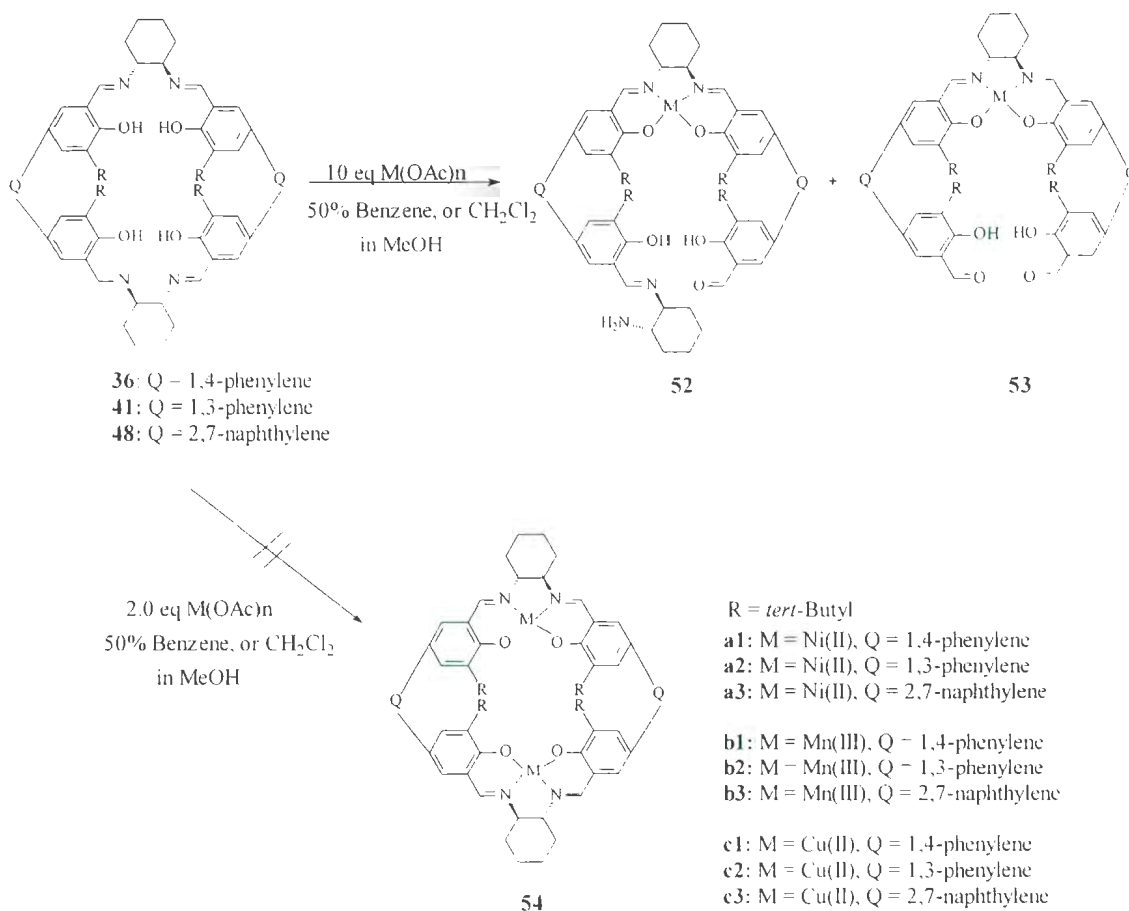


**Figure 1.3-18:** (a) Computer-generated model<sup>30</sup> of complex **51** showing the relative orientation of the M(III)-OH bonds, each of which are above the planes of their respective cyclohexyl groups; (b) The chemical structure of **51**.

A similar Ni-templated protocol was then used in an attempt to synthesize the Ni(II) complex analogue but unfortunately, Ni(ClO<sub>4</sub>)<sub>2</sub> failed to give any of the desired complex. The same methodology was employed with each of bisaldehydes **35**, **40** or **47** in the presence of either Mn(ClO<sub>4</sub>)<sub>2</sub> or Ni(ClO<sub>4</sub>)<sub>2</sub>, but again, none of the target respective bimetallic complexes **54a1** and **54b1**; **54a2** and **54b2**; or **54a3** and **54b3** were not

Brown solids were obtained with  $\text{Mn}(\text{ClO}_4)_2$ , but neither MALDI-TOF nor APCI MS-spectra afforded any significant mass data, thus indicating that only polymeric mixtures were produced from these reactions. With  $\text{Ni}(\text{ClO}_4)_2$ , only unreacted starting materials were recovered.



**Scheme 1.3-15:** Complexation reactions of **36**, **41** and **48** with  $\text{Mn}^{3+}$ ,  $\text{Ni}^{2+}$  and  $\text{Cu}^{2+}$ .

### 1.3.2.5 Complexation of **36**, **41** and **48** with $\text{Mn}^{3+}$ , $\text{Ni}^{2+}$ and $\text{Cu}^{2+}$

In order to circumvent the problem of decomposition of the Schiff base macrocycles during their attempted purification on silica gel, it was decided to form the corresponding Mn(III) complexes directly from the crude mixtures, followed by

separation on silica gel. A solution of the crude mixture of the 1,4-phenylene-linked macrocycles **36-38** in dichloromethane, was stirred with a solution of two molar equivalents of  $\text{Mn}(\text{OAc})_3$  in methanol. A light brown solution resulted, to which 8 molar equivalents of  $\text{LiCl}$  were added. The MALDI-TOF mass spectrum (Figure 1.3-19) of the resulting mixture showed peaks at  $m/z$  1047.0, 1071.1, 1580.3, 2148.4 and 2185.4 which are assigned to the  $[\text{Mn}(\text{III})+\mathbf{53b1}]^+$ ,  $[\text{Mn}(\text{III})+\mathbf{36-2H}]^+$ ,  $[\text{Mn}(\text{III})+\mathbf{37-2H}]^+$ ,  $[\text{Mn}(\text{III})+\mathbf{38-2H}]^+$  and  $[\text{Mn}(\text{III})+\mathbf{38-2H+Cl}]^+$  fragments of the resulting mono-manganese complexes, respectively. No dimanganese complexes were observed.

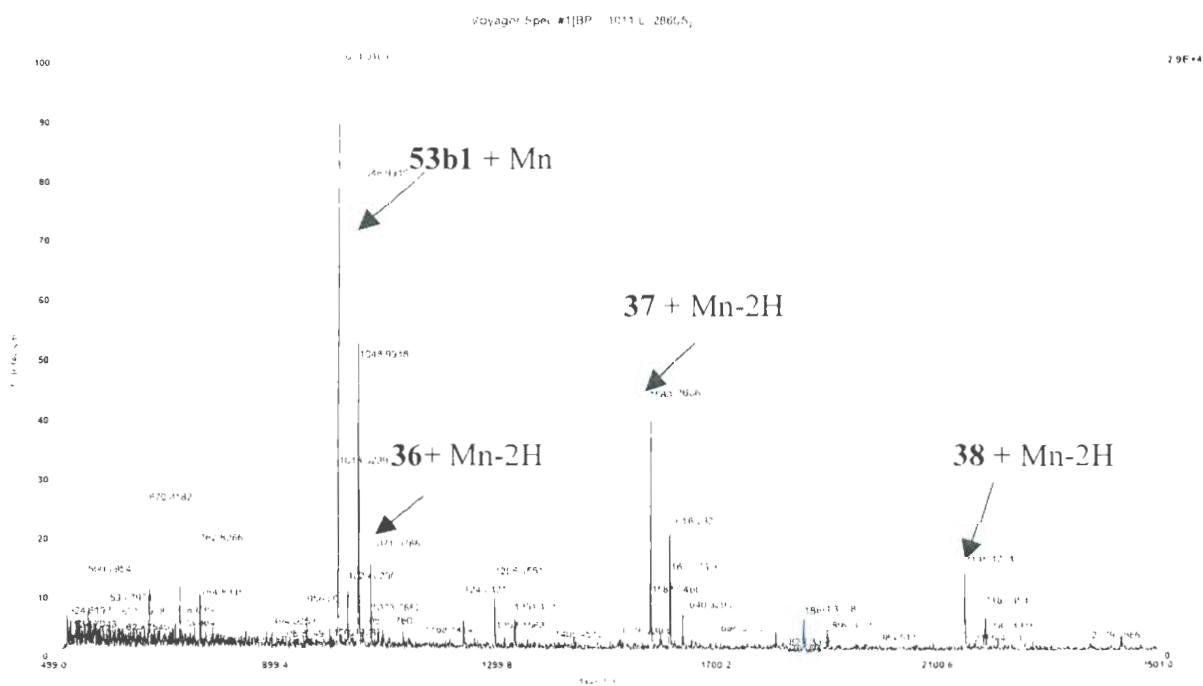


**Figure 1.3-19:** MALDI-TOF mass spectrum of the mono-metal-salen-macrocycles from the manganese complexation reaction with the mixture of salen-macrocycles **36-38**.

In order to produce the corresponding Ni(II) complexes, the crude mixture of salen-macrocycles **36-38** was reacted with a solution of Ni(OAc)<sub>2</sub> in 1:1 methanol:dichloromethane. An insoluble brown solid, and also a small amount (5% yield) of a different, dichloromethane-soluble brown solid were obtained. The latter substance showed a strong peak in its MALDI-TOF mass spectrum, corresponding to **52a1**, and its <sup>1</sup>H NMR spectrum showed an aldehydic proton signal at  $\delta = 10.0$  ppm. These results suggested that the ligands were hydrolyzed under the nickel complexation conditions, and likely formed open-chain salen complexes. The insoluble brown solid was presumed to be a nickel complex of either a polymeric or oligomeric imine-containing mixture which could not be characterized by MALDI-TOF mass spectrometry.

Complexation reactions of purified ligands **41** and **48**, with stoichiometric amounts of Mn(OAc)<sub>3</sub>, Ni(OAc)<sub>2</sub>, or Cu(OAc)<sub>2</sub> failed to give the desired corresponding complexes **54** (Scheme 1.3-15). On the other hand, decomposition occurred when excess amounts of the metal salts were used. Table 1.3-2 shows the MALDI-TOF data obtained from the reactions of 10 molar equivalents of Mn(OAc)<sub>3</sub>, Ni(OAc)<sub>2</sub>, or Cu(OAc)<sub>2</sub>, with either **41** or **48**. The peaks highlighted are those related to the decomposition products **52** and **53**.

**Table 1.3-2: Complexation of 41 and 48 with Mn<sup>3+</sup>, Ni<sup>2+</sup> and Cu<sup>2+</sup>**

Metal	Ligand 41		Ligand 48	
	MALDI-TOF MS	Product No.	MALDI-TOF mass	Product No.
Mn(III)	1088.3540	<b>52b2</b>	1187.1345	<b>52b3</b>
			1091.2782	<b>53b3</b>
Ni(III)	1070.6454	<b>52a2</b>	1190.2716	<b>52a3</b>
Cu(II)	1018.4327	<b>41</b>	1099.4686	<b>52c3</b>
			1194.9782	<b>53c3</b>

The <sup>1</sup>H NMR spectrum of the crude product of the reaction of Ni(OAc)<sub>2</sub> with either **41** or **48** showed an aldehydic peak at  $\delta = 10.0$  ppm which suggested that, once again, hydrolysis occurred. The reactions usually gave reddish-brown solids as major products that were insoluble in all of the common solvents and did not afford any mass spectral data under a variety of mass spectroscopic techniques *e.g.* APCI, ESI and MALDI-TOF. These solids were again, presumably, oligomeric or polymeric complexes which were produced *via* the decomposition of **41** and **48** in the presence of Ni<sup>2+</sup> ions.

It is further postulated that **41** and **48** coordinate a metal ion with one of the salen units, but that the other salen unit becomes partially, or completely, hydrolyzed to form the ring-opened products such as amino-aldehyde **52**, or bisaldehyde **53** (Scheme 1.3-15). The decomposition of **41** and **48** likely occurs because these tetraimine macrocycles are strained, and can easily be hydrolyzed under the Lewis acid conditions. The first molar equivalent of Mn(OAc)<sub>3</sub>·3H<sub>2</sub>O or Ni(OAc)<sub>2</sub> reacts with salen dimer ligand to give the mono-metal-salen dimer complexes (Table 1.3-2). Subsequently, acetic acid which is

formed in the reaction catalyzes hydrolysis and subsequent ring-opening of the unreacted salen units.

In contrast, ligands such as **34** (Scheme 1.3-9) which were previously prepared by the Jablonski group,<sup>28</sup> gave the corresponding Mn(III) and Ni(II) complexes in very good yields without any significant hydrolysis under the same conditions. It is concluded, that ligands **44**, are less strained than ligands **36**, **41**, and **48**, described in this thesis, which are more reactive to hydrolysis.

**Table 1.3-3: Calculated (MMFF94)<sup>30</sup> lowest-energy conformations of ligands 36, 41 and 48 and complexes 54a1-3 and 54b1-3 (Scheme 1.3-15)**

Ligand	MMM calculated energy (kcal/mol)	Mn(III) complexes	Free energy (kcal/mol)	Ni(II) complexes	Free energy (kcal/mol)
<b>36</b>	327.0	<b>54b1</b>	177.5	<b>54a1</b>	325.4
<b>41</b>	278.2	<b>54b2</b>	222.8	<b>54a2</b>	265.3
<b>48</b>	326.8	<b>54b3</b>	128.6	<b>54a3</b>	287.8

MMM<sup>30</sup> study was conducted in order to compare the relative calculated energy of **36**, **41** and **48** and their corresponding Mn(III) and Ni(II) complexes **54b1-54b3** and **54a1-54a3**, and are summarized in Table 1.3-3. These calculations suggest that the ligands have higher free energies than their corresponding Mn(III) and Ni(II) complexes, **54b1-54b3** and **54a1-54a3**. It is hypothesized that this difference could be a result of the

relatively high imine bond energies in the free ligands. Furthermore, the lone pairs of electrons on the nitrogen atoms are coordinated with the metal ions in the complexes, and consequently, would tend to lower the free energies of the complexes relative to the free ligands. As well, ligands **36** and **48** have higher free energies than **41** owing to possible additional ring strain and the steric interactions between the bulky *tert*-butyl group.

### 1.3.3 Summary

Calix[2]salens **41** and **48** bearing 1,3-phenylene and 2,7-naphthylene groups were successfully synthesized in seven steps, starting from commercially available 2-*tert*-butylphenol. Both **41** and **48** were crystallized from CH<sub>2</sub>Cl<sub>2</sub> and CHCl<sub>3</sub>, respectively, and were fully characterized by <sup>1</sup>H NMR, <sup>13</sup>C NMR and MALDI-TOF mass spectrometry. The <sup>1</sup>H NMR and <sup>13</sup>C NMR data are consistent with highly symmetrical structures. Calix[2]salen **41** was obtained from the Schiff base reaction of bisaldehydes **40** and **47** with (*R,R*)-DACH **39** in dichloromethane solvent, at room temperature. Applying high dilution conditions improved the yields of **41** to greater than 70%. The use of dichloromethane as the solvent was found to be critical for the preparation of both **41** and **48**, as it minimizes the formation of oligo- or polyimine by-products. The formation of these undesired reaction products occurs competitively in other solvents such as THF:methanol, methanol, or THF. For example, the Schiff base reaction of **40** in methanol gave high yields of polyimines (42%). The Schiff base macrocyclization reactions in these solvents also afforded different product mixtures of the cyclic dimer **41**,

trimer **42** and tetramer **43**, but these mixtures could not be separated, or purified, and appeared to be hydrolyzed on silica gel.

The Schiff base reactions of the bisaldehyde **35** with (*S,S*)-DACH **33** in THF:methanol also afforded inseparable mixtures of **36-38**. However, near-homogenous samples of calix[2]salen **36** were isolated in up to 38% yield by precipitation from THF:acetonitrile. In contrast, the anthracene-based bisaldehyde **49** gave a very low yield of the Schiff base macrocycle using dichloromethane as a solvent, and the major products were oligomers and/or polymers. Compound **49** gave the desired Mn(III)-salen dimer **40** *via* McAuliffe's manganese(II) template-assisted methodology.

The complexation reactions of crude reaction mixtures of **36-38** with Mn(OAc)<sub>2</sub> gave the corresponding mono-Mn(II)-calix[*n*]salen complexes. The Schiff base macrocycles **36**, **41** and **48** failed to give the corresponding binuclear Mn(III), Ni(III) and Cu(III) complexes, presumably because they decomposed during the complexation reactions with the metal acetate salts in methanol:dichloromethane. MMM-based calculations suggested that the ligands **36**, **41** and **48** are strained macrocycles and this could support the hypothesis that they are easily hydrolyzed.

### 1.3.4 Experimental Section

#### Materials

Chemical reagents and solvents were purchased from Aldrich and used as received. THF used for synthesizing calixsalens was further purified by fractional distillation.  $\text{CH}_2\text{Cl}_2$  was dried over  $\text{P}_4\text{O}_{10}$  then distilled over  $\text{CaH}_2$ . (*1R,2R*)- or (*1S,2S*)-diaminocyclohexane-L-tartrate salts were obtained as a gift from SeptraChem Inc. Extreme care should be taken when handling  $\text{Ba}(\text{ClO}_4)_2$  since it is shock sensitive.

#### Methods

All reactions in the syntheses were performed under a dry nitrogen atmosphere. Nitrogen gas was purified by passing through a series of columns containing DEOX (Alpha) catalyst heated to  $120\text{ }^\circ\text{C}$ , granular  $\text{P}_4\text{O}_{10}$ , and activated  $3\text{ \AA}$  molecular sieves. Flash chromatography was performed on SAI silica gel, particle size  $32\text{-}63\text{ }\mu\text{m}$ , pore size  $60\text{ \AA}$ , Batch number 02826-25. Preparative thin-layer chromatography plates (PLC) were made from SAI F-254 silica gel for TLC (particle size  $5\text{-}15\text{ }\mu\text{m}$ ), Batch number 04860-5. Thin-layer chromatography was performed using percolated SAI F-254 silica gel plates (Plastic Backed TLC, Hard layer, Batch number 79011) layer thickness  $200\text{ }\mu\text{m}$ .

#### Instrumentation

Melting points (mp) were determined on a MEL-TEMP II apparatus and are uncorrected. Mass spectra of compounds were obtained using LCMS (HP series 1100) or MaLDI-TOF MS (Voyager-DE PRO). Analytical thin layer chromatography was performed with fluorescent indicator  $\text{UV}_{254}$  (Macherey-Nagel GmbH & Co. KG,

Germany).  $^1\text{H}$  NMR and  $^{13}\text{C}$  NMR were recorded in  $\text{CDCl}_3$  on a GE-300 MHz spectrometer or on a Bruker AM-500 Fourier Transform spectrometer with  $\text{Me}_4\text{Si}$  as an internal standard. Data were reported as follows: chemical shift, multiplicity (s = singlet, d = doublet, dd = doublet of doublets, t = triplet, b = broad, h = heptet, m = multiplet), coupling constant ( $J$ , Hz), integration and assignment (mH-x, m for the H numbers in the position x of a molecule).  $^1\text{H}$  NMR and  $^{13}\text{C}$  NMR spectra were processed using "Nuts" software. Chemical shifts for  $^{13}\text{C}$  NMR spectra are relative to the solvent 77.23 ppm for  $\text{CDCl}_3$ .

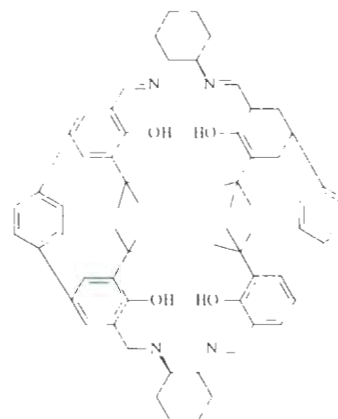
MS spectra were recorded on Applied Biosystems DE-RP instrument equipped with a reflection, delayed ion extraction, and high performance nitrogen laser (337 nm). Samples were prepared at a concentration of 1 mg/mL in 1:1 THF: $\text{CH}_2\text{Cl}_2$ . The sample was mixed with a matrix compound of  $\alpha$ -cyano-4-hydroxycinnamic acid at a concentration of 10 mg/mL in 1:1  $\text{CH}_2\text{Cl}_2$ :EtOH, or, THF:EtOH to promote desorption and ionization.

## **Syntheses:**

### **Macrocyclization reaction procedure in THF:MeOH**

Both solutions of (*S,S*)-(DACH) **33** (0.360 g, 3.16 mmol) in MeOH (40 mL) and a solution of bisaldehyde **35** (0.550 g, 1.28 mmol) in THF (50 mL), were simultaneously added with stirring at room temperature over 24 h to a solution of  $\text{Ba}(\text{ClO}_4)_2$  (0.473 g, 1.41 mmol) in 1:1 THF:MeOH (100 mL) and activated molecular sieves 4 Å (2.0 g). At the end of the addition, the solvent was evaporated and the residue was dissolved in

dichloromethane (20 mL). The solution was filtered and the solvent was evaporated from the filtrate. The product was washed with hexane (3 x 5 mL) then with MeOH (5 mL). The crude product was dissolved in THF (20 mL) then acetonitrile (50 mL) was added dropwise, and then the mixture was stirred for 2 h. The mixture was filtered and the solid was dried under vacuum to give **36** (213.9



**36**

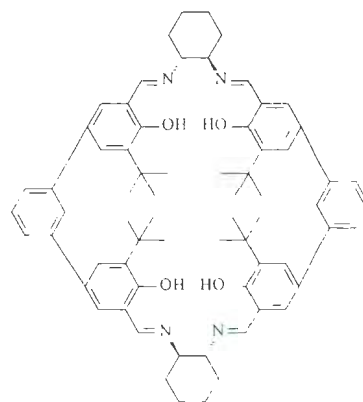
mg, 38.%): decomposition > 270 °C; <sup>1</sup>H NMR (CDCl<sub>3</sub>) δ 1.54 (s, 36H), 7.22 (s, 4H), 7.45 (s, 8H), 7.49 (s, 4H), 8.36 (s, 4H), 13.95 (s, 4H); <sup>13</sup>C NMR (CDCl<sub>3</sub>) δ 24.51, 29.73, 29.96, 35.38, 72.61, 119.08, 127.29, 128.44, 128.77, 130.90, 137.91, 138.05, 139.65, 160.13, 165.88. MALDI-TOF/MS 1018.8 [M<sup>+</sup>+H], calcd for C<sub>68</sub>H<sub>80</sub>N<sub>4</sub>O<sub>4</sub> 1016.6.

### Macrocyclization reactions in dichloromethane

The solution of (*R,R*)-DACH **39** (23.1 mg, 0.20 mmol, weighed under a nitrogen gas environment) and bisaldehyde (**40** or **47**) (0.20 mmol) in 400 mL of dichloromethane, which had been dried over P<sub>2</sub>O<sub>5</sub> and distilled over CaH<sub>2</sub>, was stirred at room temperature and under a nitrogen environment. After 1 d, the colour of the reaction changed to greenish-yellow. The reaction was stirred for 8 d for **40**, and for 30 d for **47** under a nitrogen gas environment at room temperature. The solvent was evaporated under reduced pressure to give a yellow solid.

### Calix[2]salen **41**

The crude product was re-dissolved in dichloromethane (10 mL). Initially, the solution was clear but then became turbid after 1 min. The solution was filtered and the collected solid was washed with dichloromethane (10 mL), dissolved in benzene and collected in a 50 mL round-bottom flask. The benzene was evaporated under reduced pressure to give **41** as a

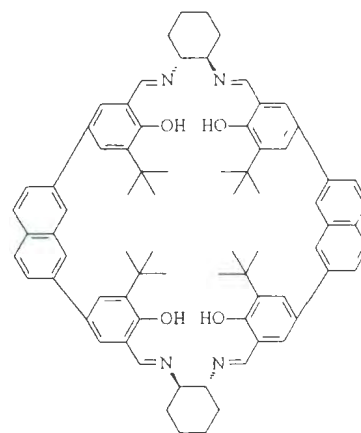


**41**

yellow solid in 43% yield. The filtrate was collected and the dichloromethane was evaporated to give a solid. This crude product was dissolved in ethyl ether (10 mL), then acetonitrile (10 mL) was added. The solution was stirred for 10 min, then filtered. The filtrate was evaporated to give a yellow solid which was dissolved in dichloromethane (10 mL). Initially, the solution was clear, but it slowly became turbid. After standing overnight, the suspension was filtered to give **41** in 29% yield (total yield 142.2 mg, 70% yield); mp 289 °C;  $^1\text{H NMR}$  ( $\text{C}_6\text{D}_6$ )  $\delta$  1.67 (s, 36H), 7.06 (s, 4H), 7.16 (s, 4H), 7.31 (t,  $J = 8.0$  Hz, 2H), 7.41 (dd,  $J = 2.5, 8.0$  Hz, 4H), 7.59 (d,  $J = 2.5$  Hz, 2H), 7.81 (s, 4H), 14.56 (s, 4H);  $^{13}\text{C NMR}$  ( $\text{CDCl}_3$ )  $\delta$  23.87, 29.62, 32.33, 35.18, 71.09, 118.67, 125.01, 126.03, 128.53, 128.86, 129.21, 131.14, 137.97, 141.79, 160.28, 165.55; MS (MALDI-TOF) 1018.4 [ $\text{M}^+ + \text{H}$ ], calcd for  $\text{C}_{68}\text{H}_{80}\text{N}_4\text{O}_4$  1016.6

### Calix[2]salen **48**

The crude yellow product obtained above was dissolved dry chloroform (5 mL). A yellow precipitate was recovered overnight. The mixture was filtered to give **48** as yellow solid (67.0 mg, 30%): decomposition > 290 °C; <sup>1</sup>H NMR (CD<sub>2</sub>Cl<sub>2</sub>) δ 1.59 (s, 36H), 7.07 (d, *J* = 2.0 Hz, 4H), 7.47 (dd, *J* = 1.5 Hz, 8.0 4H), 7.61 (d, *J* = 2.0 Hz, 4H), 7.61 (d, *J* = 1.5 Hz, 4H), 7.75 (d, *J* = 8.0 Hz, 4H), 8.18 (s, 4H) 14.27 (s, 4H); <sup>13</sup>C NMR (CD<sub>2</sub>Cl<sub>2</sub>) δ 24.78, 29.83, 32.96, 35.52, 71.54, 118.94, 125.49, 125.63, 128.35, 129.33, 134.22, 138.33, 139.38, 160.82, 165.26; MS (MALDI-TOF) 1116.9 [M<sup>+</sup>], calcd for C<sub>76</sub>H<sub>84</sub>N<sub>4</sub>O<sub>4</sub> 1116.7.



**48**

### 1.3.5 References

1. Schiff, H. *Annalen* **1864**, *131*, 118.
2. (a) Martinez, L. E.; Leighton, J. A.; Carsten, D. H.; Jacobsen, E. N. *J. Am. Chem. Soc.* **1995**, *117*, 5897. (b) Larrow, J. F.; Schaus, S. E.; Jacobsen, E. N. *J. Am. Chem. Soc.* **1996**, *118*, 7420. (c) Tokunaga, M.; Larrow, J. F.; Kakiuchi, F.; Jacobsen, E. N. *Science* **1997**, *277*, 936.
3. Myers, J. K.; Jacobsen, E. N. *J. Am. Chem. Soc.* **1999**, *121*, 8959.
4. (a) Evans, D. A.; Lectka, T.; Miller, S. J. *Tetrahedron Lett.* **1993**, *34*, 7027.
5. Schaus, S. E.; Branalt, J.; Jacobsen, E. N. *J. Org. Chem.* **1998**, *63*, 403.
6. (a) Tararov, V. I.; Hibbs, D. E.; Hursthouse, M. B.; Ikonnikov, N. S.; Malik, K. M. A.; North, M.; Orizu, C.; Belokon, Y. N. *J. Chem. Soc., Chem. Commun.* **1998**, 387.
7. Belokon, Y. N.; Caveda-Cepas, S.; Green, B.; Ikonnikov, N. S.; Khrustalev, V. N.; Larichev, V. N.; Moscalenko, M. A.; North, M.; Orizu, C.; Tararov, V. I.; Tasinazzo, M.; Timofeeva, G. I.; Yashkina, L. V. *J. Am. Chem. Soc.* **1999**, *121*, 3968.
8. Sigman, M. S.; Jacobsen, E. N. *J. Am. Chem. Soc.* **1998**, *120*, 5315.
9. Amendola, V.; Fabbrizzi, L.; Linati, L.; Mangano, C.; Pallavicini, P.; Pedrizzini, V.; Zema, M. *Chem. Eur. J.* **1999**, *5*, 3679.
10. Bennani, Y. L.; Hanessian, S. *Chem. Rev.* **1997**, *97*, 3161.
11. Hong, B. K.; Lee, I. S.; Shin, D. M.; Chung, Y. K. *J. Chem. Soc., Chem. Commun.* **2004**, 936.
12. Kuhnert, N.; Rossignolo, G. M.; Lopez-Peñago, A. *Org. Biomol. Chem.* **2003**, *1*, 1157.

13. Gao, J.; Martell, A. E. *Org. Biomol. Chem.* **2003**, *1*, 2795.
14. (b) Brunner, H.; Schiessling, H. *Bull. Soc. Chim. Belg.* **1994**, *103*, 119.
15. Li, Z.; Pu, L. *Org. Lett.* **2004**, *6*, 1065.
16. Lin, J.; Zhang, H.; Pu, L. *Org. Lett.* **2002**, *4*, 3297.
17. Li, Z.; Lin, J.; Zhang, H.; Sabat, M.; Hyacinth, M.; Pu, L. *J. Org. Chem.* **2004**, *69*, 6284.
18. Kim, G.; Park, D.; Tak, Y. *Catal. Lett.* **2000**, *65*, 127.
19. (a) Shimakoshi, H.; Kai, T.; Aritome, I.; Hisaeda, Y. *Tetrahedron Lett.* **2002**, *43*, 8261. (b) Gawroński, J.; Kolbon, H.; Kwit, M.; Katrusiak, A. *J. Org. Chem.* **2000**, *65*, 5768.
20. van Veggel, F.; Bos, M.; Harkema, S.; van de Bovenkamp, H.; Verboom, W.; Reedijk, J.; Reinhoud, D. N. *J. Org. Chem.* **1991**, *56*, 225.
21. Gao, J.; Reibenspies, J. H.; Zingaro, R. A.; Woolley, F. R.; Martell, A. E.; Clearfield, A. *Inorg. Chem.* **2005**, *44*, 232.
22. Shimakoshi, H.; Takemoto, H.; Aritome, I.; Hisaeda, Y. *Tetrahedron Lett.* **2002**, *43*, 4809.
23. (a) Akine, S.; Taniguchi, T.; Nabeshima, T. *Tetrahedron Lett.* **2001**, *42*, 8861. (b) Gallant, A. J.; Patrick, B. O.; MacLachlan, M. J. *J. Org. Chem.* **2004**, *70*, 7936. (c) Gallant, A. J.; MacLachlan, M. J. *Angew. Chem. Int. Ed.* **2003**, *42*, 5307. (d) Ma, C.; Lo, A.; Abdolmaleki, A.; MacLachlan, M. J. *Org. Lett.* **2004**, *6*, 3841.
24. Brunner, H.; Schiessling, H. *Angew. Chem., Int. Ed. Engl.* **1994**, *33*, 125.

25. (a) Srimurugan, S.; Viswanathan, B.; Varadarajan, T. K.; Varghese, B. *Tetrahedron Lett.* **2005**, *46*, 3151. (b) Srimurugan, S.; Viswanathan, B.; Varadarajan, T. K.; Varghese, B. *Org. Biomol. Chem.* **2006**, *4*, 3044.
26. Song, Y.; Yao, X.; Chen, H.; Pan, G.; Hu, X.; Zheng, Z. *J. Chem. Soc., Perkin Trans. 1* **2002**, *8*.
27. Wastkinson, M.; Whiting, A.; McAuliffe, C. A. *J. Chem. Soc., Chem. Commun.* **1994**, 2141.
28. Li, Z. **Ph. D. Thesis**; Memorial University of Newfoundland, **1998**, 70.
29. Wang, L.; Coulter, K.; Jablonski, C., *Unpublished results*.
30. Molecular mechanics calculations were conducted using *Titan for Windows 98* by Wavefunction, Inc. USA.

## **Part 2**

## Chapter 2.1. Modification of thiacalix[4]arene to form thiacalix[2]phenoxathiins—structural and complexation studies

### 2.1.1 Introduction

Interest in the study of host-guest phenomena has grown enormously and many advances have been made since the pioneering works of Pedersen,<sup>1</sup> Cram,<sup>2</sup> and Lehn.<sup>3</sup> This branch of chemistry deals with complexes which are formed based on noncovalent (“supramolecular”) bonding between “host” and “guest” species in well-defined structures. There are many molecular receptors such as the cyclodextrins, calixarenes, cucurbiturils, porphyrins, crown ethers, and cryptands which have been specifically designed in order to potentially enhance their particular host-guest properties. Some of these host molecules are selective for guests such as “hard” metals (*e.g.* alkali and alkali earth cations),<sup>4</sup> “soft” metals (*e.g.*, transition metal cations),<sup>5</sup> or neutral substances such as C<sub>60</sub>- and C<sub>70</sub>-fullerenes. These selective receptors therefore can act as chemical sensors,<sup>6</sup> as agents for the selective removal of poisonous or radioactive metal cations from waste streams,<sup>7</sup> as membrane transports by coordinating ions and creating channels to transport these ions,<sup>8</sup> as agents for the immobilization of radioisotopes,<sup>8</sup> or as phase-transfer catalysts<sup>10</sup> in other molecular recognition applications.<sup>11</sup> In addition, to be useful in these demanding applications, the receptors should be easily prepared in relatively large amounts and have structures that can easily be modified.

Calix[*n*]arene compounds such as **1** and **2** (Figure 2-1) are some of the most easily accessible candidates which can meet some of these crucial requirements. As a result,

they have been extensively studied and tested in many different applications, including incorporating modifications in order to improve their host-guest properties, and other diverse applications, such as their use as non-linear optical (NLO) materials.<sup>12</sup>

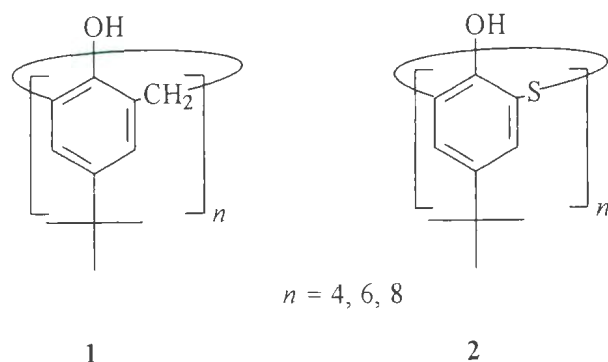
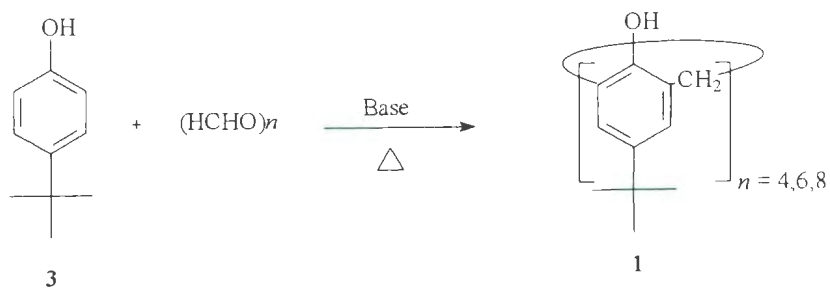
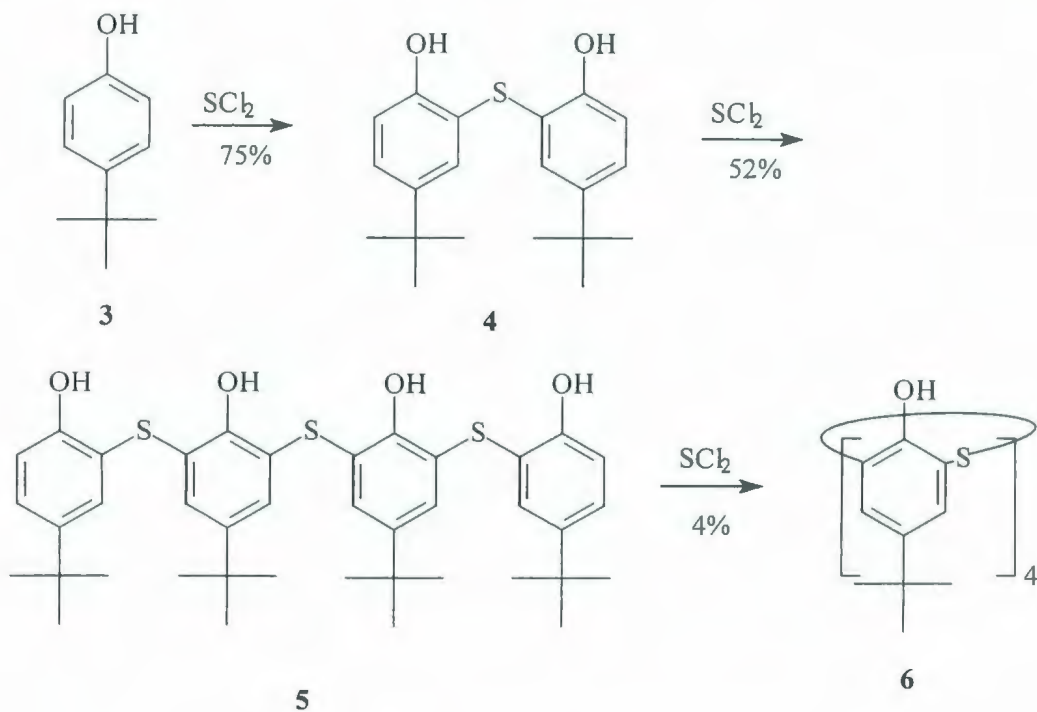


**Figure 2-1:** Calixarenes **1** and thiacalixarenes **2**.

Calix[*n*]arenes such as **1**,<sup>13</sup> in which methylene groups link the phenol units, are easily and reproducibly prepared by the reaction of *p*-*tert*-butylphenol **3** with paraformaldehyde in basic solution, following Gutsche's ground-breaking efforts and procedures (Scheme 2-1).<sup>14</sup>

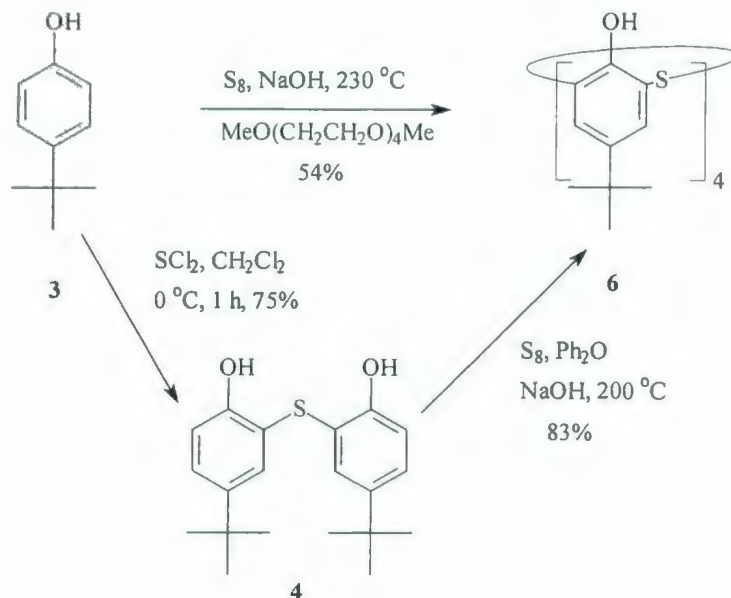


**Scheme 2-1:** Synthesis of calix[*n*]arenes **1**.



**Scheme 2-2:** The Sone synthesis of thiacalixarene **6**.

In 1997, a new generation of calixarene was first introduced by Sone in a conference abstract.<sup>15</sup> The new calixarene was formed only in poor yields *via* a multi-step synthesis starting from the reaction of *p*-*tert*-butylphenol (**3**) with  $\text{SCl}_2$  (Scheme 2-2) to form **4** which was reacted with  $\text{SCl}_2$  to form **5**. *p*-*Tert*-butylthiacalix[4]arene (**6**) formed from further reaction of **5** with  $\text{SCl}_2$ , in which the methylene linking groups in **1** are replaced by sulfur atoms. In the same year, Kumagai and Miyano reported the formation of **6** in 54% yield from a one-pot reaction of **3** with sulfur, under basic conditions.<sup>16</sup> Subsequently, **6** was obtained in even higher yields by reacting pre-formed dimer **4** with sulfur in basic solution (Scheme 2-3).<sup>17</sup>



**Scheme 2-3:** Different synthetic approaches for thiacalixarene **6**.

The X-ray structure of **6** revealed that, under the conditions of crystallization, dichloromethane became included within the cavity of the molecule.<sup>18</sup> In the solid state, **6** has a  $C_{4v}$ -symmetrical cone conformation similar to that of the methylene-bridged analogue **1**, although the thiacalix[4]arene **6** cavity is *ca.* 15% larger due to the increased S-C (1.78 Å in **6**) vs C-C (1.53 Å in **1**) bond lengths.<sup>19</sup>

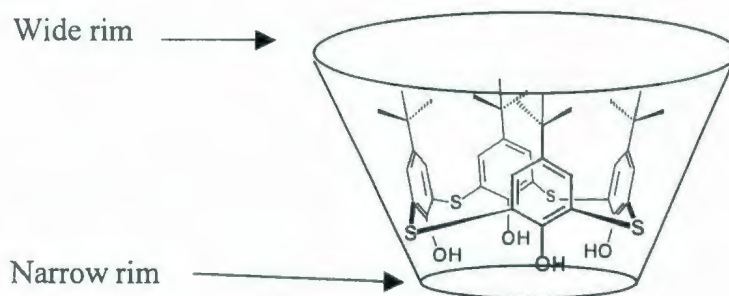


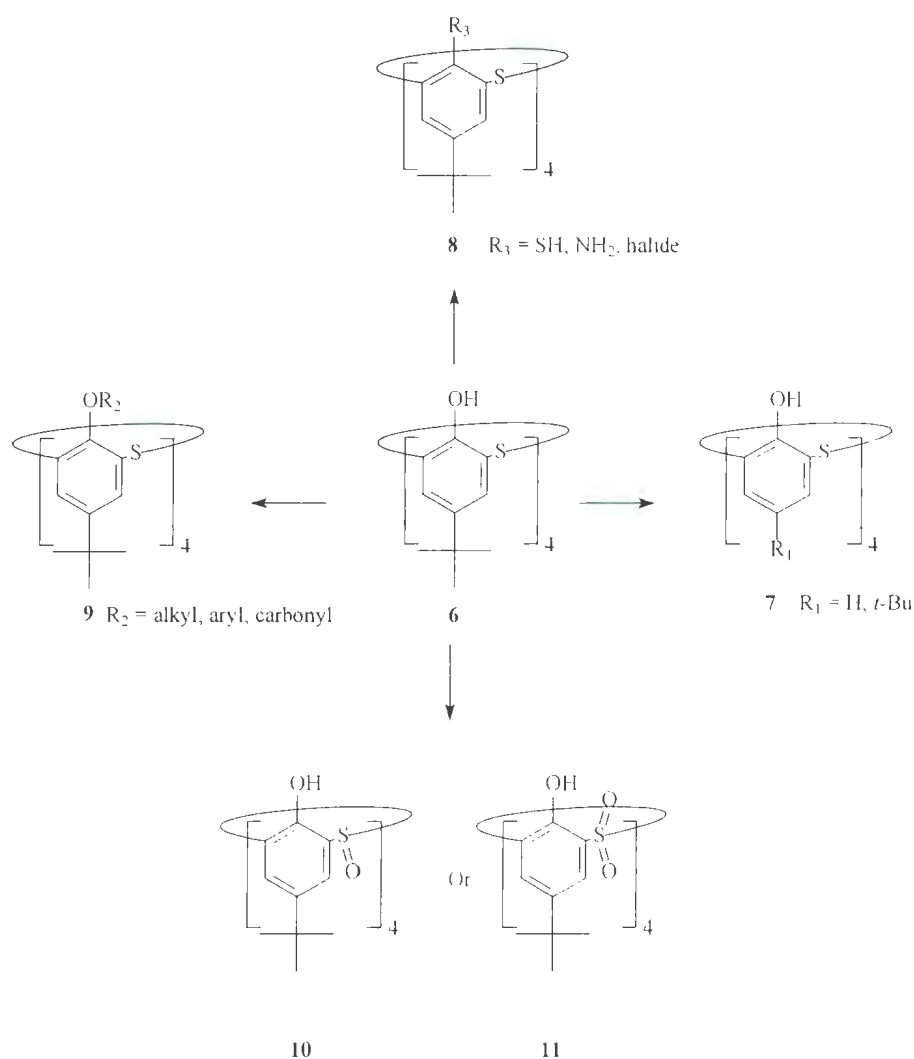
**Figure 2-2:** The calix-like shape of thiacalixarenes **6**.

Thiacalixarene **6** has a calix-like shape similar to that of calix[4]arenes (**1**) in which the *tert*-butyl group-substituted side is called the "wide" rim and the phenol group-substituted side is called the "narrow" rim (Figure 2-2). Furthermore, theoretical calculations at the B3LYP/6-31G(d,p) level of theory indicated that in the cone conformer of **6**, the intramolecular hydrogen bonds are longer (1.82 Å)<sup>20</sup> than in the cone conformer of calix[4]arene **1** (1.58 Å).<sup>21</sup> This is in agreement with the experimental evidence that thiacalixarene **6** is more conformationally flexible than **1**. The same study also revealed that there is a significant difference between the dipole moments of the cone conformers of **6** and calix[4]arene **1** (5.7 and 1.6 D, respectively, along the vertical  $C_{4v}$  axes). These structural and polarity differences between **1** and **6** could be due to the difference between the contributions from the partial charges of the methylene groups in **1** and sulfur atoms in **6**.

The relatively large cavity and dipole moment of thiacalix[4]arene (**6**) make it a good ligand for many different metals.<sup>22</sup> This has been proven by the isolation and structural characterization of complexes of **6** with Co(II),<sup>23,24</sup> Ni(II),<sup>23</sup> Cu(II),<sup>25</sup> Zn(II),<sup>24,26</sup> UO<sub>2</sub>,<sup>27</sup> Nd(III),<sup>28</sup> and also with alkali metals.<sup>29</sup> These complexes are either mononuclear (UO<sub>2</sub> and Zn(II)),<sup>26,27</sup> dinuclear (Co(II) and Ni(II)),<sup>27</sup> trinuclear (Co(II) and Zn(II))<sup>24</sup> or tetranuclear (Cu(II) and Nd(III)).<sup>25,28</sup>

The design and modification of a host molecule is crucial for improving its host-guest complexation properties. In **6**, all of the modifications which have been reported to date have been limited to either substituting, or removing, the functionalities at the wide rim, as in *e.g.* **7** (Scheme 2-4), or the phenolic groups at the narrow rim, as in **8** and **9**.

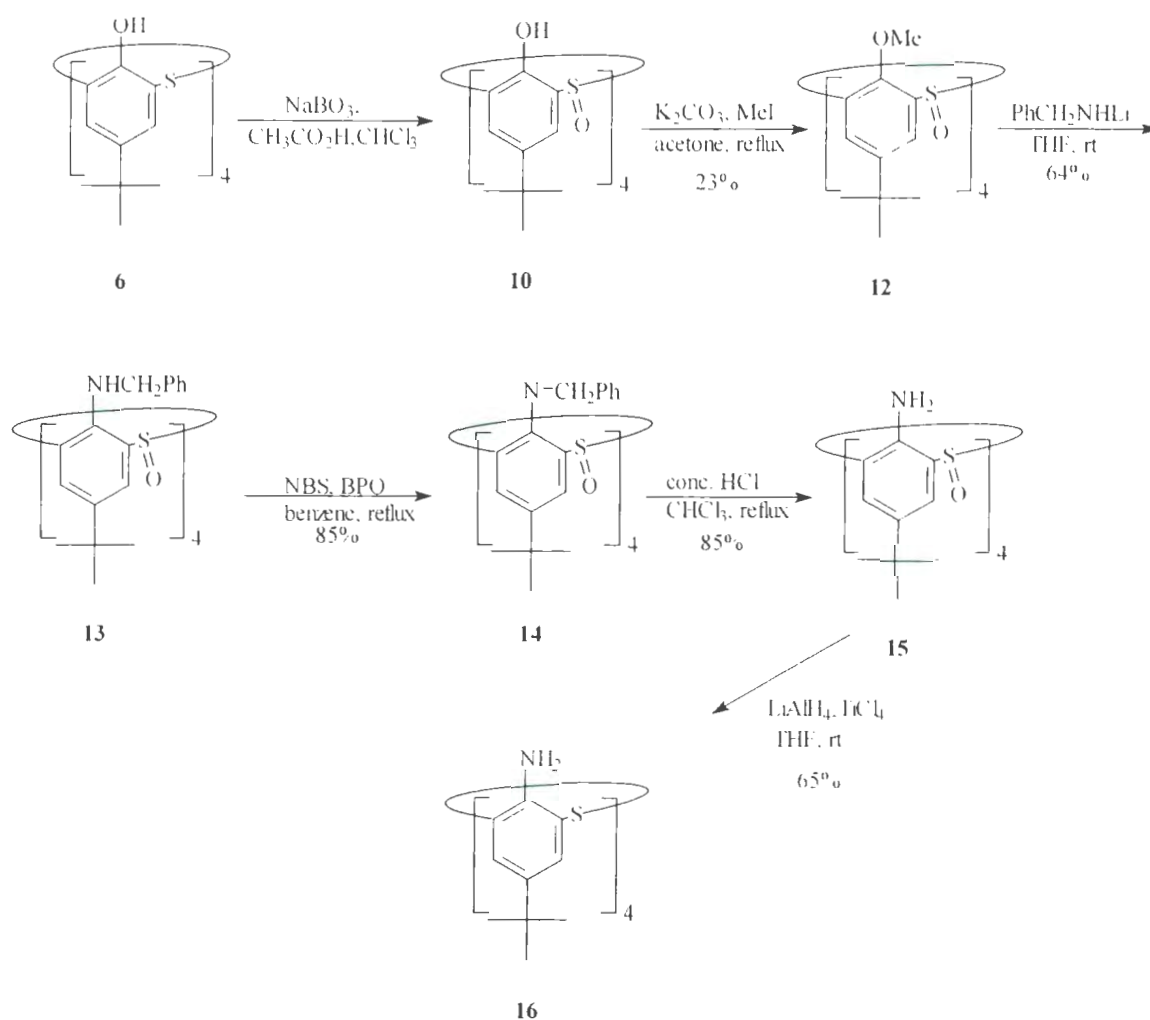
Also, oxidation of the bridging sulfur atoms to form the corresponding  $-SO-$  or  $-SO_2-$  bridging groups, as in **10** and **11**, shifts the complexation abilities of thiacalixarenes to bind better with “harder” metals (*e.g.* alkali earth metals and lanthanides).<sup>30</sup>



**Scheme 2-4:** Modification of thiacalix[4]arene **6**.

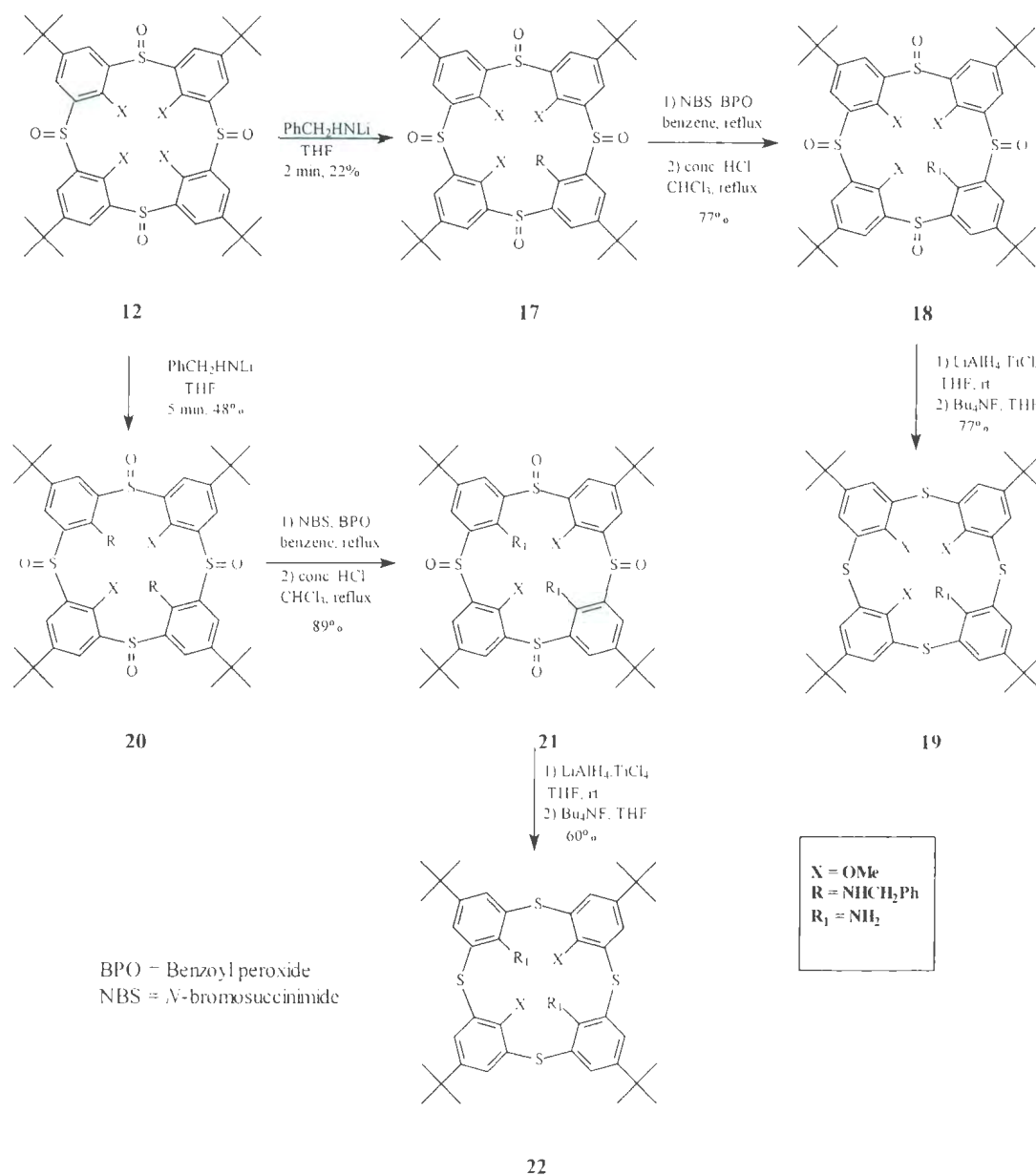
Functionalization of the phenolic groups, using different groups such as methyl acetate, methyl amide or porphyrins, and others.<sup>31</sup> as in **9** (Scheme 2-4), is the most widely used approach to functionalize the narrow rim of calixarenes and thiacalixarenes.

In contrast, there are very few known examples in which the narrow rim phenolic oxygen atoms have been replaced with other functionalities since they are highly resistant to direct substitution-displacement reactions. Iki and Miyano reported the multi-step substitution of the phenol hydroxy groups in **12** which was previously derived from **6**, by amino groups *via* nucleophilic aromatic substitution ( $S_NAr$ ) with lithium *N*-benzylamide, to form **13**. Subsequent bromination-elimination, hydrolysis and reduction *via* **14** and **15** afforded **16**, the tetraamine analogue of **6**, in 67% overall yield (Scheme 2-5).<sup>32</sup>



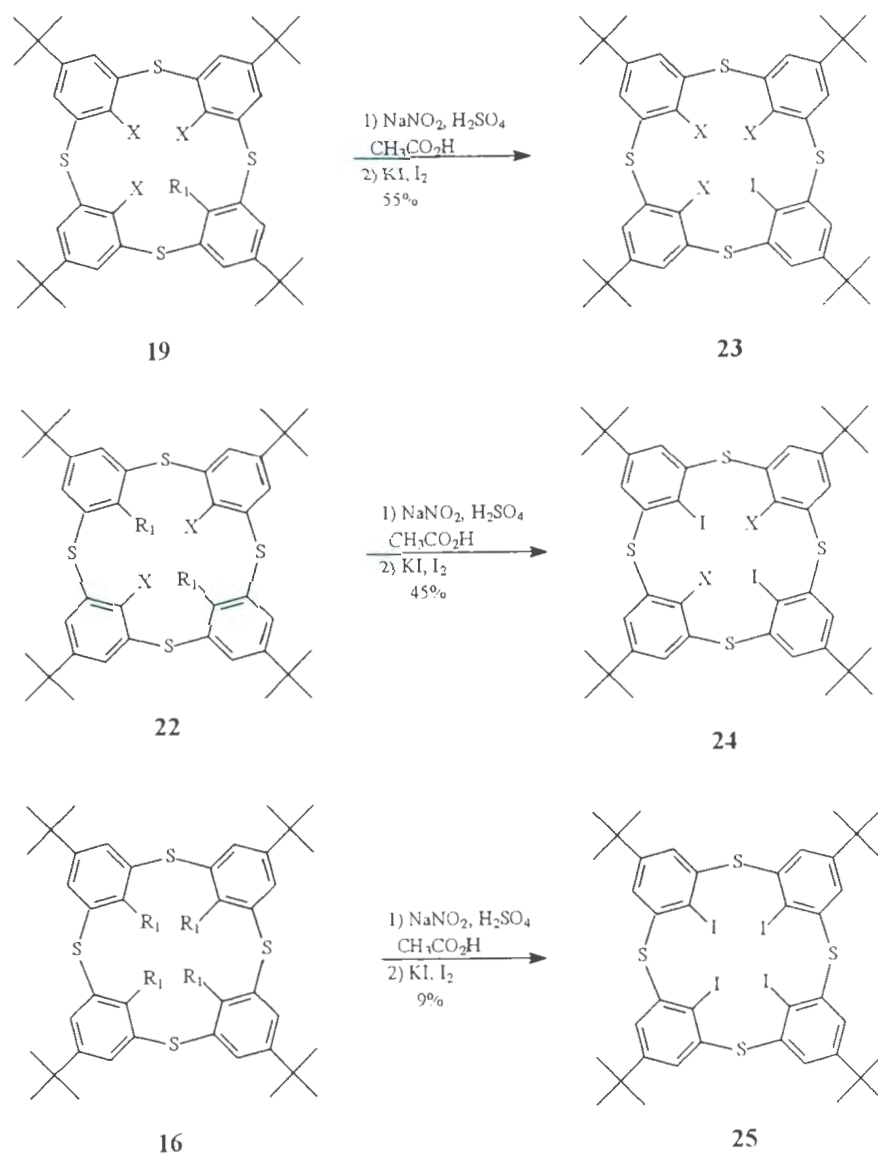
**Scheme 2-5:** Synthetic approach towards aminothiacalix[4]arene **16**.

Time-controlled  $S_NAr$  reactions of **12** with lithium *N*-benzylamide over 2 to 5 minutes afforded monoamino- **17** and diaminothiacalix[4]arene **20** in 22% and 48% yields, respectively (Scheme 2-6). Both **19** and **22** were also prepared by multi-step reactions involving removing the benzyl moieties followed by reductions.<sup>32b</sup>



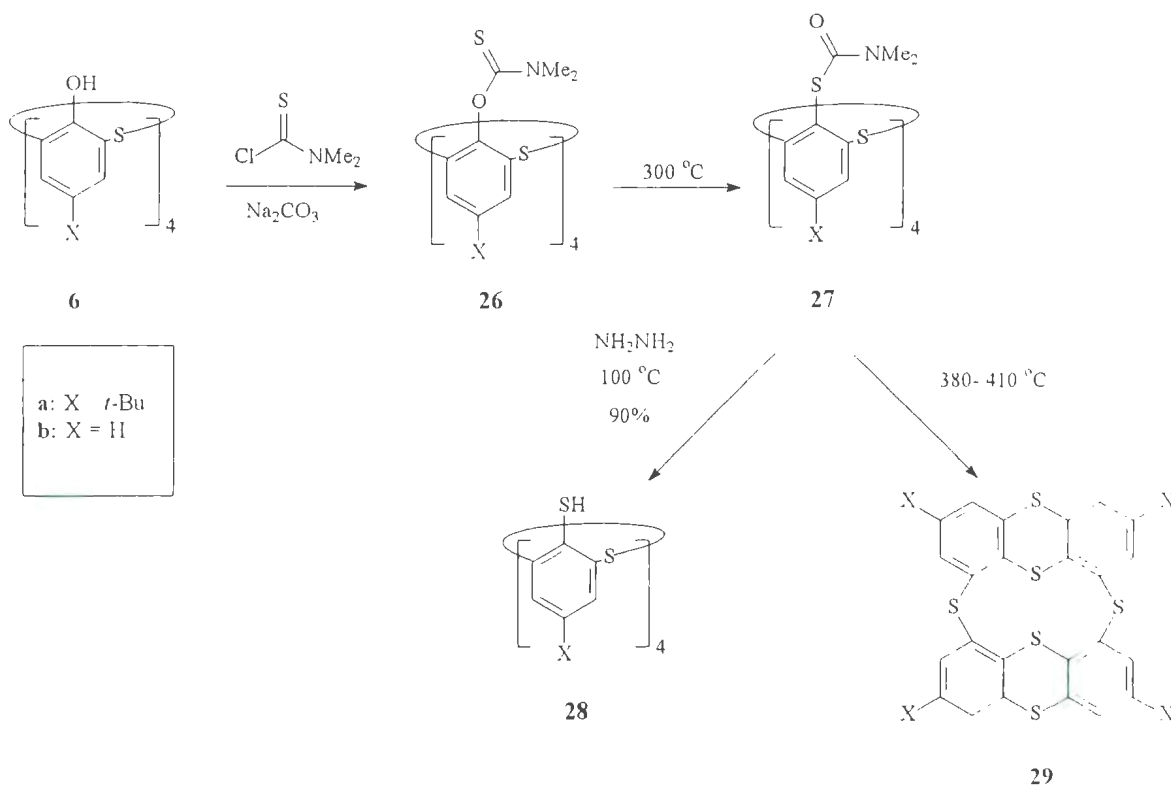
**Scheme 2-6:** Preparation of mono-, and diaminothiacalix[4]arenes **19** and **22**.

Further substitution of thiacalix[4]arene has been accomplished by replacement of the amino groups in **19**, **22** and **16** by iodide to give the mono-, di- and tetraiodothiacalix[2]arenes **23**, **24** and **25** respectively.<sup>32b</sup> These iodination steps took place *via* Griess reactions of the corresponding diazonium salts of the amines **19**, **22** and **16** with KI and I<sub>2</sub> (Scheme 2-7).



**Scheme 2-7:** Preparation of mono-, di- and tetraiodothiacalixarene **23-25**

The only other example of replacement of the phenolic hydroxyl groups with other functionalities involved conversion of the hydroxyls to sulfhydryl groups *via* the Newman-Kwart reaction (Scheme 2-8). Acylation of **6** with *N,N*-dimethylthiocarbamoyl chloride gave thioamide **26** which was thermally rearranged at 300 °C to give **27**. Deprotection of the sulfhydryls by hydrazine at 100 °C afforded **28** in good yield.<sup>33</sup>

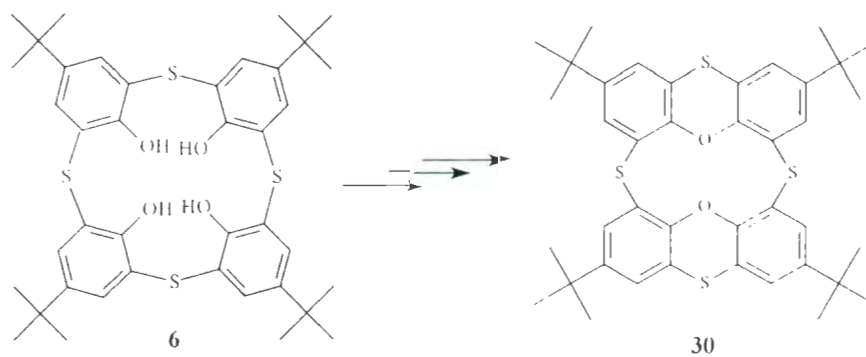


**Scheme 2-8:** Preparation of thiothiacalixarene **28** and thiacalix[2]thianthrenes **29**

Recently, Parola and coworkers,<sup>34</sup> reported that heating compounds **27** (X = H, *t*-Bu) up to 410 °C led to rearrangement, affording thiacalix[2]thianthrenes **29** (Scheme 2-8). The *tert*-butyl-substituted analogue **29a** (X = *t*-Bu) was formed in 36% yield and the unsubstituted thianthrene **29b** (X = H) was obtained in 44% yield.<sup>34</sup> Both of these

thianthrene macrocycles formed coloured radical intermediates in sulfuric acid medium, or in the presence of a Lewis acid.<sup>35</sup>

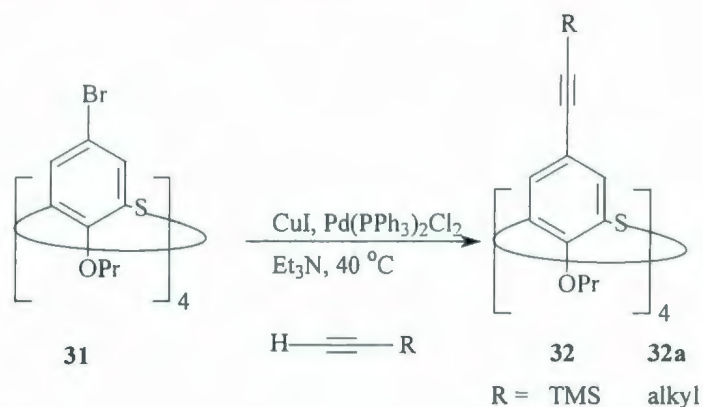
This chapter presents the results of attempts by this author to functionalize the narrow rim of thiacalix[4]arene **6** with acetylene groups, using the Sonogashira coupling reaction. Also, a Cu(I)-catalyzed rearrangement of thiacalixarene **6** to form a thiacalix[2]phenoxathiin compound **30**, is reported. In addition, a mechanism is proposed to account for this rearrangement reaction (Scheme 2-9). In a limited complexation study, the phenoxathiin compounds obtained showed modest affinities towards complexation with Ag(I) and Hg(II) ions.



**Scheme 2-9:** Preparation of thiacalix[2]phenoxathiin (**30**).

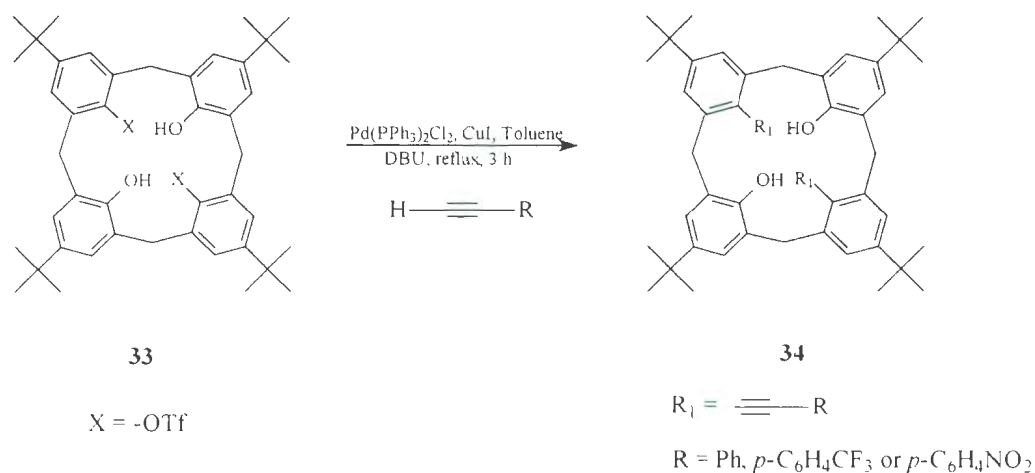
## 2.1.2 Results and discussion

Parola's group modified thiacalix[4]arene by substituting its wide rim by alkynyl groups in order to study its non-linear optical (NLO) properties.<sup>36</sup> The thiacalixarene sulfur bridging atoms and the wide rim acetylene groups enhance  $\pi$ -electron delocalization which contributes to the NLO properties for this class of compounds. Parola used modified Sonogashira reaction conditions to substitute the wide rim of the *O*-propyloxy derivative of *p*-bromothiacalix[4]arene (**31**) by TMS-acetylene, to produce **32** in 72% yield (Scheme 2-10). Further modification of **32** to produce compounds such as **32a** gave a product with significant 3<sup>rd</sup> order NLO properties.



**Scheme 2-10:** Upper-rim substitution of thiacalixarene **31** by acetylene.

Georghiou and Al-Saraierh reported the first narrow-rim phenolic group substitution reactions in calix[4]arenes by ethynyl groups (Scheme 2-11).<sup>37</sup> The 1,3-bistriflate calix[4]arene **33** was reacted with various terminal acetylene group-containing compounds under typical Sonogashira-type coupling conditions to afford the ethynyl-substituted calix[4]arenes **34** in synthetically useful yields (up to 64%).

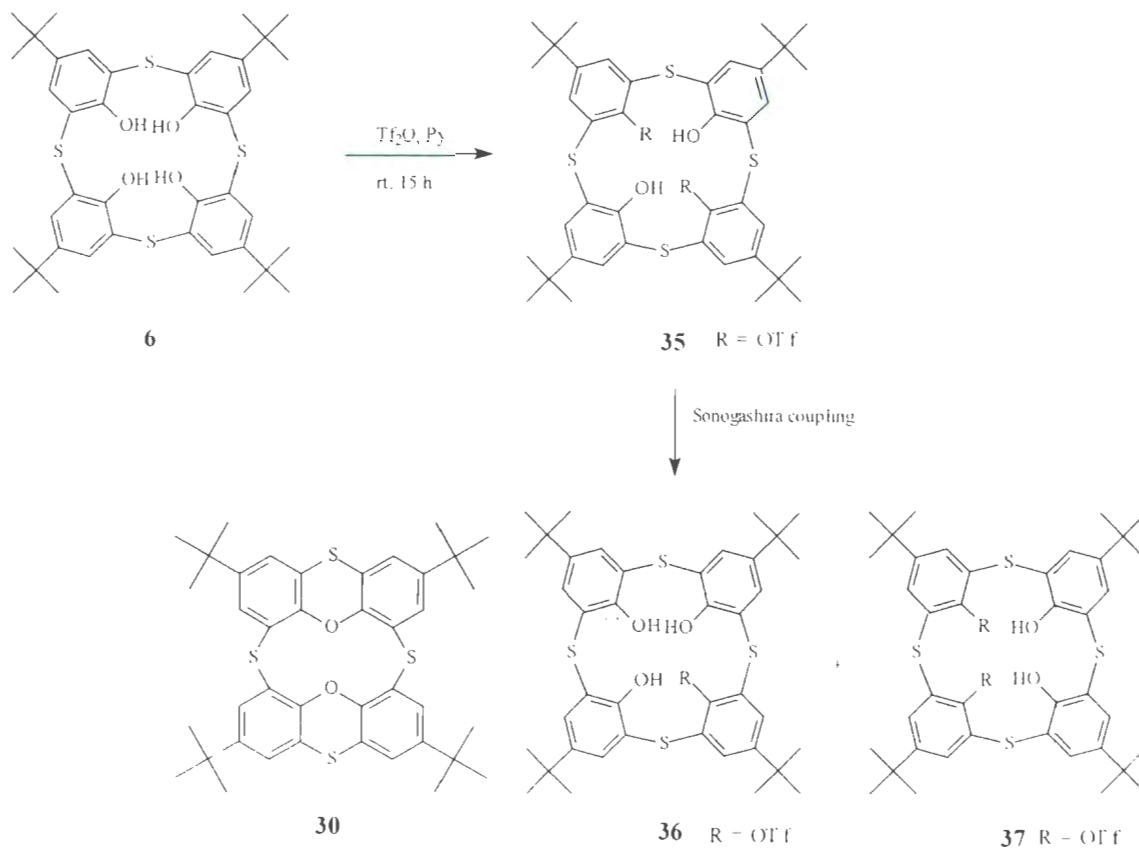


**Scheme 2-11:** Narrow-rim substitution of calixarene **33** by acetylenes.

It was of interest to extend these findings with the Sonogashira reaction<sup>37</sup> to the 1,3-bistriflate of thiacalix[4]arene **6** in order to study both the potential NLO, and also the complexation properties, of suitably designed narrow-rim arylethynyl derivatives of thiacalix[4]arene itself.

The 1,3-bistriflate thiacalix[4]arene **35** was easily prepared by reaction of **6** with triflic anhydride in anhydrous pyridine (Scheme 2-12).<sup>38</sup> The crude product crystallized from hexane to give a 60% yield of **35**. The residual product was purified by column chromatography on silica gel using (1:7)  $\text{CH}_2\text{Cl}_2$ :hexane as the eluent to afford an additional 27% yield of **35** as a colourless solid. The  $^1\text{H}$  NMR and  $^{13}\text{C}$  NMR spectra confirmed that the structure of 1,3-bistriflate **35** is highly symmetric and in the *cone* conformation. The  $^1\text{H}$  NMR spectrum of **35** showed that the phenolic hydrogen atoms were shifted to higher field at  $\delta$  6.13 ppm and the two aromatic signals appear at  $\delta$  7.17 and 7.75 ppm. In addition, two singlets at  $\delta$  1.35 and 0.96 ppm were observed for the two

*tert*-butyl groups. The  $^{13}\text{C}$  NMR spectrum showed eight aromatic signals, four upfield signals due to the *tert*-butyl groups and the characteristic peak for the carbon atom of the triflate group appeared as a quartet at 122.78 ppm.



**Scheme 2-12:** Products from the reactions of **35** under Sonogashira conditions.

Different Sonogashira reaction conditions were used (Table 2-1) in attempts to displace the triflate groups by phenylethynyl groups. However, none of these reactions gave the desired phenylethynyl products and instead other products such as **30**, **36**, and **37** (Scheme 2-12) were detected.

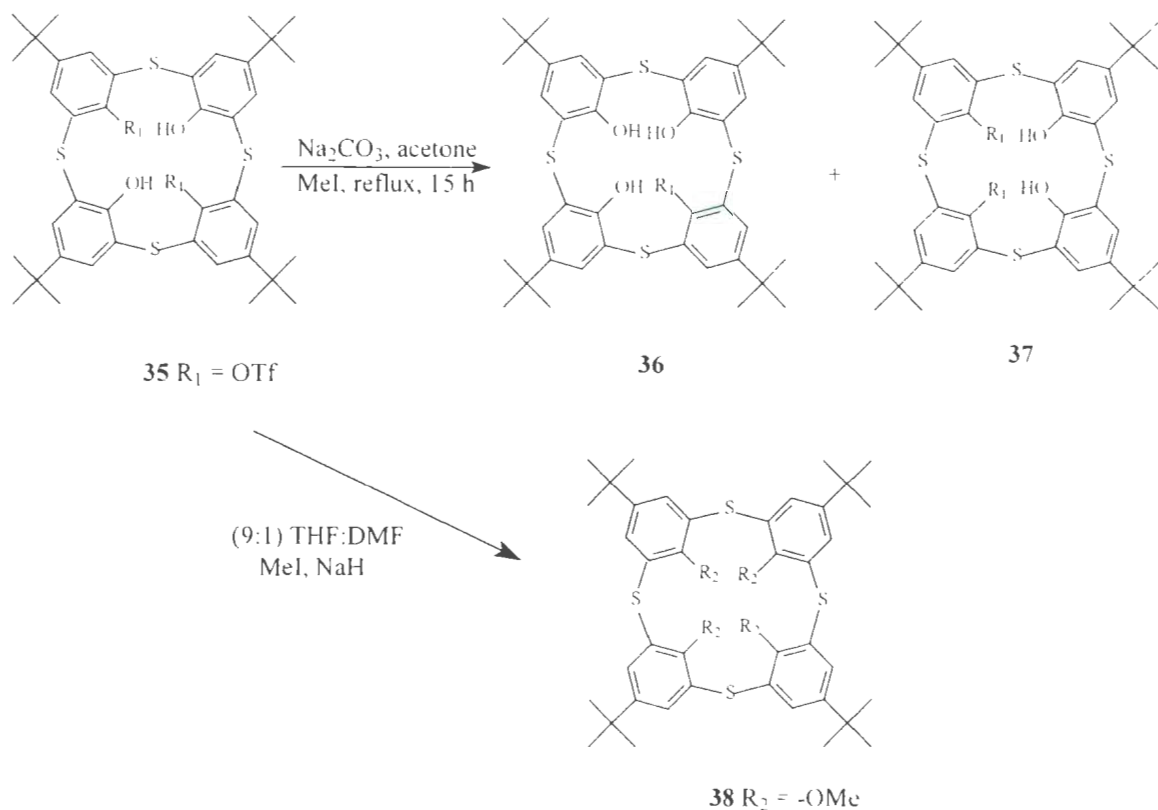
**Table 2-1: Different Sonogashira conditions used with 1,3-bistriflate 35.**

Entry	CuI	Base	Pd catalyst	Solvent	Temp. °C	Yield <sup>a</sup> (%)		
						Time (h)	36	37
	mol eq.	(mol eq.)	(mol%).					
1	5	DBU (4.4)	PdCl <sub>2</sub> (PPh <sub>3</sub> ) <sub>2</sub> (10)	Toluene	reflux 24	11	8	60
2	-	Cs <sub>2</sub> CO <sub>3</sub> (5)	PdCl <sub>2</sub> (PPh <sub>3</sub> ) <sub>2</sub> (5)	CH <sub>3</sub> CN	reflux 10	-	-	-
3	0.1	Et <sub>3</sub> N	PdCl <sub>2</sub> (PPh <sub>3</sub> ) <sub>2</sub> (5)	Et <sub>3</sub> N	40 24	30	40	28
4	0.2	Et <sub>3</sub> N	Pd(PPh <sub>3</sub> ) <sub>4</sub> (20)	CH <sub>3</sub> CN	25 3	-	-	-
5	-	Et <sub>3</sub> N	PdCl <sub>2</sub> (PPh <sub>3</sub> ) <sub>2</sub> (5)	DMF	90 5	58	37	-
6	-	piperidine	Pd(PPh <sub>3</sub> ) <sub>4</sub> (5)	piperidine	80 3	80	15	-
7	-	Et <sub>3</sub> N	Pd(OAc) <sub>2</sub> (15)	DMF DMA	25 7	-	-	-

Note: In Entry 2 only starting materials **6** and **35** were recovered.

Surprisingly, the same Sonogashira-type reaction conditions (CuI, DBU and phenylacetylene in anhydrous degassed toluene) which afforded the corresponding 1,3-bis(phenylethynyl)calix[4]arene **34** from **33**,<sup>37,38</sup> instead gave bis(phenoxathiin) **30** (60%), monotriflate **36** (11%) and 1,2-bistriflate **37** (8%) (Table 2-1, Entry1). The same products were isolated when triethylamine was employed both as a base and solvent, but phenoxathiin **30** was the minor product (28%) (Entry 3). In contrast, no **30** was detected in the absence of CuI when Et<sub>3</sub>N was used in DMF as solvent. Instead, monotriflate **36** (58%) and 1,2-bistriflate **37** (35%) were obtained (Entry 5).<sup>41</sup> Compounds **36** and **37** were also produced in different yields in the absence of CuI, when piperidine was used as both the base and solvent with Pd(PPh<sub>3</sub>)<sub>4</sub> as a catalyst (Entry 6).<sup>42</sup> Buchwald's

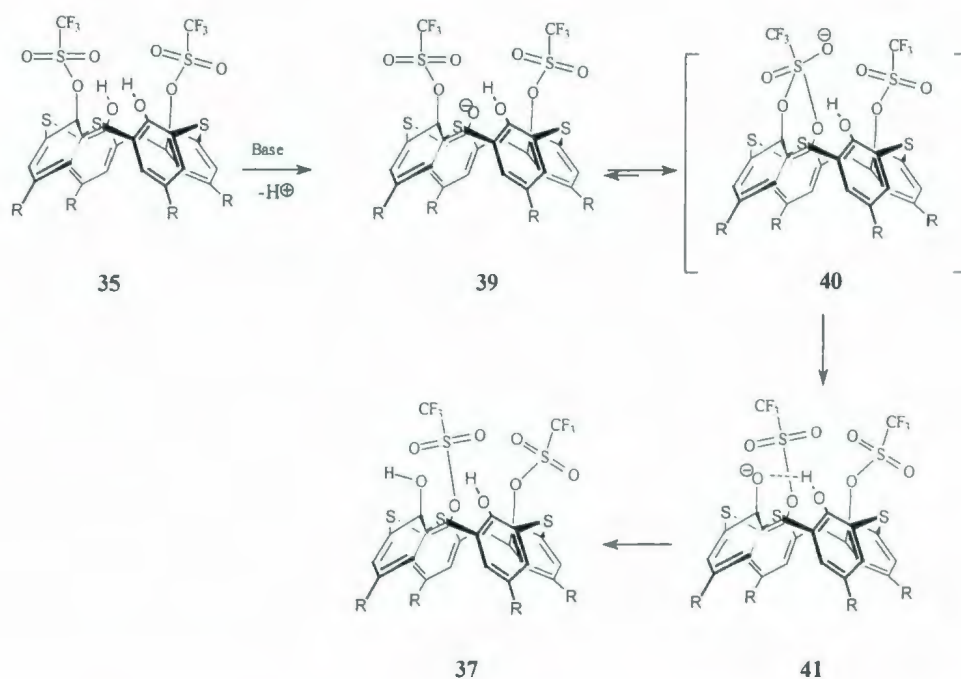
conditions<sup>39</sup> (Pd(II) in acetonitrile with Cs<sub>2</sub>CO<sub>3</sub>) afforded only thiacalix[4]arene **6** itself, the product of hydrolysis of **35** (Entry 2). No reaction was observed when triethylamine was used as base with either Pd(PPh<sub>3</sub>)<sub>4</sub> as catalyst in CH<sub>3</sub>CN (Entry 4),<sup>40</sup> or with Pd(OAc)<sub>2</sub> as catalyst in (1:1) DMF:DMA (Entry 7).<sup>43</sup>



**Scheme 2-13:** Methylation reactions of 1,3-bistriflate **35**.

It is clear that the reaction affording 1,2-bistriflate **37** and phenoxathiin **30** is associated with the presence of free phenolic groups –OH in the reactant **35**. Therefore, protection of the phenolic groups, in principle, should diminish the hydrolysis and rearrangement processes and promote the Sonogashira coupling. Various methods to

methylate 1,3-bistriflate **35** were attempted but none provided the desired methylated 1,3-triflate thiacalix[4]arene (Scheme 2-13). Instead, hydrolyzed products were obtained. For example, heating **35** with  $\text{Na}_2\text{CO}_3$  in acetone at reflux in the presence of methyl iodide afforded **36** and **37**.<sup>44</sup> Treatment of **35** with NaH in (9:1) THF:DMF, and then methyl iodide<sup>45</sup> removed the triflate groups and methylated all phenolic groups to give the tetramethoxy thiacalix[4]arene **38**.<sup>44</sup>



**Scheme 2-14:** A proposed mechanism of the migration reaction of triflate in **35** to form **37**.

1,2-Bistriflate **37** was formed by migration of triflate from position 3 to position 2, presumably *via* intermediate **40**, which is formed by the nucleophilic attack of the oxide at electrophilic sulfur in the triflate group (Scheme 2-14). This mechanism is in agreement with one proposed by Hattori *et al.* recently.<sup>46</sup> Stabilization of the anion by

hydrogen bonding between proximal hydroxyl groups favours collapse of intermediate **40** and formation of anion **41**. The importance of intramolecular hydrogen bonding was confirmed by a MMM<sup>52</sup> study, which concluded that 1,2-bistriflate **37** (407.7 kcal/mol) is more stable than the 1,3-triflate **35** (412.0 kcal/mol).

**Table 2-2: Cu-Pd conditions for the rearrangement reactions of 35 in toluene.**

Entry	CuI	Pd(PPh <sub>3</sub> ) <sub>2</sub> Cl <sub>2</sub>	Reflux	Yield <sup>a</sup> (%)		
	mol eq.	(mol%)	Time (h)	<b>36</b>	<b>37</b>	<b>30</b>
1	5	10	24	11	8	60
2	2.5	10	24	32	8	41
3	1	10	24	40	7	28
4	-	-	15	-	89	8
5	-	10	15	-	81	13
6	5	-	12	-	12	77
7	5	10	15	-	-	-

<sup>a</sup> In Entry 5 only starting material **35** was recovered.

Further investigations were performed in order to understand the mechanism of formation of phenoxathiin **30** (Table 2-2). According to Table 2-1, only Entries 1 and 3 afforded **30**. When triethylamine or DBU were used as the base with Pd(II),<sup>36,37</sup> phenoxathiin **30** was afforded in 60% and 28% yields, respectively.

Clearly, when CuI was used in excess (5 eq.), phenoxathiin **30** was produced in higher yield (60%, Entry 1). Lower yields (Entries 2 and 3, 41% and 28%, respectively) were obtained when less CuI was used (2.5 eq. and 1.0 eq., respectively). Unexpectedly,

when only 1.0 eq. of CuI (Entry 3) was used with 10 mol% Pd(II) catalyst and DBU, compound **42** was obtained as a minor product in 9% yield. In **42**, one of the hydroxyl groups of the starting material **35** was replaced by a hydrogen atom. The mechanism of its formation is uncertain, but presumably, the reaction initially forms the more stable 1,2-bistriflate **37**, followed by displacement of one of the triflate groups by a hydride under Pd-catalyzed conditions. Further mechanistic clarification requires additional investigation, but this is the first time that replacement of a narrow rim thiacalixarene hydroxy group by a hydrogen atom has been reported.

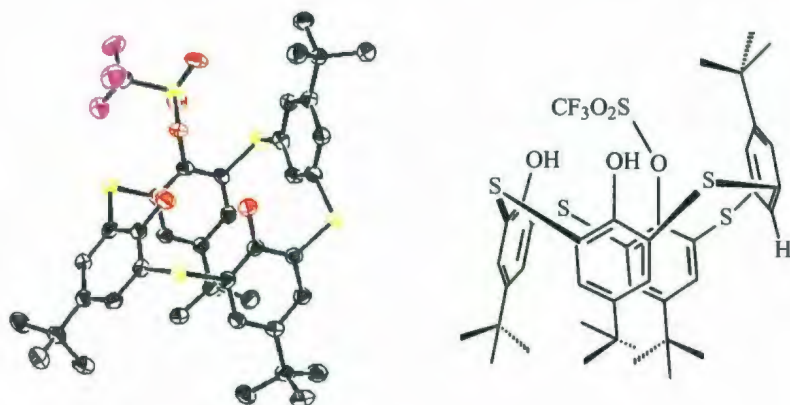
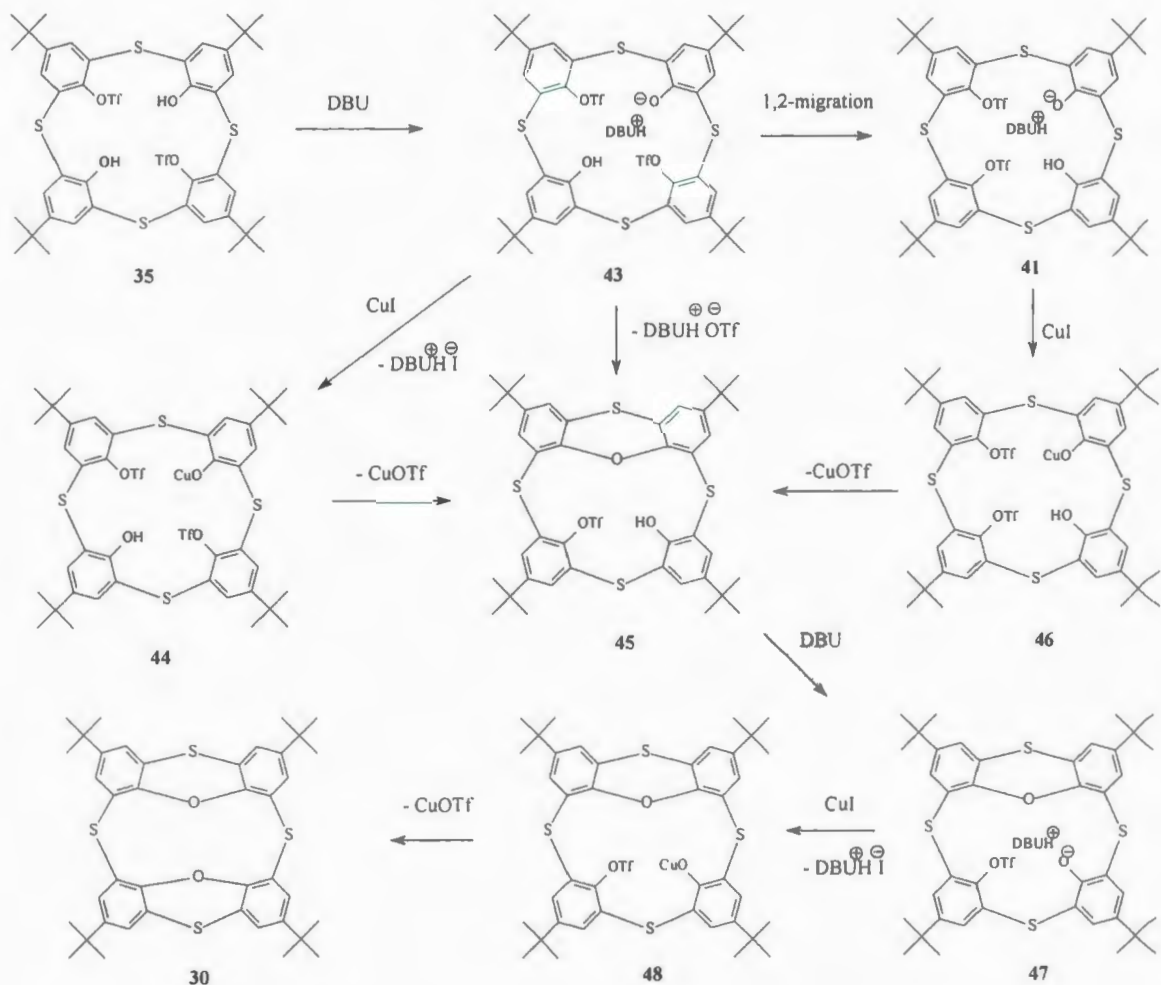


**Figure 2-3:** X-ray structure of monotriflate **42**.

The X-ray crystal structure of monotriflate **42** confirms a *partial pinched-cone* conformation (Figure 2-3). The two proximal hydroxy groups and the triflate group are all in the same face with the *tert*-butyl group of the deoxygenated aromatic ring. The aromatic ring which bears the triflate group is angled inwards toward the distal phenolic ring, and the intraannular hydrogen appears at  $\delta = 6.92$  ppm in the  $^1\text{H}$  NMR spectrum.



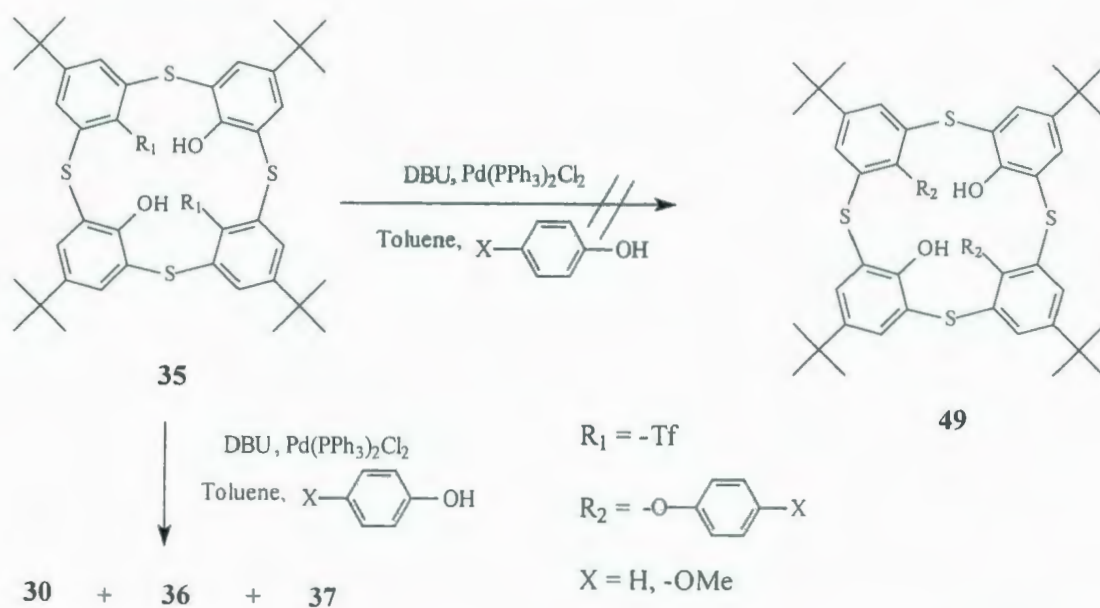
**Scheme 2-15:** A proposed mechanism for reaction of **35** to form **30**.

In the absence of **CuI**, the reaction gave low yields of **30** (8% to 13%, Entries 4 and 5). No new product formation was observed when only **CuI** and **Pd(II)** together were used without any **DBU** and only unreacted starting material was recovered (Entry 6). Subsequent to the initial observations, it was found that reaction of **35** in toluene, without any **Pd** catalyst but with **CuI** and **DBU**, produced **30** in 77% yield. This evidence suggests that the reaction to form **30** proceeds *via* an Ullmann-type reaction

mechanism, and the presence of CuI and DBU is crucial to produce **30** in high yield. The mechanism in Scheme 2-15 is in basic agreement with that proposed by Hattori<sup>47c</sup> which appeared after our own work had been completed and reported by us.<sup>47a</sup>

Deprotonation of **35** by DBU forms the anion **43**. In the absence of CuI, **43** forms the phenoxathiin *via* direct displacement of the triflate group and this pathway usually gives **45** in low yield. In the presence of CuI, a phenoxide coordinates to the Cu(I) to form **44** which in turn, leads to **45** *via* an Ullmann-type reaction. Also, **43** could rearrange to form the more stable anion **41** (Scheme 2-14), which forms **46** in the presence of CuI, and leads also, to **45**. Subsequently, deprotonation of **45** leads to phenoxide **47** which reacts with CuI, to form **48**. Phenoxathiin **30** is obtained from Cu(I) complex **48** *via* an Ullmann-type reaction.

In order to see whether **35** could react in an intermolecular fashion under these same Cu(I)-catalyzed conditions, the following two experiments were conducted. Bistriflate **35** was reacted with 10 mol equivalents of either phenol, or 4-methoxyphenol, in the presence of DBU, CuI, and Pd(PPh<sub>3</sub>)<sub>2</sub>Cl<sub>2</sub> in toluene (Scheme 2-16). None of the possible products of the corresponding intermolecular reactions (**49**) were detected, however, and the product mixture again contained the product phenoxathiin **30** in 18% or 26% yields, respectively.



X	Yield (%)		
	30	36	37
H	18	63	22
OMe	26	48	31

**Scheme 2-16:** Reactions of **35** in the presence of phenols.

The structure of a sample of **30**, which had crystallized from benzene, was determined by single crystal X-ray crystallography (Figure 2-4). This structure was virtually identical to that subsequently reported by Hattori *et al.*,<sup>47c</sup> except for a single molecule of benzene in the unit cell (Hattori's crystal was derived from  $\text{CH}_2\text{Cl}_2:\text{CH}_3\text{CN}$  with the resultant differences in the crystal packing). It should be noted that the molecule of benzene is not within the "cavity" of the macrocycle, and is thus not a "guest" molecule.

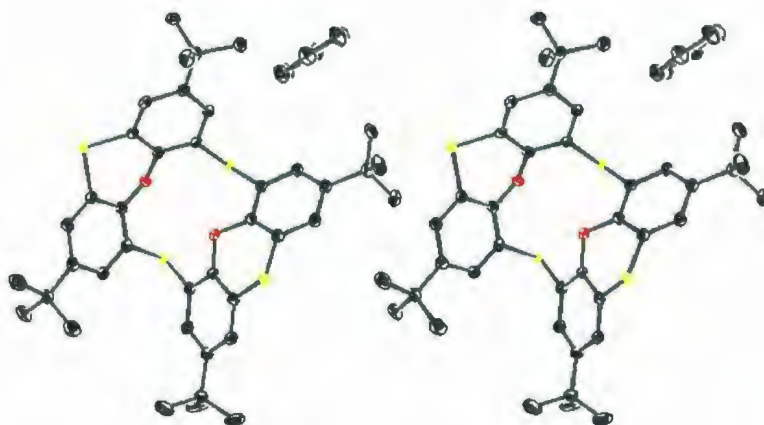


**Figure 2-4:** X-ray structure stereoview of **30:C<sub>6</sub>H<sub>6</sub>**.

The phenoxathiin C-S-C and C-O-C bond angles in **30** are comparable with those of Hattori's X-ray structure:  $97.28^\circ$  and  $114.72^\circ$ ; and  $97.60^\circ$  and  $115.89^\circ$  in **30** compared with  $97.51^\circ$  and  $116.17^\circ$ ; and  $97.88^\circ$  and  $115.95^\circ$  in Hattori's structure, respectively. The C-S-C bond angles incorporating the two sulphur atoms connecting the two phenoxathiins in **30:C<sub>6</sub>H<sub>6</sub>** are  $98.02^\circ$  and  $100.49^\circ$  vs.  $98.29^\circ$  and  $100.92^\circ$ , respectively.

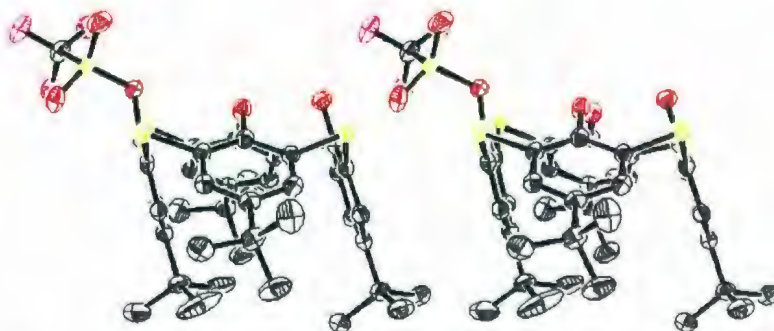


**Figure 2-5:** X-ray structure stereoview of monotriflate **36**.

The X-ray crystal structure of monotriflate **36** shows it to be in a “skewed” *pinched-cone* conformation in which the aromatic ring which bears the triflate group is angled inwards, toward the distal phenolic ring (Figure 2-5).

The X-ray crystal structure of 1,2-bistriflate **37** was also solved and it also revealed that there are two molecules in the unit cell. Each of the molecules is in a *pinched-cone* conformation and are oriented in opposite directions to each other (Figure 2-6). Hattori's group has also reported the formation of **37** produced by the intramolecular rearrangement of the precursor **35** under basic conditions,<sup>46</sup> but did not obtain its crystal structure. Previously, Georghiou<sup>48</sup> and others<sup>49</sup> reported a similar intramolecular rearrangement of 1,3-bistriflate *p*-*tert*-butylcalix[4]arene, the analogous 1,3-bistriflate of *p*-*tert*-thiabutylcalix[4]arene under Pd-catalyzed reaction conditions.

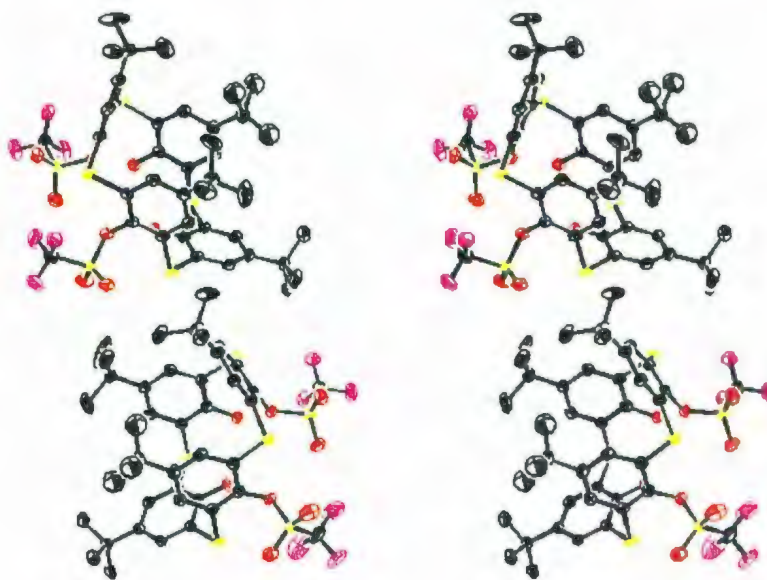
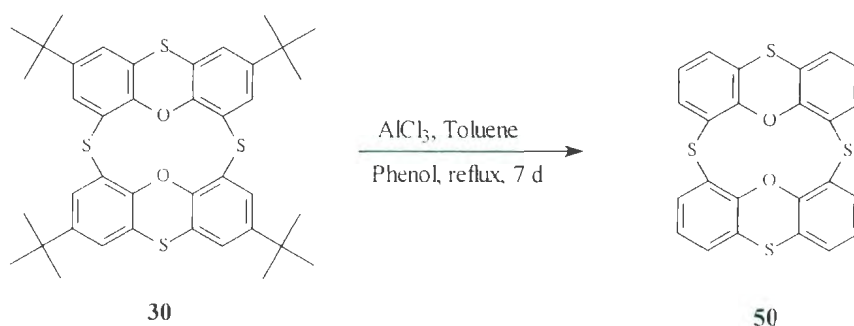


**Figure 2-6:** X-ray structure stereoview of 1,2-bistriflate **37** showing the orientation of the two molecules in the unit cell. The hydrogen atoms and the solvent molecule ( $\text{CHCl}_3$ ) have been removed for clarity.

MMM<sup>51</sup> calculations suggested that the new bowl-shaped compound **30** might be capable of complexation with C<sub>60</sub> or C<sub>70</sub>. However, all of the experimental conditions which were tried failed to provide evidence for any such complexation. Further effort was therefore focused on the synthesis of new derivatives of **30** containing different wide rim ethynyl substituents, which in principle, could be introduced *via* Sonogashira coupling reactions, as was demonstrated in 2003 by Parola *et al.* for tetra-*O*-propylthiacalix[4]arene.



**Scheme 2-17:** De-*tert*-butylation reaction of tetra-*tert*-butylphenoxathiin **30**.

The prerequisite removal of the *tert*-butyl groups from **30** as a first step towards this goal was achieved using the AlCl<sub>3</sub>-phenol protocol described by Hosseini *et al.*, (Scheme 2-17).<sup>18</sup> The desired de-*tert*-butylated bis(phenoxathiin) **50** was obtained in 26% yield and its X-ray structure (Figure 2-5) revealed it to be quite different to that of Desroches and Parola's comparable "thiacalix[2]thianthrene" **29b**.<sup>36</sup> The X-ray structure of **50** reveals that there is a pair of "interlocked L-shaped" molecules in the unit cell (Figure 2-7). The planes of each of the phenoxathiin units of one of these molecules are approximately antiparallel to the corresponding phenoxathiin units of its partner molecule. Each of the C-S-C bond angles which incorporate the sulphur atoms connecting the pair

phenoxathiins in each molecule are  $100.76^\circ$  and  $100.15^\circ$ ; and  $99.70^\circ$  and  $98.82^\circ$ , respectively.

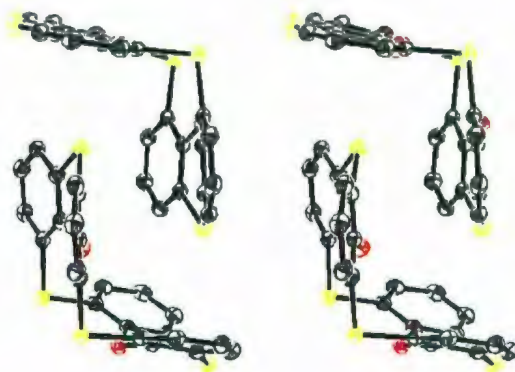


**Figure 2-7:**X-ray structure stereoview of de-*tert*-butylated bis(phenoxathiin) **50**.

These angles are not much different than the corresponding ones seen in either Hattori's, or in compound **30**. However, significant differences are clearly evident in the C-S-C and C-O-C bond angles for each of the phenoxathiin moieties of each molecule of **50** in the unit cell when compared with those of **30**. In **50**, these angles are respectively  $97.73^\circ$  and  $117.17^\circ$ ; and  $99.21^\circ$  and  $118.3^\circ$  for one of the molecules; and, for the second molecule, the respective angles are  $99.81^\circ$  and  $120.32^\circ$ ; and  $101.01^\circ$  and  $122.9^\circ$ . The three rings of the phenoxathiin moiety having the largest C-O-C angle are nearly coplanar when compared with the other three phenoxathiins in the unit cell.

### 2.1.3 Complexation studies

The Georghiou group has been interested in the complexation behaviour of the neutral fullerenes  $C_{60}$  and  $C_{70}$  with diverse bowl-shaped host molecules, including

thiocorannulene derivatives **51-56**,<sup>52</sup> and calix[4]naphthalenes such as **57**. They reported that compounds **51-57** were modest receptors ( $K_{\text{assoc}} \sim 280\text{-}1420$ ) for  $C_{60}$  and  $C_{70}$ . The sulfur atoms in these compounds, it was rationalized, enhanced their binding with fullerenes, since corannulene itself was not a receptor for these fullerenes.<sup>53</sup> On the other hand, the deeper cavity-containing *tert*-butyl substituted calix[4]naphthalene, has also been reported to have modest binding affinity with fullerenes.<sup>53</sup>

Since **30** contains both sulphur atoms and can adopt a roughly bowl-shaped cavity, it was hypothesized that it could also show some binding affinity towards fullerenes, and MMM<sup>52</sup> calculations supported this suggestion.

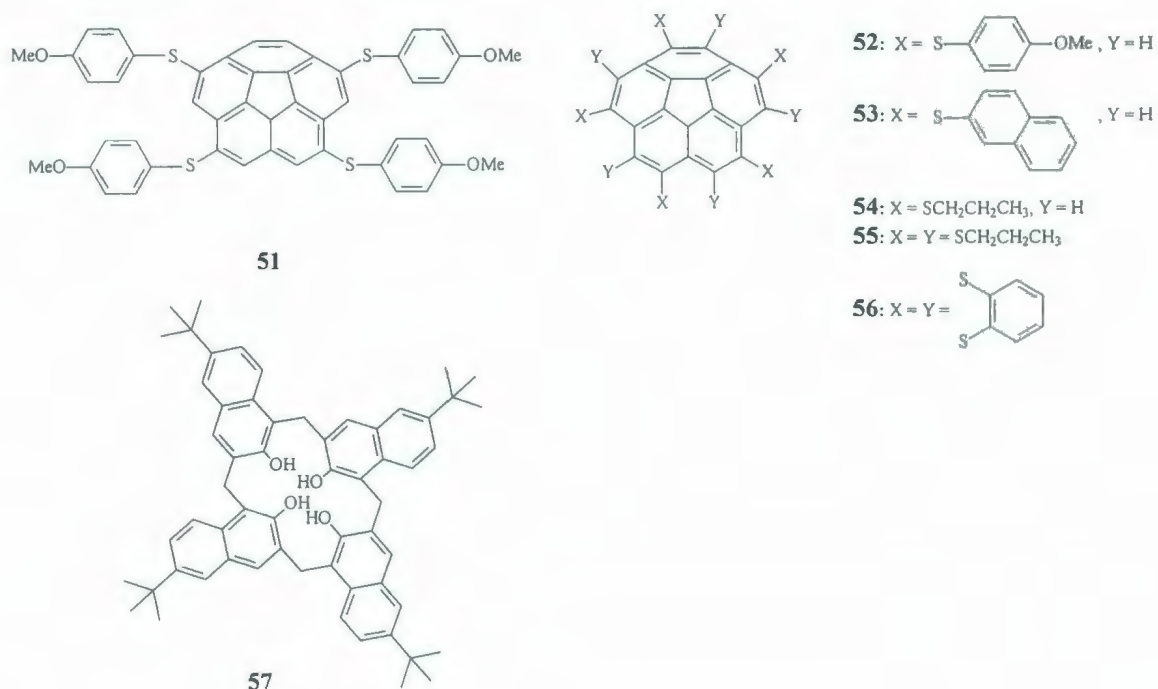


**Figure 2-8:** Thiocorannulenes **51-56** and *tert*-butylcalix[4]naphthalene (**57**).

However, none of the conditions which were tried provided evidence for any such complexation. One possible reason for this lack of experimentally demonstrable

complexation ability is suggested by the two structures shown in Figure 2-9. Figure 2-9(a) is the MMM<sup>51</sup> computer-generated structure of the hypothetical **30**:C<sub>60</sub> complex; and Figure 2-9(b) is that of the complex of C<sub>60</sub> with tetra-*tert*-butylcalix[4]naphthalene (**57**), a molecule which has shown experimentally demonstrable complexation behaviour towards C<sub>60</sub> and C<sub>70</sub>.

It is hypothesized that in the case of **30**, a C<sub>60</sub> molecule is not as deeply embedded, or as tightly embraced by this host molecule, in comparison with the deeper, basket-shaped calixnaphthalene **57**. Another factor could be that the barrier to conformational interconversion in the case of **30** is smaller than that in **57**. In the latter the narrow-rim hydroxyl groups are hydrogen-bonded to one another, thus allowing for a greater degree of pre-organization for effective complexation with a C<sub>60</sub> molecule.

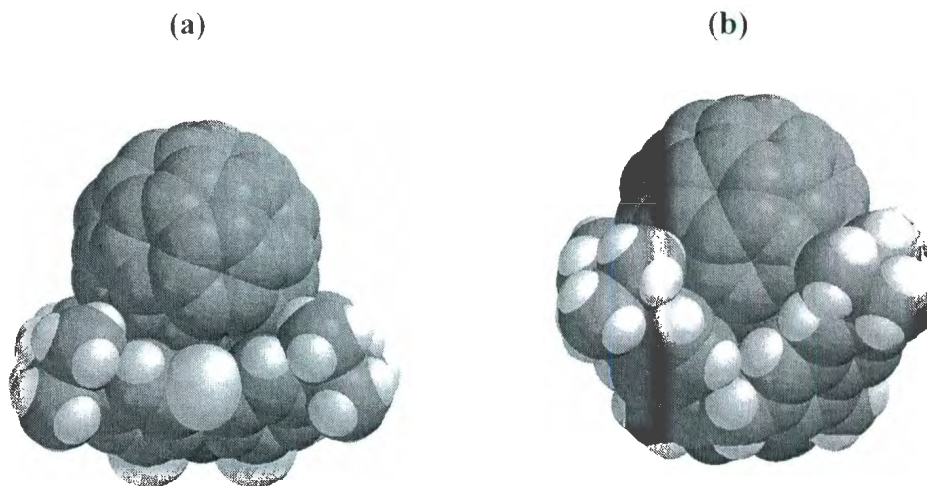


**Figure 2-9:** MMM computer-generated hypothetical structures of supramolecular complexes of C<sub>60</sub> with (a) phenoxathiin **30** and (b) tetra-*tert*-butylcalix[4]naphthalene (**57**).

Sulfur atom-containing calix compounds are known to be good receptors for soft ions such as  $\text{Ag}^+$  and  $\text{Hg}^{2+}$  ions. Georghiou and Tran reported moderate binding abilities for thiaisocalixnaphthalenes **56** and **57** (Figure 2-8) with  $\text{Ag}^+$  and  $\text{Hg}^{2+}$  ions in 1:9  $\text{CD}_3\text{CN}:\text{CDCl}_3$  solvent. This binding ability was attributed to  $\pi$ -cation and/or S-cation interactions.<sup>54</sup> Therefore, it was anticipated that thiacalixphenoxathiins **30** and **50** would have similar binding properties. Indeed, as expected, both **30** and **50** did form 1:1 complexes with  $\text{Ag}^+$  with apparent  $K_{\text{ASSOC}}$  values of  $2200 \pm 200$  and  $630 \pm 50$ , as determined by  $^1\text{H}$  NMR spectroscopy in 1:9  $\text{CD}_3\text{CN}:\text{CDCl}_3$  (v/v) as the solvent (Figures 2-10, 2-11).

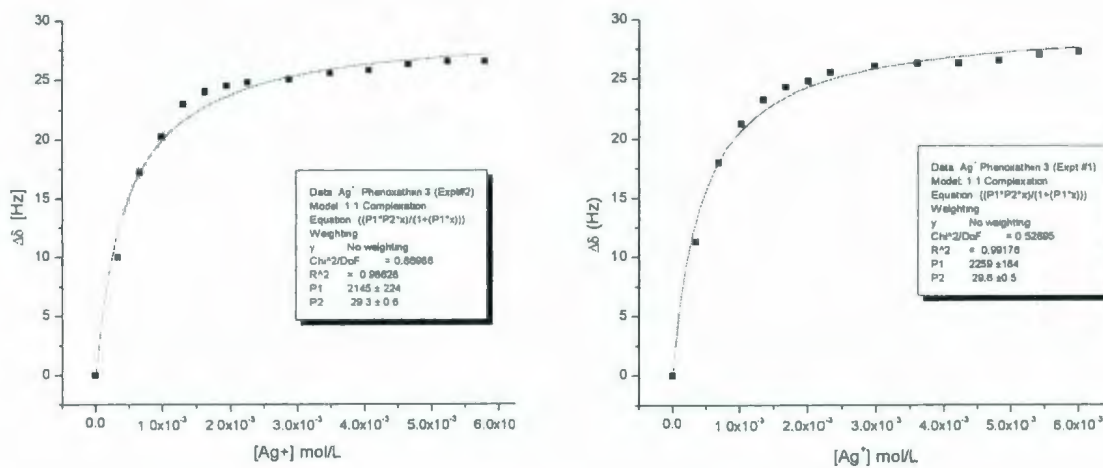


**Figure 2-10:**  $^1\text{H}$  NMR titration curve of  $\text{AgCO}_2\text{CF}_3$  with **30**.

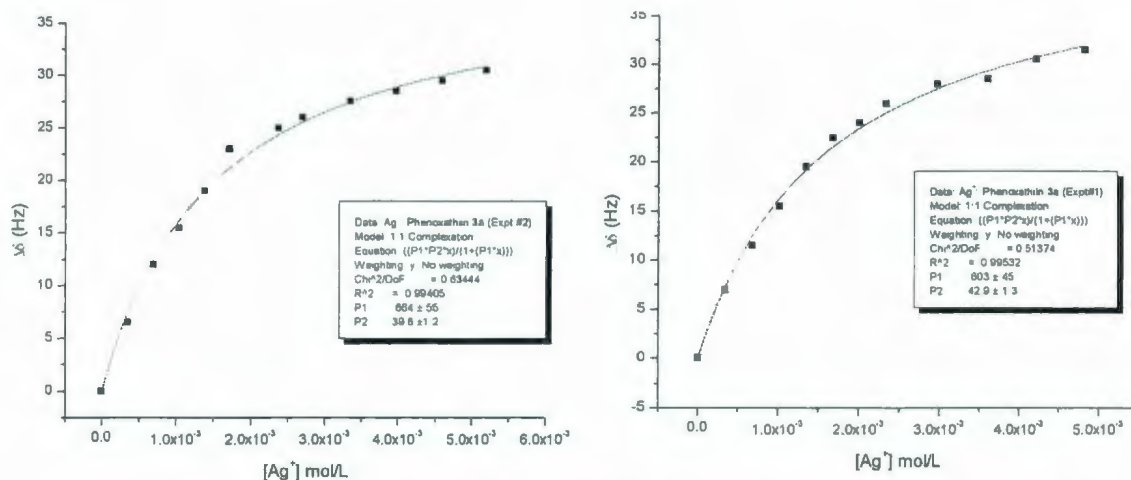


**Figure 2-11:**  $^1\text{H}$  NMR titration curves for  $\text{AgCO}_2\text{CF}_3$  complexation with **50**.

To avoid any solvent effect, all host and guest solutions were prepared using the same solvent mixture. Upon addition of aliquots of solutions of  $\text{Ag}^+$  ( $\sim 6 \times 10^{-2}$  M) to the host solutions of **30** or **50** ( $\sim 7 \times 10^{-4}$  M), the  $^1\text{H}$  NMR spectra showed clear induced changes in the chemical shifts of all of the host signals (Figures 2-10, 2-11). With  $[\text{Guest}]/[\text{Host}]$  ratios  $\geq 10:1$ , the observed chemical shifts leveled off very rapidly so the complexation studies were conducted at lower ratios, ranging from 0.5–9.0. In these ranges, addition of  $\text{Ag}^+$  solutions to the **30** (Figure 2-12) host solutions, resulted in shifts of the singlet and the doublets at  $\delta = 1.255$  ppm and 7.123 ppm to lower field at  $\delta = 1.266$  and 7.176 ppm, respectively. In contrast, the doublet at  $\delta = 7.594$  ppm was shifted to higher field ( $\delta = 7.598$  ppm). In the  $^1\text{H}$  NMR titration experiment of adding  $\text{Ag}^+$  to **50**, all the peaks were shifted downfield (Figure 2-13). The mole ratio plots, in both cases indicated the formation of 1:1 host-guest complexes with  $\text{Ag}^+$  in the concentration ranges

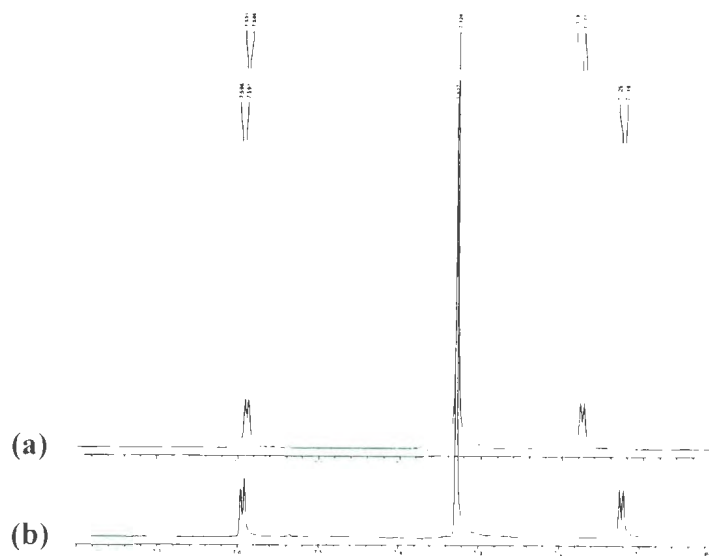


**Figure 2-12:** (a) The  $^1\text{H}$  NMR spectrum of a solution of  $\text{Ag}^+$  and **30** in 1:9  $\text{CD}_3\text{CN}:\text{CDCl}_3$ . (b) The  $^1\text{H}$  NMR spectrum of a solution of **30** in 1:9  $\text{CD}_3\text{CN}:\text{CDCl}_3$ .

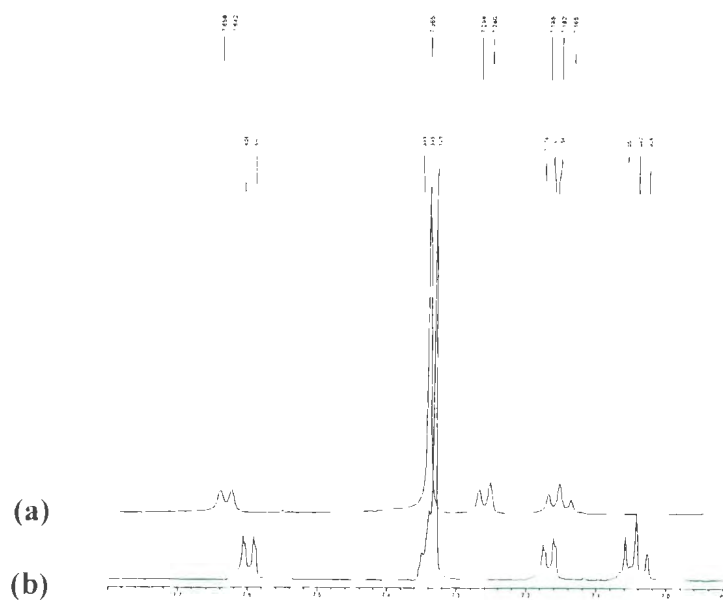


**Figure 2-13:** (a) The  $^1\text{H}$  NMR spectrum of a solution of  $\text{Ag}^+$  and **50** in 1:9  $\text{CD}_3\text{CN}:\text{CDCl}_3$ . (b) The  $^1\text{H}$  NMR spectrum of a solution of **50** in 1:9  $\text{CD}_3\text{CN}:\text{CDCl}_3$ .

which were studied. For the non-linear curve fitting plots, 1:1 binding isotherms as described by Connors<sup>50</sup> were employed.

The complexation of  $\text{Hg}^{2+}$  with **30** was investigated in the same solvent system using a number of  $\text{Hg}^{2+}$  salts ( $\text{HgCl}_2$ ,  $\text{Hg}(\text{OCOCF}_3)_2$  and  $\text{Hg}(\text{ClO}_4)_2$ ). The 500 MHz  $^1\text{H}$  NMR spectra of **30** did not reveal any complexation-induced chemical shifts even when the maximum possible concentration of added  $\text{HgCl}_2$  was used. In contrast, very small complexation-induced chemical shifts were observed when **30** was added to saturated solutions of either  $\text{Hg}(\text{OCOCF}_3)_2$  or  $\text{Hg}(\text{ClO}_4)_2$ . However, the relatively low solubilities of either  $\text{Hg}(\text{OCOCF}_3)_2$  or  $\text{Hg}(\text{ClO}_4)_2$  in 1:9  $\text{CD}_3\text{CN}:\text{CDCl}_3$  solvent limited the ability to accurately determine  $K_{\text{assoc}}$  values for either of these two salts with **30**. Therefore, a different solvent system (1.5:9  $\text{D}_3\text{COD}:\text{CDCl}_3$ ) in which the solubilities of these  $\text{Hg}^{2+}$  salts were higher, was used to measure  $K_{\text{assoc}}$  values for  $\text{Hg}(\text{ClO}_4)_2$  with **30** and **50**. The *tert*-butyl signals in **30** did not show any significant shifts in the titration experiments within the accessible concentration ranges (Figure 2-14). However, the aromatic doublet signal at  $\delta = 7.596$  ppm was shifted upfield by 49.5 Hz while the aromatic doublet signal at  $\delta = 7.122$  ppm was shifted downfield by 75.5 Hz.

In the case of **50** (Figure 2-15), all the peaks were shifted to lower field: the aromatic doublet signal at  $\delta = 7.595$  ppm showed the smallest shift (49.5 Hz), the triplet aromatic signal at  $\delta = 7.034$  ppm revealed the largest shift (72.0 Hz) and the doublet signal at  $\delta = 7.161$  ppm was shifted by 62.3 Hz.

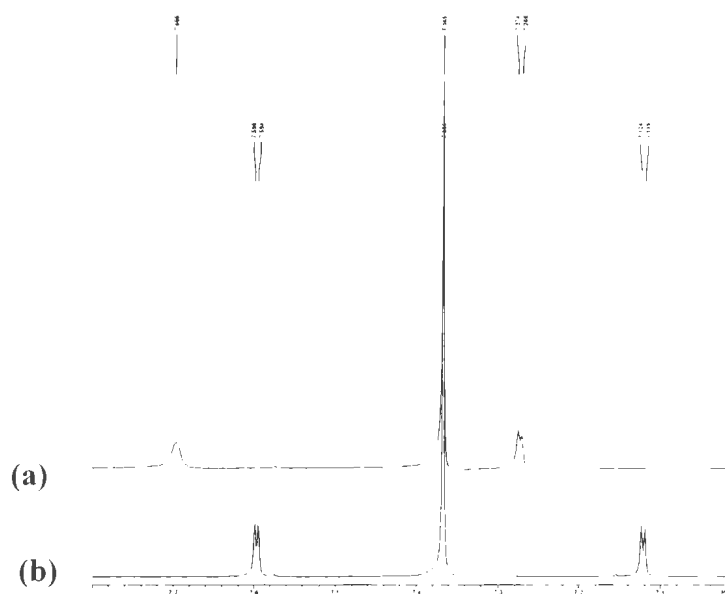


**Figure 2-14:** (a) The  $^1\text{H}$  NMR spectrum of a solution of  $\text{Hg}^{2+}$  and **30** in 1.5:9  $\text{D}_3\text{COD}:\text{CDCl}_3$ . (b) The  $^1\text{H}$  NMR spectrum of a solution of **30** in 1.5:9  $\text{D}_3\text{COD}:\text{CDCl}_3$ .

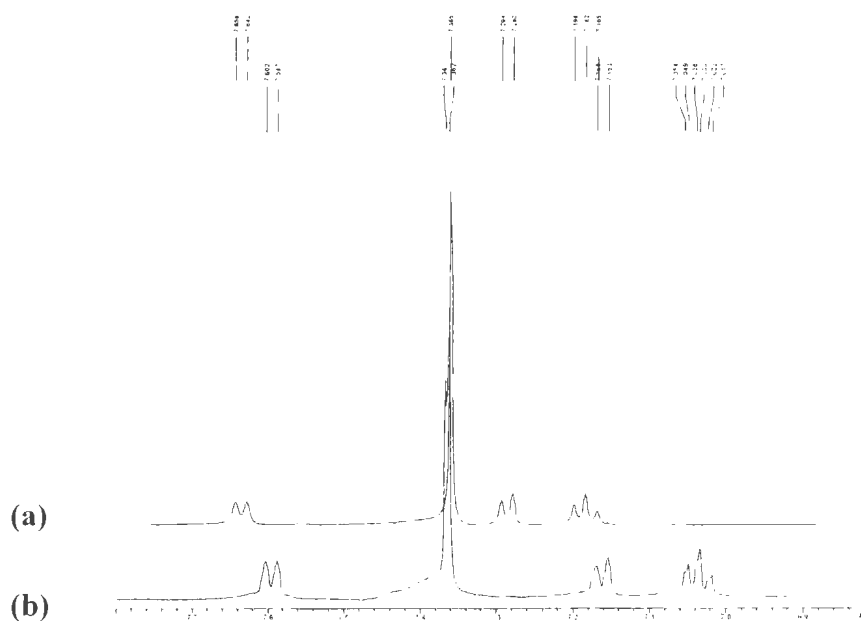


**Figure 2-15:** (a) The  $^1\text{H}$  NMR spectrum of the solution of  $\text{Hg}^{2+}$  and **50** in 1.5:9  $\text{D}_3\text{COD}:\text{CDCl}_3$ . (b) The  $^1\text{H}$  NMR spectrum of the solution of **50** in 1.5:9  $\text{D}_3\text{COD}:\text{CDCl}_3$ .

The same titration protocol used in the determination of  $K_{assoc}$  of  $Ag^+$  with **30** and **50** in 1:9  $CD_3CN:CDCl_3$  solvent was also employed to investigate  $K_{assoc}$  with  $Hg^{2+}$  in 1.5:9  $D_3COD:CDCl_3$  solvent. The isothermal non-linear curve fitting plots method showed that both macrocycles **30** and **50** revealed similar 1:1 binding with  $Hg^{2+}$  with  $K_{assoc}$  values of  $540 \pm 75$  for **30** and  $475 \pm 36$  for **50** (Figures 2-16, 2-17).

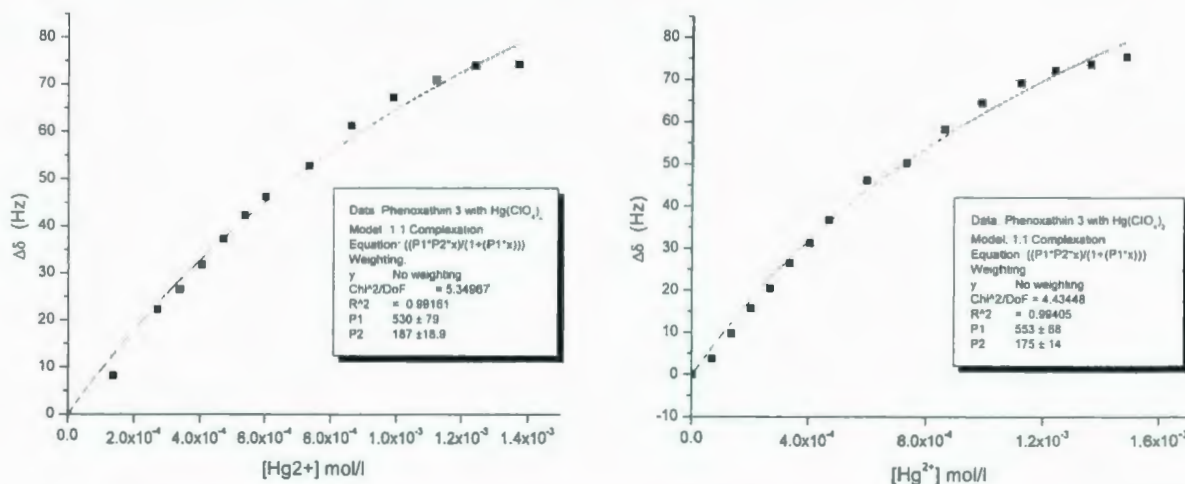


Figure 2-16: 500 MHz  $^1H$  NMR titration curve of  $Hg(ClO_4)_2$  with **30**.

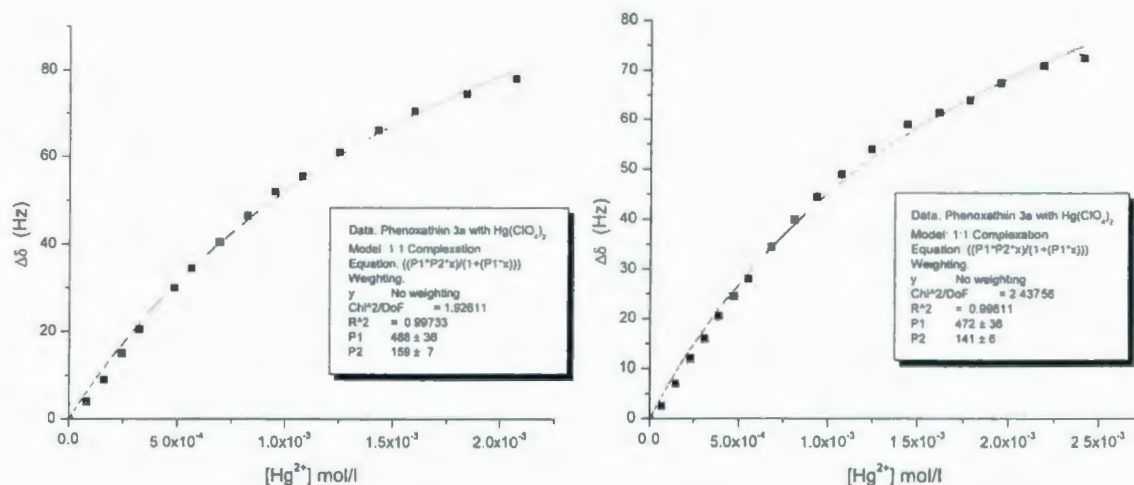


Figure 2-17: 500 MHz  $^1H$  NMR titration curve of  $Hg(ClO_4)_2$  with **50**.

It was rationalized that the abilities of **30** and **50** to bind with the  $\text{Ag}^+$  and  $\text{Hg}^{2+}$  ions studied are due to the  $\text{Ag}^+ - \pi$  and  $\text{Hg}^{2+} - \pi$ , and/or  $\text{Ag}^+ - \text{S}$  and  $\text{Hg}^{2+} - \text{S}$  interactions, and that these likely occur within the cavities of the host molecules. It is noteworthy that *tert*-butyl-substituted phenoxathiin **30** showed larger  $K_{\text{assoc}}$  values than **50** for both  $\text{Ag}^+$  and  $\text{Hg}^{2+}$ , and this enhancement is attributed to the larger cavity of **30**. The affinity of **30** for  $\text{Ag}^+$  was  $\sim 4 \times$  greater than that of **50**. In contrast, compounds **30** and **50** had almost the same affinity for  $\text{Hg}^{2+}$  which possibly could be ascribed to solvent effects. In the case of the  $\text{Ag}^+$ , the solvent system which was used is less polar than that used for the  $\text{Hg}^{2+}$  determinations. The more polar solvent, therefore, could possibly be more effectively dissociating any formed phenoxathiin- $\text{Hg}^{2+}$  complexes by favouring the solvation of the  $\text{Hg}^{2+}$  ions, instead.

#### 2.1.4 Summary

Replacement of the hydroxyl groups at the narrow rim of *p-tert*-butyl thiacalixarene could not be achieved *via* Sonogashira coupling reaction of 1,3-bistriflate **35**. This is likely as a result of the sensitivity of **35** to the basic conditions which are necessary, which results in rearrangement to form the more stable 1,2-bistriflate **37**. Cu(I)-catalyzed intramolecular rearrangements occurred to form phenoxathiin **30** in 70% yield in the presence of excess CuI (5 mol eq.). An unprecedented displacement of a hydroxyl group in *p-tert*-butyl thiacalixarene by a hydrogen atom to form **42**, using Pd(II) and DBU in toluene in the presence of CuI (1.0 mol eq.) was also observed.

The structure of the phenoxathiin **30** was successfully modified by removing the *tert*-butyl substituents to form the de-*tert*-butylated phenoxathiin **50**. This new compound could open the door for substitution of the wide rim by various functionalities which could improve potentially the host-guest capacity, or for studying other properties such as their NLO properties of these new products.

Complexation studies confirmed that phenoxathiins **30** and **50** are modest receptors for  $\text{Ag}^+$  in 1:9  $\text{CD}_3\text{CN}:\text{CDCl}_3$  solvent and for  $\text{Hg}^{2+}$  in 1.5:9  $\text{D}_3\text{COD}:\text{CDCl}_3$  solvent.  $^1\text{H}$  NMR titration experiments to determine the  $K_{\text{assoc}}$  values for **30** with  $\text{Ag}^+$  and  $\text{Hg}^{2+}$  solutions revealed that  $K_{\text{assoc}}$  values were  $2200 \pm 200$  for  $\text{Ag}^+$  and  $540 \pm 75$  for  $\text{Hg}^{2+}$ . On the other hand, the  $K_{\text{assoc}}$  values **50** with  $\text{Ag}^+$  and  $\text{Hg}^{2+}$  were  $630 \pm 50$  and  $475 \pm 36$ , respectively.

## 2.1.5 Experimental Section

### Materials

Chemical reagents and solvents were purchased from Aldrich or Fluka and used as received. THF was further purified by distillation over sodium. The  $\text{CH}_2\text{Cl}_2$  was dried over  $\text{P}_4\text{O}_{10}$  then distilled over  $\text{CaH}_2$ .

### General methods

All experiments with moisture- or air-sensitive compounds were carried out in anhydrous solvents under Ar or  $\text{N}_2$  atmosphere unless otherwise indicated. Organic solvents were evaporated under reduced pressure using a rotary evaporator. Flash chromatography was performed on SAI silica gel, particle size 32-63  $\mu\text{m}$ , pore size 60  $\text{\AA}$ , Batch number 02826-25. Preparative thin-layer chromatography plates (PLC) were made from SAI F-254 silica gel for TLC (particle size 5-15  $\mu\text{m}$ ), Batch number 04860-5. Thin-layer chromatography was performed using percolated SAI F-254 silica gel plates (Plastic Backed TLC, Hard layer, Batch number 79011) layer thickness 200  $\mu\text{m}$ .

### Instrumentation

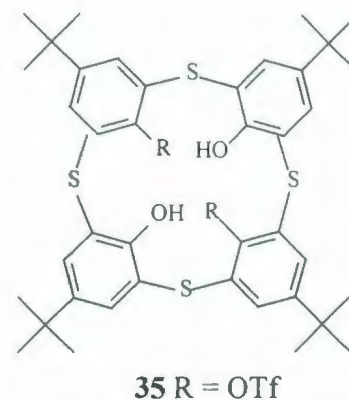
Melting points (mp) were determined on a MEL-TEMP II apparatus and are uncorrected. Mass spectra of compounds were obtained using LCMS (HP series 1100). Analytical thin layer chromatography was performed with fluorescent indicator  $\text{UV}_{254}$  (Macherey-Nagel GmbH & Co. KG, Germany). Unless otherwise specified, all  $^1\text{H}$ - and  $^{13}\text{C}$  NMR were recorded on a GE-300 MHz spectrometer or on a Bruker AM-500 Fourier Transform spectrometer using  $\text{CDCl}_3$  containing  $\text{Me}_4\text{Si}$  as an internal standard and

chemical shifts for the  $^1\text{H}$  NMR spectra are relative to the internal standard at 0.00 ppm. Data were reported as follows: chemical shift, multiplicity (s = singlet, d = doublet, dd = doublet of doublets, t = triplet, b = broad, h = heptet, m = multiplet), coupling constant ( $J$ , Hz), integration and assignment ( $m\text{H}-x$ , where  $m$  denotes the number of protons at position  $x$  in the molecule).  $^1\text{H}$ - and  $^{13}\text{C}$  NMR spectra were processed using "Nuts" software. Chemical shifts for  $^{13}\text{C}$  NMR spectra are relative to the solvent 77.23 ppm for  $\text{CDCl}_3$ .

## Synthesis

### 1,3-Bistriflate 35

Triflic anhydride (1.6 g, 5.8 mmol) was added dropwise with stirring over 10 min at 0 °C to a solution of thiacalix[4]arene **6** (2.0 g, 2.8 mmol) in 10 mL dry pyridine. The reaction mixture was stirred overnight at room temperature under argon and then poured over 200 mL of ice-water mixture. The resulting precipitate was



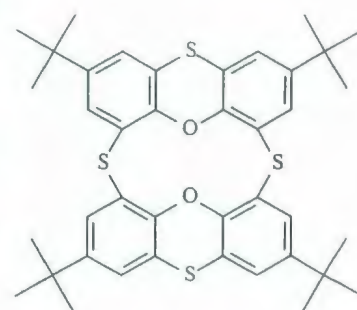
filtered, washed with cooled water (2 x 30 mL) and crystallized from hexane to give **35** (1.6 g, 60%). The supernatant hexane solution was evaporated and chromatographed on silica gel with (1:7)  $\text{CH}_2\text{Cl}_2$ :hexane as an eluent to give an additional (0.74 g, 27%) of product: mp 319-321 °C;  $^1\text{H}$  NMR ( $\text{CDCl}_3$ , 500 MHz)  $\delta$  7.75 (s, 4H), 7.17 (s, 4H), 6.13 (s, 4H, OH), 1.35 (s, 18H), 0.93 (s, 18H);  $^{13}\text{C}$  NMR ( $\text{CDCl}_3$ , 500 MHz)  $\delta$  155.64, 151.72, 147.91, 144.04, 135.07, 133.59, 129.05, 121.23, 120.23, 122.78, 34.67, 34.51, 31.59, 30.87; MS (APCI-)  $m/z$  983.1 (M-H), calcd. for  $\text{C}_{42}\text{H}_{46}\text{F}_6\text{O}_8\text{S}_6$  984.1.

**Reaction of 1,3-bistriflate **35** with DBU in the presence of PdCl<sub>2</sub>(PPh<sub>3</sub>)<sub>2</sub> and 5.0 mole eq. CuI**

DBU (70 mg, 0.46 mmol) was added to a stirred mixture of PdCl<sub>2</sub>(PPh<sub>3</sub>)<sub>2</sub> (8.0 mg, 0.011 mmol), CuI (100 mg, 0.530 mmol), and **35** (110 mg, 0.11 mmol) in refluxing dry-degassed toluene (30 mL). The reaction mixture was stirred for a further 24 h under argon at reflux. Removal of volatiles on a rotary evaporator gave the crude product which was dissolved in CH<sub>2</sub>Cl<sub>2</sub> (40 mL) and washed with aqueous saturated NH<sub>4</sub>Cl (15 mL) and with H<sub>2</sub>O (20 mL). The CH<sub>2</sub>Cl<sub>2</sub> extract was dried (MgSO<sub>4</sub>) and the solvent was removed under vacuum to give the crude product, which was purified by PLC (3:7) CH<sub>2</sub>Cl<sub>2</sub>:hexane to give the following compounds:

**Tetra-tert-butyl-thiacalix[2]phenoxathiin (**30**)**

(45.0 mg, 59%): mp 376-378 °C; <sup>1</sup>H NMR (CDCl<sub>3</sub>, 500 MHz) δ 7.60 (d, *J* = 1.5 Hz, 4H), 7.12 (d, *J* = 2.0 Hz, 4H), 1.262 (s, 36H); <sup>13</sup>C NMR (CDCl<sub>3</sub>, 500 MHz) 151.95, 148.20, 133.14, 125.11, 122.41, 34.67, 31.40; MS (APCI+) *m/z* 685.3 (M+H), calcd for C<sub>40</sub>H<sub>44</sub>O<sub>2</sub>S<sub>4</sub> 684.2.



**30**

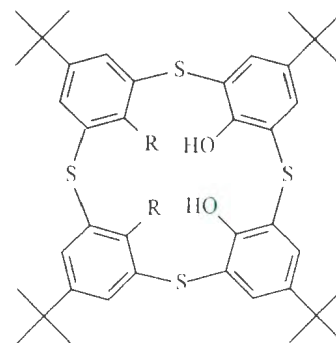
Crystallographic data for **30**: C<sub>46</sub>H<sub>50</sub>O<sub>2</sub>S<sub>4</sub>, fw = 763.14,

*P*2<sub>1</sub>(#4), *a* = 13.5552(9) Å; *b* = 10.8734(6) Å; β = 111.6526(14)°; *c* = 14.9307(10) Å; *V* = 2045.4(2) Å<sup>3</sup>, *Z* = 2, *D*<sub>calc</sub> = 1.239 g/cm<sup>3</sup>. Data was collected at a temperature of -160 ± 1° C to a maximum 2θ value of 61.5°. A total of 19278 reflections were collected, 9291 were unique (*R*<sub>int</sub> = 0.017). The data was processed using CrystalClear (Rigaku). No. of

variables = 470; reflection/ parameter ratio = 19.77;  $R_1$  ( $I > 2.00\sigma(I)$ ) = 0.0388;  $R$  (all reflections) = 0.0391;  $wR_2$  (all reflections) = 0.1034. GoF = 1.038.

### 1,2-Bistriflate **37**

(7.0 mg, 7%): mp 234-236 °C:  $^1\text{H}$  NMR ( $\text{CDCl}_3$ , 500 MHz)  $\delta$  7.72 (br, s, 3H),  $\delta$  7.56 (d,  $J = 2.5$ , 2H), 7.54 (d,  $J = 2.0$  Hz, 2H), 7.38 (d,  $J = 2.0$  Hz, 2H), 7.25 (d,  $J = 2.5$  Hz, 2H), 1.23 (s, 18H), 0.99 (s, 18H);  $^{13}\text{C}$  NMR ( $\text{CDCl}_3$ , 500 MHz)  $\delta$  155.19, 151.67, 147.33, 144.10, 135.67, 135.29, 134.45, 134.39, 132.65, 129.50, 120.59, 120.42, 119.13, 34.74, 34.40, 31.44, 31.05. MS (APCI-)  $m/z$



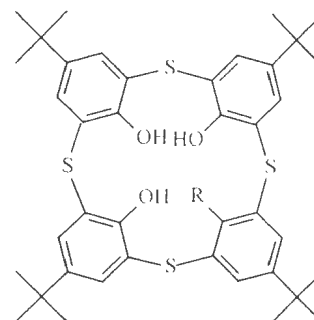
**37** R = OTf

983.1(M-H), calcd. for  $\text{C}_{42}\text{H}_{46}\text{F}_6\text{O}_8\text{S}_6$  984.1.

Crystallographic data for **37**:  $\text{C}_{42.35}\text{H}_{46.35}\text{F}_6\text{O}_8 \text{S}_6\text{Cl}_{1.05}$ , fw = 1026.95, primitive triclinic cell, P-1 (#2)  $a = 13.1289(15)$  Å,  $\alpha = 110.835(2)^\circ$ ,  $b = 19.649(3)$  Å,  $\beta = 98.5680(18)^\circ$ ,  $c = 22.054(3)$  Å,  $\gamma = 104.8480(17)^\circ$ ,  $V = 4954.7(11)$  Å<sup>3</sup>,  $Z = 4$ ,  $D_{\text{calc}} = 1.377$  g/cm<sup>3</sup>. The data was collected at a temperature of  $-160 \pm 1$  °C to a maximum  $2\theta$  value of  $61.5^\circ$ . 42658 reflections were collected, 20234 were unique ( $R_{\text{int}} = 0.032$ ). The data was collected and processed using CrystalClear (Rigaku). No. of variables = 1117; reflection/parameter ratio = 18.20;  $R_1$  ( $I > 2.00\sigma(I)$ ) = 0.0862;  $R$  (all reflections) = 0.0944;  $wR_2$  (all reflections) = 0.2550. GoF = 1.065.

### Monotriflate **36**

(10.5 mg, 11%): mp 270-273 °C:  $^1\text{H}$  NMR ( $\text{CDCl}_3$ , 500 MHz)  $\delta$  7.71 (d,  $J = 3.0$ , 2H), 7.69 (d,  $J = 2.5$ , 2H), 7.50 (s, 2H), 7.08 (s, 2H), 1.31 (s, 18H), 1.16 (s, 9H), 0.80 (s, 9H);  $^{13}\text{C}$  NMR ( $\text{CDCl}_3$ , 500 MHz)  $\delta$  155.77, 155.66, 151.74, 147.48, 144.50, 144.07, 136.30, 135.64, 135.37, 133.19, 129.99, 121.31, 121.19, 120.19, 34.53, 34.46, 34.36, 31.61,



**36** R = OTf

31.38, 30.67; MS (APCI-)  $m/z$  851.1 (M-H), calcd. for  $\text{C}_{41}\text{H}_{47}\text{F}_3\text{O}_6\text{S}_5$  852.2.

Crystallographic data for **36**:  $\text{C}_{41}\text{H}_{47}\text{F}_3\text{O}_6\text{S}_5$ , fw = 853.11,  $P2_1/c$  (#14),  $a = 12.490(3)$  Å;  $b = 16.513(2)$  Å;  $\beta = 104.682(5)^\circ$ ;  $c = 21.792(4)$  Å;  $V = 4347.6(14)$  Å<sup>3</sup>,  $Z = 4$ ,  $D_{\text{calc}} = 1.303$  g/cm<sup>3</sup>. The data was collected at a temperature of  $-160 \pm 1$  °C to a maximum  $2\theta$  value of  $61.5^\circ$ . 46060 reflections were collected, 8526 were unique ( $R_{\text{int}} = 0.069$ ). The data was collected and processed using CrystalClear (Rigaku). No. of variables = 497; reflection/parameter ratio = 17.15;  $R_1$  ( $I > 2.00\sigma(I)$ ) = 0.0695;  $R$  (all reflections) = 0.0760;  $wR_2$  (all reflections) = 0.1976. GoF = 1.079.

### Reaction of 1,3-bistriflate with DBU

A solution of DBU (35 mg, 0.46 mmol) and **35** (55 mg, 0.056 mmol) in toluene (15 mL) was stirred at reflux temperature for 15 h under argon. The solvent was evaporated on a rotary evaporator and the resulting crude product was dissolved in  $\text{CH}_2\text{Cl}_2$  (25 mL) and washed with aqueous 10% HCl (15 mL). The  $\text{CH}_2\text{Cl}_2$  extract was dried ( $\text{MgSO}_4$ ) and the solvent removed under vacuum to give the crude product which was purified by PLC (3:7)  $\text{CH}_2\text{Cl}_2$ :hexane to give the following compounds: 1,2-

bistriflate **37** (49 mg, 89%) and tetra-*tert*-butyl-thiacalix[2]phenoxathiin (**30**) (3.0 mg, 8%).

#### **Reaction of 1,3-bistriflate with DBU in the presence of PdCl<sub>2</sub>(PPh<sub>3</sub>)<sub>2</sub>**

To a stirred mixture of PdCl<sub>2</sub>(PPh<sub>3</sub>)<sub>2</sub> (4.0 mg, 0.0055 mmol) and 1,3-bistriflate **35** (55 mg, 0.055 mmol) in dry degassed toluene (30 mL), DBU (35 mg, 0.23 mmol) was added at reflux temperature. The reaction mixture was stirred for a further 15 h at the reflux temperature under argon. The solvent was evaporated on a rotary evaporator and the resulting crude product was dissolved in CH<sub>2</sub>Cl<sub>2</sub> (20 mL) and washed with aqueous 10% HCl (15 mL) and with H<sub>2</sub>O (20 mL). The CH<sub>2</sub>Cl<sub>2</sub> extract was dried (MgSO<sub>4</sub>) and the solvent was removed under vacuum to give the crude product which was purified by PLC (3:7) CH<sub>2</sub>Cl<sub>2</sub>:hexane to give the following compounds: 1,2-bistriflate **37** (45 mg, 81%) and tetra-*tert*-butyl-thiacalix[2]phenoxathiin **30** (5.0 mg, 13%).

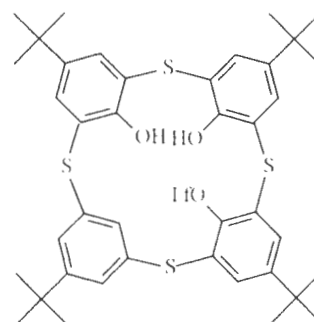
#### **Reaction of 1,3-bistriflate with DBU in the presence of CuI.**

To a stirred mixture of CuI (50 mg, 0.27 mmol), and 1,3-bistriflate **35** (55 mg, 0.055 mmol) in dry-degassed toluene (20 mL), DBU (35 mg, 0.23 mmol) was added at reflux temperature. The reaction mixture was stirred for a further 15 h at the reflux temperature under argon. The solvent was evaporated on a rotary evaporator and the resulting crude product was dissolved in CH<sub>2</sub>Cl<sub>2</sub> (40 mL) and washed with aqueous saturated NH<sub>4</sub>Cl (15 mL) and with H<sub>2</sub>O (20 mL). The CH<sub>2</sub>Cl<sub>2</sub> extracts was dried (MgSO<sub>4</sub>) and the solvent was removed under vacuum to give the crude product which was purified

by PLC (3:7) CH<sub>2</sub>Cl<sub>2</sub>:hexane to give the following compounds: tetra-*tert*-butyl-thiacalix[2]phenoxathiin **30** (26.8 mg, 77%) and 1,2-bistriflate **37** (6.0 mg, 12%).

**Reaction of 1,3-bistriflate with DBU in the presence of PdCl<sub>2</sub>(PPh<sub>3</sub>)<sub>2</sub> and 1.0 mole eq. CuI**

DBU (70 mg, 0.46 mmol) was added to a stirred mixture of PdCl<sub>2</sub>(PPh<sub>3</sub>)<sub>2</sub> (8.0 mg, 0.011 mmol), CuI (20 mg, 0.11 mmol), and **35** (110 mg, 0.11 mmol) in refluxing dry-degassed toluene (30 mL). The reaction mixture was stirred for a further 24 h under argon at reflux. Removal of



**42**

volatiles on a rotary evaporator gave the crude product which was dissolved in CH<sub>2</sub>Cl<sub>2</sub> (40 mL) and washed with aqueous saturated NH<sub>4</sub>Cl (15 mL) and with H<sub>2</sub>O (20 mL). The CH<sub>2</sub>Cl<sub>2</sub> extract was dried (MgSO<sub>4</sub>) and the solvent was removed under vacuum to give the crude product which was purified by PLC (5:5) CH<sub>2</sub>Cl<sub>2</sub>:hexane to give the following compounds:

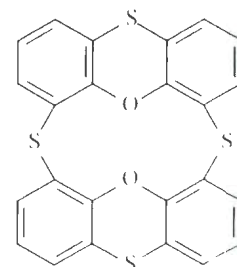
Tetra-*tert*-butyl-thiacalix[2]phenoxathiin **30** (21.5 mg, 28% yield), monotriflate **36** (37.5 mg, 40% yield), 1,2-bistriflate **37** (8.00 mg, 7.0% yield) and monotriflate **42** (8.5 mg, 9%): 218-220 mp; <sup>1</sup>H NMR (CDCl<sub>3</sub>, 500 MHz) δ 7.67 (s, 1H), 7.64 (s, 1H), 7.63 (s, 1H), 7.61 (s, 1H), 7.41 (s, 1H), 7.39 (s, 1H), 7.31 (s, 1H), 7.24 (s, 1H), 6.92 (s, 1H), 6.14 (s, 2H), 1.32 (s, 4H), 1.31 (s, 4H), 1.21 (s, 4H), 1.18 (s, 4H); <sup>13</sup>C NMR (CDCl<sub>3</sub>, 500 MHz) 155.25, 155.16, 153.15, 151.40, 147.83, 145.16, 143.70, 138.14, 137.31, 37.09, 135.60, 135.45, 134.15, 134.01, 133.98, 130.01, 128.85, 126.90, 126.20, 125.03, 121.11, 120.03,

117.51, 116.98, 35.14, 34.87, 34.43, 34.33, 31.79, 31.51, 31.39, 31.31; MS (APCI-)  $m/z$  834.2 (M-H),, calcd. for  $C_{41}H_{47}F_3O_5S_5$  835.2.

Crystallographic data for **42**:  $C_{41}H_{47}F_3O_5S_5$ , fw = 837.11, P-1 (#2), Lattice Parameters  $a = 10.9907(13)$  Å,  $b = 14.3416(11)$  Å,  $c = 15.5658(8)$  Å,  $\alpha = 61.816(9)^\circ$ ,  $\beta = 75.573(13)^\circ$ ,  $\gamma = 81.851(13)^\circ$ ,  $V = 2093.6(3)$  Å<sup>3</sup>,  $Z = 2$ ,  $D_{\text{calc}} = 1.338$  g/cm<sup>3</sup>. The data was collected at a temperature of  $-135 \pm 1$  °C to a maximum  $2\theta$  value of  $61.7^\circ$ . 20163 reflections were collected, 8573 were unique ( $R_{\text{int}} = 0.064$ ). The data was collected and processed using CrystalClear (Rigaku). No. of variables = 488; reflection/parameter ratio = 17.57;  $R_1$  ( $I > 2.00\sigma(I)$ ) = 0.0865;  $R$  (all reflections) = 0.0973;  $wR_2$  (all reflections) = 0.2403 GoF = 1.106.

### Thiacalix[2]phenoxathiin (**50**)

A mixture of phenol (267 mg, 2.8 mmol) and  $AlCl_3$  (1.5 mg, 11.2 mmol) was added to a solution of **30** (194 mg, 0.280 mmol) in dry toluene (5 mL). After heating for the reaction mixture on reflux for 8 days, it was allowed to cool to room temperature and the resulting dark solution was poured onto aqueous solution of 10% HCl (10 mL). The organic layer was separated and the aqueous phase was further extracted with  $CH_2Cl_2$  (2 x 50 mL). The combined organic layers were dried ( $MgSO_4$ ) and evaporated to dryness leaving black oil which was triturated with hexane to give a precipitate. Further purification by column chromatography on silica gel and (1:9)  $CH_2Cl_2$ :hexane gave a product which was crystallized from a  $CHCl_3$ :hexane to



**50**

give *de-tert*-butylated-phenoxathiin **50** (39 mg, 26% yield) mp °C;  $^1\text{H}$  NMR ( $\text{CDCl}_3$ , 500 MHz)  $\delta$  7.59 (d,  $J = 7.0$  Hz, 4H), 7.14 (d,  $J = 6.5$  Hz, 4H), 7.02 (t,  $J = 7.0$  Hz, 4H);  $^{13}\text{C}$  NMR ( $\text{CDCl}_3$ , 500 MHz)  $\delta$  154.42, 136.13, 128.29, 125.84, 125.27, 123.51; MS (APCI-)  $m/z$  461.0, calcd for  $\text{C}_{24}\text{H}_{12}\text{O}_2\text{S}_4$  460.0. Crystallographic data for **50**:  $\text{C}_{24}\text{H}_{12}\text{O}_2\text{S}_4$ , fw = 460.60, monoclinic,  $P 2_1/c$  (#14),  $a = 17.027(4)$  Å,  $b = 10.3137(18)$  Å,  $c = 24.212(5)$  Å,  $\beta = 117.240(6)$  °,  $V = 3780.3(13)$  Å<sup>3</sup>,  $Z = 8$ ,  $D_{\text{calc}} = 1.618$  g/cm<sup>3</sup>. The data were collected at a temperature of  $-160 \pm 1^\circ$  C to a maximum  $2\theta$  value of  $61.5^\circ$ . 42852 reflections were collected, 7814 ( $R_{\text{int}} = 0.049$ ), equivalent reflections were merged. Data were collected and processed using CrystalClear (Rigaku). No. Variables = 542, Reflection/Parameter Ratio = 14.42,  $R_1$  ( $I > 2.00\sigma(I)$ ) = 0.0519,  $R$  (All reflections) = 0.0544,  $wR_2$  (All reflections) = 0.1251. GoF = 1.176.

#### Association constant determinations

Association constant ( $K_{\text{assoc}}$ ) silver-binding studies in 1:9  $\text{CD}_3\text{CCN}:\text{CDCl}_3$  solutions between bisphenoxathiin with  $\text{AgO}_2\text{CCF}_3$  were determined by  $^1\text{H}$  NMR spectroscopy from the changes in the chemical shift of the respective aromatic hydrogen signals. In determination of  $K_{\text{assoc}}$ , the non-linear curve fitting plots a 1:1 binding isotherm as described by Connors<sup>51</sup> was employed.

In a typical experiment, aliquots of the guest solutions, *e.g.*  $\text{AgO}_2\text{CCF}_3$  ( $6.90 \times 10^{-2}$  M ranging from 30–885  $\mu\text{L}$ ) in (1:9)  $\text{CD}_3\text{CN}:\text{CDCl}_3$  (v/v) were added to individual NMR tubes which contained 1  $\mu\text{L}$  of either **30** ( $7.3 \times 10^{-7}$  M), or **50** ( $7.3 \times 10^{-7}$  M). The resulting solutions were sonicated for approx. 5 min before NMR measurements were

recorded at 298 K at 500 MHz. A similar methodology was employed with  $\text{Hg}(\text{ClO}_4)_2$  in 1.5:9  $\text{D}_3\text{COD}:\text{CDCl}_3$  solutions ( $2.74 \times 10^{-2}$  M).

## 2.1.6 References

1. Pedersen, C. J. *Angew. Chem.* **1988**, *100*, 1053.
2. Cram, D. J. *Angew. Chem.* **1988**, *100*, 1041.
3. Lehn, J.-M. *Angew. Chem.* **1988**, *100*, 91.
4. Izatt, R. M.; Pawlak, K.; Bradshaw, J. S. *Chem. Rev.* **1991**, *91*, 1721. (b) Cooper, S. R., Ed. *Crown Compounds Toward Future Applications*; VCH Publishers, Inc.: New York, **1992**. (c) Hiraoka, M., Ed. *Crown Ethers and Analogous Compounds*, Studies in Organic Chemistry 45; Elsevier: Amsterdam, **1992**.
5. Pearson, R. G. *Hard and Soft Acids and Bases*; Dowden, Hutchinson, Ross: Stroudsburg, PA, **1973**.
6. (a) Kimura, K.; Shono, T. *Applications of Crown Compounds to Analytical and Separation Chemistry: Ion Sensor and Liquid Chromatography*; Chapter 4 in ref 4 (b) Cobben, P. L. H. M.; Egberink, R. J. M.; Bomer, J. G.; Bergveld, P.; Verboom, W.; Reinhoudt, D. N. *J. Am. Chem. Soc.* **1992**, *114*, 10573.
7. Dozol, J. F. *Future Industrial Prospects of Membrane Processes*; Cecille, L., Toussaint, J.-C., Eds.; Elsevier: London, **1989**.
8. Van Straaten-Nijenhuis, W. F.; De Jong, F.; Reinhoudt, D. N. *Recl. Trav. Chim. Pays-Bas* **1993**, *112*, 317.
9. Parker, D. *Chem. Soc. Rev.* **1990**, *19*, 271.
10. Patai, S.; Rappoport, Z. *Crown Ethers and Analogs*; John Wiley & Sons: Chichester, **1989**; Chapter 2.

11. Lehn, J. M. *Supramolecular Chemistry: Concepts and Perspectives*; Wiley-VCH: New York, 1995. (b) Lehn, J.-M. *Science* **2002**, *295*, 2400
12. Hennrich, G.; Murillo, M. T.; Prados, P.; Al-Saraiher, H.; El-Dali, A.; Thompson, D. W.; Collins, J.; Georghiou, P. E.; Teshome, A.; Asselberghs, I.; Clays, K. *Chem. Eur. J.* **2007**, *13*, 7753.
13. (a) Gutsche, C. D. *Calixarenes*; Stoddart, J. F., Ed.; Monographs in Supra-molecular Chemistry; The Royal Society of Chemistry: Cambridge, **1989**. (b) Ikeda, A.; Shinkai, S. *Chem. Rev.* **1997**, *97*, 1713. (c) Gutsche, C. D. In *Calixarenes Revisited*; Stoddart, J. F., Ed.; Monographs in Supramolecular Chemistry; The Royal Society of Chemistry: Cambridge, **1998**. (d) *Calixarenes in Action*; Mandolini, L.; Ungaro, R., Eds.; Imperial College Press: London, **2000**. (e) *Calixarenes 2001*; Asfari, Z.; Bohmer, V.; Harrowfield, J. M.; Vicens, J.; Eds.; Kluwer Academic Publishers: Dordrecht, **2001**.
14. (a) Gutsche, C. D.; Iqbal, M. *Org. Synth.* **1990**, *68*, 234. (b) Gutsche, C. D.; Dhawan, B.; Leonis, M.; Stewart, D. R. *Org. Synth.* **1990**, *68*, 238. (c) Munch, J. H.; Gutsche, C. D. *Org. Synth.* **1990**, *68*, 243.
15. (a) Sone, T.; Ohba, Y.; Moriya, K.; Kumada, H. Abstract Book of Workshop on Calixarenes and Related Compounds, Fukuoka, Japan, 1993, PS/B-36. (b) Sone, T.; Ohba, Y.; Moriya, K.; Kumada, H.; Ito, K. *Tetrahedron* **1997**, *53*, 10689. (c) Ito, K.; Ohba, Y.; Sone, T. *Nippon Kagaku Kaishi* **1999**, 217.
16. Kumagai, H.; Hasegawa, M.; Miyanari, S.; Sagawa, Y.; Sato, Y.; Hori, T.; Ueda, S.; Kamiyama, H.; Miyano, S. *Tetrahedron Lett.* **1997**, *38*, 3971.

17. Kon, N.; Iki, N.; Miyano, S. *Tetrahedron Lett.* **2002**, *43*, 2231.
18. Akdas, H.; Bringel, L.; Graf, E.; Hosseini, M. W.; Mislin, G.; Pansanel, J.; Cian, A. D.; Fischer, J. *Tetrahedron Lett.* **1998**, *39*, 2311.
19. Ungaro, R.; Pochini, A.; Andreetti, G. D.; Sangermano, V. *J. Chem. Soc., Perkin Trans. 2* **1984**, 1979.
20. Bernardino, R. J.; Costa Cabral, B. J. C. *J. Mol. Struct. (THEOCHEM)* **2001**, *549*, 253.
21. Bernardino, R. J.; Costa Cabral, B. J. *J. Phys. Chem. A* **1999**, *103*, 9080.
22. (a) Iki, N.; Morohashi, N.; Suzuki, T.; Ogawa, S.; Aono, M.; Kabuto, C.; Kumagai, H.; Takeya, H.; Miyanari, S.; Miyano, S. *Tetrahedron Lett.* **2000**, *41*, 2587. (b) Iki, N.; Miyano, S. *J. Inclusion Phenom. Macrocyclic Chem.* **2001**, *41*, 99. (c) Iki, N.; Morohashi, N.; Narumi, F.; Miyano, S. *Bull. Chem. Soc. Jpn.* **1998**, *71*, 1597.
23. Kajiwara, T.; Yokozawa, S.; Ito, K.; Iki, N.; Morohashi, N.; Miyano, S. *Chem. Lett.* **2001**, 6.
24. Bilyk, A.; Hall, A. K.; Harrowfield, J. M.; Hosseini, M. W.; Mislin, G.; Skelton, B. W.; Taylor, C.; White, A. H. *Eur. J. Inorg. Chem.* **2000**, 823.
25. Mislin, G.; Graf, E.; Hosseini, M. W.; Bilyk, A.; Hall, A. K.; Harrowfield, J. M.; Skelton, B. W.; White, A. H. *Chem. Commun.* **1999**, 373.
26. Kajiwara, T.; Yokozawa, S.; Ito, K.; Iki, N.; Morohashi, N.; Miyano, S. *Angew. Chem. Int. Ed.* **2002**, *41*, 2076.
27. Asfari, Z.; Bilyk, A.; Dunlop, J. W. C.; Hall, A. K.; Harrowfield, J. M.; Hosseini, M. W.; Skelton, B. W.; White, A. H. *Angew. Chem. Int. Ed.* **2001**, *40*, 721.

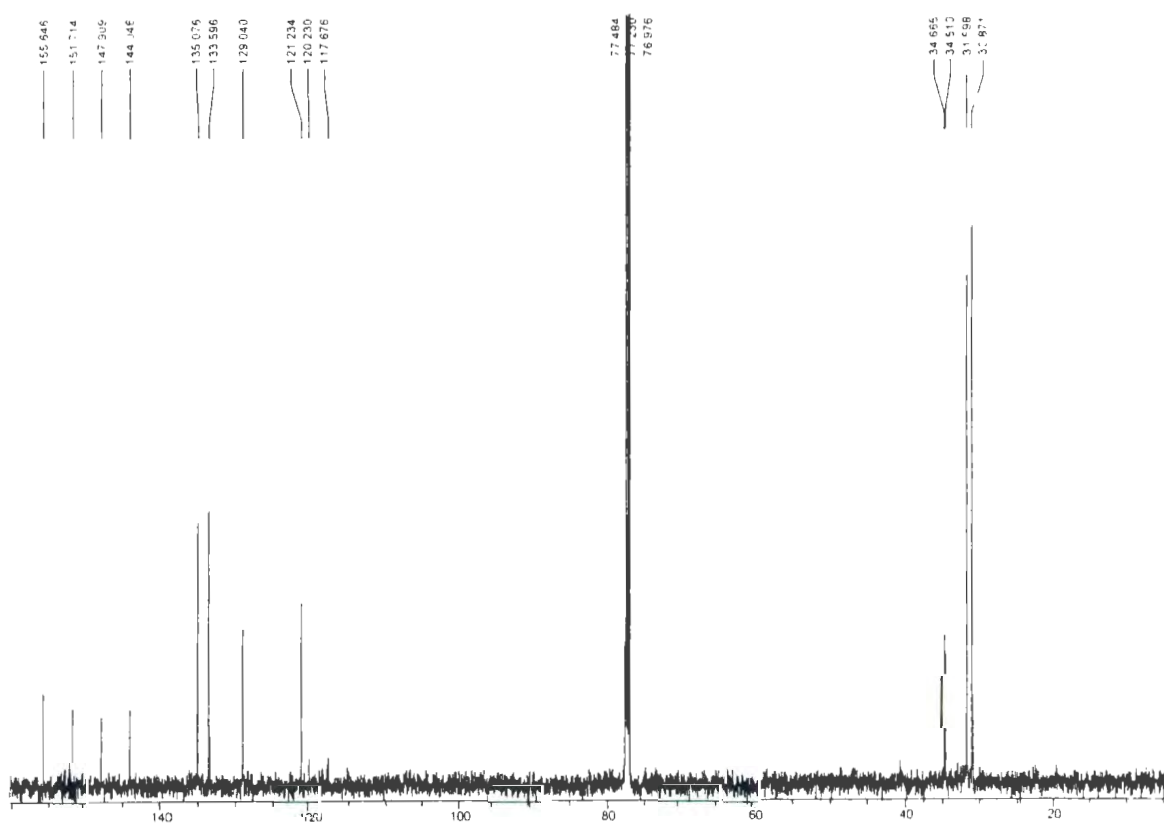
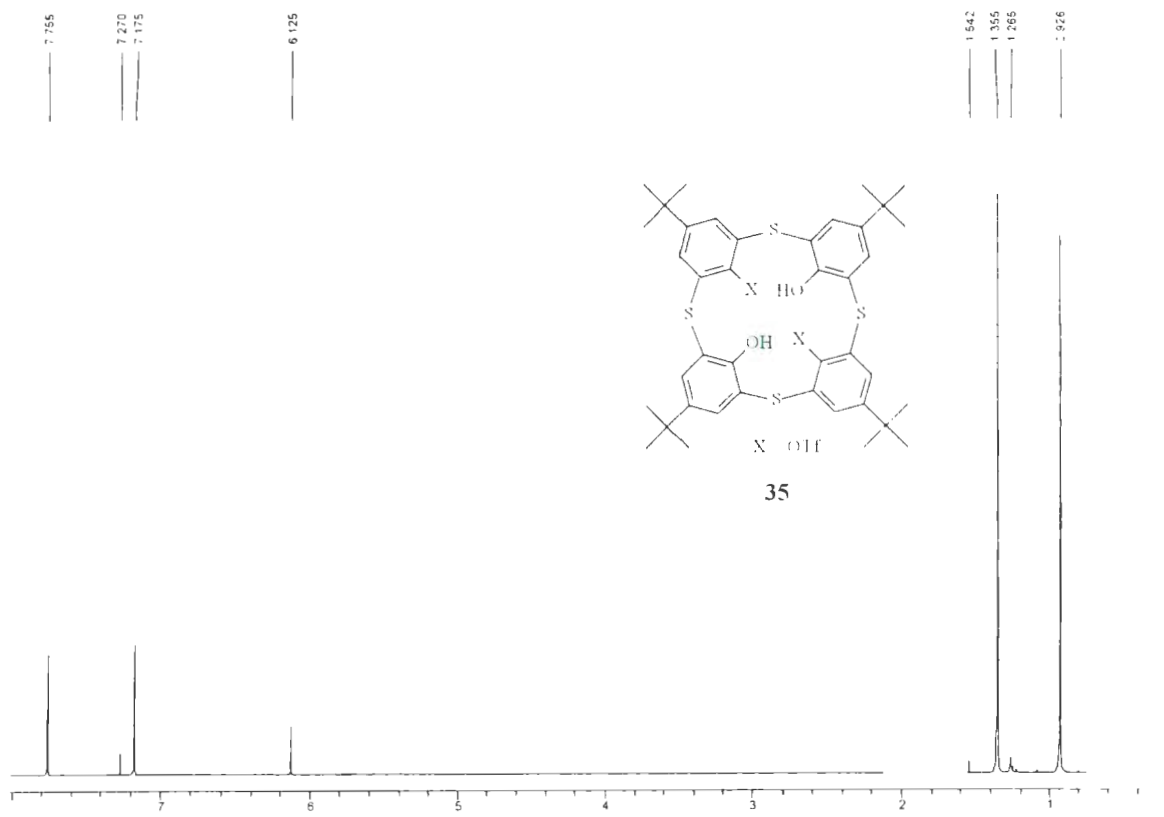
28. Bilyk, A.; K. Hall, A.; Harrowfield, J. M.; Hosseini, M. W.; Skelton, B. W.; White, A. H. *Aust. J. Chem.* **2000**, *53*, 895.
29. Bilyk, A.; Hall, A. K.; Harrowfield, J. M.; Hosseini, M. W.; Skelton, B. W.; White, A. H. *Inorg. Chem.* **2001**, *40*, 672.
30. (a) Iki, H.; Kumagai, H.; Morohashi, N.; Ejima, K.; Hasegawa, M.; Miyanari, S.; Miyano, S. *Tetrahedron Lett.* **1998**, *39*, 7559. (b) Morohashi, N.; Iki, N.; Sugawara, A.; Miyano, S. *Tetrahedron* **2001**, *57*, 5557. (c) Iki, N.; Horiuchi, T.; Oka, H.; Koyama, K.; Morohashi, N.; Kabuto, C.; Miyano, S. *J. Chem. Soc., Perkin Trans. 2* **2001**, 2219.
31. Morohashi, N.; Narumi, F.; Iki, N.; Hattori, T.; Miyano, S. *Chem. Rev.* **2006**, *106*, 5291.
32. (a) Katagiri, H.; Iki, N.; Hattori, T.; Kabuto, C.; Miyano, S. *J. Am. Chem. Soc.* **2001**, *123*, 779. (b) Tanaka, S.; Katagiri, H.; Iki, N.; Hattori, T.; Kabuto, C.; Miyano, S. *Tetrahedron Lett.* **2007**, *48*, 5293.
33. Rao, P.; Hosseini, M. W.; Cian, A. D.; Fischer, J. *Chem. Commun.* **1999**, 2169.
34. (a) Zieba, R.; Desroches, C.; Chaput, F.; Sigala, C.; Jeanneau, E.; Parola, S. *Tetrahedron Lett.* **2007**, *48*, 5401. (b) Zieba, R.; Desroches, C.; Chaput, F.; Parola, S. *FP07 52*, 926, **2007**.
35. Zieba, R.; Desroches, C.; Jeanneau, E.; Parola, S. *Tetrahedron* **2007**, *63*, 10809.
36. Desroches, C.; Lopes, C.; Kessler, V.; Parola, S. *Dalton Trans* **2003**, 2085.
37. Al-Saraierh, H.; Miller, D. O.; Georghiou, P. E. *J. Org. Chem.* **2005**, *70*, 8273.

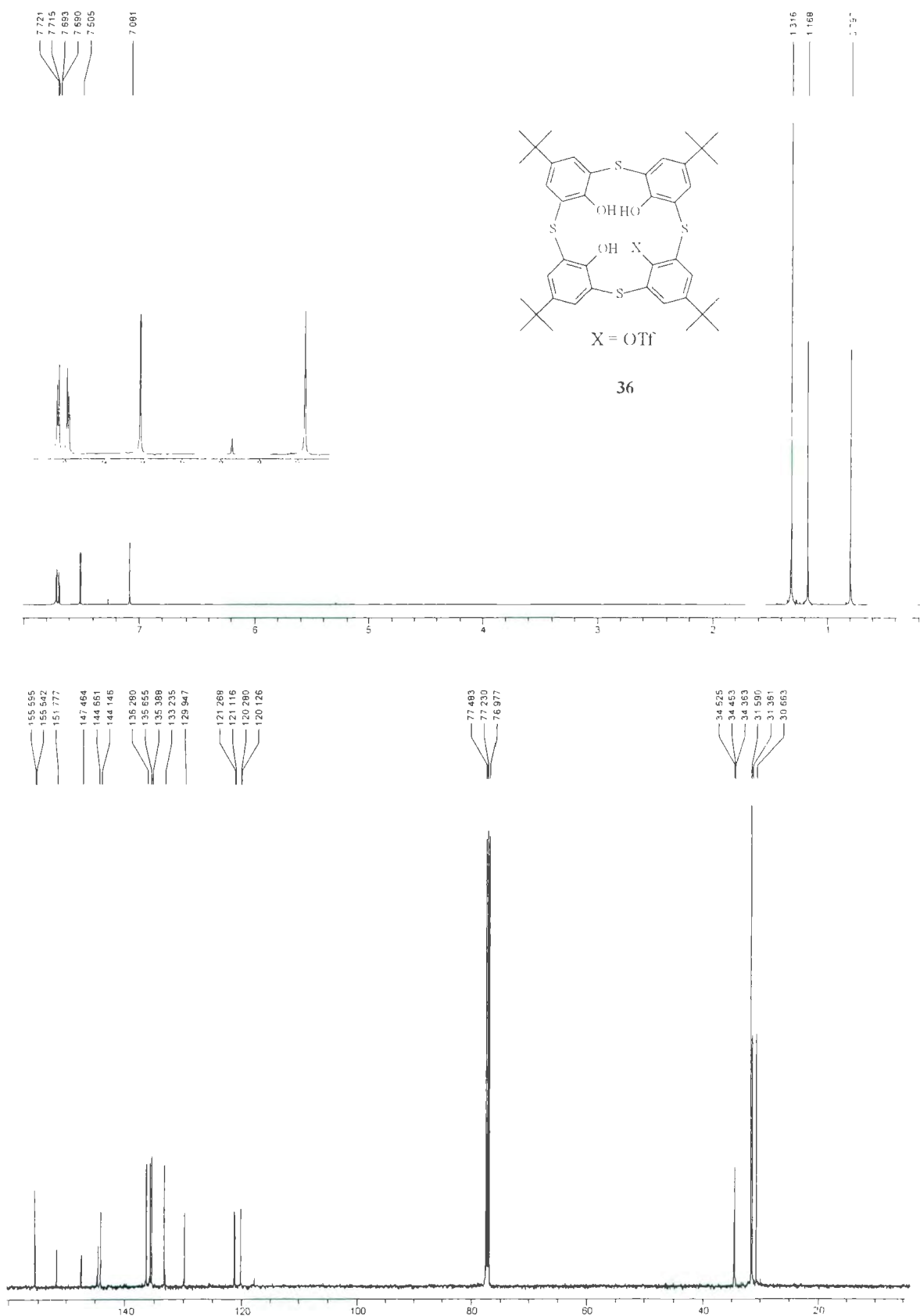
38. Al-Saraierh, H. **Ph. D. Thesis**: "Synthesis of new *narrow* rim modified calix[4]arenes *via* Sonogashira reactions and their photochemistry"; Memorial University of Newfoundland, 2007.
39. Gelman, D.; Buchwald, S. L. *Angew. Chem. Int. Ed. Engl.* **2003**, *42*, 5993.
40. Nicolaou, K. C.; Dai, W.; Hong, Y.; Tsay, S.; Baldrige, K. K.; Siegel J. S. *J. Am. Chem. Soc.* **1993**, *115*, 7944.
41. Chen, Q.Y.; Yang, Z. Y. *Tetrahedron Lett.* **1986**, *27*, 1171.
42. Alami, M.; Ferri, F.; Linstumelle, G. *Tetrahedron Lett.* **1993**, *34*, 6403.
43. Fu, X.; Zhang, S.; Yin, J.; Schumacher, D. P. *Tetrahedron Lett.* **2002**, *43*, 6673.
44. Lhoták, P.; Himl, M.; Pakhomova, S.; Stibor, I. *Tetrahedron Lett.* **1998**, *39*, 8915.
45. Gutsche, C. D.; Dhawran, B.; Levine, J. A.; No, K. H.; Bauer, I. J. *Tetrahedron* **1983**, *39*, 409.
46. Serizawa, R.; Tanaka, S.; Morohashi, N.; Narumi, F.; Hattori, T. *Tetrahedron Lett.* **2007**, *48*, 6281.
47. (a) Our findings were first reported at *calix2007*, the 9<sup>th</sup> international conference, August 6-9, **2007**. (b) Habashneh, A.; Jablonski, C. R.; Collins, J.; Georghiou, P. E. *New J. Chem.* **2008**, *32*, 1590. (c) Tanaka, S.; Serizawa, R.; Morohashi, N.; Hattori, T. *Tetrahedron Lett.* **2007**, *48*, 7660 (First published on the web August 31, **2007**).
48. Chowdhury, S.; Bridson, J. N.; Georghiou, P. E. *J. Org. Chem.* **2000**, *65*, 3299.
49. González, J. J.; Nieto, P. M.; Fraños, P.; Echavarren, A. M.; de Mendoza, J. *J. Org. Chem.* **1995**, *60*, 7419.

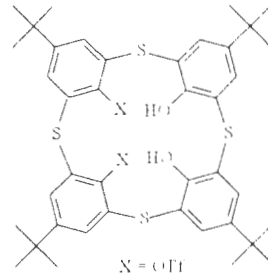
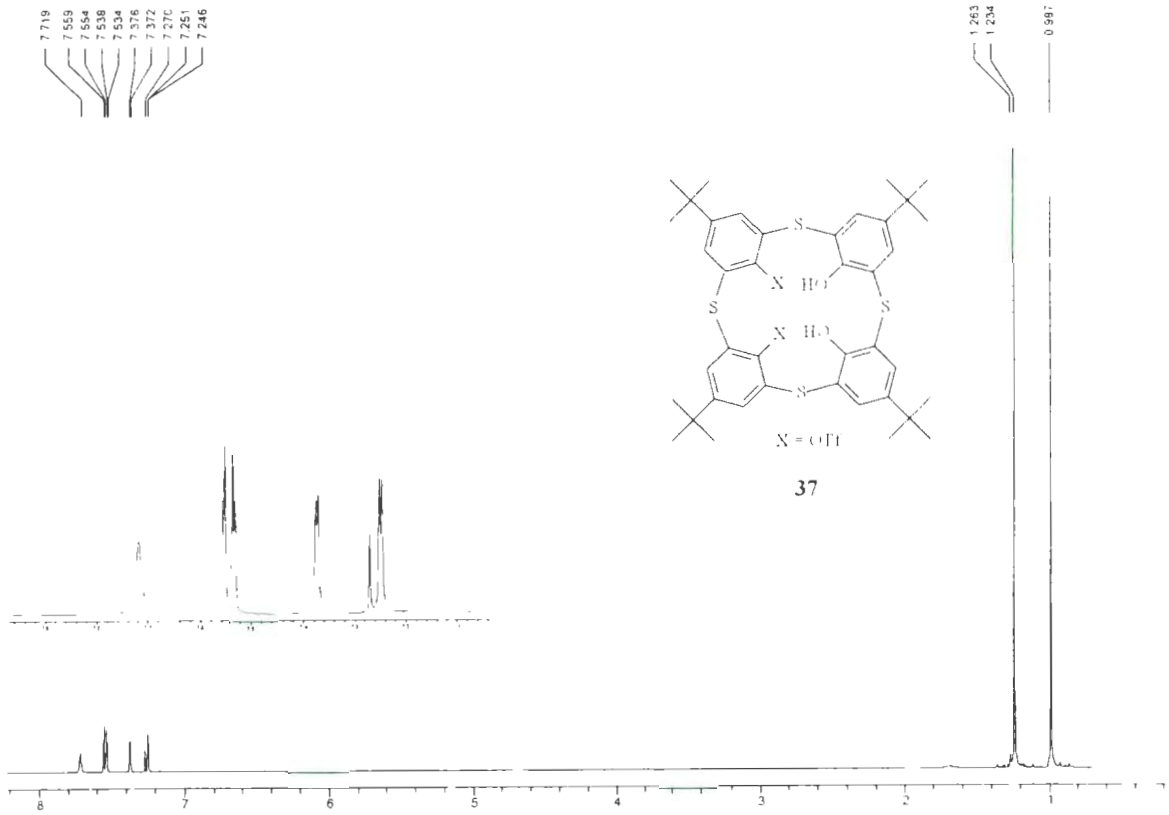
50. Akdasa, H.; Bringel L.; Grafa, E.; Hosseini, M. W.; Mislina, G.; Pansanela, J.; De Cian A.; Fischer, J. *Tetrahedron Lett.* **1998**, *39*, 2311.
51. (a) K. A. Connors, *Binding Constants*, Wiley, New York, 1987. (b) association constants were calculated using non-linear curve fitting using the program ORIGINPro 7.5 from OriginLab Corporation, or with Excel for simple linear regression analysis.
52. Molecular mechanics calculations were conducted using *Titan for Windows 95/98* by Wavefunction, Inc., USA.
53. (a) Mizyed, S.; Georghiou, P. E.; Bancu, M.; Cuadra, B.; Rai, A. K.; Cheng, P.; Scott, L. T. *J. Am. Chem. Soc.* **2001**, *123*, 12770. (b) Georghiou, P. E.; Tran, A. H.; Mizyed, S.; Bancu, M.; Scott, L. T. *J. Org. Chem.* **2005**, *70*, 6158.
54. Georghiou, P. E.; Tran, A. H.; Stroud S. S.; Thompson, D. W. *Tetrahedron* **2006**, *62*, 2036.
55. Tran, A. H.; Georghiou, P. E. *New. J. Chem.* **2007**, *31*, 921.

## **Appendix B**

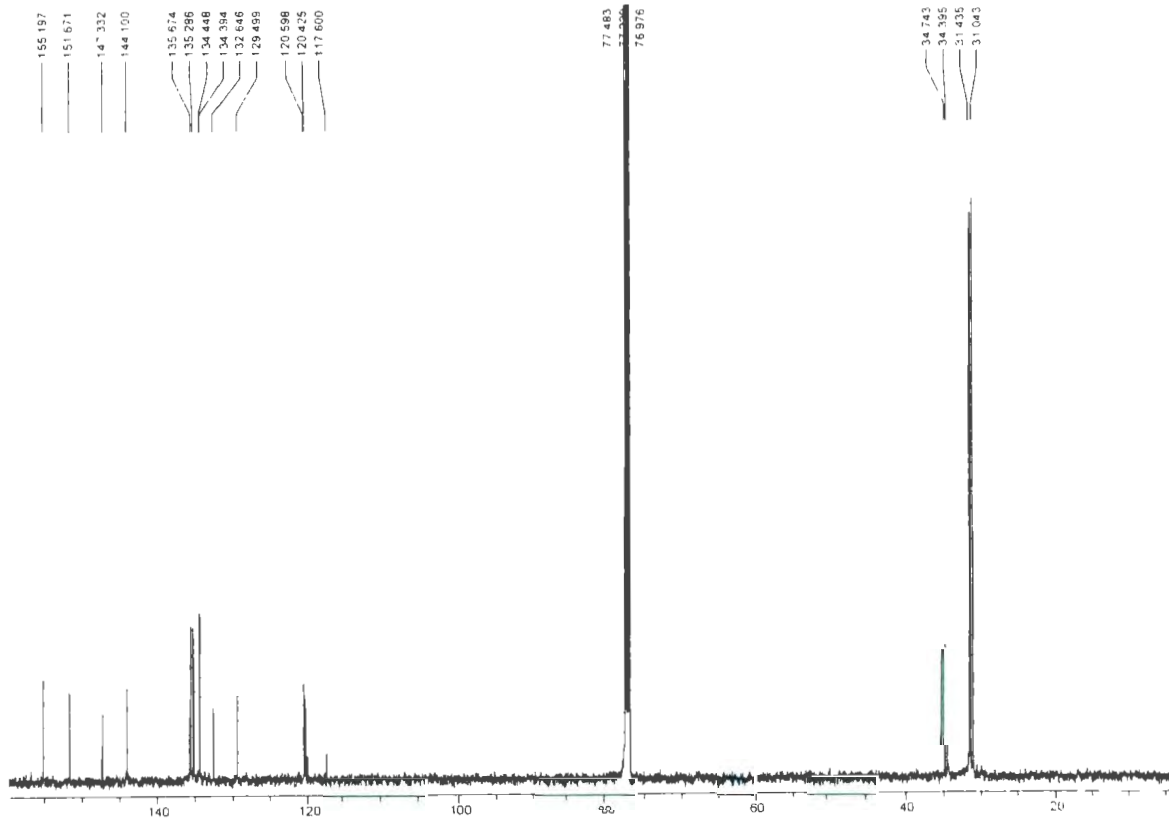
**Selected NMR spectra for synthesized compounds in Chapter 2.1**

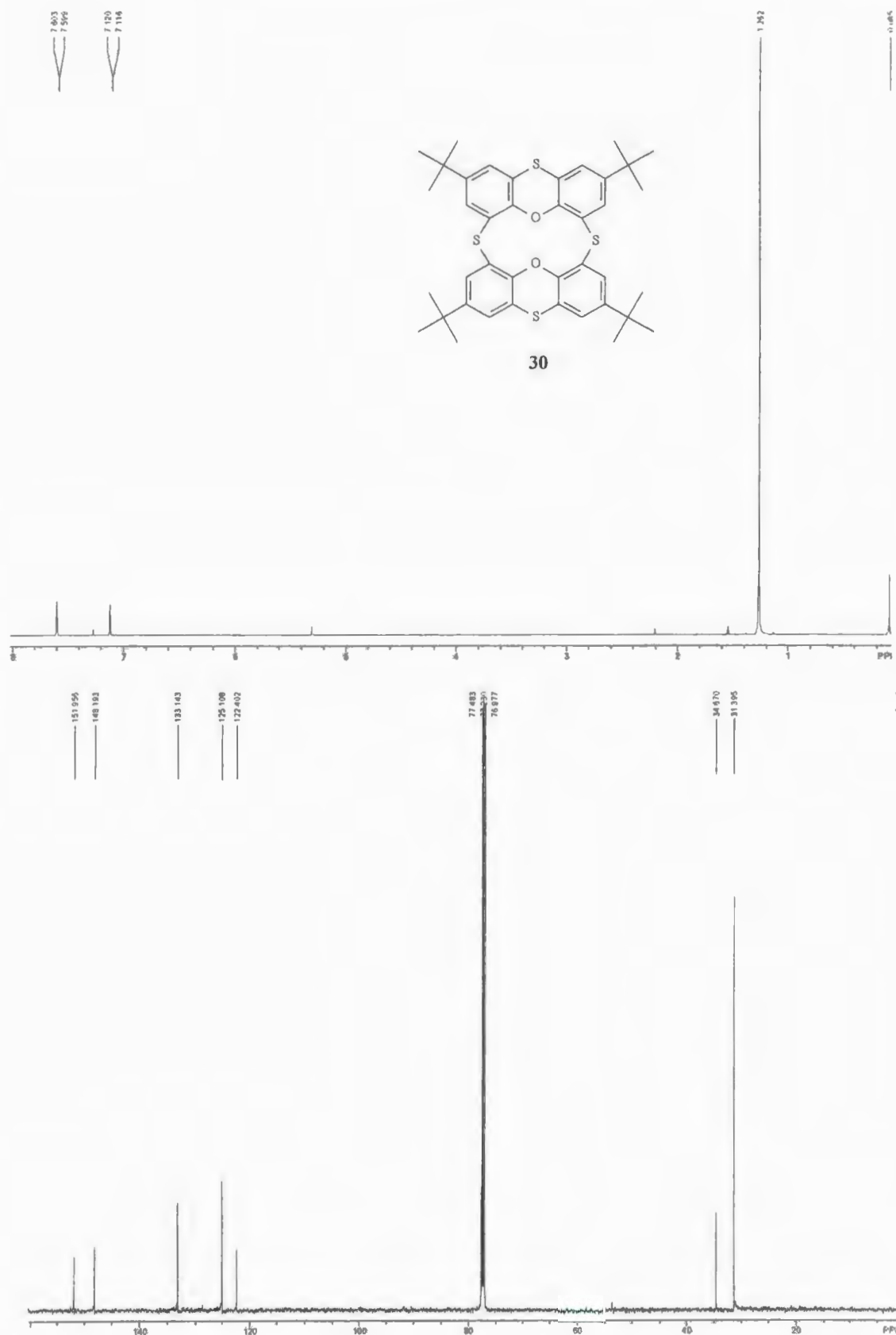


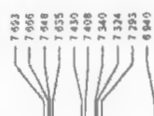




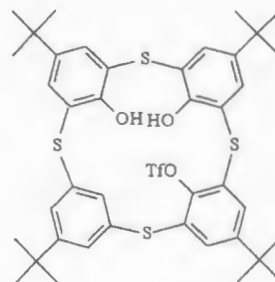
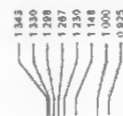
37



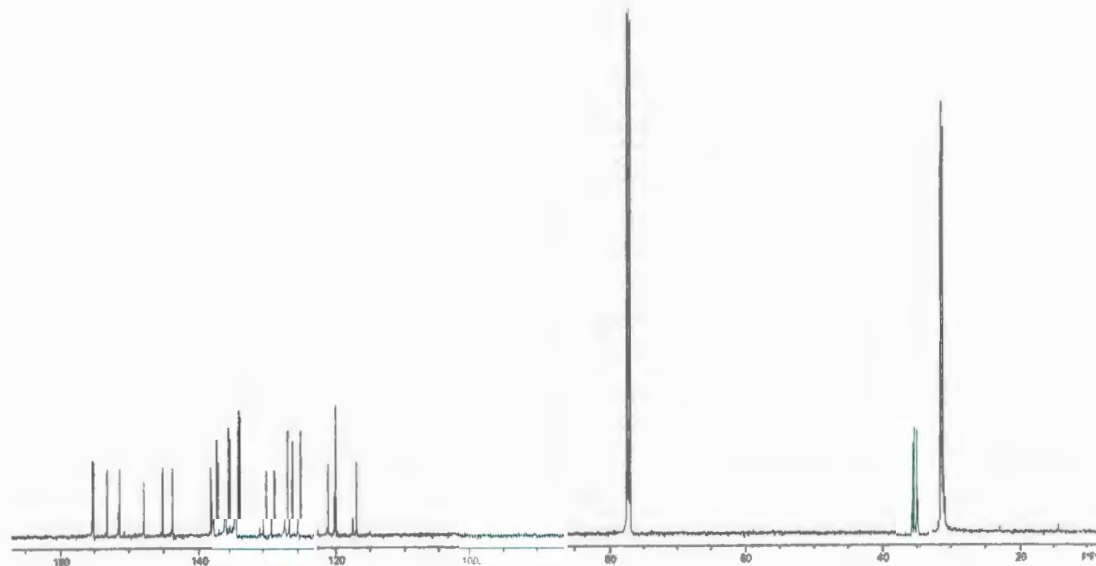
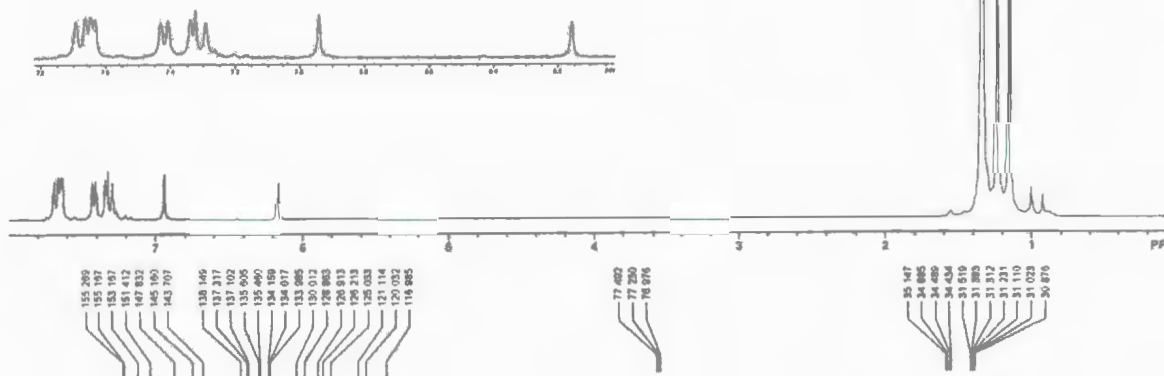


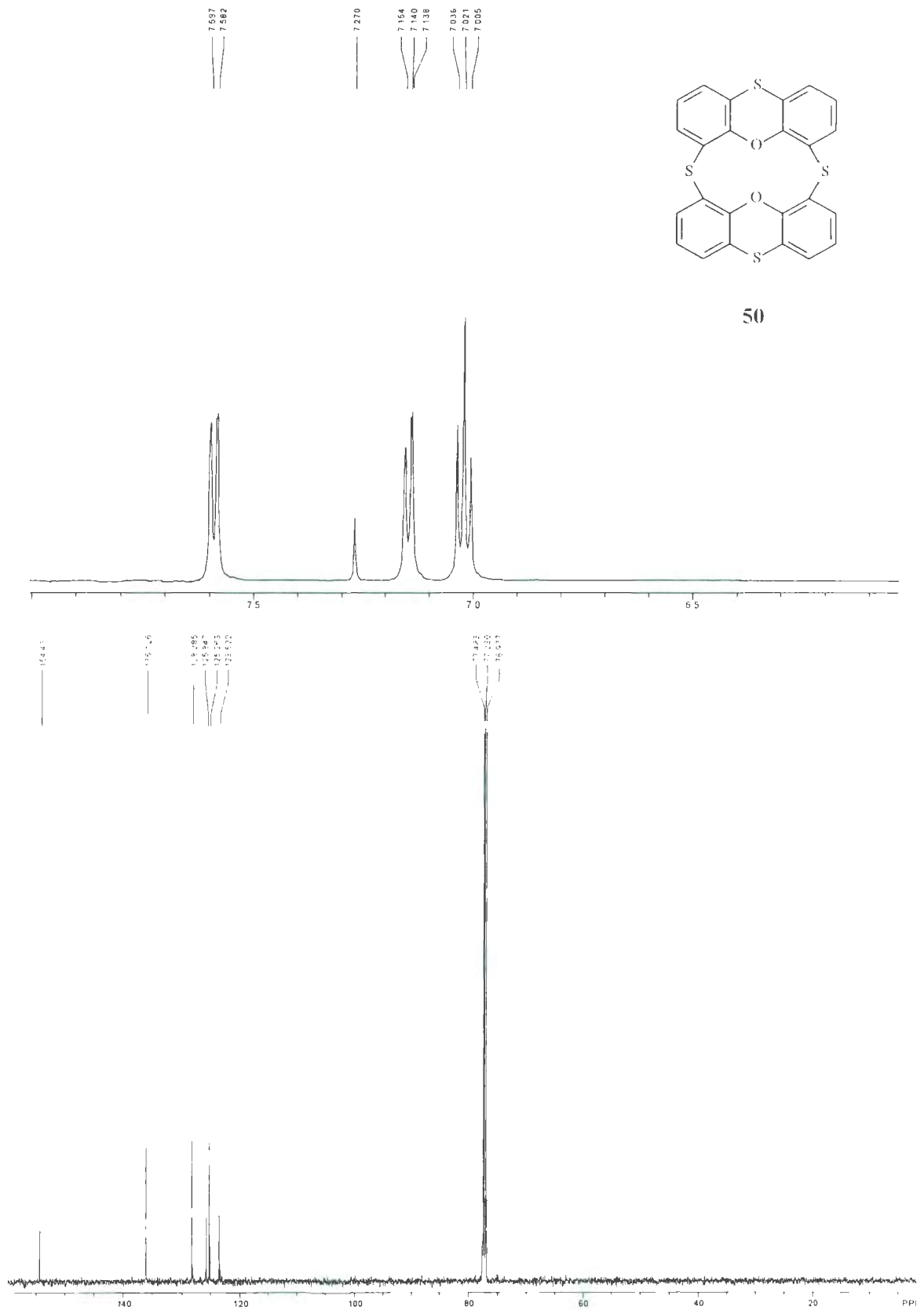


6.158



42





## **Appendix C**

**Complexation data for compounds 30 and 50 in Chapter 2.1**

**Appendix 1** Chemical shift changes ( $\Delta\delta$ ) for protons on **30** in 1:9 CD<sub>3</sub>CN:CDCl<sub>3</sub> at 298 K *versus* added AgCO<sub>2</sub>CF<sub>3</sub> solution ( $6.90 \times 10^{-2}$  M) ( $\Delta\delta$  are absolute values), Run No. 1.

Entry #	Added uL	Total addition (L)	Total volume	Mol Ag <sup>+</sup>	[Ag <sup>+</sup> ]	No. eq. Ag <sup>+</sup>	$\delta$ (ppm)	$\Delta\delta$ (ppm)	$\Delta$ (Hz)
1	0	0	1.000E-3	0	0.000E+0	0.00	7.1380	0	0
2	5.0	5.00E-6	1.005E-3	3.45E-7	3.43E-4	0.47	7.1545	0.0165	8.25
3	5.0	1.00E-5	1.010E-3	6.90E-7	6.83E-4	0.95	7.1635	0.0255	12.75
4	5.0	1.50E-5	1.015E-3	1.03E-6	1.02E-3	1.42	7.1680	0.0300	15.00
5	5.0	2.00E-5	1.020E-3	1.38E-6	1.35E-3	1.89	7.1705	0.0325	16.25
6	5.0	2.50E-5	1.025E-3	1.72E-6	1.68E-3	2.36	7.1730	0.0350	17.50
7	5.0	3.00E-5	1.030E-3	2.07E-6	2.01E-3	2.84	7.1740	0.0360	18.00
8	5.0	3.50E-5	1.035E-3	2.41E-6	2.33E-3	3.31	7.1745	0.0365	18.25
9	10.0	4.50E-5	1.045E-3	3.10E-6	2.97E-3	4.25	7.1740	0.0360	18.00
10	10.0	5.50E-5	1.055E-3	3.79E-6	3.60E-3	5.20	7.1760	0.0380	19.00
11	10.0	6.50E-5	1.065E-3	4.48E-6	4.21E-3	6.14	7.1765	0.0385	19.25
12	10.0	7.50E-5	1.075E-3	5.17E-6	4.81E-3	7.09	7.1760	0.0380	19.00
13	10.0	8.50E-5	1.085E-3	5.86E-6	5.41E-3	8.03	7.1765	0.0385	19.25
14	10.0	9.50E-5	1.095E-3	6.55E-6	5.99E-3	8.98	7.1770	0.0390	19.50

**Appendix 2** Chemical shift changes ( $\Delta\delta$ ) for protons on **30** in 1:9  $\text{CD}_3\text{CN}:\text{CDCl}_3$  at 298 K *versus* added  $\text{AgCO}_2\text{CF}_3$  solution ( $6.67 \times 10^{-3} \text{ M}$ ) ( $\Delta\delta$  are absolute values), Run No. 2.

Entry #	Added uL	Total addition (L)	Total volume	Mol $\text{Ag}^+$	$[\text{Ag}^+]$	No. eq. $\text{Ag}^+$	$\delta$ (ppm)	$\Delta\delta$ (ppm)	$\Delta$ (Hz)
1	0	0	1.000E-3	0.00E-0	0.00E+0	0.00	7.1225	0	0
2	5.0	5.00E-6	1.005E-3	3.33E-7	3.32E-4	0.46	7.1425	0.0200	10.00
3	5.0	1.00E-5	1.010E-3	6.67E-7	6.60E-4	0.92	7.1570	0.0345	17.25
4	5.0	1.50E-5	1.015E-3	1.00E-6	9.86E-4	1.38	7.1630	0.0405	20.25
5	5.0	2.00E-5	1.020E-3	1.33E-6	1.31E-3	1.84	7.1685	0.0460	23.00
6	5.0	2.50E-5	1.025E-3	1.67E-6	1.63E-3	2.30	7.1705	0.0480	24.00
7	5.0	3.00E-5	1.030E-3	2.00E-6	1.94E-3	2.76	7.1715	0.0490	24.50
8	5.0	3.50E-5	1.035E-3	2.33E-6	2.26E-3	3.22	7.1720	0.0495	24.75
9	10.0	4.50E-5	1.045E-3	3.00E-6	2.87E-3	4.15	7.1725	0.0500	25.00
10	10.0	5.50E-5	1.055E-3	3.67E-6	3.48E-3	5.07	7.1735	0.0510	25.50
11	10.0	6.50E-5	1.065E-3	4.34E-6	4.07E-3	5.99	7.1740	0.0515	25.75
12	10.0	7.50E-5	1.075E-3	5.00E-6	4.65E-3	6.91	7.1750	0.0525	26.25
13	10.0	8.50E-5	1.085E-3	5.67E-6	5.23E-3	7.83	7.1755	0.0530	26.50
14	10.0	9.50E-5	1.095E-3	6.34E-6	5.79E-3	8.75	7.1755	0.0530	26.50

**Appendix 3** Chemical shift changes ( $\Delta\delta$ ) for protons on **50** in 1:9  $\text{CD}_3\text{CN}:\text{CDCl}_3$  at 298 K *versus* added  $\text{AgCO}_2\text{CF}_3$  solution ( $6.90 \times 10^{-3} \text{ M}$ ) ( $\Delta\delta$  are absolute values), Run No. 1.

Entry #	Added uL	Total addition (L)	Total volume	Mol $\text{Ag}^+$	$[\text{Ag}^+]$	No. eq. $\text{Ag}^+$	$\delta$ (ppm)	$\Delta\delta$ (ppm)	$\Delta$ (Hz)
1	0	0	1.00E-3	0	0.00E+0	0.00	7.0420	0	0
2	5.0	5.00E-6	1.005E-3	3.45E-7	3.44E-4	0.49	7.0560	0.0140	7.00
3	5.0	1.00E-5	1.010E-3	6.90E-7	6.84E-4	0.98	7.0650	0.0230	11.50
4	5.0	1.50E-5	1.015E-3	1.04E-6	1.02E-3	1.47	7.0730	0.0310	15.50
5	5.0	2.00E-5	1.020E-3	1.38E-6	1.35E-3	1.96	7.0810	0.0390	19.50
6	5.0	2.50E-5	1.025E-3	1.73E-6	1.68E-3	2.46	7.0870	0.0450	22.50
7	5.0	3.00E-5	1.030E-3	2.07E-6	2.01E-3	2.95	7.0900	0.0480	24.00
8	5.0	3.50E-5	1.035E-3	2.42E-6	2.33E-3	3.44	7.0940	0.0520	26.00
9	10.0	4.50E-5	1.045E-3	3.11E-6	2.97E-3	4.42	7.0980	0.0560	28.00
10	10.0	5.50E-5	1.055E-3	3.80E-6	3.60E-3	5.40	7.0990	0.0570	28.50
11	10.0	6.50E-5	1.065E-3	4.49E-6	4.21E-3	6.39	7.1030	0.0610	30.50
12	10.0	7.50E-5	1.075E-3	5.18E-6	4.82E-3	7.37	7.1050	0.0630	31.50

**Appendix 4** Chemical shift changes ( $\Delta\delta$ ) for protons on **50** in 1:9  $\text{CD}_3\text{CN}:\text{CDCl}_3$  at 298 K *versus* added  $\text{AgCO}_2\text{CF}_3$  solution ( $7.01 \times 10^{-3} \text{ M}$ ) ( $\Delta\delta$  are absolute values), Run No.2

Entry #	Added uL	Total addition (L)	Total volume	Mol $\text{Ag}^+$	$[\text{Ag}^+]$	No. eq. $\text{Ag}^+$	$\delta$ (ppm)	$\Delta\delta$ (ppm)	$\Delta$ (Hz)
1	0	0	1.00E-3	0	0.00E+0	0.00	7.0420	0	0
2	5.0	5.00E-6	1.005E-3	3.51E-7	3.49E-4	0.46	7.0550	0.0130	6.50
3	5.0	1.00E-5	1.010E-3	7.01E-7	6.94E-4	0.92	7.0660	0.0240	12.00
4	5.0	1.50E-5	1.015E-3	1.05E-6	1.04E-3	1.38	7.0730	0.0310	15.50
5	5.0	2.00E-5	1.020E-3	1.40E-6	1.38E-3	1.85	7.0800	0.0380	19.00
6	10.0	3.00E-5	1.030E-3	2.10E-6	2.04E-3	2.77	7.0880	0.0460	23.00
7	10.0	4.00E-5	1.040E-3	2.81E-6	2.70E-3	3.69	7.0920	0.0500	25.00
8	5.0	4.50E-5	1.045E-3	3.16E-6	3.02E-3	4.15	7.0940	0.0520	26.00
9	10.0	5.50E-5	1.055E-3	3.86E-6	3.66E-3	5.07	7.0970	0.0550	27.50
10	10.0	6.50E-5	1.065E-3	4.56E-6	4.28E-3	6.00	7.0990	0.0570	28.50
11	10.0	7.50E-5	1.075E-3	5.26E-6	4.89E-3	6.92	7.1010	0.0590	29.50
12	10.0	8.50E-5	1.085E-3	5.96E-6	5.49E-3	7.84	7.1030	0.0610	30.50

**Appendix 5** Chemical shift changes ( $\Delta\delta$ ) for protons on **30** in 1.5:9  $D_3COD:CDCl_3$  at 298 K *versus* added  $Hg(ClO_4)_2$  solution ( $2.74 \times 10^{-2}$  M) ( $\Delta\delta$  are absolute values), Run No. 1

Entry #	Added uL	Total addition (L)	Total volume	Mol $Hg^{2+}$	$[Hg^{2+}]$	No. eq. $Hg^{2+}$	$\delta$ (ppm)	$\Delta\delta$ (ppm)	$\Delta$ (Hz)
1	0	0	1.000E-3	0	0.00E+0	0.00	7.1215	0	0
2	5.0	5.00E-6	1.005E-3	1.37E-7	1.36E-4	0.20	7.1380	0.0165	8.25
3	5.0	1.00E-5	1.010E-3	2.74E-7	2.71E-4	0.40	7.1660	0.0445	22.25
4	2.5	1.25E-5	1.013E-3	3.42E-7	3.38E-4	0.50	7.1745	0.0530	26.50
5	2.5	1.50E-5	1.015E-3	4.11E-7	4.05E-4	0.60	7.1850	0.0635	31.75
6	2.5	1.75E-5	1.018E-3	4.79E-7	4.71E-4	0.70	7.1960	0.0745	37.25
7	2.5	2.00E-5	1.020E-3	5.47E-7	5.37E-4	0.80	7.2060	0.0845	42.25
8	2.5	2.25E-5	1.023E-3	6.16E-7	6.02E-4	0.89	7.2140	0.0925	46.25
9	5.0	2.75E-5	1.028E-3	7.53E-7	7.33E-4	1.09	7.2270	0.1055	52.75
10	5.0	3.25E-5	1.033E-3	8.90E-7	8.62E-4	1.29	7.2440	0.1225	61.25
11	5.0	3.75E-5	1.038E-3	1.03E-6	9.89E-4	1.49	7.2560	0.1345	67.25
12	5.0	4.25E-5	1.043E-3	1.16E-6	1.12E-3	1.69	7.2635	0.1420	71.00
13	5.0	4.75E-5	1.048E-3	1.30E-6	1.24E-3	1.89	7.2695	0.1480	74.00
14	5.0	5.25E-5	1.053E-3	1.44E-6	1.37E-3	2.09	7.2700	0.1485	74.25

**Appendix 6** Chemical shift changes ( $\Delta\delta$ ) for protons on **30** in 1.5:9  $D_3COD:CDCl_3$  at 298 K *versus* added  $Hg(ClO_4)_2$  solution ( $2.74 \times 10^{-2}$  M) ( $\Delta\delta$  are absolute values), Run No. 2.

Entry #	Added uL	Total addition (L)	Total volume	Mol $Hg^{2+}$	$[Hg^{2+}]$	No. eq. $Hg^{2+}$	$\delta$ (ppm)	$\Delta\delta$ (ppm)	$\Delta$ (Hz)
1	0	0	1.000E-3	0	0.00E+0	0.00	7.1215	0	0
2	2.5	2.50E-6	1.003E-3	6.84E-8	6.83E-5	0.10	7.1290	0.0075	3.75
3	2.5	5.00E-6	1.005E-3	1.37E-7	1.36E-4	0.19	7.1410	0.0195	9.75
4	2.5	7.50E-6	1.008E-3	2.05E-7	2.04E-4	0.29	7.1530	0.0315	15.75
5	2.5	1.00E-5	1.010E-3	2.74E-7	2.71E-4	0.38	7.1625	0.0410	20.50
6	2.5	1.25E-5	1.013E-3	3.42E-7	3.38E-4	0.48	7.1745	0.0530	26.50
7	2.5	1.50E-5	1.015E-3	4.11E-7	4.05E-4	0.58	7.1840	0.0625	31.25
8	2.5	1.75E-5	1.018E-3	4.79E-7	4.71E-4	0.67	7.1950	0.0735	36.75
9	5.0	2.25E-5	1.023E-3	6.16E-7	6.02E-4	0.87	7.2140	0.0925	46.25
10	5.0	2.75E-5	1.028E-3	7.53E-7	7.33E-4	1.06	7.2220	0.1005	50.25
11	5.0	3.25E-5	1.033E-3	8.90E-7	8.62E-4	1.25	7.2380	0.1165	58.25
12	5.0	3.75E-5	1.038E-3	1.03E-6	9.89E-4	1.44	7.2505	0.1290	64.50
13	5.0	4.25E-5	1.043E-3	1.16E-6	1.12E-3	1.64	7.2600	0.1385	69.25
14	5.0	4.75E-5	1.048E-3	1.30E-6	1.24E-3	1.83	7.2660	0.1445	72.25
15	5.0	5.25E-5	1.053E-3	1.437E-6	1.36E-3	2.020	7.269	0.1475	73.75
16	5.0	5.75E-5	1.058E-3	1.574E-6	1.49E-3	2.214	7.2725	0.1510	75.50

**Appendix 7** Chemical shift changes ( $\Delta\delta$ ) for protons on **50** in 1.5:9  $D_3COD:CDCl_3$  at 298 K *versus* added  $Hg(ClO_4)_2$  solution ( $2.74 \times 10^{-2}$  M) ( $\Delta\delta$  are absolute values), Run No. 1.

Entry #	Added uL	Total addition (L)	Total volume	Mol $Hg^{2+}$	$[Hg^{2+}]$	No. eq. $Hg^{2+}$	$\delta$ (ppm)	$\Delta\delta$ (ppm)	$\Delta$ (Hz)
1	0	0	1.00E-03	0	0.00E+00	0.00	7.0340	0	0
2	3.0	3.00E-06	1.003E-03	8.21E-08	8.19E-05	0.12	7.0420	0.0080	4.00
3	3.0	6.00E-06	1.006E-03	1.64E-07	1.63E-04	0.25	7.0520	0.0180	9.00
4	3.0	9.00E-06	1.009E-03	2.46E-07	2.44E-04	0.37	7.0640	0.0300	15.00
5	3.0	1.20E-05	1.012E-03	3.28E-07	3.25E-04	0.49	7.0750	0.0410	20.50
6	6.0	1.80E-05	1.018E-03	4.93E-07	4.84E-04	0.74	7.0940	0.0600	30.00
7	3.0	2.10E-05	1.021E-03	5.75E-07	5.63E-04	0.86	7.1030	0.0690	34.50
8	5.0	2.60E-05	1.026E-03	7.12E-07	6.94E-04	1.06	7.1150	0.0810	40.50
9	5.0	3.10E-05	1.031E-03	8.49E-07	8.23E-04	1.27	7.1270	0.0930	46.50
10	5.0	3.60E-05	1.036E-03	9.85E-07	9.51E-04	1.47	7.1380	0.1040	52.00
11	5.0	4.10E-05	1.041E-03	1.12E-06	1.08E-03	1.67	7.1450	0.1110	55.50
12	7.0	4.80E-05	1.048E-03	1.31E-06	1.25E-03	1.96	7.1560	0.1220	61.00
13	7.0	5.50E-05	1.055E-03	1.51E-06	1.43E-03	2.25	7.1660	0.1320	66.00
14	7.0	6.20E-05	1.062E-03	1.70E-06	1.60E-03	2.53	7.1750	0.1410	70.50
15	10.0	7.20E-05	1.072E-03	1.97E-06	1.84E-03	2.94	7.1830	0.1490	74.50
16	10.0	8.20E-05	1.082E-03	2.24E-06	2.07E-03	3.35	7.1900	0.1560	78.00

**Appendix 8** Chemical shift changes ( $\Delta\delta$ ) for protons on **50** in 1.5:9  $D_3COD:CDCl_3$  at 298 K *versus* added  $Hg(ClO_4)_2$  solution ( $2.74 \times 10^{-2}$  M) ( $\Delta\delta$  are absolute values), Run No. 2.

Entry #	Added uL	Total addition (L)	Total volume	Mol $Hg^{2+}$	$[Hg^{2+}]$	No. eq. $Hg^{2+}$	$\delta$ (ppm)	$\Delta\delta$ (ppm)	$\Delta$ (Hz)
1	0	0	1.000E-03	0	0.00E+00	0.00	7.0350	0	0
2	2.5	2.50E-06	1.003E-03	6.84E-08	6.83E-05	0.09	7.0400	0.0050	2.50
3	3.0	5.50E-06	1.006E-03	1.51E-07	1.50E-04	0.20	7.0490	0.0140	7.00
4	3.0	8.50E-06	1.009E-03	2.33E-07	2.31E-04	0.31	7.0590	0.0240	12.00
5	3.0	1.15E-05	1.012E-03	3.15E-07	3.11E-04	0.41	7.0670	0.0320	16.00
6	3.0	1.45E-05	1.015E-03	3.97E-07	3.91E-04	0.52	7.0760	0.0410	20.50
7	3.0	1.75E-05	1.018E-03	4.79E-07	4.71E-04	0.63	7.0840	0.0490	24.50
8	3.0	2.05E-05	1.021E-03	5.61E-07	5.50E-04	0.74	7.0910	0.0560	28.00
9	5.0	2.55E-05	1.026E-03	6.98E-07	6.81E-04	0.92	7.1040	0.0690	34.50
10	5.0	3.05E-05	1.031E-03	8.35E-07	8.10E-04	1.10	7.1150	0.0800	40.00
11	5.0	3.55E-05	1.036E-03	9.72E-07	9.38E-04	1.28	7.1240	0.0890	44.50
12	5.0	4.05E-05	1.041E-03	1.11E-06	1.07E-03	1.46	7.1330	0.0980	49.00
13	7.0	4.75E-05	1.048E-03	1.30E-06	1.24E-03	1.71	7.1430	0.1080	54.00
14	8.0	5.55E-05	1.056E-03	1.52E-06	1.44E-03	2.00	7.1530	0.1180	59.00
15	7.0	6.25E-05	1.063E-03	1.71E-06	1.61E-03	2.25	7.1580	0.1230	61.50
16	7.0	6.95E-05	1.070E-03	1.90E-06	1.78E-03	2.50	7.1630	0.1280	64.00
17	7.0	7.65E-05	1.077E-03	2.09E-06	1.95E-03	2.76	7.1700	0.1350	67.50
18	10.0	8.65E-05	1.087E-03	2.37E-06	2.18E-03	3.12	7.1770	0.1420	71.00
19	10.0	9.65E-05	1.097E-03	2.64E-06	2.41E-03	3.48	7.1800	0.1450	72.50



